TECHNISCHE UNIVERSITÄT WIEN

Gutachter der Dissertation:

1. Gutachter: _____
Prof. Dr. A. Pimenov
TU Wien

2. Gutachter: _____
Prof. Dr. W. Schranz
Universität Wien

DISSERTATION

Dielectric spectroscopy at the spin-driven ferroelectric phase transition in chiral multiferroic DyMnO$_3$

ausgeführt zum Zwecke der Erlangung des akademischen Grades eines

Doktors der Naturwissenschaften unter der Leitung von

Univ.Prof.Dr.rer.nat. Andrei Pimenov

E138- Institut für Festkörperphysik

eingereicht an der TU Wien

Fakultät für Physik

von

Ing.Dipl.Ing. Markus Schiebl, BSc.
Matrikelnummer: 0225960
Vorgartenstraße 221/3/1, 1020 Wien

Wien, am 18. Jänner 2016

Abstract

In magnetoelectric multiferroics the onset of ferroelectricity is coupled to the onset of a magnetic structure that breaks the inversion symmetry. The dynamics of such coupled ordering transition can be probed via the dielectric response of the system. Generally, the question which type of ferroelectric transition (order-disorder or displacive) applies for multiferroics is important and $DyMnO_3$ belongs to the most prominent members of this interesting material class. In the ferroelectric state, the Mn^{3+}- spins form a cycloidal magnetic structure whereas in the paraelectric state, a collinear sinusoidal modulated spin structure is proposed to exist. However, the exact role in the formation of multiferroicity of the so-called collinear sinusoidal magnetic state, preceding the multiferroic state under cooling, is not yet fully clarified.

Detailed dielectric studies near the spin-driven ferroelectric phase transition reveals the indication of an order-disorder type ferroelectric transition with a double well potential. This potential reflects a dynamical switching between magnetic cycloids of the opposite chirality in the vicinity of the ferroelectric phase transition boundary by applying an electric field. Several parameters of the model correlate well with physical properties of $DyMnO_3$. Thus, the characteristic energies of magnetic ordering and the value of the static electric polarization are in agreement with known values. Most importantly, the experimental data and the simple model suggest to explain the paraelectric sinusoidal phase in rare-earth manganate as a dynamical equilibrium of cycloids with opposite chiralities. In addition to the dielectric results, this hypothesis resolve several experimental constraints which contradicted the concept of static sinusoidally modulated magnetic phase.

Kurzfassung

Ferroelektrizität in einem magnetoelektrischen Multiferroikum ist verbunden mit der Entstehung von nicht inversionssymmetrischen magnetischen Strukturen. Diese Multiferroika zeichnen sich dadurch aus, dass sich deren Magnetisierung durch ein elektrisches Feld bzw. deren elektrische Polarisation durch ein magnetisches Feld beeinflussen lässt. In diesen Materialien sind die polare und die magnetische Ordnung stark aneinander gekoppelt. Diese spezielle Eigenschaft eröffnet ein ganz neues Feld von Anwendungen in Optik, elektronischer Schaltungstechnik und elektronischer Speichertechnik.

Die Dynamik solch komplexer Ordnungsstrukturen kann mittels dielektrischer Antwort untersucht werden. Ein typisches Merkmal ist die Anregung von Elektro-Magnonen mittels eines elektrischen Feldes im THz-Bereich. Zudem können auch dispersive dielektrische Merkmale im Niederfrequenzbereich (<1MHz) in der Nähe des multiferroischen Phasenübergangs beobachtet werden. Diesbezüglich wurde das Verhalten der dielektrischen Antwort von $DyMnO_3$ im Frequenzbereich von 10^{-1}-10^6 Hz in der Nähe des multiferroischen Phasenübergangs untersucht. Die Ursache von Ferroelektrizität in $DyMnO_3$ unterhalb der kritischen Temperatur liegt in der Bildung einer zykloidalen magnetischen Struktur, wobei oberhalb der kritischen Temperatur nach bisheriger wohl akzeptierter Meinung eine sinusoidale magnetische Struktur vorliegt.

Die Resultate zeigen eine kritische Verlangsamung der Ordnungsparameterdynamik in der Nähe des multiferroischen Phasenübergangs. Es kann gezeigt werden, dass diese Verlangsamung als Ursache eines Ordnungs-Unordnungs Phasenüberganges gesehen werden kann, bei dem sich elektrische Dipole in einem Doppelmuldenpotential unterhalb von T_C langreichweitig ordnen. Dies lässt den Schluss zu, dass die paraelektrische sinusoidale magnetische Phase oberhalb von T_C als dynamisches Gleichgewicht von kurzreichweitig geordneten zykloidalen magnetischen Strukturen mit gegensätzlicher Händigkeit gesehen werden kann. Demzufolge existiert eine Kopplung zwischen Spin-und Ladungsträgerfreiheitsgraden auch oberhalb der kritischen Temperatur.

Contents

List of Figures

List of Abbreviations

CW	Clock Wise
CCW	Counter-Clock Wise
DM	Dzyaloshinskii-Moriya
IDM	Inverse Dzyaloshinskii-Moriya
GKA	Goodenough-Kanamori-Anderson
NN	Nearest Neighbour
NNN	Next Nearest Neighbour
FM	Ferro Magnetic
AFM	Anti Ferro Magnetic
MW	Maxwell Wagner
AC	Alternating Current

Statement of Original Authorship

I declare that this thesis is my own work and has not been submitted in any form for another degree or diploma at any university or other institution of tertiary education. Information arrived from the published or unpublished work of others has been acknowledged in the text and a list of references is given

Signed: _____

Date: _____

Acknowledgments

Finally, I would like to thank following people:

Prof. Dr. Andrei Pimenov for giving me the opportunity of doing my PhD in this interesting scientific field and his support and guidance throughout the years.

Anna Pimenov for preparing various sorts of polycristalline samples and for encouraging me in times when I made slow progress. I also thank Anna for her effort in introducing social life into the workgroup.

Dr. Alexey Shuvaev, Dr. Graehme Eoin Johnstone and Wlad Dziom for the fruitful discussion on the principles of solid state physics.

Sonja, Lennard Pau, Lilli Marleen and Ben Julian without whose support it would not have been completed.

Ing.Dipl.Ing. Markus Schiebl, BSc.

CHAPTER 1

Introduction

Magnetoelectric multiferroic materials with a coupling of electric and magnetic degrees of freedom have attracted considerable interest after the discovery of a large magnetoelectric effect (ME) in several compounds [1, 2, 3, 4]. They allow a cross-control of the electric polarization via a magnetic field and the magnetization via an electric field and thus in turn they are currently the subject of intensive study due to fascinating physical properties and potential for applications as multifunctional devices [1, 5, 6, 7, 8, 9, 10, 11, 12, 13, 14, 15, 16, 17, 18, 19, 20, 21, 22, 23, 24, 25].

The rare-earth $RMnO_3$ manganites (R=Gd, Tb, Dy, Eu/Y) with orthorhombically distorted perovskite structure have emerged as a new class of multiferroics with strongly coupled antiferromagnetic and ferroelectric properties [26, 27]. Several rare earth manganites orders antiferromagnetically below $T_N \sim 40K$ into collinear paraelectric phase [28] with sinusoidal modulations of the M_n^{3+}- spins. This phase is followed by a cycloidal spin order with nonzero electric polarization below $T_C \sim 20K$.

It should be noted that the M_n^{3+} atom is supposed [29] to have a Heisenberg spin with a fixed length of $S = 2$. The purely sinusoidally modulated spin phase contradicts this property. Model calculations [29] have obtained the sinusoidal order only as a time-space average of the simulated cluster. Thus, there is a possibility that a short-range dynamic order exists in the intermediate temperature range $T_C < T < T_N$ which is responsible for the "hidden" spin. As the magnetic order at low temperatures is spin cycloid, it is natural to assume that the dynamic short-range order is also a spin cycloid. This would imply that there are fluctuating ferroelectric regions in the sinusoidal phase and that the ferroelectric transition is actually of the order-disorder type. Such transition has been also suggested in Ref. [30] where a **c**-axis relaxation typical for the order-disorder type transitions has been investigated. The fact that the wave vector q_{Mn} of the spin wave does not change at the transition temperature T_C [31] is also an indirect evidence that the ferroelectric transition is not of the displacive type.

The data by terahertz spectroscopy [32, 33] evidence the nonzero dielectric contribution of electromagnon in the sinusoidal phase. According to the commonly accepted mechanism of the electromagnon [34, 35], the majority of the spectral weight of this mode originates from exchange striction mechanism and can only exist in magnetic phases with non-collinear spin arrangement. These facts again favor the hypothesis of dynamical cycloidal spin order in the sinusoidal phase.

Recent theoretical analysis of the terahertz dynamics in the sinusoidal phase suggested

an explanation based on anomalous magnetoelectric coupling. Investigations of the collinear sinusoidal phase in the diluted compounds $TbMn_{1-x}Al_xO_3$ [36] and the observation of the memory effect in the low temperature sinusoidal phase in the multiferroic $MnWO_4$[37] have suggested the presence of the nanosize ferroelectric domains and support relaxor order-disorder type transition.

In this work we present the analysis of the critical behavior of the low-frequency relaxation in $DyMnO_3$. The observed critical behavior confirms that the sinusoidal to cycloidal phase transition is of the order-disorder type. The model suggests the presence of the short-range cycloidal order in the collinear spin phase.

CHAPTER 2

Fundamental properties of magnetoelectrics

2.1 Thermodynamic potential in electromagnetism and the magnetoelectric effect

Landau and Lifshitz first predicted the linear magnetoelectric effect published in the famous book "*Electrodynamics of continuous media*" [38]. It describes the influence of a magnetic field on the electric polarization and - vice versa - the influence of an electric field on the magnetization of a material. This phenomenon was fist observed by Astrov [39] and Folen et al. [40] in Cr_2O_3.

The electric polarization and magnetization of a material is described within the framework of thermodynamics with the basic principle of energy conservation - the first law of thermodynamic. It is given by,

$$\mathrm{d}U = \mathrm{d}Q - \mathrm{d}W + \bar{\mu}\mathrm{d}N \tag{2.1}$$

Where U is the internal energy, Q is the heat energy, W is the work, $\bar{\mu}$ is the chemical potential, and N is the particle number. Nota bene there exists different sign conventions. Here, the elementary work (differential form of work), $\mathrm{d}W$, is the work exerted to the environment by the system. In this case, positive work means loss of energy by the system. In general, the expression of the differential form of work is

$$\mathrm{d}W_{mech} = \sum_i f_i \mathrm{d}X_i \tag{2.2}$$

where f_i are the coordinates of the generalized force and X_i the coordinates of the generalized displacement. Neglecting the work related to the surface energy and elastic deformation, only the work related to the change of the volume and the change of the electromagnetic energy must be accounted in Eq. (2.1). The conservation of energy in electrodynamics is given by [41],

$$\frac{\mathrm{d}W_{mech}}{\mathrm{d}t} = -\frac{\mathrm{d}E_{field}}{\mathrm{d}t} - \oint_S \mathbf{S} \cdot \mathrm{d}\mathbf{a} \tag{2.3}$$

The field energy is given by, $E_{field} = \frac{1}{2}\int_V (\mathbf{E} \cdot \mathbf{D} + \mathbf{B} \cdot \mathbf{H})\, d\tau$ where $\mathbf{D}$ is the displace-

ment field, $\mathbf{B}$ is the induction field,$\mathbf{E}$ is the electric field and $\mathbf{H}$ is the magnetic field. $\mathbf{S}$ denotes the pointing vector with $\mathbf{S} = \frac{1}{\mu_0}\left(\mathbf{E} \times \mathbf{B}\right)$. For uniform fields, the energy flux in and out of V across the bounding surface (=material surface) are balanced, thus $\oint_S \mathbf{S} \cdot d\mathbf{a} = 0$. Hence,

$$\frac{dW_{mech}}{dt} = -\frac{dE_{field}}{dt} \Rightarrow dW_{mech} = -dE_{field} \tag{2.4}$$

The change of the field energy is given by,

$$dE_{field} = \frac{1}{2}\int_V \left(\mathbf{E} \cdot d\mathbf{D} + d\mathbf{E} \cdot \mathbf{D} + \mathbf{B} \cdot d\mathbf{H} + d\mathbf{B} \cdot \mathbf{H}\right)d\tau \tag{2.5}$$

With the definition of the dielectric displacement field,

$$\mathbf{D} = \varepsilon_0 \mathbf{E} + \mathbf{P}\left(\mathbf{E}, \mathbf{H}\right) \tag{2.6}$$

where $\mathbf{P}$ is the polarization dependent on $\mathbf{E}$ and $\mathbf{H}$ and the magnetic induction,

$$\mathbf{B} = \mu_0 \left[\mathbf{H} + \mathbf{M}\left(\mathbf{H}, \mathbf{E}\right)\right] \tag{2.7}$$

where $\mathbf{M}$ is the magnetization dependent on $\mathbf{E}$ and $\mathbf{H}$ and with the definitions of the electric and magnetic susceptibilities as, $\overline{\overline{\chi_E}} = \frac{1}{\varepsilon_0}\frac{d\mathbf{P}}{d\mathbf{E}}$, $\overline{\overline{\chi_M}} = \frac{d\mathbf{M}}{d\mathbf{H}}$ where the double bar denotes a second rank tensor, the change of the displacement field with respect to a change of the electric field becomes,

$$\begin{aligned}
\frac{d\mathbf{D}}{d\mathbf{E}} &= \varepsilon_0 + \frac{d\mathbf{P}\left(\mathbf{E}, \mathbf{H}\right)}{d\mathbf{E}} \\
&= \varepsilon_0\left(1 + \overline{\overline{\chi_E}}\right) \\
&= \overline{\overline{\varepsilon}}
\end{aligned} \tag{2.8}$$

Thus, $d\mathbf{D} = \overline{\overline{\varepsilon}}d\mathbf{E}$ and $\mathbf{D} = \overline{\overline{\varepsilon}}\mathbf{E}$. The change of the induction field with respect to a change of the magnetic field becomes,

$$\begin{aligned}
\frac{d\mathbf{B}}{d\mathbf{H}} &= \mu_0 + \mu_0\frac{d\mathbf{M}\left(\mathbf{E}, \mathbf{H}\right)}{d\mathbf{H}} \\
&= \mu_0\left(1 + \overline{\overline{\chi_M}}\right) \\
&= \overline{\overline{\mu}}
\end{aligned} \tag{2.9}$$

Hence, $d\mathbf{B} = \overline{\overline{\mu}}d\mathbf{H}$ and $\mathbf{B} = \overline{\overline{\mu}}\mathbf{H}$. Consequently, Eq. (2.5) becomes,

$$dE_{field} = \int_V \left(\mathbf{E} \cdot d\mathbf{D} + \mathbf{H} \cdot d\mathbf{B}\right)d\tau \tag{2.10}$$

Thus,

$$dW_{mech} = -\int_V \left(\mathbf{E} \cdot d\mathbf{D} + \mathbf{H} \cdot d\mathbf{B}\right)d\tau \tag{2.11}$$

Equation (2.11) can be interpreted as the work carried out by the system which is equival-

ent to the decrease of the field energy. With Eq. (2.11), the energy conservation principle (Eq. 2.1), becomes,

$$\mathrm{d}U\left(S, N, V, \mathbf{D}, \mathbf{B}\right) = T\mathrm{d}S - p\mathrm{d}V + \bar{\mu}\mathrm{d}N + \int_V \left(\mathbf{E} \cdot \mathrm{d}\mathbf{D} + \mathbf{H} \cdot \mathrm{d}\mathbf{B}\right)\mathrm{d}\tau \qquad (2.12)$$

Where S is the entropy, T is the temperature, p is the pressure and V is the volume. In this description, the natural variable of the system are given by the entropy, S, the particle number, N, the volume, V, the dielectric displacement field, $\mathbf{D}$, and the magnetic induction field, $\mathbf{B}$. Material parameters like the permittivity, ε, and the permeability, μ, contained in the electric and magnetic field must be expressed as functions of the natural variables.

In more detail, this implies that ε and μ must be expressed as functions of the entropy. However, this is very inconvenient since the temperature is the choice as a natural variable in the experiment in contrast to the entropy –it is much easier to control the temperature instead of the entropy. Thus, the free energy becomes the thermodynamic potential to describe a material in a certain thermodynamic state. The free energy is obtained by a Legrende-Transformation of the internal energy. It is defined as,

$$F\left(T, N, V, \mathbf{D}, \mathbf{B}\right) = U - \frac{\partial U}{\partial S}S = U - TS \qquad (2.13)$$

Thus, with Eq. (2.12), the differential of the free energy, F, becomes,

$$\mathrm{d}F = -S\mathrm{d}T - p\mathrm{d}V + \bar{\mu}\mathrm{d}N + \int_V \left(\mathbf{E} \cdot \mathrm{d}\mathbf{D} + \mathbf{H} \cdot \mathrm{d}\mathbf{B}\right)\mathrm{d}\tau \qquad (2.14)$$

Here ε and μ are functions of temperature. Since free charges are sources of the electric displacement, $\mathbf{D}$, and the vector potential, $\mathbf{A}$, is the source of the magnetic induction, $\mathbf{B}$, the free energy given by Eq. (2.14) is the choice for problems with fixed free charges of conductors and fixed vector potential.

For other cases, at which the natural variables T, $\mathbf{E}$ and $\mathbf{H}$ are the choice for describing the state of the problem, a new potential should be formed by a suitable Legendre-Transformation,

$$\begin{aligned} F\left(T, N, V, \mathbf{E}, \mathbf{H}\right) = \quad & U - \frac{\partial U}{\partial S}S - \frac{\partial U}{\partial \mathbf{D}}\mathbf{D} - \frac{\partial U}{\partial \mathbf{B}}\mathbf{B} \\ = \quad & U - TS - \int_V \left(\mathbf{E} \cdot \mathbf{D} + \mathbf{H} \cdot \mathbf{B}\right)\mathrm{d}\tau \end{aligned} \qquad (2.15)$$

Thus,

$$\mathrm{d}F = -S\mathrm{d}T - p\mathrm{d}V + \bar{\mu}\mathrm{d}N - \int_V \left(\mathbf{D} \cdot \mathrm{d}\mathbf{E} + \mathbf{B} \cdot \mathrm{d}\mathbf{H}\right)\mathrm{d}\tau \qquad (2.16)$$

Hence, this potential obtains extremum with constant electric field, $\mathbf{E}$, and magnetic field, $\mathbf{H}$. Hence, Eq. (2.16) is suitable for cases with fixed electric potential and fixed currents.

2.1.1 Material equation for magnetoelectric media

With the definition of the dielectric displacement field Eq. (2.6), and the magnetic induction, Eq. (2.7), the change of the free energy of the medium, Eq. (2.16), becomes at constant temperature, volume and particle number,

$$dF_{EM} = -\int_V \left(\varepsilon_0 \mathbf{E} \cdot d\mathbf{E} + \mathbf{P} \cdot d\mathbf{E} + \mu_0 \mathbf{H} \cdot d\mathbf{H} + \mu_0 \mathbf{M} \cdot d\mathbf{H} \right) d\tau \tag{2.17}$$

Equation (2.17) includes also the contribution of the free space to the change of the electromagnetic free energy, dF_{EM}. For further calculations, it is convenient to exclude the free space contribution to the total electromagnetic free energy. That means of course, only contributions arising from material properties will be considered to derive the material equations. Thus the change of the electromagnetic free energy considering only material properties becomes,

$$
\begin{aligned}
d\mathcal{F}_{EM} =\;& dF_{EM} + \int_V \left(\varepsilon_0 \mathbf{E} \cdot d\mathbf{E} + \mu_0 \mathbf{H} \cdot d\mathbf{H} \right) d\tau \\
=\;& -\int_V \left(\mathbf{P} \cdot d\mathbf{E} + \mu_0 \mathbf{M} \cdot d\mathbf{H} \right) d\tau
\end{aligned}
\tag{2.18}
$$

The material equations for a magnetoelectric media are derived by expanding Eq. (2.18) into a Taylor series with respect to $\mathbf{E}$ and $\mathbf{H}$. Using Einstein summation convention and considering only linear terms, the free energy, $\mathcal{F}_{EM}$, is given by,

$$
\begin{aligned}
\mathcal{F}_{EM}(\mathbf{E}, \mathbf{H}) =\;& \mathcal{F}_0 + \int_V \left(\left. \frac{\partial \mathcal{F}_{EM}}{\partial H_i} \right|_{H_i=0} H_i + \frac{1}{2} \left. \frac{\partial^2 \mathcal{F}_{EM}}{\partial H_j \partial H_i} \right|_{H_i=H_j=0} H_i H_j \right) d\tau \\
& + \int_V \left(\left. \frac{\partial \mathcal{F}_{EM}}{\partial E_i} \right|_{E_i=0} E_i + \frac{1}{2} \left. \frac{\partial^2 \mathcal{F}_{EM}}{\partial E_j \partial E_i} \right|_{E_i=E_j=0} E_i E_j \right) d\tau \\
& + \frac{1}{2} \int_V \left(\left. \frac{\partial^2 \mathcal{F}_{EM}}{\partial E_j \partial H_i} \right|_{E_j=H_i=0} H_i E_j + \left. \frac{\partial^2 \mathcal{F}_{EM}}{\partial H_j \partial E_i} \right|_{H_j=E_i=0} E_i H_j \right) d\tau
\end{aligned}
\tag{2.19}
$$

The last term in Eq. (2.19) becomes,

$$\frac{1}{2} \int_V \left(\left. \frac{\partial (\mu_0 M_i)}{\partial E_j} \right|_{E_j=H_i=0} H_i E_j + \left. \frac{\partial P_i}{\partial H_j} \right|_{H_j=E_i=0} E_i H_j \right) d\tau \tag{2.20}$$

With the classic linear material equations for the electric polarization and magnetization, $\frac{dM_i^S}{dH_j} = \chi_{ij}^M$, $\frac{dP_i^S}{dE_j} = \varepsilon_0 \chi_{ij}^E$, where $-M_i^S = \left. \frac{\partial \mathcal{F}_{EM}}{\partial H_i} \right|_{H_i=0}$ and $-P_i^S = \left. \frac{\partial \mathcal{F}_{EM}}{\partial E_i} \right|_{E_i=0}$, and the definition of the linear magnetoelectric susceptibilities, $\frac{\partial M_i}{\partial E_j} = \alpha_{ij}$, $\frac{\partial P_i}{\partial H_j} = \mu_0 \beta_{ij}$, Eq. (2.19) becomes,

$$\mathcal{F}_{EM}\left(\mathbf{E},\mathbf{H}\right) = \mathcal{F}_0 - \int_V \left(\mu_0 M_i^S H_i + \frac{1}{2}\mu_0\chi_{ij}^M H_i H_j \right) \mathrm{d}\tau$$
$$- \int_V \left(P_i^S E_i + \frac{1}{2}\varepsilon_0\chi_{ij}^E E_i E_j \right) \mathrm{d}\tau \qquad (2.21)$$
$$- \frac{1}{2}\int_V \left(\mu_0\alpha_{ij}H_i E_j + \mu_0\beta_{ij}E_i H_j \right) \mathrm{d}\tau$$

Where $\mathcal{F}_0$ represents all field independent contribution to the free energy, and χ_{ij}^E and χ_{ij}^M are the electric and magnetic susceptibilities respectively. The magnetoelectric susceptibilities, α_{ij} and β_{ij} correspond to the induction of polarization by a magnetic field respectively, to the induction of magnetization by an electric field.

With the definition of the electrical polarization and magnetization, Eq. (2.18),

$$\int_V P_i \mathrm{d}\tau = -\frac{\partial \mathcal{F}_{EM}}{\partial E_i} \qquad \int_V M_i \mathrm{d}\tau = -\frac{1}{\mu_0}\frac{\partial \mathcal{F}_{EM}}{\partial H_i} \qquad (2.22)$$

the material equations for a magnetoelectric media are given by,

$$\int_V P_i \mathrm{d}\tau = -\frac{\partial}{\partial E_i}\int_V \left(-P_l^S E_l - \frac{1}{2}\varepsilon_0\chi_{lm}^E E_l E_m - \frac{1}{2}\mu_0\alpha_{lm}H_l E_m - \frac{1}{2}\mu_0\beta_{lm}E_l H_m \right) \mathrm{d}\tau$$
$$= \int_V \left(P_l^S \delta_{li} + \frac{1}{2}\varepsilon_0\delta_{li}\left(\chi_{lm}^E + \chi_{ml}^E\right)E_m + \frac{1}{2}\mu_0\alpha_{lm}H_l\delta_{mi} + \frac{1}{2}\mu_0\beta_{lm}H_m\delta_{li} \right) \mathrm{d}\tau$$
$$= \int_V \left(P_i^S + \frac{1}{2}\varepsilon_0\left(\chi_{ij}^E + \chi_{ji}^E\right)E_j + \frac{1}{2}\mu_0\left(\alpha_{ji} + \beta_{ij}\right)H_j \right) \mathrm{d}\tau$$

$$(2.23)$$

$$\int_V M_i \mathrm{d}\tau = -\frac{1}{\mu_0}\frac{\partial}{\partial H_i}\int_V \mu_0\left(-M_l^S H_l - \frac{1}{2}\chi_{lm}^M H_l H_m - \frac{1}{2}\alpha_{lm}H_l E_m - \frac{1}{2}\beta_{lm}E_l H_m \right) \mathrm{d}\tau$$
$$= \int_V \left(M_l^S \delta_{li} + \frac{1}{2}\delta_{li}\left(\chi_{lm}^M + \chi_{ml}^M\right)H_m + \frac{1}{2}\alpha_{lm}E_m\delta_{li} + \frac{1}{2}\beta_{lm}E_l\delta_{mi} \right) \mathrm{d}\tau$$
$$= \int_V \left(M_i^S + \frac{1}{2}\left(\chi_{ij}^M + \chi_{ji}^M\right)H_j + \frac{1}{2}\left(\alpha_{ij} + \beta_{ji}\right)E_j \right) \mathrm{d}\tau$$

$$(2.24)$$

with,

$$\delta_{ij} = \begin{cases} 1 & i = j \\ 0 & i \neq j \end{cases} \qquad (2.25)$$

where P_i^S and M_i^S denote the spontaneous polarization and magnetization respectively. For isotropic material the electric polarization is always parallel to the electric field ($\mathbf{P}\|\mathbf{E}$)

as well as the magnetization is always parallel to the magnetic field $(\mathbf{M}||\mathbf{H})$. Therefore, $\chi_{ij}^E = \chi_{ji}^E$, $\chi_{ij}^M = \chi_{ji}^M$, $\alpha_{ij} = \alpha_{ji}$, $\beta_{ij} = \beta_{ji}$. The free energy in Eq. (2.21) is twice differentiable anywhere with respect to the fields. Hence, Young's theorem holds and $\alpha_{ij} = \beta_{ij}$. Consequently, the induction of polarization by a magnetic field and the induction of magnetization by an electric field is symmetric. The final material equations become,

$$
\begin{aligned}
P_i &= P_i^S + \varepsilon_0 \chi_{ij}^E E_j + \mu_0 \gamma_{ij} H_j + \dots \\
M_i &= M_i^S + \chi_{ij}^M H_j + \gamma_{ij} E_j + \dots
\end{aligned}
\tag{2.26}
$$

where γ_{ij} is the linear magnetoelectric susceptibility.

2.1.2   Upper bound of the linear magnetoelectric susceptibility

From thermodynamic considerations a fundamental property of the linear magnetoelectric susceptibility can be obtained which is given by an upper bound of attainable values. Although the assumption of an anisotropic behaviour of the media leads to a more accurate and complete relation for this boundary, an isotropic media is assumed to simplify the considerations. This simplification transfers tensor properties to scalar properties but it does not change the characteristic of that boundary.

With $\chi^E = \left(\frac{\varepsilon}{\varepsilon_0} - 1 \right)$, Eq. (2.18) and Eq. (2.21), the electromagnetic free energy including the free space contribution becomes with negligible static electric and magnetic polarization, $P^S = M^S = 0$,

$$
\begin{aligned}
F_{EM} &= \mathcal{F}_{EM} - \int_V \left(\frac{1}{2}\varepsilon_0 E^2 + \frac{1}{2}\mu_0 H^2 \right) \mathrm{d}\tau \\
&= -\int_V \left(\frac{1}{2}\varepsilon E^2 + \frac{1}{2}\mu H^2 + \gamma H E \right) \mathrm{d}\tau
\end{aligned}
\tag{2.27}
$$

In equilibrium the electromagnetic free energy extremizes. Thus the Hessians given by,

$$
\mathrm{H}_1 = \begin{pmatrix} \frac{\partial^2 F_{EM}}{\partial E^2} & \frac{\partial^2 F_{EM}}{\partial E \partial H} \\ \frac{\partial^2 F_{EM}}{\partial H \partial E} & \frac{\partial^2 F_{EM}}{\partial H^2} \end{pmatrix} = \begin{pmatrix} -\varepsilon & -\gamma \\ -\gamma & -\mu \end{pmatrix}
\tag{2.28}
$$

$$
\mathrm{H}_2 = \begin{pmatrix} \frac{\partial^2 F_{EM}}{\partial H^2} & \frac{\partial^2 F_{EM}}{\partial E \partial H} \\ \frac{\partial^2 F_{EM}}{\partial H \partial E} & \frac{\partial^2 F_{EM}}{\partial E^2} \end{pmatrix} = \begin{pmatrix} -\mu & -\gamma \\ -\gamma & -\varepsilon \end{pmatrix}
\tag{2.29}
$$

of the electromagnetic free energy must be positive or negative definite. In case that H_1 and H_2 are positive definite, hence the electromagnetic free energy minimizes, the principal minors of the Hessian,

$$
\det (H_k) > 0 \quad \forall k \quad H_k = \begin{pmatrix} h_{11} & \cdots & h_{1k} \\ \vdots & \ddots & \vdots \\ h_{k1} & \cdots & h_{kk} \end{pmatrix}
\tag{2.30}
$$

must be positive. Hence,

$$-\varepsilon > 0 \tag{2.31}$$

$$\varepsilon\mu - \gamma^2 > 0 \tag{2.32}$$

$$-\mu > 0 \tag{2.33}$$

If the electromagnetic free energy maximizes, the Hessians are negative definite and the odd and even principal minors of the Hessian are negative and positive. Thus,

$$(-1)^k \det\left(H_k\right) > 0 \quad \forall k \tag{2.34}$$

Hence,

$$\varepsilon > 0 \tag{2.35}$$

$$\varepsilon\mu - \gamma^2 > 0 \tag{2.36}$$

$$\mu > 0 \tag{2.37}$$

Equation (2.31) and (2.33) implicate a negative permittivity and permeability. Therefore, for materials with negative refraction (e.g. metamaterials) the electromagnetic free energy minimizes. For conventional materials (positive refraction) the electromagnetic free energy maximizes.

A fundamental relation for magnetoelectric media is given by Eq. (2.32) and (2.36) which limits the magnetoelectric susceptibility,

$$\gamma < \sqrt{\varepsilon\mu} \tag{2.38}$$

For an anisotropic medium the theoretical limit to the linear magnetoelectric coupling is governed by the appropriate diagonal elements of the permittivity and the permeability, [1],

$$\gamma_{ij} < \sqrt{\varepsilon_{ii}\mu_{jj}} \tag{2.39}$$

In fact, assuming free localized magnetic moments in the medium, the diamagnetic contribution to the magnetic susceptibility can be neglected, a more rigorous constraint for the linear magnetoelectric susceptibility can be obtained [42]

$$\gamma_{ij} < \sqrt{\chi_{ii}^E \chi_{jj}^M} \tag{2.40}$$

Therefore, to obtain large linear magnetoelectric effect, systems with large permittivity and large permeability are required. Hence for materials being ferroelectric and ferromagnetic simultaneously (materials showing a ferroelectric, ferromagnetic or multiferroic phase transition), a large linear magnetoelectric coupling might be expected.

Examples of large linear magnetoelectric coupling are $R\mathrm{Fe}_3\left(\mathrm{BO}_3\right)_4$, $R\mathrm{Al}_3\left(\mathrm{BO}_3\right)_4$ with $R = Sm, Ho$ [18, 43, 44]. They posess colossal magnetic-field-induced changes in the dielec-

tric constant [45, 46] caused by a large electromagnon in the gigahertz frequency range [47].

2.2   Symmetry considerations of linear magnetoelectric coupling and the magnetodielectric effect

The absence or presence of the linear magnetoelectric effect is on an phenomenological level a symmetry property of the system and hence can be solely determined by symmetry arguments regarding the invariance of time and space inversion of the free energy of the system.

The electromagnetic free energy given by Eq. (2.18) is rather inconvenient for symmetry analysis since its natural variables are E and H. Usually, for phase transition studies the free energy of the system is expanded into a power series of P and M. Accordingly, the free energy of choice is obtained by a Legrende-Transformation of Eq. (2.18) and becomes,

$$
\begin{aligned}
\mathcal{F}_{EM}\left(\mathbf{P},\mathbf{M}\right) = \ & \mathcal{F}_{EM}\left(\mathbf{E},\mathbf{H}\right) - \frac{\partial \mathcal{F}_{EM}\left(\mathbf{E},\mathbf{H}\right)}{\partial \mathbf{E}}\mathbf{E} - \frac{\partial \mathcal{F}_{\mathbf{EM}}\left(\mathbf{E},\mathbf{H}\right)}{\partial \mathbf{H}}\mathbf{H} \\
= \ & \mathcal{F}_{EM}\left(\mathbf{E},\mathbf{H}\right) + \int_{V}\left(\mathbf{P}\cdot\mathbf{E} + \mu_0\mathbf{M}\cdot\mathbf{H}\right)\mathrm{d}\tau
\end{aligned}
\tag{2.41}
$$

Thus,

$$
\begin{aligned}
\mathrm{d}\mathcal{F}_{EM}\left(\mathbf{P},\mathbf{M}\right) = \ & \mathrm{d}\mathcal{F}_{EM}\left(\mathbf{E},\mathbf{H}\right) + \int_{V}\left(\mathbf{E}\cdot\mathrm{d}\mathbf{P} + \mathbf{P}\cdot\mathrm{d}\mathbf{E} + \mu_0\mathbf{H}\cdot\mathrm{d}\mathbf{M} + \mu_0\mathbf{M}\cdot\mathrm{d}\mathbf{H}\right)\mathrm{d}\tau \\
= \ & -\int_{V}\left(\mathbf{P}\cdot\mathrm{d}\mathbf{E} + \mu_0\mathbf{M}\cdot\mathrm{d}\mathbf{H}\right)\mathrm{d}\tau \\
& + \int_{V}\left(\mathbf{E}\cdot\mathrm{d}\mathbf{P} + \mathbf{P}\cdot\mathrm{d}\mathbf{E} + \mu_0\mathbf{H}\cdot\mathrm{d}\mathbf{M} + \mu_0\mathbf{M}\cdot\mathrm{d}\mathbf{H}\right)\mathrm{d}\tau \\
= \ & \int_{V}\left(\mathbf{E}\cdot\mathrm{d}\mathbf{P} + \mu_0\mathbf{H}\cdot\mathrm{d}\mathbf{M}\right)\mathrm{d}\tau
\end{aligned}
\tag{2.42}
$$

Expanding Eq. (2.42) into a Taylor series with respect to $\mathbf{P}$ and $\mathbf{M}$ and assuming isotropic behaviour, the free energy, $\mathcal{F}_{EM}(P, M)$, is given by,

For linear magnetoelectric media, the lowest term in the the free energy depends on the bi-linear term, $F \propto -\gamma EH$, (Eq. 2.27). Assuming scalar properties and negligible static polarization and magnetization the material equations are given by,

$$
\begin{aligned}
\mathcal{F}_{EM}\left(P,M\right) = \ & \mathcal{F}_0 + \int_{V}\left(\frac{\partial \mathcal{F}_{EM}}{\partial M}M + \frac{\partial^2 \mathcal{F}_{EM}}{\partial^2 M}M^2 + \dots\right)\mathrm{d}\tau \\
& + \int_{V}\left(\frac{\partial \mathcal{F}_{EM}}{\partial P}P + \frac{\partial^2 \mathcal{F}_{EM}}{\partial^2 P}P^2 + \dots\right)\mathrm{d}\tau \\
& + \frac{1}{2}\int_{V}\left(\frac{\partial^2 \mathcal{F}_{EM}}{\partial P\partial M}PM + \frac{\partial^2 \mathcal{F}_{EM}}{\partial M\partial P}MP + \dots\right)\mathrm{d}\tau
\end{aligned}
\tag{2.43}
$$

With Eq. (2.42) follows,

$$
\begin{aligned}
\mathcal{F}_{EM}\left(P, M\right) = \quad & \mathcal{F}_0 + \int\limits_V \left(\mu_0 H M + \mu_0 \frac{dH}{dM} M^2 + \dots\right) d\tau \\
& + \int\limits_V \left(EP + \frac{dE}{dP} P^2 + \dots\right) d\tau \\
& + \frac{1}{2} \int\limits_V \left(\frac{\partial}{\partial P}\left(\mu_0 H\right) PM + \frac{\partial E}{\partial M} MP + \dots\right) d\tau
\end{aligned}
\tag{2.44}
$$

From Eq. (2.26) follows with negligible static electric polarization and magnetization,

$$
\begin{aligned}
P = \quad & \varepsilon_0 \chi_E E + \mu_0 \gamma H \\
M = \quad & \chi_M H + \gamma E
\end{aligned}
\tag{2.45}
$$

Thus,

$$
\begin{aligned}
E = \quad & \frac{\chi_M P - \mu_0 \gamma M}{\varepsilon_0 \chi_E \chi_M - \mu_0 \gamma^2} \\
H = \quad & \frac{\varepsilon_0 \chi_E M - \gamma P}{\varepsilon_0 \chi_E \chi_M - \mu_0 \gamma^2}
\end{aligned}
\tag{2.46}
$$

Hence,

$$
\begin{aligned}
\frac{\partial H}{\partial P} &= \frac{-\gamma}{\varepsilon_0 \chi_E \chi_M - \mu_0 \gamma^2} & \frac{\partial E}{\partial M} &= \frac{-\mu_0 \gamma}{\varepsilon_0 \chi_E \chi_M - \mu_0 \gamma^2} \\
\frac{\partial H}{\partial M} &= \frac{\varepsilon_0 \chi_E}{\varepsilon_0 \chi_E \chi_M - \mu_0 \gamma^2} & \frac{\partial E}{\partial P} &= \frac{\chi_M}{\varepsilon_0 \chi_E \chi_M - \mu_0 \gamma^2}
\end{aligned}
\tag{2.47}
$$

Consequently, Eq. (2.44) becomes with Eq. (2.47),

$$
\begin{aligned}
\mathcal{F}_{EM}\left(P, M\right) = \quad & \mathcal{F}_0 + \int\limits_V \left(\mu_0 H M + \frac{\mu_0 \varepsilon_0 \chi_E}{\varepsilon_0 \chi_E \chi_M - \mu_0 \gamma^2} M^2 + \dots\right) d\tau \\
& + \int\limits_V \left(EP + \frac{\chi_M}{\varepsilon_0 \chi_E \chi_M - \mu_0 \gamma^2} P^2 + \dots\right) d\tau \\
& + \int\limits_V \left(\frac{-\mu_0 \gamma}{\varepsilon_0 \chi_E \chi_M - \mu_0 \gamma^2} PM + \dots\right) d\tau
\end{aligned}
\tag{2.48}
$$

Thus the magnetoelectric free energy considering only the lowest order coupling between P and M is given by,

$$
F_{ME} = - \int d\tau_V \frac{\mu_0 \gamma}{\varepsilon_0 \chi_E \chi_M - \mu_0 \gamma^2} PM
\tag{2.49}
$$

For simplicity, it is assumed that $\gamma^2 \ll \chi^E \chi^M$. Accordingly, Eq. (2.49) becomes,

$$
F_{ME} = - \int d\tau_V \frac{\mu_0}{\varepsilon_0 \chi_E \chi_M} \gamma PM
\tag{2.50}
$$

Due to the definition of the electric dipole moment, $\mathbf{d} = q\mathbf{r}$, and magnetic moment, $\boldsymbol{\mu} = qv\mathbf{A}$, where q is the charge, v is the velocity, $\mathbf{r}$ is the distance between the positive and negative charge and $\mathbf{A}$ is the enclosed area of the moving charge and by the conservation of charge during space and time inversion, the elementary electric dipole reverses, $\mathbf{d}(-\mathbf{r}) \rightarrow -\mathbf{d}(\mathbf{r})$ under space inversion while the space inversion does not change the direction of currents, thus $\boldsymbol{\mu}(-\mathbf{r}) \rightarrow \boldsymbol{\mu}(\mathbf{r})$. On the contrary, time inversion will reverse the sign of the magnetic moment, $\boldsymbol{\mu}(-t) \rightarrow -\boldsymbol{\mu}(t)$, while the sign of the electric dipole remains unaffected, $\mathbf{d}(-t) \rightarrow \mathbf{d}(t)$. The given arguments are summarized in Fig. (2.1).
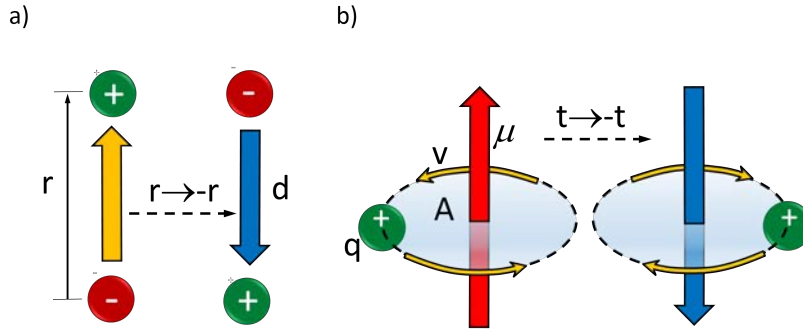
Figure 2.1: *Space and time inversion symmetries of elementary magnetic and electric dipoles.* **a**) An electric dipole changes sign under space inversion but is not affected by time inversion. **b**) A magnetic dipole is generated by a circular current. By applying time inversion the sense of rotation of the charge reverses and thus in turn the magnetic dipole reverses too.

According to the arguments above, the ferroelectric chain breaks the space inversion symmetry, i.e. the macroscopic electric polarization changes sign under space inversion, but keeps the time inversion symmetry, $\mathbf{P}(-\mathbf{r}, t) = -\mathbf{P}(\mathbf{r}, t)$, $\mathbf{P}(-t, \mathbf{r}) = \mathbf{P}(t, \mathbf{r})$ (Fig. 2.2).

Vice versa, the ferromagnetic chain breaks time inversion symmetry but keeps space inversion symmetry, $\mathbf{M}(-\mathbf{r}, t) = \mathbf{M}(\mathbf{r}, t)$, $\mathbf{M}(-t, \mathbf{r}) = -\mathbf{M}(t, \mathbf{r})$. For an antiferromagnetic chain the order parameter is given by the staggered magnetization which is defined as, $\mathbf{L} = \frac{1}{2}(\mathbf{M}_A - \mathbf{M}_B)$, where $\mathbf{M}_A$ and $\mathbf{M}_B$ is the magnetization of the both sublattices. Just like the ferromagnetic chain it keeps space inversion symmetry but breaks time inversion symmetry, $\mathbf{L}(-\mathbf{r}, t) = \mathbf{L}(\mathbf{r}, t)$, $\mathbf{L}(-t, \mathbf{r}) = -\mathbf{L}(t, \mathbf{r})$.

According to Eq. (2.50) the magnetoelectric contribution to the free energy is, $F_{ME} \propto -\gamma PM$. It is evident, that the magnetoelectric free energy changes sign under space and time inversion, $F(-\mathbf{r}, t) = -F(\mathbf{r}, t)$ and $F(\mathbf{r}, -t) = -F(\mathbf{r}, t)$. The Neumann's principle states that if a crystal is invariant with respect to certain symmetry operations, any of its physical properties must also be invariant with respect to the same symmetry operations, or otherwise stated, the symmetry operations of any physical property of a crystal must include the symmetry operations of the point group of the crystal [48] . Accordingly, the symmetry operations of the free energy is inevitably connected to the symmetry operations of the crystal. Consequently, the crystal must break both symmetries in order to allow for the linear magnetoelectric effect. Since magnetic order always breaks the time inversion
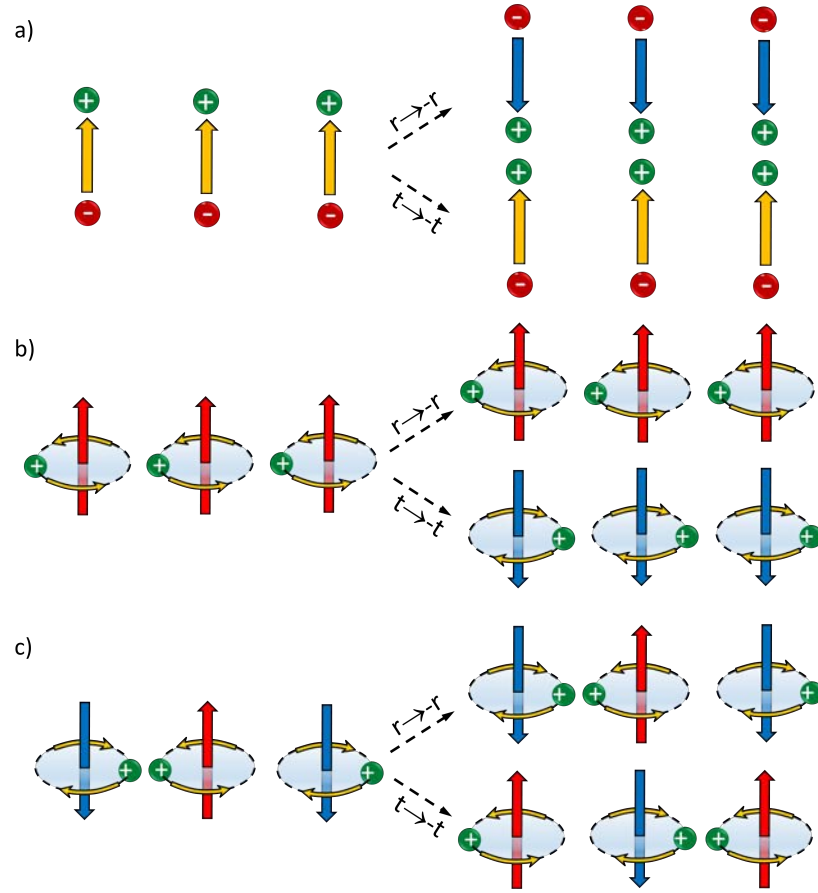
Figure 2.2: *Space and time inversion symmetry for a chain of elementary magnetic and electric dipoles.* **a**) A ferroelectric chain of elementary electric dipoles breaks only space inversion symmetry **b**) A ferromagnetic chain of elementary magnetic dipoles breaks only time inversion symmetry. **c**) An antiferromagnetic chain of elementary magnetic dipoles behaves in exactly the same way as a ferromagnetic chain.

symmetry the crystal must belong to a space group where the space inversion symmetry is broken. For a centro-symmetric crystal structure, the space inversion symmetry is not broken and thus in turn the magnetic order must break the space inversion as well as the time inversion symmetry for allowing the linear magnetoelectric effect. Hence, the linear magnetoelectric coupling is not allowed in ferromagnets and most antiferromagnets with a centro-symmetric crystal structure since the magnitization in these systems is invariant under space inversion. Additionally, if the crystal is centro-symmetric in the disordered state (unpolarized state), space inversion is always fulfilled and odd powers of P are not allowed. Furthermore, the paramagnetic phase is time-reversal invariant [49]. Thus odd powers of M are not allowed in the non-ordered state. Hence, the bilinear coupling of P with M is not allowed in the free energy expansion above the transition temperature. Therefore, $\gamma = 0$ for $T > T_C$. Consequently, for simplicity it is assumed that the linear magnetoelectric susceptibility behaves as $\gamma \rightarrow \gamma \Theta \left(T_C - T \right)$ where $\Theta \left(T_C - T \right)$ is the heaviside step function.

Nota bene, nonlinear magnetoelectric contributions like $\kappa P M^2$ or $\zeta P^2 M^2$ which is gen-

erally allowed by symmetry, may still be presents, but they are typically rather weak [50, 51]. These higher order couplings between electric polarization and magnetization are summarized under the term "*magnetodielectric effect*" whereas the term "*magnetoelectric effect*" should be reserved for special symmetries where a free energy invariant proportional to, $F \propto \gamma PM$, is allowed [52].

The terminology "*magnetodielectric effect*" is used for systems that are not known to be linear magnetoelectrics by symmetry but though display a change in the dielectric constant at magnetic ordering temperatures, or show finite magnetocapacitance such as $EuTiO_3$[51], $TmFeO_3$[53], MnF_2[54], MnO[55], Mn_3O_4[56], $Tb_3Fe_5O_{12}$[57], $Dy_2Ti_2O_7$[58], $Tb_2Ti_2O_7$ [59], and $ZnFe_2O_4$[60]. Of course, the fulfilment of the symmetry requirements alone does not guarantee the existence of the linear magnetoelectric effect in magnetoelectrics, but the converse is always true that is, that the existence of the linear magnetoelectric effect requires broken space and time inversion symmetry of the crystal. For centro-symmetric crystals structures, the linear magnetoelectric effect requires the existence of broken space inversion symmetry in the magnetic point group (nota bene: the linear magnetoelectric effect can only occur in magnetic point groups since it vanishes for all symmetry groups containing time reversal symmetry [61]).

CHAPTER 3

Spin-Lattice coupling: Ferroelectricity induced by magnetic order

3.1 Spin frustration as an origin of linear magnetic ferroelectrics

As seen in Sec.(2.2) the linear magnetoelectric effect is only allowed in centro-symmetric systems in which the magnetic structure breaks the spatial inversion symmetry. Consequently, spatial variation of the magnetization must exist in the system.

This is where spin frustration comes into play. In some lattices it is not possible to satisfy all exchange interactions and energy can not be minimized (Fig. 3.1). On the square lattice it
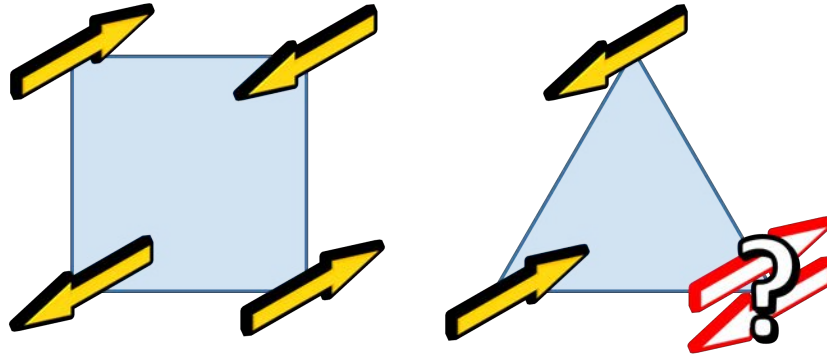
Figure 3.1: *Geometrically frustration of spins.* On a rectangular lattice an anti-ferromagnetic order of the spins does not lead to spin frustration whereas on a triangular lattice neighbouring spins are frustrated for an antiferromagnetic exchange interaction.

is possible to satisfy the requirement of antiparallel ordering. However, on a triangular lattice things are not so straightforward. If two neighbouring spins are placed antiparallel, the third spin is faced with a dilemma. In any case the one of two neighbours will not have their energy minimized.

As a result the system is frustrated and tends to release this frustration by forming unusual magnetic order where magnetization is inhomogeneous in space. This order is developed usually at very low temperatures and entails simultaneously the onset of electric polarization.

Such magnetoelectric materials belong to the class of Type-II or joint-order-parameter multiferroics. In this class of materials, ferroelectricity is directly caused by magnetic order

whereas in Type-I or split-order-parameter multiferroics magnetic and electric order are not inherently related to each other (Fig. 3.2)
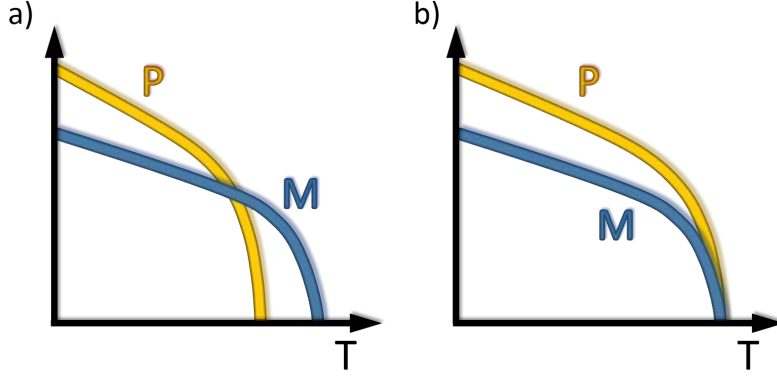
Figure 3.2: *Type-I and Type-II Multiferroics.* (**a**) Magnetic and electric order are not directly related to each other in Type-I magnetoelectric multiferroics. They set in at different temperatures and do not allow the linear magnetoelectric coupling. Hence, both orders are usually weak coupled. (**b**) Magnetic and electric order have a common cause in Type-II magnetoelectric multiferroics. Thus they appear simultaneously and allow the linear magnetoelectric effect. Therefore they exhibit a strong magnetoelectric coupling.

3.2   Ferroelectricity in cycloidal magnets

As mentioned in the previous section, competing interactions between spins would lead to highly frustrated magnetic structures and in order to "release" this frustration, specific kind of magnetic order is developed in frustrated magnets.

For example, the one-dimensional Heisenberg spin chain given by,

$$H = -J_1 \sum_i \mathbf{S}_i \cdot \mathbf{S}_{i+1} \tag{3.1}$$

with a ferromagnetic interaction $J_1 > 0$ between neighbouring spins has a uniform ground state with all spins parallel. An additional antiferromagnetic next-nearest-neighbour interaction $J_2 < 0$,

$$H = -J_1 \sum_i \mathbf{S}_i \cdot \mathbf{S}_{i+1} - J_2 \sum_i \mathbf{S}_i \cdot \mathbf{S}_{i+2} \tag{3.2}$$

frustrates this simple ordering, and when sufficiently strong, $|J_2| > \frac{J_1}{4}$[4], it stabilizes a cycloidal magnetic state (Fig. 3.3). This can be seen as follows: The energy of the system only depends on the relative angle between neighbouring moments and in the ordered ground state the Hamiltonian per site in Eq. (3.2) can be written as,

$$H_i \propto -J_1 \cos\left(\varphi_{i,i+1}\right) - J_2 \cos\left(2\varphi_{i,i+1}\right) \tag{3.3}$$

The ground state is given by $\frac{\partial H_i}{\partial \varphi_{i,i+1}} = 0$, thus[1]

$$J_1 \sin\left(\varphi_{i,i+1}\right)\left[1 + \frac{4J_2}{J_1}\cos\left(\varphi_{i,i+1}\right)\right] = 0 \Rightarrow \cos\left(\varphi_{i,i+1}\right) = -\frac{J_1}{4J_2} \tag{3.4}$$

In order to obtain a solution, $\frac{J_1}{4J_2} \leq 1$.
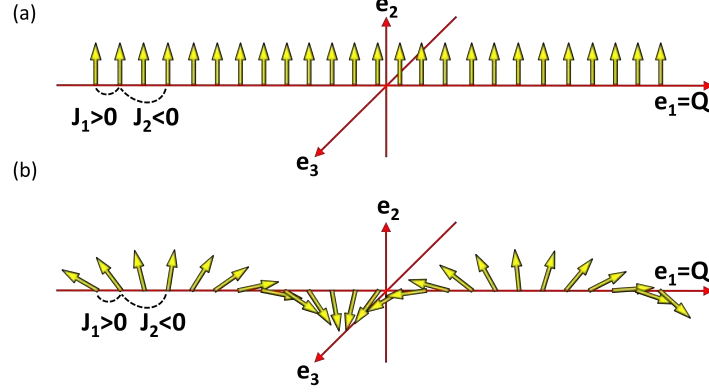
Figure 3.3: *Frustrated Heisenberg spin chain.* (**a**) Ferromagnetic nearest neighbour and antiferromagnetic next nearest neighbour interaction frustrates the Heisenberg spin chain. (**b**) The system tends to minimize the energy and thus develops a cycloidal spin structure.

Like any other antiferromagnetic order, the cycloidal magnetic structure breaks time reversal symmetry. In addition it breaks space inversion symmetry, because the change of the sign of all coordinates inverts the direction of the rotation of spins, clockwise (CW) respectively counter-clockwise (CCW), in the cycloid and thus the cycloidal structure is a chiral object, i.e. the CW cycloid cannot be mapped to its inverted (mirror) image by rotations and translations (Fig. 3.4). Hence, the symmetry of the cycloidal state allows for a linear magnetoelectric coupling.

In general, such magnetic structure can be described for CW and CCW cycloidal order by,

$$\mathbf{M_n} = M \begin{cases} \mathbf{e}_1 \cos\left(-\mathbf{Qx_n}\right) + \mathbf{e}_2 \sin\left(-\mathbf{Qx_n}\right) & \text{CW} \\ \mathbf{e}_1 \cos\left(\mathbf{Qx_n}\right) + \mathbf{e}_2 \sin\left(\mathbf{Qx_n}\right) & \text{CCW} \end{cases} \tag{3.5}$$

where $\mathbf{e}_1$ and $\mathbf{e}_2$ are versors of the corresponding euclidean space, $\mathbf{x}_n$ is the coordinate vector of the spins, M is the absolute value of the magnetic moment and $\mathbf{Q}$ is the wave vector of the cycloid. The period of the spin-cycloid depends on strengths of competing interactions and is often incommensurate (out of proportion) with the period of the crystal lattice. With $\mathbf{x}_n = na$ and $Q = \frac{2\pi}{ma}$ where a is the distance between two neighbouring spins, n is a integer number defining the site of the spin, and m is a multiple of the distance between two

---

[1]$\sin\left(2\varphi\right) = 2\sin\varphi\cos\varphi$
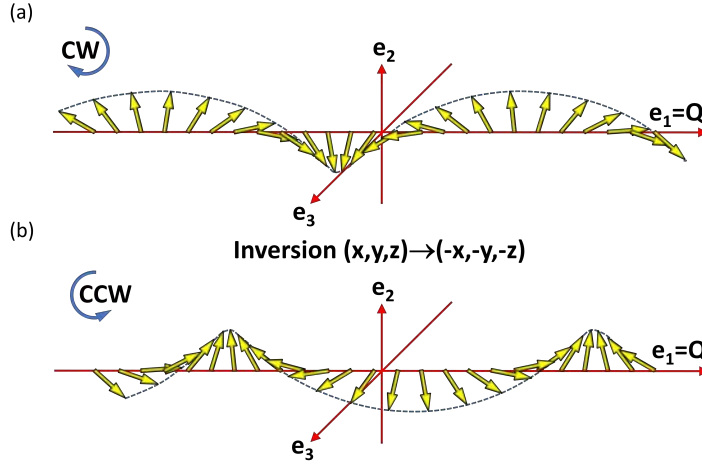
Figure 3.4: *Broken space inversion symmetry of cycloidal magnetic structure.* (**a**) Clockwise (CW) rotation of the spins. (**b**) Space inversion leads to a counter-clockwise rotation (CCW) of the spins and thus to a broken space inversion symmetry.

neighbouring spins defining the wave length[2] as $\lambda = ma$. Thus the product $\mathbf{Q}\mathbf{x}_n$ in Eq. (3.5) is, $\mathbf{Q}\mathbf{x}_n = qn$ with $q = \frac{2\pi}{m}$. The parameter m is given by, $m = \frac{2\pi}{\varphi_{i,i+1}}$, thus $\varphi_{i,i+1} = q$. Consequently, for the wave vector follows according to Eq. (3.4),

$$\cos(q) = -\frac{J_1}{4J_2} \tag{3.6}$$

From a phenomenological point of view, the inhomogeneous magnetic structure given by a cycloidal distribution of spins can induce electric polarization via a Lifshitz term, $(\mathbf{M} \cdot \nabla)\mathbf{M} - \mathbf{M}(\nabla \cdot \mathbf{M})$, in the free energy [62] . Mostovoy [63] proposed a free energy term which describes the linear coupling between electric polarization and non-uniform distribution of magnetization in a cubic environment as,

$$F_P = \frac{\mathbf{P}^2}{2\chi^E} + \lambda\mathbf{P}\left[\mathbf{M}(\nabla \cdot \mathbf{M}) - (\mathbf{M} \cdot \nabla)\mathbf{M}\right] \tag{3.7}$$

with $\mathbf{M}(\nabla \cdot \mathbf{M}) = M_i\partial_j M_j$ and $(\mathbf{M} \cdot \nabla)\mathbf{M} = M_j\partial_j M_i$. The induced electric polarization is found by $\frac{\partial F_P}{\partial \mathbf{P}} = 0$, which is,

$$\mathbf{P} = \chi^E\lambda\left[(\mathbf{M} \cdot \nabla)\mathbf{M} - \mathbf{M}(\nabla \cdot \mathbf{M})\right] \tag{3.8}$$

Substituting Eq. (3.5) into Eq. (3.8) the cycloidal spin distribution gives rise to electric polarization by (Appendix A.1),

---

[2]Nota bene, by describing phonons the smallest wave length is equal to $\lambda = m \cdot 2a$ with $m = 1$. Thus, the wave vector is $Q = \frac{2\pi}{m \cdot 2a} = \frac{\pi}{ma}$. For describing magnetic structures the smallest wave length is equal to $\lambda = m \cdot a$ with $m = 1$. This can be understood by considering a ferromagnetic spin chain. In that case the spins can be described by $M_n = M\cos\left(\frac{2\pi}{a}na\right) = M\cos(2\pi n) = M$

$$\mathbf{P} = \chi^E \lambda M^2 \begin{cases} -(\mathbf{e}_3 \times \mathbf{Q}) & \text{CW} \\ (\mathbf{e}_3 \times \mathbf{Q}) & \text{CCW} \end{cases} \tag{3.9}$$

The versors $\mathbf{e}_1$ and $\mathbf{e}_2$ define the cycloidal plane and $\mathbf{e}_3$ is the spin rotation axis. Thus the induced electric polarization is orthogonal to the propagation vector and lies in the cycloidal plane. Furthermore it is obvious, that the helicity[3] of the cycloidal structure defines the direction of the electric polarization vector.

This specific type of magnetic structure and consequently a ferroelectric behaviour is found in systems like $TbMnO_3$[64], $Ni_3V_2O_8$[65] and $MnWO_4$ [66, 67, 68], in multiferroic pyroxenes [69] and in some other systems.

3.2.1 Microscopic mechanism of electric polarization in cycloidal spin magnets

Microscopically, two possible mechanisms have been proposed to explain the coupling between spin and charge degrees of freedom and thus in turn the appearance of a spontaneous electric polarization induced by a cycloidal magnetic order:

3.2.1.1 Spin-Current mechanism

A spin current is a quantum mechanical effect that arises from virtual hopping of electrons, e.g. across a Mn−O−Mn bond and taking into account the spin of the electrons [70, 71, 72] . In that sense it is the spin-polarized equivalent of double-exchange or superexchange.

In that model, a spin current arises between two neighbouring coupled non-collinear spins, $\mathbf{J}_{i,i+1}^S \propto \mathbf{S}_i \times \mathbf{S}_{i+1}$. A unique feature of a spin current is given by the fact, that in contrast to a charge current, it is time symmetric, $\mathbf{J}_{i,i+1}^S(-t) = +\mathbf{J}_{i,i+1}^S(t)$, since the spin polarization is also reversed together with the direction. Thus, from the symmetry point of view, the spin current belongs to the same class as the electric polarization and hence it is natural to expect the linear coupling between these two.

Indeed, a spontaneous electric polarization is induced that is proportional to the vector product of spin current and the unit vector, $\mathbf{e}_{i,i+1}$, that connect the two neighbouring spins,

$$\mathbf{P}_{i,i+1} \propto \left(\mathbf{e}_{i,i+1} \times \mathbf{J}_{i,i+1}^S\right) \tag{3.10}$$

It is worth mentioning, that since this effect is based on virtual hopping of electrons, the ferroelectric polarization result purely from a shift of electrons [73] and the ions remain fixed.

3.2.1.2 Inverse Dzyaloshinskii-Moriya interaction

A second possible mechanism for the generation of an electric polarization induced by a cycloidal spin structure is based on the Dzyaloshinskii-Moriya (DM) interaction [74, 75, 76, 77].

---

[3]often described as chirality

It describes a relativistic correction to the superexchange which accounts for the spin-orbit coupling.

In non-relativistic quantum mechanics the Heisenberg superexchange interaction is due to the second order virtual hopping of the electrons, and the spin of every electron is conserved during the hopping. However, in relativistic quantum mechanics, the z-component of spin, m_s, is no longer a good quantum number and thus it is not conserved: it may flip once during the second order virtual hopping.

These virtual hopping with one time spin flip will lead to the DM interaction in the same way as non-relativistic hopping lead to the Heisenberg interaction. The DM interaction is a antisymmetric superexchange interaction that appears in addition to the symmetric Heisenberg exchange, $H_{Heis} = -J_{ij} \sum_{ij} \mathbf{S}_i \cdot \mathbf{S}_j$, and is given by,

$$H_{DM} = \sum_{ij} \mathbf{D}_{i,j} \cdot (\mathbf{S}_i \times \mathbf{S}_j) \tag{3.11}$$

Here $\mathbf{D}_{i,j} \propto \lambda \Delta \mathbf{x}_{i,j} \times \mathbf{r}_{i,j}$ is the so-called Dzyaloshinskii-vector, where $\mathbf{r}_{i,j}$ is the unit vector connecting the magnetic ions i and j, $\mathbf{x}_{i,j}$ is the distance between the ligand (mostly oxygen) mediating the superexchange and the line $\mathbf{r}_{i,j}$, and λ is the spin-orbit coupling constant. Since the DM interaction is proportional to the vector product of spins, it favours non-collinear spin ordering with an angle between neighbouring spins given by,

$$\frac{\mathrm{d}H}{\mathrm{d}\varphi} = \frac{\mathrm{d}\left(H_{Heis} + H_{DM}\right)}{\mathrm{d}\varphi} = J_{ij} S_i S_j \sin \varphi_{ij} + \lambda \Delta x_{ij} r_{ij} \sin \beta_{ij} S_i S_j \cos \varphi_{ij} = 0$$

$$\tan \varphi_{ij} = -\frac{\lambda \Delta x_{ij} r_{ij} \overbrace{\sin \beta}^{1}}{J_{ij}} = -\frac{\lambda \Delta x_{ij} r_{ij}}{J_{ij}} \tag{3.12}$$

where φ is the angle between two neighbouring spins and β is the angle between $\Delta \mathbf{x}_{i,j}$ and $\mathbf{r}_{i,j}$. By definition, the vectors $\Delta \mathbf{x}_{i,j}$ and $\mathbf{r}_{i,j}$ are orthogonal thus $\sin \beta = 1$. The spin-spin interaction, determined by J, depends upon the bond angle, α, between the magnetic ions and the ligand according to the Goodenough-Kanamori-Anderson (GKA) rules [78][4]. In turn, the bond angle is determined by the position of the ligand ion (Fig. 3.5). Consequently, the spin-spin interaction depends on Δx_{ij}. Therefore, for a fixed distance between magnetic ions, $r = R$, the angle between neighbouring spins is solely dependent on the position of the ligand ion as,

$$\varphi_{ij}\left(\Delta x_{ij}\right) = \arctan \left[-\lambda R \frac{\Delta x_{ij}}{J_{ij}\left(\Delta x_{ij}\right)} \right] \tag{3.13}$$

For a given bond angle, α, the position of the ligand ion can be $\pm X$. Thus $J_{ij}\left(+X\right) = J_{ij}\left(-X\right)$. Therefore, according to Eq. (3.13) the angle between two neighbouring spins changes sign for opposite ligand positions as, $\varphi_{ij}\left(+X\right) < 0$ and $\varphi_{ij}\left(-X\right) > 0$. This

---

[4]If the bond angle is 180°, an antiferromagnetic alignment is preferred. Thus $J > 0$. In contrast, a bond angle of 90° leads to a ferromagnetic alligment, thus $J < 0$
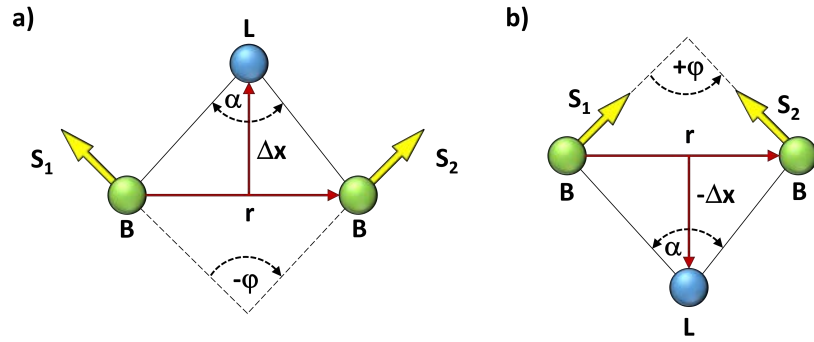
Figure 3.5: *Microscopic mechanism of the Spin-Lattice coupling due to Dzyaloshinskii-Moriya interaction.* The angle, φ, between the neighbouring spins is governed by spin-spin interaction and depends on the bond angle, α, between the magnetic ions (B) and the ligand ion (L). Thus in turn, it depends on the position, Δx, of the ligand ion. (a) If $\Delta x > 0$, the angle between two neighbouring spins is negative thus the spin rotates clockwise. (b) If $\Delta x < 0$, the angle between two neighbouring spins is positive thus the spin rotates counter-clockwise. Charge and spin degrees of freedom are coupled, if the magnetic ions and the ligand ion are oppositely charged.

peculiar behaviour of the angle between neighbouring spins can lead to weak ferromagnetism in canted antiferromagnets, although the DM interaction is rather weak.

This can be explained as follows. A chain of magnetic ions with nearest-neighbour interaction arising from superexchange via intermediate ligand ions and if the ligand ions are distorted from the plane formed by the magnetic ions in a zig-zag pattern, results in an alternating Dzyaloshinskii-vector (Fig. 3.6).
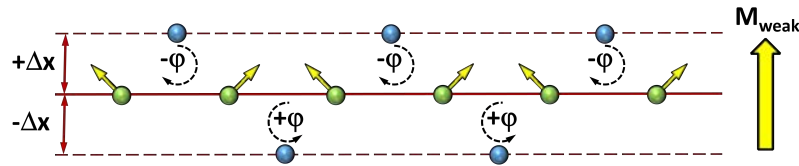
Figure 3.6: *Weak magnetism in canted antiferromagnets.* Alternating Dzyaloshinskii-vector leads to alternating helicity of neighbouring spins and thus to a weak ferromagnetism in canted antiferromagnets.

Consequently, for a alternating Dzyaloshinskii-vector, the helicity (direction of rotation from spin to spin) changes. This behaviour leads to a weak ferromagnetism in canted antiferromagnets, e.g in La_2CuO_4 [79].

Magnetically induced ferroelectricity in cycloidal ordered spins works exactly the other way round. It is therefore also called the inverse Dzyaloshinskii-Moriya interaction (IDM) [74]. That means, that the displacement, Δx, of the ligand ions becomes a function of the angle, φ, between the spins. Therefore, with Eq. (3.4), Eq. (3.12) must be interpreted as,

$$\Delta x_{ij} = \frac{J_{ij}\tan\varphi_{ij}}{\lambda r_{ij}} = \frac{J_1\tan\left[\arccos\left(-\frac{J_1}{4J_2}\right)\right]}{\lambda r_{ij}} \tag{3.14}$$

If a cycloidal order is present, the angle between the spins is equal for each pair of spins. Thus the IDM interaction pushes the ligand ions in one common direction transverse to the chain of magnetic ions. If the magnetic ions are charged, e.g. positive and the ligand ions are charged negative, an electric polarization is induced (Fig. 3.7).
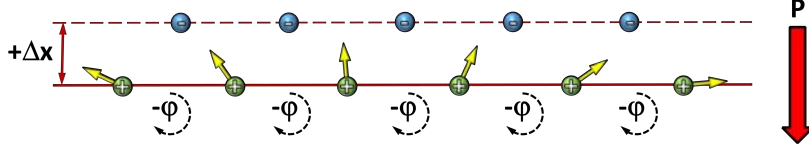
Figure 3.7: *Inverse Dzyaloshinskii-Moriya interaction.* In a cycloidal spin order, the IDM interaction leads to a displacement of the ligand ions (blue) in the same direction due to same helicity between neighbouring spins. If the magnetic (green) and ligand ions are charged oppositely, a macroscopic electric polarization (red arrow) is induced leading to a linear magneto electric effect.

The electric polarization is proportional to the displacement of the ligand ions given by Eq. (3.14). With $\sin\varphi = (S_iS_j)^{-1}(\mathbf{S}_i\times\mathbf{S}_j)$, $\cos\varphi = (S_iS_j)^{-1}\mathbf{S}_i\cdot\mathbf{S}_j$ and $xr\sin\beta = \Delta\mathbf{x}_{\mathrm{i,j}}\times\mathbf{r}_{i,j}$ follows,

$$\Delta\mathbf{x}_{\mathrm{i,j}}\times\mathbf{r}_{i,j} = -\frac{J_{ij}}{\lambda}\frac{\mathbf{S}_i\times\mathbf{S}_j}{\mathbf{S}_i\cdot\mathbf{S}_j} \tag{3.15}$$

Thus, the displacement becomes,

$$
\begin{aligned}
-\frac{J_{ij}}{\lambda\mathbf{S}_i\cdot\mathbf{S}_j}\mathbf{e}_{\mathbf{r}i,j}\times(\mathbf{S}_i\times\mathbf{S}_j) =\ & \mathbf{e}_{\mathbf{r}i,j}\times(\Delta\mathbf{x}_{\mathrm{i,j}}\times\mathbf{r}_{i,j}) \\
=\ & \Delta\mathbf{x}_{\mathrm{i,j}}\left(\mathbf{e}_{\mathbf{r}i,j}\cdot\mathbf{r}_{i,j}\right) - \mathbf{r}_{i,j}\left(\underbrace{\mathbf{e}_{\mathbf{r}i,j}\cdot\Delta\mathbf{x}_{\mathrm{i,j}}}_{0}\right) \\
=\ & \Delta\mathbf{x}_{\mathrm{i,j}}r_{i,j} \\
\Rightarrow \Delta\mathbf{x}_{\mathrm{i,j}} =\ & -\frac{J_{ij}}{r_{i,j}\lambda\mathbf{S}_i\cdot\mathbf{S}_j}\mathbf{e}_{\mathbf{r}i,j}\times(\mathbf{S}_i\times\mathbf{S}_j)
\end{aligned}
\tag{3.16}
$$

where $\mathbf{e}_{\mathbf{r}i,j}$ denotes the unit vector connecting the spins $\mathbf{S}_i$ and $\mathbf{S}_j$. Therefore, the electric polarization is given by,

$$\mathbf{P} = \sum_{i,j}A_{i,j}\mathbf{e}_{\mathbf{r}i,j}\times(\mathbf{S}_i\times\mathbf{S}_j) \tag{3.17}$$

with $A_{i,j} = -\frac{qJ_{ij}}{r_{i,j}\lambda\mathbf{S}_i\cdot\mathbf{S}_j}$ where q is the charge of the ligand ion.

Equation (3.17) shows the direct one-to-one correlation between the polarization direction and the helicity of the spin cycloid. Furthermore, according to Eq. (3.17) the absolut value of

the displacement depends on the angle between two spins (Fig. 3.8).
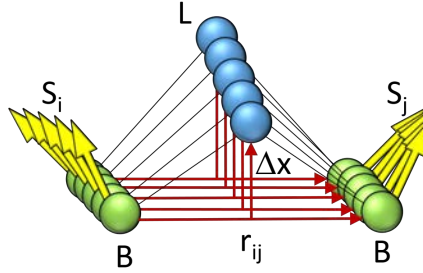
Figure 3.8: *Displacement as a function of spin angle.* The size of the displacement of the ligand ion depends on the size of the spin angle. For collinear spins the displacement vanishes whereas for $\frac{\pi}{2}$ the displacement is maximal.

The physical interpretation of the IDM interaction is that the relativistic correction can be expressed by a spin-orbital interaction, which will try to rotate the atomic orbitals in order to align with the spins. This rotation of the atomic orbitals will repulse the ligand ion between the two magnetic ions via Coulomb force. Thus, the IDM interaction leads to an ionic polarization in contrast to the spin-current which generates an electric polarization.

From an experimental point of view the prove of which mechanism leads to the induced electric polarization in cycloidal spin structures is a non-trivial process because only small electric polarization of $\approx 100\mathrm{nC}/\mathrm{cm}^2$ corresponds to an ionic shift of approximately 1 pm. This is at the resolution limit of methods that can measure the crystal structure, like neutron scattering and X-ray diffraction. Often, it is unclear whether the ions or the electrons induces the polarization [80, 81, 82].

Both effects are supported by theoretical calculations and they may even be present simultaneously [73, 83]. Nevertheless, the IDM interaction and its related ionic displacement is the mechanism that explains the emergence of a net electric polarization in $\mathrm{TbMnO_3}$[84, 85, 86] Dynamic magnetoelectric switching processes may clarify this question since electronic and ionic systems can have different dynamic properties.

3.3   Ferroelectricity in charge ordered collinear magnets

A second mechanism called exchange striction, explains the linear coupling between electric and magnetic degrees of freedom and thus in turn the emergence of electric polarization due to magnetic order in collinear magnetic structures.

It does not require the presence of spin-orbit coupling and is based on magnetostriction. For the magnetostriction to give magneto electric behaviour the presence of inequivalent magnetic ions with different charges is essential. These in turn may be either just different ions, or the same element in different valence states.

3.3.1   Electric polarization due to magnetostriction for a straight charged ordered chain

A simple model that describes the emergence of ferroelectricity in charge ordered collinear magnets is the Ising model with both nearest-neighbour and next-nearest-neighbour interaction,

$$H = -J_1 \sum_i \sigma_i \sigma_{i+1} - J_2 \sum_i \sigma_i \sigma_{i+2} \tag{3.18}$$

where $J_1 \lessgtr 0$ and $J_2 < 0$ are the ferromagnetic and antiferromagnetic exchange constant respectively, and $\sigma_i = \pm 1$ represents the Ising spin at site i. If the antiferromagnetic exchange constant is sufficiently large, $|J_2| > \frac{|J_1|}{2}$, the magnetic ordering will be of the up–up–down–down type [87].

This specific type of magnetic order is space inversion symmetric and thus is not able to lead to a linear magneto electric effect in principle (Fig. 3.9).
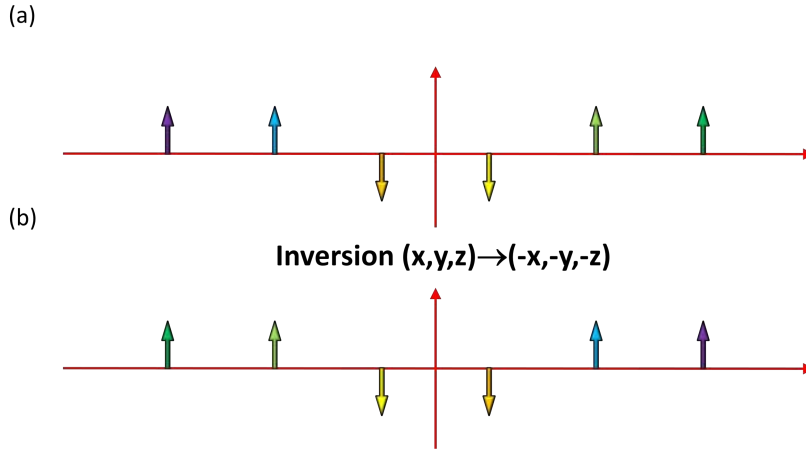
Figure 3.9: *Up-up-down-down spin structure.* The up-up-down-down spin structure does not break the space inversion symmetry.

Also the bare charged ordered chain without accounting the spin order does not break the space inversion symmetry (Fig. 3.10).

However, taking both charge and magnetic structure together, the system loses space inversion symmetry (Fig. 3.11) and in turn can lead to the linear magneto electric effect.

The exchange striction shifts neighbouring ions in a way that optimizes the spin-exchange energy since in general the exchange constant is a function of the distance between these spins, $J = f(r)$. Thus depending on the sign of J_1, the bond with parallel spins (for $J_1 > 0$) will shorten and with antiparallel spins will stretch, respectively the bond with antiparallel spins (for $J_1 < 0$) will shorten and parallel spins will stretch, increasing the magnetic energy gain on the corresponding bond (Fig. 3.12).

In both cases this will lead to a induced electric polarization. An almost ideal realization of this scenario seems to have been found in Ca_3CoMnO_6 [88]. In this system with a quasi-

(a)

(b)

Inversion (x,y,z)→(-x,-y,-z)
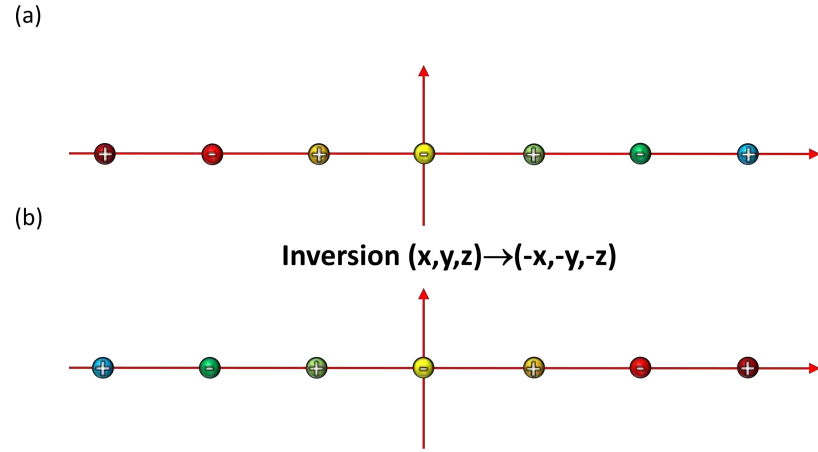
Figure 3.10: *Charged ordered chain.* The charged ordered chain does not break space inversion symmetry.

(a)

(b)

Inversion (x,y,z)→(-x,-y,-z)
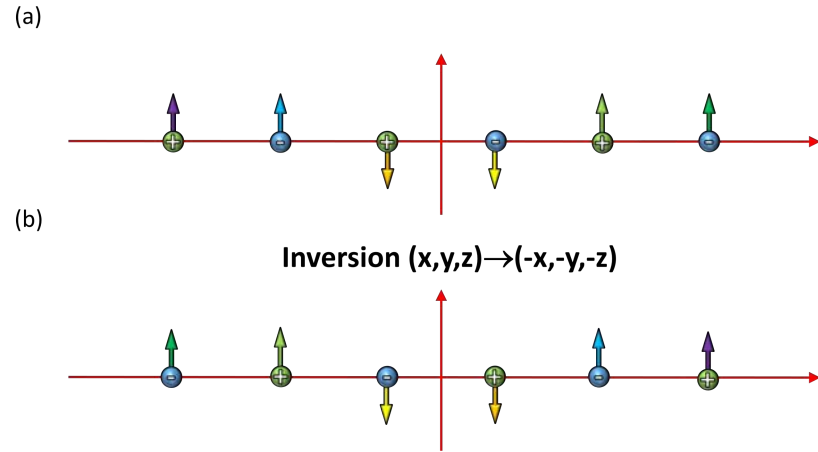
Figure 3.11: *Charged ordered chain with spin structure.* A chain with alternating charges and with the spin structure up-up-down-down breaks the space inversion symmetry and thus allows in principle the emergence of the linear magneto electric effect.

onedimensional structure the ions Co^{2+} and Mn^{4+} alternate along the chain, and magnetic structure is of the up–up–down–down type. Indeed, below $T_N = 16\,K$, Choi *et al.* [88] observe an electric polarization in this system. In addition the coexistence of site-centred charge ordering and spin ordering of the up-up-down-down type has been observed in $RNiO_3$[89]. Furthermore, this example is closely related to the origin of ferroelectricity in orthorhombic RMn_2O_5 (R = rare-earth). In this family of multiferroics the strongly interacting Mn^{3+} and Mn^{4+} spins form a five-fold loop of antiferromagnetic bonds, which leads to frustration [80].

3.3.2 Electric polarization due to exchange striction for a zig-zag charged ordered chain

In zig-zag charged ordered chains the most important influence to the spatially dependent exchange constant comes not directly from the relative position of the ions itself, but indirectly from the change of the bond angle caused by the change of the relative position. If **x** is the
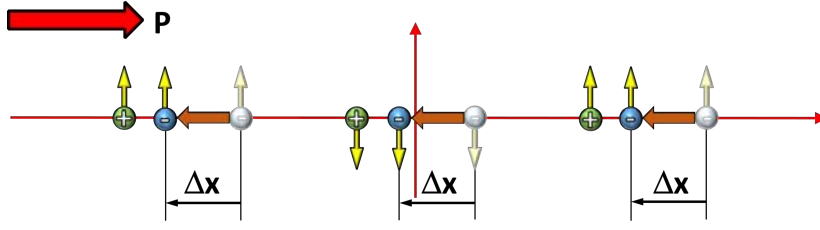
Figure 3.12: *Effect of Magnetostriction.* Shortening (in this example) the ferro-magnetic bonds, produces a electric polarization, indicated by the red arrow.

distance of the ligand ion to the line connecting the magnetic ions, then to first order in $\mathbf{x}$ the exchange interaction has the form ($\nabla = \frac{\mathrm{d}}{\mathrm{d}\mathbf{x}}$),

$$J\left(x, y, z\right) = J\left(x_0, y_0, z_0\right) + \left.\frac{\partial J}{\partial \alpha}\right|_{\alpha_0} \left.\boldsymbol{\nabla}\alpha\right|_{\mathbf{x}_0} \cdot \left(\mathbf{x} - \mathbf{x}_0\right) \qquad (3.19)$$

where α is the bond angle and x_0 is the equilibrium position. The exchange constant J is maximal for $\alpha = \pi$, $\left.\frac{\partial J}{\partial \alpha}\right|_{\pi} = 0$, and decreases with decreasing angle as it follows from the Goodenough-Kanamori-Anderson rules. The Heisenberg exchange interaction then has the form,

$$H_{i,i+1} = \left[J\left(x_{i_0}, y_{i_0}, z_{i_0}\right) + \left.\frac{\partial J_i}{\partial \alpha_i}\right|_{\alpha_{i_0}} \left.\boldsymbol{\nabla}\alpha_i\right|_{\mathbf{x}_{i_0}} \cdot \left(\mathbf{x_i} - \mathbf{x_{i_0}}\right)\right] \mathbf{S}_i \cdot \mathbf{S}_{i+1} \qquad (3.20)$$

If the bond angle in equilibrium position substantially differs from π, the first derivative $\left.\frac{\partial J_i}{\partial \alpha_i}\right|_{\alpha_0} \neq 0$ exists and is the same for all bonds. In a zig-zag chain the derivative of the bond angle with respect to the position of the ligand ion alternates, $\left.\boldsymbol{\nabla}\alpha_i\right|_{\mathbf{x}_{i_0}} \sim (-1)^i$, in the same manner as the scalar product of two neighbouring spins alternates, $\mathbf{S}_i \cdot \mathbf{S}_{i+1} \sim (-1)^i$. In equilibrium, the gain of the Heisenberg exchange energy becomes maximized. Therefore all $\Delta\mathbf{x}_i = \mathbf{x}_i - \mathbf{x}_{i_0} < 0$ and thus in turn pushes all ligand ions in the same direction away from the equilibrium position. This displacement generates an electric polarization accordingly if the ligand and magnetic ions are differently charged (Fig. 3.13).
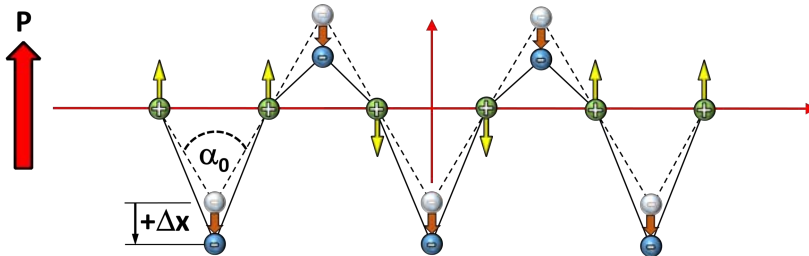
Figure 3.13: *Zig-Zag charge ordered chain with up-up-down-down spin structure.* Electric polarization is induced in a charged ordered zig-zag chain with up-up-down-down spin structure.

Nota bene, in zig-zag chains with a cycloidal spin arrangement and a Heisenberg interaction, the scalar product of two neighbouring spins is constant and always positive, $\mathbf{S}_i \cdot \mathbf{S}_{i+1} >$

0. Hence the displacement of the ligand ion alternates, $\Delta\mathbf{x}_i = \mathbf{x}_i - \mathbf{x}_{i_0} \sim (-1)^i$ and no electric polarization (static property) is induced (Fig.3.14).
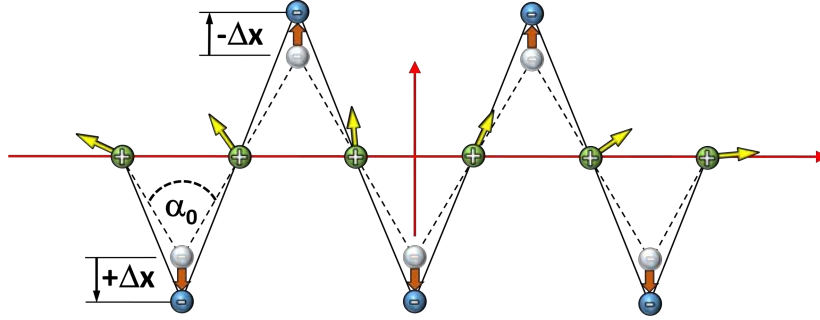
Figure 3.14: *Zig-Zag charge ordered chain with cycloidal spin structure.* The cycloidal spin order in a zig-zag charged ordered chain causes a shift of the ligand ions in opposite directions. Thus no electric polarization is generated..

However, the exchange striction is most likely the driving mechanism of the existence of novel coupled magnon-phonon excitations called electromagnons (dynamic property) [90, 91] in charged ordered zig-zag chains with a cycloidal spin order.

It was found out, that these excitations does not depend on direction of the spins and thus in turn do not obey the selection rule of the IDM interaction namely that the electric component of the excitation field should be in-plane with the spin cycloid, $\mathbf{E} \parallel \mathbf{P} \propto \mathbf{e}_{ij} \times (\mathbf{S}_i \times \mathbf{S}_j)$[90, 92, 93, 94, 95, 96, 97]. Therefore the violation of the this selection rule implies that a different dynamical megnetoelectric coupling is responsible for the appearance of electromagnons in cycloidal ordered magnets.

CHAPTER 4

Theory of ferroelectric phase transition

4.1 Static critical phenomena

The thermodynamic properties of a system in equilibrium can be analysed by considering its thermodynamic potential expressed in terms of natural variables. The potential which is commonly used in describing phase transitions is the free energy, $F = U - TS$ [1](Eq. 2.13).

The fundamental concept on which all thermodynamic theories of ferroelectric phase transitions are based on is that the phase transition can be described in terms of an order parameter, Ω, whose appearance at the phase transition temperature, T_C, breaks the symmetry of the system. Hence Ω vanishes above T_C and is non-zero below T_C.

The order parameter thus measures the extent to which the atomic configuration in the less symmetrical phase departs from the configuration of the more symmetrical phase [98]. Therefore, for studying phase transitions it is essential to know the free energy of the system.

The procedure to calculate the free energy is linked to the problem to find the partition function for system composed by N particles,

$$F = -k_B T \ln \mathcal{Z} \tag{4.1}$$

where $\mathcal{Z}$ is the partition function given by [2]

$$\mathcal{Z} = \int\limits_{-\infty}^{+\infty} e^{-(k_B T)^{-1} \mathcal{H}(\mathbf{p}_n, \mathbf{r}_n)} \prod_n \mathrm{d}\mathbf{p}_n \mathrm{d}\mathbf{r}_n \tag{4.2}$$

where k_B is the Boltzmann's constant, T is the temperature and H is the Hamiltonian of the system given by,

$$\mathcal{H}(\mathbf{p}_n, \mathbf{r}_n) = \sum_{n=1}^{N} \frac{p_n^2}{2m} + V(\mathbf{r}_1, ..., \mathbf{r}_N) \tag{4.3}$$

---

[1]The free energy is a function of temperature and volume,$F = f(T, V)$. Thus thermodynamic equilibrium is given by $dT = 0$ and $dV = 0$. Processes with $dV = 0$ are difficult to realize experimentally. Therefore it is convenient to consider the Gibbs free energy which is a function of temperature and pressure, $G(T, p) = F + pV$. Hence, $dF = dG - V dp - pdV$. For in isobaric process follows, $dF = dG - pdV$. In solid state physics dV is usually very small and hence negligible. Thus in turn $dF \approx dG$.

[2]Here it is assumed that the system can be considered classically. For quantum mechanical systems $\mathcal{Z} = \mathrm{Tr}\left[\exp\left(-\frac{H}{k_B T}\right)\right]$.

with the total kinetic energy, $\sum_{n=1}^{N} \frac{p_n^2}{2m}$, and the total interaction energy, $V\left(\mathbf{r}_1, ..., \mathbf{r}_N\right)$, where $\mathbf{p}_n$ and $\mathbf{r}_n$ are the momentum and position of the nth particle, respectively. The partition function and thus in turn the free energy of a system can only be evaluated if the multiple integral can be split into the product of singular integrals.

If the interaction energy between the particles has to be accounted, it is no longer possible to break up the integral into the product of singular integrals and usually perturbation theory with respect to the interaction energy has to be applied [99].

There exists one ideal case where, in spite of interaction between the particles, the multiple integral splits into the product of simple integrals. This is the case for a so called *harmonic crystal*. The potential energy for such a crystal is a quadratic function of the atomic displacements. In that case, it is possible to pass over from spatial coordinates, $\mathbf{r}_i$, to the normal coordinates $\mathbf{u}_q$ of which the function $V\left(\mathbf{r}_1, ..., \mathbf{r}_N\right)$ becomes $V = \frac{1}{2}\sum_{q=0}^{N} v_q u_q^2$ where v_q are certain coefficients [99].

In the harmonic approximation on the other hand the breaking of symmetry at ferroelectric phase transitions can not be described. Anharmonic effects must be considered such as the dependence of the potential energy on higher order atomic displacements [99, 100]. This in turn entails that the transition to the normal coordinates does not allow to split the integrals in Eq. (4.2) and perturbation theory must be applied.

In doing so, one assumes small anharmonic corrections, but in the vicinity of the phase transition, i.e. in the anomalous region of the response function (electric susceptibility) anharmonic effects cannot be considered to be small. Thus, the problem of calculating anomalies in the region of phase transitions or thermodynamic potentials within the framework of statistical physics is extremely complicated [99].

As a matter of fact, phase transitions are usually investigated within the framework of Ginzburg-Landau theory as a first stage.

4.1.1   Thermodynamics and Ginzburg-Landau Hamiltonian

In practice, the expression in Eq. (4.2) is not of much use, since the microscopic Hamiltonian, and the degrees of freedom, are too much complicated to make a calculation possible in most cases [101].

On the contrary, near the phase transition temperature, the degrees of freedom which controls the phase transition are long wavelength collective excitations of electric dipoles. Thus it is possible to introduce a coarse-grained electric polarization field [101, 102], $\pi\left(\mathbf{r}\right)$ which represents the average of the elemental electric dipoles in the vicinity of a point $\mathbf{r}$.

That means, that the volume is divided into small cells where each cell is small enough to be represented by a differential volume element $\mathrm{d}^3 r$ but large enough to include many electric dipoles in it. It is important to emphasize that while $\mathbf{r}$ is treated as a continuous variable, the function $\pi\left(\mathbf{r}\right)$ does not exhibit any variations at distances of the order of the volume dimensions. That is that the Fourier transform involves only wave vectors with magnitude less than some upper cut-off $\left|\mathbf{q}\right|_{max} \sim \frac{1}{d}$ where d is of the order of the volume dimension.

By focusing only on the coarse-grained electric polarization field, the original problem

given by Eq. (4.1) is simplified since the partition function can be written as [101, 102],

$$\mathcal{Z} = \int \mathcal{D}\pi\left(\mathbf{r}\right) e^{-(k_B T)^{-1}\mathcal{H}[\pi(\mathbf{r})]} \tag{4.4}$$

Hence, in thermal equilibrium the probability to find a specific configuration of the order parameter field is given by,

$$\mathcal{P}\left[\pi\left(\mathbf{r_i}\right)\right] = \frac{1}{\mathcal{Z}} e^{-(k_B T)^{-1}\mathcal{H}[\pi(\mathbf{r_i})]} \tag{4.5}$$

The functional integration $\int \mathcal{D}\pi\left(\mathbf{r}\right)$ is an integral over all possible values of $\pi\left(\mathbf{r}\right)$ at all positions $\mathbf{r}$. That is a sum over all possible macrostates (different configurations of the order parameter field) in which the Boltzmann factor determines the probability for a given macrostate. It is a shorthand notation which reads [102],

$$\int \mathcal{D}\pi\left(\mathbf{r}\right) = \int \prod_i \mathrm{d}\pi\left(\mathbf{r_i}\right) \tag{4.6}$$

The coarse-grained Hamiltonian $\mathcal{H}\left[\pi\left(\mathbf{r}\right)\right]$ is the so called Ginzburg-Landau Hamiltonian and can be constructed by appropriate assumptions which are [101]: The crystal energy may be represented as a sum over all volume energies and energies of interactions between them. The energy of interaction can be expressed through gradient expansions. In a continuum representation the sum goes over to an integral.

Furthermore, $\mathcal{H}\left[\pi\left(\mathbf{r}\right), \nabla\pi\left(\mathbf{r}\right), \cdots\right]$ must have the symmetry of the paraelectric phase which is invariant under space inversion and in an isotropic system the derivatives must be invariant under spatial rotations. Thus the Ginzburg-Landau Hamiltonian including the interaction energy with an external electric field, $E\left(\mathbf{r}\right)$, sufficiently describing phase transitions in most cases is given by [101],

$$\mathcal{H} = \int \left\{ a\pi^2\left(\mathbf{r}\right) + b\pi^4\left(\mathbf{r}\right) + c\pi^6\left(\mathbf{r}\right) + \ldots + K\left[\boldsymbol{\nabla}\pi\left(\mathbf{r}\right)\right]^2 - gE\left(\mathbf{r}\right)\pi\left(\mathbf{r}\right) \right\} \mathrm{d}V \tag{4.7}$$

The phenomenological parameters a, b, c, K, g[3] are non-universal functions of microscopic interactions as well as external parameters such as temperature and pressure.

The term $K\left[\boldsymbol{\nabla}\pi\left(\mathbf{r}\right)\right]^2$ represents the increase of the energy density due to spatial fluctuations of the order parameter[4]. A positive K leads to $\boldsymbol{\nabla}\pi\left(\mathbf{r}\right) = 0$ in equilibrium and consequently to a spatially homogeneous system, whereas for $K < 0$, $\boldsymbol{\nabla}\pi\left(\mathbf{r}\right) \neq 0$ and a

---

[3]In Kadar's textbook, g is set to one, $g = 1$. Since the Hamiltonian in Eq.(4.7) represents a series expansion of the actual total energy, the parameter g is not necessarily one, but can be also a function of temperature and microscopic parameters.

[4]This particular form of interaction energy can be understood on the basis of an Ising type interaction. Suppose that the interaction energy can be written as $\mathcal{H}_{INT} = J\sum_i S_i S_{i+1}$, where J is a exchange constant and S_i is a spin like entity. For a coarse-grained order parameter field, this relation can be written as $\mathcal{H}_{INT} = \sum_l \pi_l \pi_{l+1}$ where π_l is the coarse grained order parameter at position l which is $\pi_l = \sum_{i=la}^{(l+1)a} S_i$ where a is the region size. The interaction energy can be rewritten to $\mathcal{H}_{INT} = \frac{1}{2}J\sum_l \left(\pi_l - \pi_{l+1}\right)^2 - J\sum_l \pi_l^2$. Thus $\mathcal{H}_{INT} \propto a\sum_l \left(\frac{\pi_l - \pi_{l+1}}{a}\right)^2 a \approx a\int \left(\frac{\pi(\mathbf{r}+\mathrm{d}\mathbf{r})-\pi(\mathbf{r})}{\mathrm{d}\mathbf{r}}\right)^2 \mathrm{d}\mathbf{r} = K\int\left[\boldsymbol{\nabla}\pi\left(\mathbf{r}\right)\right]^2 \mathrm{d}\mathbf{r}$

spatially inhomogeneous system is favoured in equilibrium. Thus the gradient term accounts the energy stored in domain walls [103].

4.1.2 Saddle point approximation and Landau's theory

Although by the transformation from the original degrees of freedom, Eq. (4.2), to a field representation, $\pi(\mathbf{r})$, and consequently evaluating the partition function in Eq. (4.4) over all possible configurations of the order parameter field, Eq. (4.6), it is still challenging to calculate the partition function in Eq. (4.4). As a first step the order parameter field is replaced by the mean value, $\pi(\mathbf{r}) \rightarrow \langle \pi(\mathbf{r}) \rangle = \bar{\pi}$ thus the term considering spatial fluctuations in Eq. (4.7) vanishes, $\boldsymbol{\nabla}\pi(\mathbf{r}) \rightarrow \boldsymbol{\nabla}\bar{\pi} = 0$ and the integral in Eq. (4.4) simplifies to $\int \mathcal{D}\pi(\mathbf{r}) = \int \prod_i \mathrm{d}\pi(\mathbf{r_i}) \rightarrow \int \mathrm{d}\bar{\pi}$.

Therefore, the partition function in Eq. (4.4) with $\mathcal{H}(\bar{\pi}) = a\bar{\pi}^2 + b\bar{\pi}^4 + c\bar{\pi}^6 + \ldots - gE_0\bar{\pi}$ becomes,

$$\mathcal{Z} = \int\limits_{-\infty}^{+\infty} \mathrm{d}\bar{\pi}\, e^{-(k_BT)^{-1}V\mathcal{H}(\bar{\pi})} \tag{4.8}$$

Expanding $\mathcal{H}(\bar{\pi})$ around its minimum, $\bar{\pi}_S$, and considering that the first-order term vanishes at the minimum $\bar{\pi}_S$ (equilibrium), Eq. (4.8) becomes,

$$\mathcal{Z} \approx \int\limits_{-\infty}^{+\infty} \mathrm{d}\bar{\pi}\, e^{-(k_BT)^{-1}V\left[\mathcal{H}(\bar{\pi}_S)+\frac{1}{2}(\bar{\pi}-\bar{\pi}_S)^2\mathcal{H}''(\bar{\pi}_S)\right]} \tag{4.9}$$

Thus,

$$\begin{aligned} \mathcal{Z} &\approx\ e^{-(k_BT)^{-1}V\mathcal{H}(\bar{\pi}_S)} \int\limits_{-\infty}^{+\infty} \mathrm{d}\bar{\pi}\, e^{-(k_BT)^{-1}V\left[\frac{1}{2}(\bar{\pi}-\bar{\pi}_S)^2\mathcal{H}''(\bar{\pi}_S)\right]} \\ &\approx\ e^{-(k_BT)^{-1}V\mathcal{H}(\bar{\pi}_S)}\sqrt{\frac{2\pi k_BT}{V\mathcal{H}''(\bar{\pi}_S)}} \end{aligned} \tag{4.10}$$

According to Eq. (4.1) the free energy becomes,

$$F = V\mathcal{H}(\bar{\pi}_S) + \frac{k_BT}{2}\left\{\ln\left[V\mathcal{H}''(\bar{\pi}_S)\right] - \ln\left[2\pi k_BT\right]\right\} \tag{4.11}$$

In the limit of $V \rightarrow \infty$, the free energy is given by,

$$F = V\mathcal{H}(\bar{\pi}_S) = V\left(a\bar{\pi}_S^2 + b\bar{\pi}_S^4 + c\bar{\pi}_S^6 + \ldots - gE_0\bar{\pi}_S\right) \tag{4.12}$$

Nota bene, since the Ginzburg-Landau Hamiltonian has a minimum for $\bar{\pi} = \bar{\pi}_S$, $\bar{\pi}_S$ corresponds to the most probable mean value of the order parameter density according to Eq. (4.5). Additionally, since $\mathcal{H}(\bar{\pi}_S) = \min$, $F \rightarrow \min$ as well, according to Eq. (4.12). Bearing in mind that in thermal equilibrium the free energy becomes minimized, $\bar{\pi}_S$ corresponds to the mean value of the order parameter density in thermal equilibrium which can be obtained

by the minimum condition $\frac{\mathrm{d}F}{\mathrm{d}\bar{\pi}_S} = 0$. This is in accordance with Landau's phase transition theory.

The essential idea in the framework of Landau's theory of phase transitions relies on the fact that the free energy density can be expanded in a power series with respect to the order parameter near the critical temperature (phase transition temperature) due to a small order parameter near T_C [104]. It was first applied to the case of ferroelectrics by Devonshire [105, 106, 107] to describe the ferroelectric phase transition in uniaxial ferroelectric materials.

4.1.3   Fluctuations, Correlations & Susceptibility

According to Eq. (4.5), the most probable order parameter configuration, $\pi_M(\mathbf{r})$, is given by $\mathcal{P}[\pi_M(\mathbf{r})] = \max$. Thus $\pi_M(\mathbf{r})$ corresponds to the order parameter density in thermal equilibrium. Therefore the Ginzburg-Landau Hamiltonian must be minimal, $\mathcal{H}[\pi_M(\mathbf{r})] = \min$, i.e. the variation of $\mathcal{H}$ must be zero[5], $\delta\mathcal{H} = 0$. Thus $\pi(r)$ must satisfy the Euler-Lagrange equation,

$$\left.\frac{\partial I}{\partial\pi(\mathbf{r})}\right|_{\pi_M(\mathbf{r})} - \boldsymbol{\nabla}\cdot\left.\frac{\partial I}{\partial[\boldsymbol{\nabla}\pi(\mathbf{r})]}\right|_{\pi_{Mo}(\mathbf{r})} = 0 \tag{4.13}$$

where I is the integrand of Eq. (4.7). For second order phase transitions (continuous order parameter at $T = T_C$) it is sufficient to include only a few terms up to the quartic term [108]. Thus Eq. (4.13) becomes,

$$2a\pi_M(\mathbf{r}) + 4b\pi_M^3(\mathbf{r}) - gE(\mathbf{r}) - 2K\triangle\pi_M(\mathbf{r}) = 0 \tag{4.14}$$

where $\triangle$ is the Laplacian with $\triangle\pi_M(\mathbf{r}) = \frac{\partial^2\pi_M(\mathbf{r})}{\partial x^2} + \frac{\partial^2\pi_M(\mathbf{r})}{\partial y^2} + \frac{\partial^2\pi_M(\mathbf{r})}{\partial z^2}$. Because of the non linear term, $4b\pi_M^3(\mathbf{r})$, it is not possible to integrate this equation exactly. However, assuming a perturbing field of the form $E(\mathbf{r}) = \delta E e^{i\mathbf{q}\cdot\mathbf{r}}$, the solution is then given of the form $\pi_M(\mathbf{r}) = \bar{\pi}_S + \delta\pi e^{i\mathbf{q}\cdot\mathbf{r}}$ where $\bar{\pi}_S$ is the average electric polarization density in thermal equilibrium in zero electric field [109]. Therefore with considering only first order of smallness[6] , $\delta\pi$, Eq. (4.14) becomes,

$$\underbrace{2a\bar{\pi}_S + 4b\bar{\pi}_S^3}_{=0} + \left[2Kq^2 + 2a + 12b\bar{\pi}_S^2\right]\delta\pi e^{i\mathbf{q}\cdot\mathbf{r}} - g\delta E e^{i\mathbf{q}\cdot\mathbf{r}} = 0 \tag{4.15}$$

The susceptibility is given by $\chi = \frac{1}{\varepsilon_0}\frac{\delta\pi}{\delta E}$, thus,

$$\chi_q = \frac{1}{\varepsilon_0}\frac{g}{2Kq^2 + 2a + 12b\bar{\pi}_S^2} = \frac{1}{\varepsilon_0}\frac{\chi_0}{1 + q^2\xi^2} \tag{4.16}$$

where χ_0 is the susceptibility in case of the mean value of the electric polarization field in thermal equilibrium ($\pi(\mathbf{r}) = \bar{\pi}_S$) and ξ is the correlation length[7].

---

[5]This is equivalent to the question which $\pi(r)$ minimizes the integral

[6]Thermodynamic equilibrium requires $\frac{\mathrm{d}F}{\mathrm{d}\bar{\pi}_S} = 0$ thus $2a\bar{\pi}_S + 4b\bar{\pi}_S^3 = 0$

[7]$\chi_0 = \begin{cases} \frac{1}{2A(T-T_C)} & T > T_C \\ \frac{1}{4A(T_C-T)} & T < T_C \end{cases}$ $\xi^2 = \begin{cases} \frac{K}{A(T-T_C)} & T > T_C \\ \frac{1}{2A(T_C-T)} & T < T_C \end{cases}$

A fundamental property of phase transitions can be obtained by studying the range of spatial fluctuations. For instance, an interesting situation arises when the system is locally perturbed by an electric field, $E(\mathbf{r}) = E_0 \delta(\mathbf{r})$, and one would like to know how far away the effects of this perturbation can be seen. In that case the fluctuations of the electric polarization field become[8],

$$\delta\pi(\mathbf{r}) = \frac{\chi_0 E_0}{(2\pi)^3} \int \frac{1}{1+q^2\xi^2} e^{i\mathbf{q}\cdot\mathbf{r}} \mathrm{d}^3 q = \frac{\chi_0 E_0}{32\pi^4\xi^2} \frac{1}{|\mathbf{r}|} e^{-\frac{|\mathbf{r}|}{\xi}} \tag{4.17}$$

Equation (4.17) contains the Ornstein-Zernike correlation function for $\mathbf{r}' = 0$ in the three dimensional case ($d = 3$) which is given by [110],

$$\begin{aligned} G(\mathbf{r}, \mathbf{r}') &= \langle \delta\pi(\mathbf{r})\,\delta\pi(\mathbf{r}') \rangle \\ &= \langle [\pi(\mathbf{r}) - \langle \pi(\mathbf{r}) \rangle][\pi(\mathbf{r}') - \langle \pi(\mathbf{r}') \rangle] \rangle \\ &= \langle \pi(\mathbf{r})\pi(\mathbf{r}') \rangle - \langle \pi(\mathbf{r}) \rangle \langle \pi(\mathbf{r}') \rangle \\ &\propto \frac{1}{(|\mathbf{r} - \mathbf{r}'|)^{\frac{d-1}{2}}} e^{-\frac{|\mathbf{r}-\mathbf{r}'|}{\xi}} \end{aligned} \tag{4.18}$$

The correlation function describes the relation between fluctuation of the electric polarization field[9] at points $\mathbf{r}$ and $\mathbf{r}'$. For the infinite large, translational and rotationally invariant system, it is shown [110] that[10],

$$\chi = (k_B T)^{-1} \int G(r)\,\mathrm{d}^3 r \propto \xi^2 \tag{4.19}$$

Thus the spatial fluctuations of the electric polarization field in Eq. (4.17) becomes,

$$\delta\pi(\mathbf{r}) = \frac{E_0}{32\pi^4} \frac{1}{|\mathbf{r}|} e^{-\frac{|\mathbf{r}|}{\xi}} \tag{4.20}$$

In the vicinity of T_C, χ_q becomes very large and thus in turn even a small perturbing field can cause considerable fluctuations.

As a result, this spatial fluctuations are not only excited by a external perturbing field but also by thermal fluctuation of the electric polarization field itself. The correlation length thus plays the role of the characteristic size of thermal fluctuations.

---

[8] $\delta\pi(\mathbf{r}) = \int \delta\pi(\mathbf{q}) e^{i\mathbf{q}\cdot\mathbf{r}} \mathrm{d}^3 q$. With $\delta\pi(\mathbf{q}) = \varepsilon_0 \chi(\mathbf{q}) \delta E(\mathbf{q})$ follows, $\delta\pi(\mathbf{r}) = \int \varepsilon_0 \chi(\mathbf{q}) \delta E(\mathbf{q}) e^{i\mathbf{q}\cdot\mathbf{r}} \mathrm{d}^3 q$. With $\delta E(\mathbf{r}) = E_0 \delta(\mathbf{r})$ follows $\delta E(\mathbf{q}) = \int E_0 \delta(\mathbf{r}) e^{i\mathbf{q}\cdot\mathbf{r}} \mathrm{d}^3 q = E_0$. Thus $\delta\pi(\mathbf{r}) = E_0 \int \varepsilon_0 \chi(\mathbf{q}) e^{i\mathbf{q}\cdot\mathbf{r}} \mathrm{d}^3 q$. With Eq. (4.16) the fluctuation becomes $\delta\pi(\mathbf{r}) = \chi_0 E_0 \int \frac{1}{1+q^2\xi^2} e^{i\mathbf{q}\cdot\mathbf{r}} \mathrm{d}^3 q = \chi_0 E_0 \iiint \frac{1}{1+q^2\xi^2} e^{iqr\cos\vartheta} q^2 \sin\vartheta \mathrm{d}\vartheta \mathrm{d}\varphi \mathrm{d}q$.

[9] That means, that $G(\mathbf{r}, \mathbf{r}')$ describes the correlation of fluctuations at point $\mathbf{r}$ and $\mathbf{r}'$

[10] With $\mathcal{H} = \mathcal{H}_0 - \int \pi(\mathbf{r}) E(\mathbf{r})$, $F = -k_B T \ln \mathcal{Z}$ and $\mathcal{Z} = \int \mathcal{D}\pi(\mathbf{r}) e^{-(k_B T)^{-1}\mathcal{H}[\pi(\mathbf{r})]}$ a generalized susceptibility is given by $\chi(\mathbf{r}, \mathbf{r}') = -\frac{\partial^2 F}{\partial E(\mathbf{r})\partial E(\mathbf{r}')}$ where the susceptibility $\chi(\mathbf{r}, \mathbf{r}')$ is the response function which describes the response of the electric polarization at point $\mathbf{r}$ when an electric field is applied at point $\mathbf{r}'$, $P(\mathbf{r}, \mathbf{r}') = \chi(\mathbf{r}, \mathbf{r}') E(\mathbf{r}')$. Thus $\chi(\mathbf{r}, \mathbf{r}') = (k_B T)^{-1} \left(\frac{1}{\mathcal{Z}} \frac{\partial^2 \mathcal{Z}}{\partial E(\mathbf{r})\partial E(\mathbf{r}')} - \frac{1}{\mathcal{Z}} \frac{\partial \mathcal{Z}}{\partial E(\mathbf{r})} \cdot \frac{1}{\mathcal{Z}} \frac{\partial \mathcal{Z}}{\partial E(\mathbf{r}')} \right) = (k_B T)^{-1} [\langle \pi(\mathbf{r})\pi(\mathbf{r}') \rangle - \langle \pi(\mathbf{r}) \rangle \langle \pi(\mathbf{r}') \rangle] = (k_B T)^{-1} G(\mathbf{r}, \mathbf{r}')$. Hence for a translational and rotationally system, $G(\mathbf{r}, \mathbf{r}') = G(|\mathbf{r} - \mathbf{r}'|)$. Therefore the macroscopic susceptibility is $\chi = \int \chi(|\mathbf{r} - \mathbf{r}'|)\mathrm{d}V = 4\pi (k_B T)^{-1} \int |\mathbf{r} - \mathbf{r}'|^2 \frac{1}{(|\mathbf{r}-\mathbf{r}'|)^{\frac{d-1}{2}}} e^{-\frac{|\mathbf{r}-\mathbf{r}'|}{\xi}} \mathrm{d}(|\mathbf{r} - \mathbf{r}'|)$. Thus for $d = 3$, $\chi \propto \int_0^\infty R e^{-\frac{R}{\xi}} \mathrm{d}R \propto \xi^2$

If at a certain point, as a result of thermal fluctuation, there will arise a value of the electric polarization (density) which is substantially different from the equilibrium value, it will change the values of the electric polarization (density) at other positions. Thus, thermal fluctuations of the electric polarization (density) do not occur independently at various points of the crystal, but instead, they are intercorrelated at distances of the order of ξ, i.e. it gives the distance over which perturbations have a noticeable effect.

At $T = T_C$ the correlation of fluctuations decays as $\frac{1}{r}$. Thus at the critical temperature any small change in the electrical polarization at one point will be noticeable over all length scales (infinite range). This long range correlated fluctuations are the reason of the inherent instability of the system at $T = T_C$. Of course for a real system, fluctuations of the electric polarization will be noticeable only all over the sample[11].

These conclusions lead to a very interesting consequence for the dynamics near second order phase transitions. As the correlation length increases on approaching T_C, it will necessarily become much longer than the characteristic length (unit cell, for example) of the system. As a consequence, the behaviour of the system in the vicinity of the phase transition will not depend on the nature of microscopic interactions which drive the transition, but will exhibit a universal behaviour, that is determined by the dimensionality of the system.[12]

Since thermodynamic quantities which characterize a macroscopic system are average values, an interesting property of phase transition can be deduced by considering the fluctuations of the most probable mean value of the order parameter, $\Delta(V\bar{\pi}_S) = V\bar{\pi}_S - \langle V\bar{\pi}_S \rangle$. $\Delta(V\bar{\pi}_S)$ defines the stochastic process of fluctuations of $(V\bar{\pi}_S)$ and since for a stationary process the averaged value $\langle \Delta(V\bar{\pi}_S) \rangle$ vanishes, the mean quadratic fluctuations, $\left\langle [\Delta(V\bar{\pi}_S)]^2 \right\rangle$, is different from zero and thus a proper measure of fluctuations in a system. It becomes,

$$
\begin{aligned}
\left\langle [\Delta(V\bar{\pi}_S)]^2 \right\rangle =\ & \langle (V\bar{\pi}_S - \langle V\bar{\pi}_S \rangle)(V\bar{\pi}_S - \langle V\bar{\pi}_S \rangle) \rangle \\
=\ & \left\langle (V\bar{\pi}_S)^2 - 2V\bar{\pi}_S \langle V\bar{\pi}_S \rangle + \langle V\bar{\pi}_S \rangle^2 \right\rangle \\
=\ & \left\langle V\bar{\pi}_S^2 \right\rangle - 2\langle V\bar{\pi}_S \rangle \langle V\bar{\pi}_S \rangle + \langle V\bar{\pi}_S \rangle^2 \\
=\ & \left\langle (V\bar{\pi}_S)^2 \right\rangle - \langle V\bar{\pi}_S \rangle^2 = \text{Var}(V\bar{\pi}_S)
\end{aligned}
\tag{4.21}
$$

Hence for a confidence interval of 1σ, where σ is the standard deviation, $\sigma = \sqrt{\text{Var}(V\bar{\pi}_S)}$ the order parameter is given by ,

$$
V\bar{\pi}_S = \langle V\bar{\pi}_S \rangle \pm \sqrt{\left\langle (V\bar{\pi}_S)^2 \right\rangle - \langle V\bar{\pi}_S \rangle^2}
\tag{4.22}
$$

---

[11]This actually causes a limited susceptibility instead of an infinitely value at $T = T_C$. This singularity argument in turn is only valid for a infinite large system which implies $V \to \infty$, $N \to \infty$ such $\frac{N}{V}$ is finite

[12]To understand that fact, consider an Ising model with next nearest neighbour ineraction only. For example, if the spin at position $\mathbf{r}$ flips, the spin at $\mathbf{r} + \mathbf{L}$ may also flip for $T \approx T_C$. Here $\mathbf{L} = (n_1\mathbf{a}, n_2\mathbf{b}, n_3\mathbf{c})$with $\mathbf{a}, \mathbf{b}, \mathbf{c}$ as unit vectors describing the lattice and n_i are integer numbers determining the correlation length $\xi = \sqrt{\sum_{i=1}^{3} n_i^2}$. Although only next nearest neighbour interaction is considered, the spin at position $\mathbf{r} + \mathbf{L}$ is affected by a spin at position $\mathbf{r}$.

The expectation value of the most probable mean value of the order parameter[13] is calculated with Eq. (4.8) and Eq. (4.12) by,

$$\langle V\bar{\pi}_S \rangle = \frac{1}{\mathcal{Z}} \int\limits_{-\infty}^{+\infty} \mathrm{d}\,(V\bar{\pi}_S)\,(V\bar{\pi}_S)\,e^{-(k_BT)^{-1}\mathcal{H}(V\bar{\pi}_S)} \tag{4.23}$$

with $\mathcal{H}\,(V\bar{\pi}_S) = V\mathcal{H}\,(\bar{\pi}_S)$. The susceptibility becomes,

$$\begin{aligned}
\chi = \frac{\partial \langle V\bar{\pi}_S \rangle}{\partial E_0} \quad &= \int\limits_{-\infty}^{+\infty} \mathrm{d}\,(V\bar{\pi}_S)\,(V\bar{\pi}_S)\,e^{-(k_BT)^{-1}\mathcal{H}(V\bar{\pi}_S)} \frac{\partial}{\partial E_0}\left(\frac{1}{\mathcal{Z}}\right) \\[2mm]
&+ \frac{1}{\mathcal{Z}}\frac{\partial}{\partial E_0}\int\limits_{-\infty}^{+\infty} \mathrm{d}\,(V\bar{\pi}_S)\,(V\bar{\pi}_S)\,e^{-(k_BT)^{-1}\mathcal{H}(V\bar{\pi}_S)} \\[2mm]
&= -\frac{1}{k_BT}\left(\frac{1}{\mathcal{Z}^2}\right)\left(\int\limits_{-\infty}^{+\infty} \mathrm{d}\,(V\bar{\pi}_S)\,(V\bar{\pi}_S)\,e^{-(k_BT)^{-1}\mathcal{H}(V\bar{\pi}_S)}\right)^2 \\[2mm]
&+ \frac{1}{k_BT}\frac{1}{\mathcal{Z}}\int\limits_{-\infty}^{+\infty} \mathrm{d}\,(V\bar{\pi}_S)\,(V\bar{\pi}_S)^2\,e^{-(k_BT)^{-1}\mathcal{H}(V\bar{\pi}_S)} \\[2mm]
&= \frac{1}{k_BT}\left[\left\langle (V\bar{\pi}_S)^2 \right\rangle - \langle V\bar{\pi}_S \rangle^2\right] = \mathrm{Var}\,(V\bar{\pi}_S)
\end{aligned} \tag{4.24}$$

With Eq.(4.19) the mean quadratic fluctuations of the most probable mean value of the order parameter is proportional to the correlation length of spatial fluctuations as,

$$\left\langle (V\bar{\pi}_S)^2 \right\rangle - \langle V\bar{\pi}_S \rangle^2 \propto \xi^2 \tag{4.25}$$

As the correlation length approaches infinity, $\xi \to \infty$, the fluctuations of the order parameter diverges and they are called *critical fluctuations*. Consequently, according to Eq. (4.22) the order parameter is not longer well defined near T_C. This is an example of the inherent instability of a system at a phase transition.

4.1.4 Microscopic theory and the single ion model

The simplest model for describing ferroelectric phase transitions assumes a diatomic crystal consisting of ions of species A and B (Fig. 4.1a) [99].

At temperatures well bellow the critical temperature, $T \ll T_C$, the ions of species A are collectively displaced along a specific direction in the unit cell, whereas species B remain fixed, and thus generates a macroscopic electric polarization. Therefore, this model concerns the motion of only one ion A in the unit cell, assuming that the role of the other ions B is reduced to down to the creation of a potential field [99].

---

[13]Strictly speaking: The most probable mean value of the order parameter filed density times the system volume.

Since for a ferroelectric phase transition a macroscopic electric polarization evolves at the transition temperature, T_C, the potential field must cause a force acting on ion A which results in a displacement from the central position in the unit cell such that a non-symmetric phase in the equilibrium structure is realized at temperatures $T = 0$.

If it assumed, for the sake of simplicity, that the ions A can move only along one direction, e. g. the x-axis, it is assumed that the potential created by these forces must be symmetric in x with respect to the centre of the unit cell. The simplest version for such a potential describes a scalar (one-dimensional) displacement of each ion A and possesses two minima at $x \neq 0$ rendering the case of an electric polarization along x and $-x$ (Fig. 4.1b).
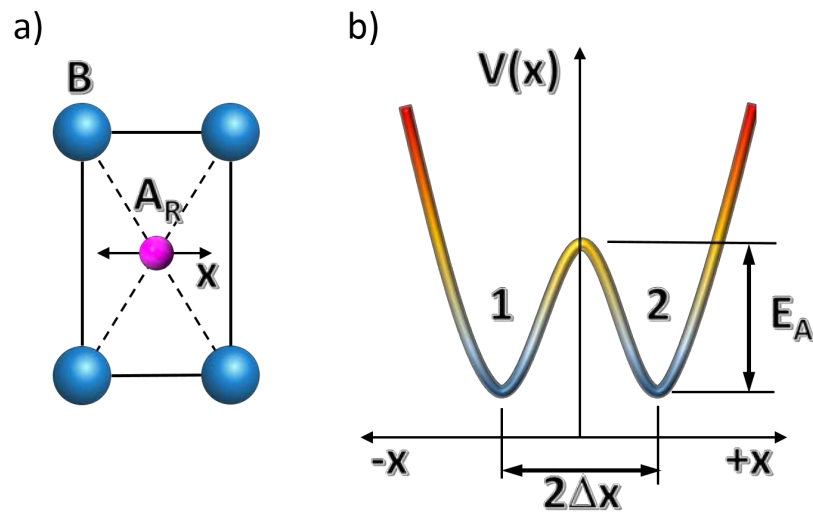
Figure 4.1: *Diatomic crystal and the single ion model.* (a) Unit cell of a diatomic crystal consisting of ions A and B. According to the single ion model, the ions A can move whereas the ions B remain immovable. (b) Potential energy of ion A in the field of ion B. After [99]

However, the forces caused by ion B acting on ion A is not sufficient to describe a ferroelectric phase transition since the ions A are independent from each other in that case, and a phase transition to a ferroelectric state will never occur [99].

Thus it is immediately clear that the introduction of an interaction between various ions A is necessary for rendering ferroelectric phase transitions because the evolvement of a spontaneous electric polarization is linked to a cooperative displacement of ions A. The unidimensional analogue of that system can be represented as an array of ions A aligned on a straight line and connected by springs, whereas each of the ion A is moving it its local double well potential. This model is called in literature the ϕ^4 single ion model [111, 112, 113, 114, 115] (Fig. 4.2).

The Hamiltonian in the three-dimensional case, assuming that the interaction of ions A with other ions A is described by the potential of the elastic spring, is given by,
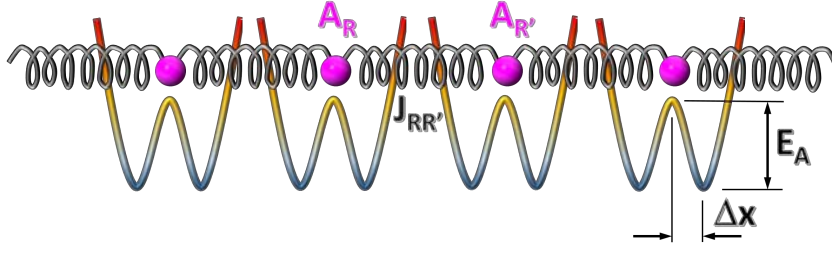
Figure 4.2: ϕ^4 *single ion model* . The model contains an one-dimensional array of ions linked by harmonic forces with one ion in each unit cell. Each ion "sees" a local double well potential which is assumed to represent the rest of the crystal. The double well potential provides the driving force for the phase ferroelectric phase transition. After [99, 100, 116]

$$\mathcal{H} = \underbrace{\frac{1}{2}\sum_{\mathbf{R}} m\left(\frac{\mathrm{d}x_{\mathbf{R}}}{\mathrm{d}t}\right)^2}_{I} + \underbrace{\sum_{\mathbf{R}}\left(-\eta x_{\mathbf{R}}^2 + \vartheta x_{\mathbf{R}}^4\right)}_{II} + \underbrace{\frac{1}{2}\sum_{\mathbf{R},\mathbf{R}'\neq\mathbf{R}}\frac{J_{\mathbf{R},\mathbf{R}'}\left(x_{\mathbf{R}} - x_{\mathbf{R}'}\right)^2}{2}}_{III} \quad (4.26)$$

The I-Term describes the kinetic energy with each atom has mass m , the II-Term defines the double-well potential $V\left(x_{\mathbf{R}}\right) = -\eta x_{\mathbf{R}}^2 + \vartheta x_{\mathbf{R}}^4$, i.e. this term describes an assembly of N uncoupled oscillators (ions A) moving in an anharmonic potential. The III-Term considers the interaction of ions A among each other. Since the energy of a given spring will appear twice if the sum $\sum_{\mathbf{R},\mathbf{R}'\neq\mathbf{R}}\frac{J_{\mathbf{R},\mathbf{R}'}\left(x_{\mathbf{R}}-x_{\mathbf{R}'}\right)^2}{2}$ is performed for each atom the factor $\frac{1}{2}$ is necessary for the correct value of the total energy. Here η, ϑ are positive constants defining the shape of the double-well potential, $x_{\mathbf{R}}$ is the displacement along the x-direction of ion A present in the unit cell, the centre of which has a coordinate given by, $\mathbf{R} = n_1\mathbf{a} + n_2\mathbf{b} + n_3\mathbf{c}$, where $\mathbf{a}, \mathbf{b}, \mathbf{c}$ are the vectors of unit translation and $J_{\mathbf{R},\mathbf{R}'}$ determines the interaction of ions A arranged at points with the radius-vector $\mathbf{R}$ and $\mathbf{R}'$. Rearrangement of Eq. (4.26) leads to[14],

$$\mathcal{H} = \frac{1}{2}\sum_{\mathbf{R}} m\left(\frac{\mathrm{d}x_{\mathbf{R}}}{\mathrm{d}t}\right)^2 + \sum_{\mathbf{R}}\left[\left(-\eta + \frac{J_0}{2}\right)x_{\mathbf{R}}^2 + \vartheta x_{\mathbf{R}}^4\right] - \frac{1}{2}\sum_{\mathbf{R},\mathbf{R}'} J_{\mathbf{R},\mathbf{R}'} x_{\mathbf{R}} x_{\mathbf{R}'} \quad (4.27)$$

where $J_0 = \sum_{\mathbf{R}'} J_{\mathbf{R},\mathbf{R}'}$ which represents the constant that characterizes the interaction of a ion A at an arbitrary position $\mathbf{R}$ with all other ions A being located within the interaction radius. It characterizes the total number of ions A, whose position is still influenced by the

---

[14]
$$\mathcal{H} = \frac{1}{2}\sum_{\mathbf{R}} m\left(\frac{\mathrm{d}x_{\mathbf{R}}}{\mathrm{d}t}\right)^2 + \sum_{\mathbf{R}}\left(-\eta x_{\mathbf{R}}^2 + \vartheta x_{\mathbf{R}}^4\right) + \frac{1}{4}\left(\underbrace{\sum_{\mathbf{R},\mathbf{R}'} J_{\mathbf{R},\mathbf{R}'} x_{\mathbf{R}}^2 + \sum_{\mathbf{R},\mathbf{R}'} J_{\mathbf{R},\mathbf{R}'} x_{\mathbf{R}'}^2}_{2\sum_{\mathbf{R},\mathbf{R}'} J_{\mathbf{R},\mathbf{R}'} x_{\mathbf{R}}^2}\right)$$
$$- \frac{1}{2}\sum_{\mathbf{R},\mathbf{R}'} J_{\mathbf{R},\mathbf{R}'} x_{\mathbf{R}} x_{\mathbf{R}'}$$

Thus, with $\frac{1}{2}\sum_{\mathbf{R},\mathbf{R}'} J_{\mathbf{R},\mathbf{R}'} x_{\mathbf{R}}^2 = \frac{1}{2}\sum_R x_{\mathbf{R}}^2 \sum_{R'} J_{\mathbf{R},\mathbf{R}'}$ and with $J_0 = \sum_{\mathbf{R}'} J_{\mathbf{R},\mathbf{R}'}$ the Hamiltonian becomes
$\mathcal{H} = \frac{1}{2}\sum_{\mathbf{R}} m\left(\frac{\mathrm{d}x_{\mathbf{R}}}{\mathrm{d}t}\right)^2 + \sum_{\mathbf{R}}\left(-\eta x_{\mathbf{R}}^2 + \vartheta x_{\mathbf{R}}^4\right) + \frac{1}{2}\sum_{\mathbf{R}} J_0 x_{\mathbf{R}}^2 - \frac{1}{2}\sum_{\mathbf{R},\mathbf{R}'} J_{\mathbf{R},\mathbf{R}'} x_{\mathbf{R}} x_{\mathbf{R}'}$

movement of one ion A arranged at point $\mathbf{R}$. The last term in Eq. (4.27) is bilinear in displacements of ions A at $\mathbf{R}$ and $\mathbf{R}'$and therefore it corresponds to a dipole-dipole interaction. Hence[15],

$$J_{\mathbf{R},\mathbf{R}'} = -\frac{q^2}{4\pi\varepsilon_0}\frac{\left[\cos\left(\varphi_{\mathbf{R},\mathbf{R}'}\right) - 3\cos\left(\varphi_{(\mathbf{R}-\mathbf{R}'),\mathbf{R}}\right)\cos\left(\varphi_{(\mathbf{R}-\mathbf{R}'),\mathbf{R}'}\right)\right]}{|\mathbf{R}-\mathbf{R}'|^3} \tag{4.28}$$

Thus,

$$J_0 = -\frac{q^2}{4\pi\varepsilon_0}\sum_{\mathbf{R}'}\frac{\left[\cos\left(\varphi_{\mathbf{R},\mathbf{R}'}\right) - 3\cos\left(\varphi_{(\mathbf{R}-\mathbf{R}'),\mathbf{R}}\right)\cos\left(\varphi_{(\mathbf{R}-\mathbf{R}'),\mathbf{R}'}\right)\right]}{|\mathbf{R}-\mathbf{R}'|^3} \tag{4.29}$$

Hence, for the simple dipole configurations follows (arrows illustrate the arrangement and direction of the dipole moment),

$$
\begin{aligned}
\downarrow\downarrow \quad J_{\mathbf{R},\mathbf{R}'} &= \quad -\frac{q^2}{4\pi\varepsilon_0\,|\mathbf{R}-\mathbf{R}'|^3} \\
\downarrow\uparrow \quad J_{\mathbf{R},\mathbf{R}'} &= \quad +\frac{q^2}{4\pi\varepsilon_0\,|\mathbf{R}-\mathbf{R}'|^3} \\
\rightarrow\rightarrow \quad J_{\mathbf{R},\mathbf{R}'} &= \quad -\frac{q^2}{2\pi\varepsilon_0\,|\mathbf{R}-\mathbf{R}'|^3} \\
\rightarrow\leftarrow \quad J_{\mathbf{R},\mathbf{R}'} &= \quad +\frac{q^2}{2\pi\varepsilon_0\,|\mathbf{R}-\mathbf{R}'|^3} \\
\uparrow\rightarrow \quad J_{\mathbf{R},\mathbf{R}'} &= \quad 0
\end{aligned}
\tag{4.30}
$$

Basically, the model defined by Eq. (4.26) has two important quantities. The first is the depth of the potential well, V_0, respectively the hight of the energy barrier, $E_A = |V_0|$ (Fig. 4.1). The minima of $V(x)$ occur at $x = \pm\Delta x$, so that distance between two local equilibrium positions is $2\Delta x$. Thus with $\frac{dV}{dx}\big|_{\Delta x} := 0$ follows,

$$
\begin{aligned}
\textbf{I)} \quad & \frac{\eta}{2\vartheta} \;=\; (\Delta x)^2 \\
\textbf{II)} \quad & V_0 \;=\; -\frac{1}{2}\eta\,(\Delta x)^2
\end{aligned}
\tag{4.31}
$$

With the set of equations in Eq. (4.31) the shape parameters of the double-well potential can be determined by fundamental properties, i.e. the hight of the energy barrier and the half-distance between two local equilibrium positions as,

---

[15]The energy between two electric dipoles are given by [41] $E = \frac{1}{4\pi\varepsilon_0}\frac{D^2\mathbf{p_R}\cdot\mathbf{p_{R'}} - 3(\mathbf{D}\cdot\mathbf{p_R})(\mathbf{D}\cdot\mathbf{p_{R'}})}{D^5}$ where D is the distance between the dipoles. With $\mathbf{p_R} = q\mathbf{x_R}$ and $\mathbf{p_{R'}} = q\mathbf{x_{R'}}$ the energy becomes $E = \frac{1}{4\pi\varepsilon_0}\frac{D^2 q^2 x_\mathbf{R} x_{\mathbf{R}'}\cos(\varphi_{\mathbf{R},\mathbf{R}'}) - 3D^2 q^2 x_\mathbf{R} x_{\mathbf{R}'}\cos(\varphi_{\mathbf{D},\mathbf{R}})\cos(\varphi_{\mathbf{D},\mathbf{R}'})}{D^5} \Rightarrow E = \frac{1}{4\pi\varepsilon_0}\frac{q^2 x_\mathbf{R} x_{\mathbf{R}'}\left[\cos(\varphi_{\mathbf{R}\mathbf{R}'}) - 3\cos(\varphi_{\mathbf{D}\mathbf{R}})\cos(\varphi_{\mathbf{D}\mathbf{R}'})\right]}{D^3}$.

$$\eta = \; 2\frac{E_A}{(\Delta x)^2}$$
$$\vartheta = \; \frac{E_A}{(\Delta x)^4} \tag{4.32}$$

The second important quantity is the interaction energy, W, of one ion A arranged at point $\mathbf{R}$ with all other ions A being located within the interaction radius. With the maximum displacement of $\pm\Delta x$ of ion A present in the unit cell, the maximal interaction energy of one ion A arranged at point $\mathbf{R}$ becomes[16],

$$\begin{aligned} W = \; & \underbrace{\sum_{\mathbf{R}' \neq \mathbf{R}} \frac{1}{2} J_{\mathbf{R},\mathbf{R}'} \left(x_{\mathbf{R}} - x_{\mathbf{R}'}\right)^2} \\ = \; & \sum_{\mathbf{R}' \neq \mathbf{R}} \frac{1}{2} J_{\mathbf{R},\mathbf{R}'} \left(2\Delta x\right)^2 \\ = \; & 2\left(\Delta x\right)^2 \sum_{\mathbf{R}' \neq \mathbf{R}} J_{\mathbf{R},\mathbf{R}'} \\ = \; & 2\left(\Delta x\right)^2 J_0 \end{aligned} \tag{4.33}$$

The ratio of these two quantities,

$$s = \frac{E_A}{W} = \frac{E_A}{2\left(\Delta x\right)^2 J_0} \tag{4.34}$$

gives the relative strengths of the local double-well potential and the energy of interaction of an ion with its neighbours [117]. Depending on the value of that ratio, two limiting cases can be distinguished.

4.1.4.1   Order-Disorder limit

The case $s \gg 1$ corresponds to the order-disorder limit [116, 100]. In this case the potential barrier between the two wells is much higher than the interaction between neighbouring ions A. Even at a temperature well above the transition temperature, $T \gg T_C$ with $J_0 \leq k_B T \leq E_A$, the ions will reside in one or other of the two wells, albeit with a random occupancy thus in turn no macroscopic electric polarization is generated, $\bar{\pi}_S = 0$ (Fig. 4.3).

On cooling toward the transition temperature, $T > T_C$, the effects of interactions become more significant and a degree of short-range order is established, i.e. on a mesoscopic scale a electric polarization exists but still on a macroscopic scale $\bar{\pi}_S = 0$. However, the spatial range of this short-range order grows on cooling toward T_C.

Below the transition temperature, $T < T_C$, the probability is greater that one side of the double-well potential (in this case the left-hand side) will be occupied. A long-range order is established and accordingly a macroscopic electric polarization appears, $\bar{\pi}_S \neq 0$. But, there is also a significant probability that some atoms will occupy the alternative potential well [116].

---

[16]Energy stored in one spring at maximal compression

At very low temperatures, $T \ll T_C$, most of the ions A occupy the same side of the double-well potential. Thus the electric polarization reaches its maximum, $\bar{\pi}_S = \bar{\pi}_{S,max}$.
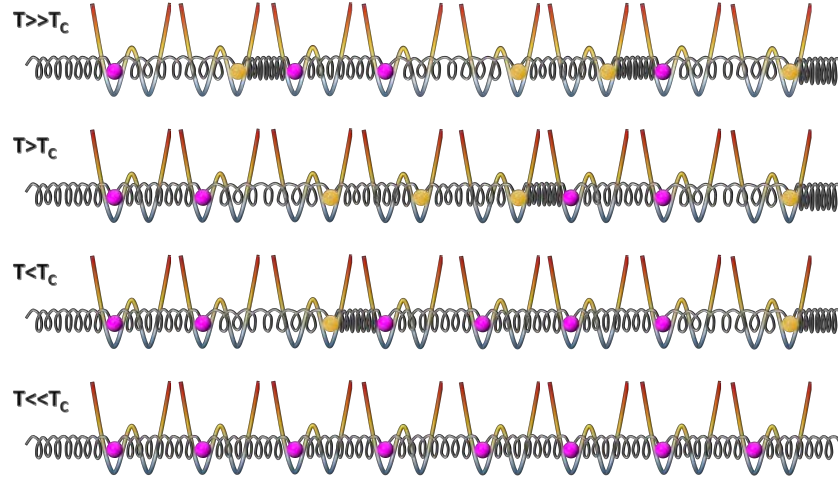
Figure 4.3: *Sequence showing the ordering of atoms in the order-disorder limit. At high temperatures $(T \gg T_C)$ the positions of neighbouring ions are not correlated in any significant way (magenta and yellow balls indicate ions in the left or in the right state of the double-well potential). Near the transition temperature a degree of short-range order is established. Below the transition temperature one side of the double-well potential is favoured and a long-range order appears. Well below the transition temperature each ion occupies the same side of the double-well potential.*

Because in this limit the displacements are all $x_{\mathbf{R}} \approx \pm \Delta x$ for most temperatures, the entropy is purely configurational. In that case, the transition temperature can be readily estimated by the equilibrium condition of the free energy. With Eqs. (2.12,2.13, 2.14), the equilibrium condition is given by,

$$\mathrm{d}F = \mathrm{d}U - S\mathrm{d}T = 0 \tag{4.35}$$

If a completely chaotic position of ions A at $T \geq T_C$ is assumed, half of the springs appear to be deformed. The energy of the system in the order-disorder limit is solely determined by these deformation of the springs (no kinetic energy exists) so that the energy of the system increases as compared with the energy at $T = 0$ whereas the interaction energy Eq. (4.33) becomes $W = 0$,

$$dU \sim U(T_C) - U(T = 0) = W\frac{N}{2} = N\left(\Delta x\right)^2 J_0 \tag{4.36}$$

The entropy, S, is a logarithmic measure of the number of possible microstates, Ω, for a given energy and is defined as,

$$S = k_B \ln \Omega \tag{4.37}$$

The number of possible microstates is given by the binomial coefficient since there are $\frac{N!}{k!(N-k)!}$ possibilities of k deformed springs of N total springs in the system. At T_C, $k = N/2$

thus with Eq. (4.35) in equilibrium follows,

$$N \left(\Delta x \right)^2 J_0 = k_B T_C \ln \frac{N!}{\left[\left(\frac{N}{2}! \right) \right]^2} \tag{4.38}$$

With Stirling's formula, $\ln N! \approx N \ln N - N$ for large N, the transition temperature can be determined from Eq. (4.38) as,

$$k_B T_C = \frac{J_0 \left(\Delta x \right)^2}{\ln 2} \tag{4.39}$$

Thus with Eq. (4.34) follows,

$$s = \frac{E_A}{k_B T_C \ln 4} \gg 1 \tag{4.40}$$

A more thorough analysis with a nearest-neighbour coupling of the ions A leads to [111],

$$k_B T_C = 2 d k_d J \frac{\eta}{\vartheta} = 4 d k_d J \left(\Delta x \right)^2 \tag{4.41}$$

where J is the nearest neighbour coupling constant, d is the dimension of the system and k_d is a constant with $k_{d=2} = 0.5673$ and $k_{d=3} = 0.76$. Thus on a cubic lattice the transition temperature is calculated as,

$$k_B T_C = 9.12 J \left(\Delta x \right)^2 \tag{4.42}$$

Hence with Eq. (4.34) for an order-disorder phase transition follows,

$$s = 4.56 \frac{E_A}{k_B T_C} \gg 1 \tag{4.43}$$

4.1.4.2 Displacive limit

Here the forces between ions are much larger than the forces due to the local potential. Unlike in the order-disorder limit, at high temperatures the local potential does not force ions to stay on one or the other side of the origin because $k_B T_C \gg E_A$ thus $\bar{\pi}_S = 0$ (Fig. 4.4).

Instead the ions vibrate about the origin, and the shape of the double-well potential has only a small effect to modify the phonon frequencies [116, 100].

Below the transition temperature the mean positions of all the ions are displaced by the same small amount to one side of the origin, thus $\bar{\pi}_S \neq 0$, and the size of this displacement increases on further cooling. Hence at $T = 0$, $\bar{\pi}_S = \bar{\pi}_{S,max}$. Displacive phase transitions have been understood in terms of the soft-mode theory [98, 118, 119, 117, 120, 121].

The central idea of the soft mode theory is that in the high-temperature phase a lattice vibration (normal mode) exists with a critical wave vector for which the frequency falls to zero on cooling toward the transition temperature [98]. It is given by,

$$\omega^2 \left(\mathbf{q} \right) = K \left(T - T_C \right) + A^2 \left(\mathbf{q} - \mathbf{q}_C \right)^2 \tag{4.44}$$
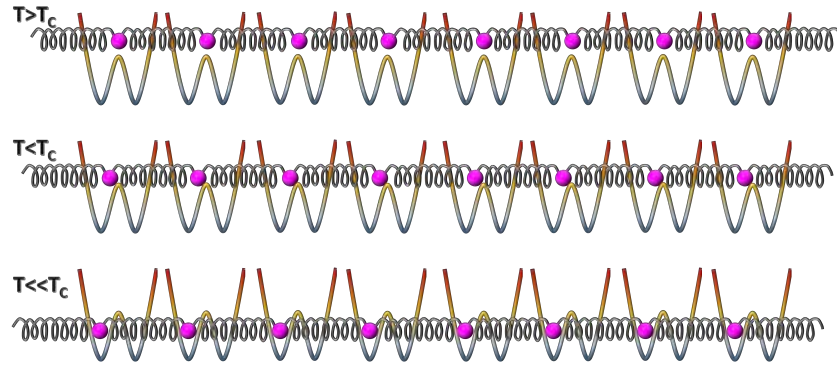
Figure 4.4: *Sequence showing the ordering of atoms in the displacive limit.* At high temperatures $(T \gg T_C)$ ions vibrate about the origin. Below the transition temperature the ions vibrate about the their new equilibrium positions which are equally displaced from the origin.

where $\mathbf{q}$ and $\mathbf{q}_C$ are the wave vector respectively the critical wave vector which measures the phase difference among the atomic displacements from one unit cell to the other. K and A are constants. The derivation of Eq. (4.44) is given in section (4.5). A vanishing frequency implies a vanishing restoring force against the corresponding deformation, i.e. one of the elementary excitations (phonon) becomes unstable as $T \to T_C$ which is the reason that it is called soft mode. The atomic displacements associated with the soft mode are the same as the deformation of the structure in the low-temperature phase.

For a ferroelectric phase transition the critical wave vector is zero, $\mathbf{q}_C = 0$, hence the displacements are identical for all unit cells. The instability occurs at the centre of the Brillouin zone and there is no change in the number of atoms per unit cell (Fig. 4.5) [100].
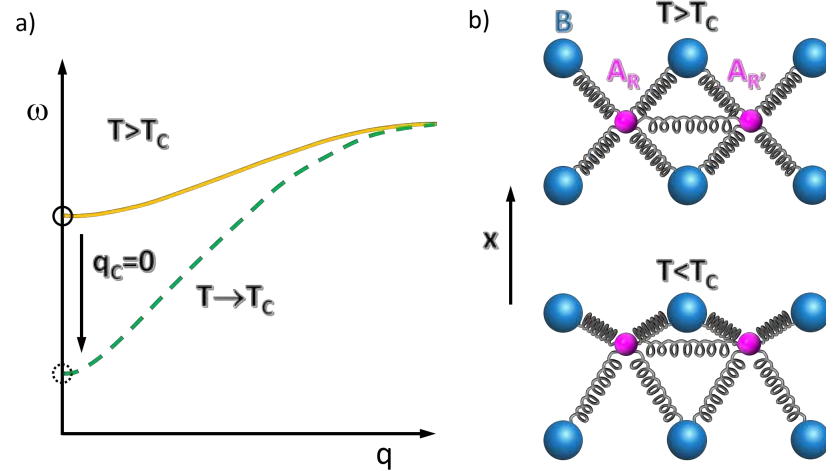
Figure 4.5: *Schematic representations of a ferroelectric soft mode behaviour.* a) behaviour of the phonon dispersion curves; b) atomic distortions. After [100]

For an antiferroelectric phase transition, $\mathbf{q}_C \neq 0$, and the magnitude and direction of $\mathbf{q}_C$ determine the size of the new unit cell. For a zone boundary soft mode (Fig. 4.6) the unit cell of the low temperature phase is doubled in one or more directions.
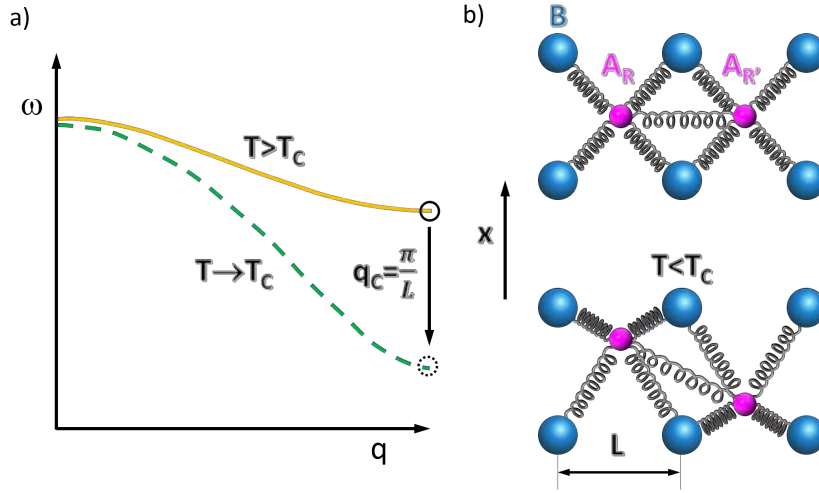
Figure 4.6: *Schematic representations of an antiferroelectric soft mode behaviour.*
a) zone boundary soft optic mode, and b) atomic displacements
showing doubling of the unit cell and the cancelling induced dipole
moments. After [100].

In the displacive case the energy difference between the symmetric, $T > T_C$, and non-symmetric phase, $T < T_C$, contains important contribution from changes in the vibrational energy and the entropy is determined by vibrational contribution rather than from any configurational term. Thus the estimation of the transition temperature based on rough calculations as in chapter 4.1.4.1 is not possible. However, with a nearest-neighbour coupling of the ions A follows [117],

$$k_B T_C = \frac{2}{3w_3} J \frac{\eta}{\vartheta} = \frac{4}{3w_3} J (\Delta x)^2 \tag{4.45}$$

where $w_3 = 0.5054$. Thus,

$$k_B T_C = 2.64 J (\Delta x)^2 \tag{4.46}$$

Hence for an displacive phase transition follows with Eq. (4.34),

$$s = 1.32 \frac{E_A}{k_B T_C} \ll 1 \tag{4.47}$$

4.2 Dynamic critical phenomena

The dynamic behaviour of a medium i.e. the relaxation from non-equilibrium back to equilibrium exhibits also anomalous characteristics near the critical temperature, T_C. Essentially, the theory of dynamic critical phenomena for a multivariable system can be formulated as a generalization of the single particle Langevin equation. The equation of motion for the time-dependent local configuration of the order parameter field is most conveniently given by the time-dependent Ginzburg-Landau equation [110, 101, 122] given by,

$$\frac{\partial \pi\left(\mathbf{r},t\right)}{\partial t} = -\Gamma \frac{\delta \mathcal{H}\left[\pi\left(\mathbf{r},t\right)\right]}{\delta \pi\left(\mathbf{r},t\right)} + \zeta\left(\mathbf{r},t\right) \tag{4.48}$$

where $\frac{\delta \mathcal{H}[\pi(\mathbf{r},t)]}{\delta \pi(\mathbf{r},t)}$ is the functional derivative of $\mathcal{H}\left[\pi\left(\mathbf{r},t\right)\right]$. Here, Γ is a dissipation para-meter, and $\zeta\left(\mathbf{r},t\right)$ is a random noise simulating the effect of thermal excitation of the order parameter.

In order to guarantee that the system reaches the canonical equilibrium probability dis-tribution at long times, $\zeta\left(\mathbf{r},t\right)$ is a random Gaussian variable satisfying $\langle \zeta\left(\mathbf{r},t\right)\rangle = 0$ and $\langle \zeta\left(\mathbf{r}',t\right)\zeta\left(\mathbf{r},t'\right)\rangle = 2Dk_B T \delta\left(\mathbf{r}-\mathbf{r}'\right)\delta(t-t')$ [123], where D is the diffusion coefficient. With Eq. (4.7), Eq. (4.13) and with $E\left(\mathbf{r}\right) = 0$, Eq. (4.48) becomes,

$$\frac{1}{\Gamma}\frac{\partial \pi\left(\mathbf{r},t\right)}{\partial t} = -\left[2a\pi\left(\mathbf{r}\right) + 4b\pi^3\left(\mathbf{r}\right) + 6c\pi^5\left(\mathbf{r}\right)\ldots - 2K\boldsymbol{\nabla}^2\pi\left(\mathbf{r}\right)\right] + \zeta\left(\mathbf{r},t\right) \tag{4.49}$$

Because of the non-linear terms in Eq. (4.49), it is not possible to integrate this equation. However, if only the high temperature phase is considered, the Gaussian model can be applied [101, 110] and Eq. (4.49) reduces to,

$$\frac{\partial \pi\left(\mathbf{r},t\right)}{\partial t} = -\Gamma\left[2a\pi\left(\mathbf{r}\right) - 2K\boldsymbol{\nabla}^2\pi\left(\mathbf{r}\right)\right] + \zeta\left(\mathbf{r},t\right) \tag{4.50}$$

Transforming Eq. (4.50) into Fourier space[17] leads to,

$$\frac{\partial \pi\left(\mathbf{q},t\right)}{\partial t} = -2\Gamma\left[a + K\mathbf{q}^2\right]\pi\left(\mathbf{q},t\right) + \zeta\left(\mathbf{q},t\right) \tag{4.51}$$

The average of $\pi\left(\mathbf{q},t\right)$ satisfies with $\langle \zeta\left(\mathbf{q},t\right)\rangle = 0$,

$$\frac{\partial \langle \pi\left(\mathbf{q},t\right)\rangle}{\partial t} = -2\Gamma\left[a + K\mathbf{q}^2\right]\langle \pi\left(\mathbf{q},t\right)\rangle \tag{4.52}$$

Thus, $\langle \pi\left(\mathbf{q},t\right)\rangle$ decay rapidly as $\exp\left(-t/\tau\right)$ with following relaxation time,

$$\tau = \frac{1}{2\Gamma\left[a + K\mathbf{q}^2\right]} \tag{4.53}$$

As a consequence, each Fourier component of the order parameter behaves as an inde-pendent particle connected to a spring [101] and the fluctuations in each mode decay with a different relaxation time. Additionally, at the critical temperature, $T = T_C$, $a = 0$ [104] and the relaxation time diverges in the long wave length limit ($q = 0$). Accordingly, at the phase transition temperature, the system does not relax but follows any perturbation without any drag.

In case when $E\left(\mathbf{r}\right)$ depends on time, Eq. (4.48) becomes in Fourier space[18] with applying Gaussian approximation,

$$-i\omega\pi\left(\mathbf{q},\omega\right) = -2\Gamma\left[a + K\mathbf{q}^2\right]\pi\left(\mathbf{q},\omega\right) + \zeta\left(\mathbf{q},\omega\right) + \Gamma gE\left(\mathbf{q},\omega\right) \tag{4.54}$$

---

[17] $\pi\left(\mathbf{r},t\right) = C\int \pi\left(\mathbf{q},t\right)\exp\left(i\mathbf{q}\mathbf{r}\right)\mathrm{d}\mathbf{r}$

[18] $\pi\left(\mathbf{r},t\right) = C\int \pi\left(\mathbf{q},\omega\right)\exp\left(i\left(\mathbf{q}\mathbf{r}-\omega t\right)\right)\mathrm{d}\mathbf{r}\mathrm{d}t$

From Eq. (4.54), the susceptibility is given with $\chi\left(\mathbf{q},\omega\right) = \frac{1}{\varepsilon_0}\frac{d\pi(\mathbf{q},\omega)}{dE(\mathbf{q},\omega)}$,

$$\chi\left(\mathbf{q},\omega\right) = \frac{1}{\varepsilon_0}\frac{g\Gamma}{2\Gamma\left[a + K\mathbf{q}^2\right] - i\omega} = \frac{1}{\varepsilon_0}\frac{g\Gamma}{\tau^{-1} - i\omega} \tag{4.55}$$

Two important properties of the susceptibility exist. First, in the static limit, $\omega \to 0$, $\chi\left(\mathbf{q},0\right) = \varepsilon_0^{-1}g\Gamma\tau$, and second, the susceptibility is purely imaginary, $\chi\left(0,\omega\right) = i\frac{g\Gamma}{\omega}\varepsilon_0^{-1}$ in the long wave length limit and at the critical temperature.

For an averaged order parameter field, i.e. homogeneous order parameter, Eq. (4.48) reduces to the Landau-Khalatnikov equation [98, 124, 125, 126, 127, 128, 129, 130] and becomes with Eq. (4.12)[19],

$$\frac{\mathrm{d}\bar{\pi}_S}{\mathrm{d}t} = -\Gamma\frac{\mathrm{d}\mathcal{H}\left(\bar{\pi}_S\right)}{\mathrm{d}\bar{\pi}_S} = -\Gamma V^{-1}\frac{\mathrm{d}F\left(\bar{\pi}_S\right)}{\mathrm{d}\bar{\pi}_S} \tag{4.56}$$

According to Eq. (4.12) the relaxation dynamic of the order parameter is given by,

$$\frac{\mathrm{d}\bar{\pi}_S}{\mathrm{d}t} = -\Gamma\left(2a\bar{\pi}_S + 4b\bar{\pi}_S^3 + 6c\bar{\pi}_S^5 + \ldots - gE_0\right) \tag{4.57}$$

Considering only second order phase transitions ($c = 0$), and substituting $E_0(t) = \delta E\exp(-i\omega t)$ and $\bar{\pi}_S(t) = \bar{\pi}_S^{static} + \delta\bar{\pi}_S\exp(-i\omega t)$ [119], Eq. (4.57) becomes,

$$
\begin{aligned}
-i\omega\delta\bar{\pi}_S\exp(-i\omega t) = \quad &-\Gamma\Bigg[2a\delta\bar{\pi}_S\exp(-i\omega t) + 4b\delta\bar{\pi}_S^3\exp(-3i\omega t) \\
&+ \quad 12b\delta\bar{\pi}_S^2\bar{\pi}_S^{static}\exp(-2i\omega t) + 12b\delta\bar{\pi}_S\left(\bar{\pi}_S^{static}\right)^2\exp(-i\omega t) \\
&+ \quad -\delta Eg\exp(-i\omega t) + 2a\bar{\pi}_S^{static} + 4b\left(\bar{\pi}_S^{static}\right)^3\Bigg]
\end{aligned}
\tag{4.58}
$$

From the stability condition ($\frac{\mathrm{d}F}{\mathrm{d}\bar{\pi}_S}\big|_{E=0} = 0$) follows,

$$2a\bar{\pi}_S^{static} + 4b\left(\bar{\pi}_S^{static}\right)^3 = 0 \tag{4.59}$$

It is assumed that $\delta\bar{\pi}_S$ is very small. Thus only first order of smallness will be regarded and higher order of smallness is assumed to be negligible ($\delta\bar{\pi}_S^2 \approx 0$, $\delta\bar{\pi}_S^3 \approx 0$). Hence, Eq.(4.58) becomes,

$$\delta\bar{\pi}_S = \frac{g\Gamma}{\Gamma\left[2a + 12b\left(\bar{\pi}_S^{static}\right)^2\right] - i\omega}\delta E \tag{4.60}$$

Comparing Eq. (4.60) with Eq. (4.55) the relaxation time in Eq. (4.60) is given by,

$$\tau^{-1} = \Gamma\left[2a + 12b\left(\bar{\pi}_S^{static}\right)^2\right] \tag{4.61}$$

and the electric susceptibility $\left(\chi = \frac{1}{\varepsilon_0}\frac{\delta\bar{\pi}_S}{\delta E}\right)$ by,

---

[19]If a kinetic energy term ($\frac{\mathrm{d}^2\bar{\pi}_S}{\mathrm{d}t^2}$) is added to the equation of motion, resonance phenomena can be described in addition to relaxation phenomena.

$$\chi\left(\omega\right) = \frac{\varepsilon_0^{-1} g \Gamma \tau}{1 - i\tau\omega} \tag{4.62}$$

where the static susceptibility is given by,

$$\chi\left(\omega = 0\right) = \chi_{static} = \varepsilon_0^{-1} g \Gamma \tau \tag{4.63}$$

With Eq.(4.59) the order parameter above and below the phase transition temperature is given by,

$$\bar{\pi}_S^{static} = \begin{cases} 0 & T > T_C \\ \sqrt{-\frac{1}{2}\frac{a}{b}} & T < T_C \end{cases} \tag{4.64}$$

Thus, the relaxation time and static susceptibility are given by,

$$\tau^{-1} = \begin{cases} 2a\Gamma & T > T_C \\ -4a\Gamma & T < T_C \end{cases} \tag{4.65}$$

$$\chi_{static}^{-1} = \begin{cases} 2\frac{a}{g}\varepsilon_0 & T > T_C \\ -4\frac{a}{g}\varepsilon_0 & T < T_C \end{cases} \tag{4.66}$$

which are in accordance to Lines and Glass [119], Mason [131], Blinc [98] and Nishimori [110]. With, $a\left(T = T_C\right) = 0$, $a\left(T > T_C\right) > 0$ and $a\left(T < T_C\right) < 0$.

According to Eq. (5.24) the permittivity becomes with Eq. (4.62) and Eq. (4.63),

$$\frac{\varepsilon\left(\omega\right)}{\varepsilon_0} = 1 + \underbrace{\frac{\chi_{static}}{1 - i\tau\omega}}_{\text{phase transition}} + \sum_{i}^{N-1} \chi_i\left(\omega\right) \tag{4.67}$$

With

$$\begin{aligned}
\varepsilon\left(\omega \gg \tau^{-1}\right) = \varepsilon\left(\infty\right) = &\ \varepsilon_0 \left[1 + \sum_{i}^{N-1} \chi_i\left(\omega\right)\right] \\
\varepsilon\left(\omega \ll \tau^{-1}\right) = \varepsilon\left(0\right) = &\ \varepsilon_0 \left[1 + \chi_{static} + \sum_{i}^{N-1} \chi_i\left(\omega\right)\right]
\end{aligned} \tag{4.68}$$

the permittivity is given by,

$$\varepsilon\left(\omega\right) = \varepsilon\left(\infty\right) + \underbrace{\frac{\Delta\varepsilon_r}{1 - i\tau\omega}}_{\text{phase transition}} \tag{4.69}$$

with $\Delta\varepsilon = \varepsilon_0 \chi_{static}$. Therefore, the relaxation strength of a relaxation mode governed by a phase transition process is given by,

$$\left(\frac{\Delta\varepsilon}{\varepsilon_0}\right)^{-1} = \Delta\varepsilon_r^{-1} = \chi_{static}^{-1} = \begin{cases} 2\frac{a}{g}\varepsilon_0 & T > T_C \\ -4\frac{a}{g}\varepsilon_0 & T < T_C \end{cases} \tag{4.70}$$

In order to determine the temperature dependence of the relaxation time and the susceptibility near the phase transition temperature, the parameters a, g, and Γ must be specified. This can be achieved either by applying statistical theories of ferroelectric phase transitions leading to an expression of the free energy or by applying microscopic theories of dynamic processes.

4.3 Statistical theory of order-disorder phase transition: The pseudo spin model

In the order disorder limit each ion is well localized in one of the two bottoms of its double well as long the thermal energy is small compared to the energy-barrier separating the two energy wells. Accordingly, all $x_{\mathbf{R}} \approx \Delta x \sigma_{\mathbf{R}}$ for all temperatures, where $\sigma_{\mathbf{R}} = \pm 1$ depending on the sign of $x_{\mathbf{R}}$. In an external electric field, an additional force with $F = qE$ is acting on each ion A where q is the charge of ion A. Hence, the additional energy, $U_{\mathbf{R}} = -qx_{\mathbf{R}}E$, has to be considered. The total energy in the order-disorder limit is then given by (Eq. 4.27),

$$\mathcal{H} = \frac{1}{2}\sum_{\mathbf{R}} m\Delta x \underbrace{\left(\frac{d\sigma_{\mathbf{R}}}{dt}\right)^2}_{0} + \underbrace{\sum_{\mathbf{R}}\left[(\Delta x)^2\left(-\eta + \frac{J_0}{2}\right)\sigma_{\mathbf{R}}^2 + (\Delta x)^4\vartheta\sigma_{\mathbf{R}}^4\right]}_{C}$$
$$- \frac{1}{2}(\Delta x)^2\sum_{\mathbf{R},\mathbf{R}'} J_{\mathbf{R},\mathbf{R}'}\sigma_{\mathbf{R}}\sigma_{\mathbf{R}'} - q\Delta xE\sum_{\mathbf{R}}\sigma_{\mathbf{R}} \tag{4.71}$$

Because in that limit, the kinetic energy vanishes and the double-well energy contribution is just a constant with $C = N\left[(\Delta x)^2\left(-\eta + \frac{J_0}{2}\right) + (\Delta x)^4\vartheta\right]$ where N is the total number of ions A, the ϕ^4 single ion model represents an array of spins with a spin pointing left or right ($\sigma_{\mathbf{R}} = \pm 1$). Since these spins are not magnetic spins, they are called "*pseudo spins*" and the total energy is represented as,

$$\mathcal{H} \propto -\frac{1}{2}(\Delta x)^2\sum_{\mathbf{R},\mathbf{R}'} J_{\mathbf{R},\mathbf{R}'}\sigma_{\mathbf{R}}\sigma_{\mathbf{R}'} - q\Delta xE\sum_{\mathbf{R}}\sigma_{\mathbf{R}} \tag{4.72}$$

Equation 4.72 describes the famous Ising model which is probably the best-studied model of a phase transition [132, 133]. With the identity transformation, $\sigma_{\mathbf{R}'} = \langle\sigma_{\mathbf{R}}\rangle + (\sigma_{\mathbf{R}'} - \langle\sigma_{\mathbf{R}}\rangle)$ and $\sigma_{\mathbf{R}} = \langle\sigma_{\mathbf{R}}\rangle + (\sigma_{\mathbf{R}} - \langle\sigma_{\mathbf{R}}\rangle)$, where $\langle\sigma_{\mathbf{R}}\rangle$ is the statistical mean value of the spin variable which is, $\langle\sigma_{\mathbf{R}}\rangle = \frac{N_+ - N_-}{N_+ + N_-}$ where N_+ and N_- being the occupation number of ions A in +1 and -1 state respectively, Eq. (4.72) becomes,

$$
\begin{aligned}
\mathcal{H} \propto \quad & -\frac{1}{2}(\Delta x)^2 \sum_{\mathbf{R},\mathbf{R}'} J_{\mathbf{R},\mathbf{R}'} \left[\langle\sigma_\mathbf{R}\rangle + (\sigma_\mathbf{R} - \langle\sigma_\mathbf{R}\rangle)\right] \left[\langle\sigma_\mathbf{R}\rangle + (\sigma_{\mathbf{R}'} - \langle\sigma_\mathbf{R}\rangle)\right] \\
& - q\Delta x E \sum_{\mathbf{R}} \sigma_\mathbf{R} \\
= & +\frac{1}{2}(\Delta x)^2 \langle\sigma_\mathbf{R}\rangle^2 J_0 \sum_{\mathbf{R}} - (\Delta x)^2 \langle\sigma_\mathbf{R}\rangle J_0 \sum_{\mathbf{R}} \sigma_\mathbf{R} \\
& - \frac{1}{2}(\Delta x)^2 \sum_{\mathbf{R},\mathbf{R}'} J_{\mathbf{R},\mathbf{R}'} (\sigma_\mathbf{R} - \langle\sigma_\mathbf{R}\rangle)(\sigma_{\mathbf{R}'} - \langle\sigma_\mathbf{R}\rangle) - q\Delta x E \sum_{\mathbf{R}} \sigma_\mathbf{R}
\end{aligned}
\tag{4.73}
$$

The term $\sum_{\mathbf{R},\mathbf{R}'} J_{\mathbf{R},\mathbf{R}'} (\sigma_\mathbf{R} - \langle\sigma_\mathbf{R}\rangle)(\sigma_{\mathbf{R}'} - \langle\sigma_\mathbf{R}\rangle)$ describes the interaction energy of fluctuations of the pseudo spin variable at different point $\mathbf{R}$ and $\mathbf{R}'$. Assuming mean-molecular-field approximation by neglecting this contribution to the total energy, Eq. (4.73) becomes with $N = \sum_\mathbf{R}$,

$$
\mathcal{H} \propto \frac{1}{2}(\Delta x)^2 \langle\sigma_\mathbf{R}\rangle^2 J_0 N - \underbrace{\left(\frac{\Delta x \langle\sigma_\mathbf{R}\rangle J_0}{q} + E\right)}_{E_{MMF}} q\Delta x \sum_\mathbf{R} \sigma_\mathbf{R}
\tag{4.74}
$$

where E_{MMF} is the mean-molecular field action on ion A. The partition function becomes[20],

$$
\begin{aligned}
\mathcal{Z} = \quad & \sum_{\sigma_{\mathbf{R}_1}=\pm 1} \cdots \sum_{\sigma_{\mathbf{R}_N}=\pm 1} \exp\left\{-\frac{\left[\frac{1}{2}(\Delta x)^2 \langle\sigma_\mathbf{R}\rangle^2 J_0 N - q\Delta x E_{MMF} \sum_\mathbf{R} \sigma_\mathbf{R}\right]}{k_B T}\right\} \\
= \quad & \underbrace{\exp\left[-\frac{(\Delta x)^2 \langle\sigma_\mathbf{R}\rangle^2 J_0 N}{2 k_B T}\right]}_{A} \sum_{\sigma_{\mathbf{R}_1}=\pm 1} \cdots \sum_{\sigma_{\mathbf{R}_N}=\pm 1} \prod_\mathbf{R} \exp\left(\frac{q\Delta x E_{MMF}}{k_B T} \sigma_\mathbf{R}\right) \\
= \quad & \left[A \sum_{\sigma_{\mathbf{R}_1}} \exp\left(\frac{q\Delta x E_{MMF}}{k_B T} \sigma_{\mathbf{R}_1}\right) \cdots \sum_{\sigma_{\mathbf{R}_{N-1}}} \exp\left(\frac{q\Delta x E_{MMF}}{k_B T} \sigma_{\mathbf{R}_{N-1}}\right)\right] \\
& \times \sum_{\sigma_{\mathbf{R}_N}=\pm 1} \exp\left(\frac{q\Delta x E_{MMF}}{k_B T} \sigma_{\mathbf{R}_N}\right)
\end{aligned}
\tag{4.75}
$$

Thus,

---

[20]Carrying out the sum over $\sigma_{\mathbf{R}_N}$ first leads to,
$\mathcal{Z} = \left[A \sum_{\sigma_{\mathbf{R}_1}} \exp(B\sigma_{\mathbf{R}_1}) \cdots \sum_{\sigma_{\mathbf{R}_{N-1}}} \exp(B\sigma_{\mathbf{R}_{N-1}})\right] \sum_{\sigma_{\mathbf{R}_N}=\pm 1} \exp(B\sigma_{\mathbf{R}_N})$ with $B = \frac{q\Delta x E_{MMF}}{k_B T}$.
The sum over $\sigma_{\mathbf{R}_N}$ is given by, $\sum_{\sigma_{\mathbf{R}_N}=\pm 1} \exp(B\sigma_{\mathbf{R}_N}) = 2\cosh(B)$. Successive evaluating of the sums leads
to $\mathcal{Z} = 2A\cosh(B)^N$

$$\mathcal{Z} = \left[A \sum_{\sigma_{\mathbf{R_1}}} \exp\left(\frac{q\Delta x E_{MMF}}{k_B T} \sigma_{\mathbf{R_1}} \right) \cdots \sum_{\sigma_{\mathbf{R}_{N-1}}} \exp\left(\frac{q\Delta x E_{MMF}}{k_B T} \sigma_{\mathbf{R_{N-1}}} \right) \right]$$

$$\times \cosh\left(\frac{q\Delta x E_{MMF}}{k_B T} \right) \tag{4.76}$$

$$= \quad 2\exp\left[-\frac{(\Delta x)^2 \langle \sigma_{\mathbf{R}} \rangle^2 J_0 N}{2k_B T} \right] \cosh\left(\frac{q\Delta x E_{MMF}}{k_B T} \right)^N$$

Substituting $\langle \sigma_{\mathbf{R}} \rangle = \frac{P}{nq\Delta x}$ where P is the electric polarization and q is the charge of the ion A, the free energy per volume with $n = N/V$ is given by,

$$\frac{F}{V} = \quad -\frac{1}{V} k_B T \ln \mathcal{Z}$$

$$= \quad \frac{J_0}{2nq^2} P^2 - nk_B T \ln\left[2\cosh\left(\frac{\frac{\Delta x J_0}{nq} P + q\Delta x E}{k_B T} \right) \right] \tag{4.77}$$

Expanding Eq. (4.77) into a Taylor series with respect to P and E and considering only even powers in P and bilinear coupling of P with E leads to,

$$\frac{F}{V} = \left(\frac{J_0}{2nq^2} - \frac{(\Delta x)^2 J_0^2}{2nq^2 k_B T} \right) P^2 + \frac{(\Delta x)^4 J_0^4}{12n^3 q^4 k_B^3 T^3} P^4 - \frac{(\Delta x)^2 J_0}{k_B T} EP \tag{4.78}$$

Hence,

$$\frac{\mathrm{d}F}{V\mathrm{d}P} = 2\left(\frac{J_0}{2nq^2} - \frac{(\Delta x)^2 J_0^2}{2nq^2 k_B T} \right) P + \frac{(\Delta x)^4 J_0^4}{3n^3 q^4 k_B^3 T^3} P^3 - \frac{(\Delta x)^2 J_0}{k_B T} E \tag{4.79}$$

With Eq. (4.56) and Eq. (4.57) it follows that $a = \left(\frac{J_0}{2nq^2} - \frac{(\Delta x)^2 J_0^2}{2nq^2 k_B T} \right)$, $b = \frac{(\Delta x)^4 J_0^4}{12n^3 q^4 k_B^3 T^3}$, and $g = \frac{(\Delta x)^2 J_0}{k_B T}$. At $T = T_C$, $a = 0$ thus,

$$a = \quad \frac{J_0}{2nq^2} \left(\frac{T - T_C}{T} \right)$$

$$T_C = \quad \frac{(\Delta x)^2 J_0}{k_B} \tag{4.80}$$

and,

$$\frac{a}{g} = \frac{k_B}{2nq^2 (\Delta x)^2} (T - T_C) \tag{4.81}$$

The equation of motion of the order parameter becomes (Eq. 4.56),

$$\frac{1}{\Gamma} \frac{\mathrm{d}P}{\mathrm{d}t} = -\left[\frac{J_0}{nq^2} \left(\frac{T - T_C}{T} \right) P + \frac{(\Delta x)^4 J_0^4}{3n^3 q^4 k_B^3 T^3} P^3 - \frac{(\Delta x)^2 J_0}{k_B T} E \right] \tag{4.82}$$

Therefore, the relaxation time and relaxation strength of the order parameter dynamic becomes (Eq. 4.65, 4.70)

$$\tau^{-1} = \begin{cases} \frac{J_0}{nq^2}\Gamma\left(\frac{T-T_C}{T}\right) & T > T_C \\ 2\frac{J_0}{nq^2}\Gamma\left(\frac{T_C-T}{T}\right) & T < T_C \end{cases} \tag{4.83}$$

$$\Delta\varepsilon_r^{-1} = \begin{cases} \frac{k_B\varepsilon_0}{nq^2(\Delta x)^2}\left(T - T_C\right) & T > T_C \\ 2\frac{k_B\varepsilon_0}{nq^2(\Delta x)^2}\left(T_C - T\right) & T < T_C \end{cases} \tag{4.84}$$

The relaxation strength exhibits a Curie-Weiss behaviour where the slope is governed by the density, charge and displacement of the ions A. The dissipation parameter can not be determined within the statistical approach. Accordingly, the exact temperature dependence of the relaxation time in the order-disorder limit can only be determined by a microscopic theory of the order parameter dynamics. However, with the phase transition temperature given in Eq.(4.80) the s-parameter (Eq.4.34) becomes,

$$s = \frac{1}{2}\frac{E_A}{k_BT_C} \gg 1 \rightarrow \frac{E_A}{k_BT_C} \gg 2 \tag{4.85}$$

4.4 Microscopic theory of the order parameter dynamics in order-disorder transitions

In order to describe the order parameter dynamics by considering a microscopic approach when a medium undergoes a phase transition from the high temperature phase to the low temperature phase, it is essential to determine the potential in which the ion A is moving. For one specific ion A, the Hamiltonian in Eq. (4.27) is given by,

$$\mathcal{H} = \frac{1}{2}m\left(\frac{dx_{\mathbf{R}}}{dt}\right)^2 + \left(-\eta + \frac{J_0}{2}\right)x_{\mathbf{R}}^2 + \vartheta x_{\mathbf{R}}^4 - \frac{1}{2}x_{\mathbf{R}}\sum_{\mathbf{R}'}J_{\mathbf{R},\mathbf{R}'}x_{\mathbf{R}'} \tag{4.86}$$

The last term in Eq. (4.86) can be replaced by the average coupling energy[21] and Eq.(4.86) becomes,

$$\mathcal{H} = \frac{1}{2}m\left(\frac{dx_{\mathbf{R}}}{dt}\right)^2 + \left(-\eta + \frac{J_0}{2}\right)x_{\mathbf{R}}^2 + \vartheta x_{\mathbf{R}}^4 - \frac{1}{2}x_{\mathbf{R}}N\left\langle J_{\mathbf{R},\mathbf{R}'}x_{\mathbf{R}'}\right\rangle \tag{4.87}$$

In the high temperature phase no order exists (the order parameter is equal to zero) and hence coupling forces along $+x$ and $-x$ are balanced (high symmetric state). Opposing coupling forces cancel each other and thus in turn the averaged interaction energy of one ion A with all other ions A vanishes. Thus, $\left\langle J_{\mathbf{R},\mathbf{R}'}x_{\mathbf{R}'}\right\rangle = 0$ and the total energy of one ion A for $T > T_C$ is given by,

$$\mathcal{H} = \frac{1}{2}m\left(\frac{dx_{\mathbf{R}}}{dt}\right)^2 + \left(-\eta + \frac{J_0}{2}\right)x_{\mathbf{R}}^2 + \vartheta x_{\mathbf{R}}^4 \tag{4.88}$$

In the order-disorder limit the forces between ions A are much smaller than the forces

---

[21] $\frac{1}{2}x_{\mathbf{R}}\sum_{\mathbf{R}'}J_{\mathbf{R},\mathbf{R}'}x_{\mathbf{R}'} = \frac{1}{2}x_{\mathbf{R}}\sum_{\mathbf{R}'}\frac{J_{\mathbf{R},\mathbf{R}'}x_{\mathbf{R}'}}{N}N = \frac{1}{2}x_{\mathbf{R}}N\left\langle J_{\mathbf{R},\mathbf{R}'}x_{\mathbf{R}'}\right\rangle$

due to the local potential. Accordingly, with Eq.(4.32) and Eq.(4.34) it follows that $J_0 \ll \frac{1}{4}\eta$. Thus in turn, $\left(-\eta + \frac{J_0}{2}\right) < 0$ and the ions A move in an effective potential with two minima. Consequently, the sign of $\left(-\eta + \frac{J_0}{2}\right)$ determines the nature of the phase transition. $\left(-\eta + \frac{J_0}{2}\right) > 0$ implies a displacive type phase transition and $\left(-\eta + \frac{J_0}{2}\right) < 0$ a order-disorder type phase transition.

It is evident that the thermal motion of an ion A is the vibration near one of the minima interrupted by relatively rare jumps to another well. From the viewpoint of the order parameter dynamics such jumps between the minima of the potential wells are of great interest since this motion of ions A implicates flipping of pseudo-spins. Assuming N ions A present in double-minima potentials, the rate equations for the change of the number of left and right displaced ions A are given by [99],

$$
\begin{aligned}
\text{I)} \quad & \frac{\mathrm{d}N_+}{\mathrm{d}t} = \nu_0\left(-w_{+-}N_+ + w_{-+}N_-\right) \\
\text{II)} \quad & \frac{\mathrm{d}N_-}{\mathrm{d}t} = \nu_0\left(+w_{+-}N_+ - w_{-+}N_-\right)
\end{aligned}
\tag{4.89}
$$

where ν_0 is the attempt frequency for a jump and w_{ij} is the probability for a jump from state i to state j. Here it is assumed, that the attempt frequency does not depend on the direction of the jump.

Subtracting equation II from equation I, and adding "0" by $w_{+-}N_- - w_{+-}N_- + w_{-+}N_+ - w_{-+}N_+$ leads to,

$$
\frac{\mathrm{d}N_+}{\mathrm{d}t} - \frac{\mathrm{d}N_-}{\mathrm{d}t} = -\left(N_+ - N_-\right)\left(w_{+-} + w_{-+}\right) + \left(N_+ + N_-\right)\left(w_{-+} - w_{+-}\right)
\tag{4.90}
$$

with $\langle\sigma_{\mathbf{R}}\rangle = \frac{N_+ - N_-}{N_+ + N_-} = \frac{P}{nq\Delta x}$ [22] Eq. (4.90) becomes,

$$
\frac{\mathrm{d}P}{\mathrm{d}t} = -P\left(w_{+-} + w_{-+}\right) + nq\Delta x\left(w_{-+} - w_{+-}\right)
\tag{4.91}
$$

Only the high-energy ions, whose kinetic energy appears to be higher than the barrier can jump. Hence, the product $w_{ij}N_i$ is the number of ions A with kinetic energy higher than that barrier. Accordingly, w_{ij} is given by the Boltzmann factor. Each ion A is acted on by a local field which is assumed to be the mean molecular field (Eq. 4.74). Therefore, one well is lowered where as the other is raised by the interaction energy of one ion A with the mean molecular field. Hence, the probabilities are given by,

$$
\begin{aligned}
w_{+-} &= \exp\left[-\frac{E_A + \left(\frac{J_0}{nq^2}P + E\right)q\Delta x}{k_B T}\right] \\
w_{+-} &= \exp\left[-\frac{E_A - \left(\frac{J_0}{nq^2}P + E\right)q\Delta x}{k_B T}\right]
\end{aligned}
\tag{4.92}
$$

---

[22] $P = P_+ - P_- = \frac{1}{V}N_+ q\Delta x - 1\frac{1}{V}N_- q\Delta x = \frac{N_+ + N_-}{V}\frac{N_+ - N_-}{N_+ + N_-}q\Delta x = n\langle\sigma_{\mathbf{R}}\rangle q\Delta x$

The electric field is assumed to be very small as well as the electric polarization near T_C. Thus the probabilities in Eq.(4.92) are expanded with respect to P and E up to the first order. Hence Eq. (4.91) becomes,

$$\frac{\mathrm{d}P}{\mathrm{d}t} = -\nu_0 \exp\left(-\frac{E_A}{k_B T}\right) \left[2\left(\frac{T-T_C}{T}\right) P + \frac{J_0 \left(\Delta x\right)^2}{n k_B^2 T^2} E P^2 - \frac{2nq^2 \left(\Delta x\right)^2}{k_B T} E\right] \tag{4.93}$$

Neglecting the term with EP^2 since $EP^2 \ll P \ \wedge \ EP^2 \ll E$ and multiplying Eq. (4.93) with $\frac{2nq^2}{J_0} \frac{J_0}{2nq^2}$ leads to,

$$\frac{1}{\nu_0 \frac{2nq^2}{J_0} \exp\left(-\frac{E_A}{k_B T}\right)} \frac{\mathrm{d}P}{\mathrm{d}t} = -\left[\frac{J_0}{nq^2}\left(\frac{T-T_C}{T}\right) P - \frac{J_0 \left(\Delta x\right)^2}{k_B T} E\right] \tag{4.94}$$

In linear approximation, Eq. (4.94) is equal to Eq. (4.82) and thus the dissipation parameter becomes,

$$\Gamma = \nu_0 \frac{2nq^2}{J_0} \exp\left(-\frac{E_A}{k_B T}\right) \tag{4.95}$$

Hence, the relaxation time and strength of the order parameter dynamics in the order-disorder limit are given by,

$$\tau^{-1} = \begin{cases} 2\nu_0 \left(\frac{T-T_C}{T}\right) \exp\left(-\frac{E_A}{k_B T}\right) & T > T_C \\ 4\nu_0 \left(\frac{T_C-T}{T}\right) \exp\left(-\frac{E_A}{k_B T}\right) & T < T_C \end{cases} \tag{4.96}$$

$$\Delta \varepsilon_r^{-1} = \begin{cases} \frac{k_B \varepsilon_0}{nq^2 (\Delta x)^2} \left(T - T_C\right) & T > T_C \\ 2\frac{k_B \varepsilon_0}{nq^2 (\Delta x)^2} \left(T_C - T\right) & T < T_C \end{cases} \tag{4.97}$$

The temperature behaviour of the relaxation time is governed by a superposition of two processes: (i) Activated behaviour with a characteristic energy and (ii) Critical slowing down of the relaxation time caused by a critical behaviour of the pre-exponential factor in the vicinity of T_C . This observation is typical for order-disorder phase transitions involving shallow double well potentials [119, 134, 135].

The temperature activated behaviour, expressed by the pre-exponential factor in Eq.(4.96), prevails for temperatures far from T_C and, therefore, causes an overall decrease of the relaxation time for decreasing temperature.

4.5   Microscopic theory of the order parameter dynamics in displacive transitions: The soft mode concept

The characteristic of displacive type phase transition rely on the fact that forces between the ions A are much larger than the forces due to the local potential. Accordingly, $J_0 > 2\eta$,

and the ions A move in an effective potential with a single minimum[23]. Applying weak-anharmonicity approximation $\left(-\eta + \frac{J_0}{2}\right) \gg \vartheta$ leads to,

$$\mathcal{H} = \frac{1}{2}m \left(\frac{\mathrm{d}x_\mathbf{R}}{\mathrm{d}t}\right)^2 + \left(-\eta + \frac{J_0}{2}\right)x_\mathbf{R}^2 \tag{4.98}$$

and the equation of motion for one ion A is given by,

$$m\frac{\mathrm{d}^2 x_\mathbf{R}}{\mathrm{d}t^2} + \rho\frac{\mathrm{d}x_\mathbf{R}}{\mathrm{d}t} = -2\left(-\eta + \frac{J_0}{2}\right)x_\mathbf{R} + qE_{eff} \tag{4.99}$$

where m is the mass of ion A, ρ is the damping constant, q is the charge of ion A and E_{eff} is the effective electric field acting on ion A. A damping term is added to the equation of motion since lattice vibrations are expected to be damped. For a ferroelectric phase transition the critical wave vector is zero (zone centre phonon) (Fig. 4.5) and therefore the displacements of ions A are identical for all unit cells, $x_\mathbf{R} \to x$. With $P = nqx$, Eq.(4.99) becomes,

$$\frac{m}{nq}\frac{\mathrm{d}^2 P}{\mathrm{d}t^2} + \frac{\rho}{nq}\frac{\mathrm{d}P}{\mathrm{d}t} = -\frac{2}{nq}\left(-\eta + \frac{J_0}{2}\right)P + qE_{eff} \tag{4.100}$$

where P is the electric polarization and n is the density of ions A. Since, if an electric field[24] is applied , each ion develops an individual dipole moment, which in turn sets up a dipolar electric field which is $\frac{1}{\varepsilon_0}P$ [136]. Thus the effective field acting on ion A is given by $E_{eff} = E + \frac{1}{\varepsilon_0}P$ and Eq. (4.100) becomes,

$$\frac{\mathrm{d}^2 P}{\mathrm{d}t^2} + \frac{\rho}{m}\frac{\mathrm{d}P}{\mathrm{d}t} = -\underbrace{\frac{2}{m}\left(-\eta + \frac{J_0}{2} - \frac{nq^2}{2\varepsilon_0}\right)}_{\omega^2}P + \frac{nq^2}{m}E \tag{4.101}$$

For a over-damped dynamic behaviour, the second derivative can be neglected and the equation of motion of the order parameter becomes,

$$\frac{\rho}{m}\frac{\mathrm{d}P}{\mathrm{d}t} = -\underbrace{\frac{2}{m}\left(-\eta + \frac{J_0}{2} - \frac{nq^2}{2\varepsilon_0}\right)}_{\omega^2}P + \frac{nq^2}{m}E \tag{4.102}$$

Comparing Eq. (4.102) with Eq. (4.57) whereas $\bar{\pi}_S = P$ and bearing in mind that in the high temperature phase only the quadratic term is relevant (Gaussian approximation) leads to $\Gamma = \frac{\rho}{m}$, $a = \frac{1}{2}\omega$ and $g = \frac{nq^2}{m}$. Hence the relaxation time and susceptibility becomes,

$$\tau^{-1} = \begin{cases} \omega^2\frac{\rho}{m} & T > T_C \\ -2\omega^2\frac{\rho}{m} & T < T_C \end{cases} \tag{4.103}$$

---

[23]From Eq.(4.32) and Eq.(4.34) follows that $J_0 \gg \frac{\eta}{4}$. This constraint is not sufficient for a single minimum potential.

[24]Nota bene, the electric field is equal to the macroscopic electric field inside the medium which is $E = \frac{1}{\varepsilon_0}(D - P)$ where D is the dielectric displacement which is equal to the macroscopic vacuum field produced by free charges.

$$\chi_{static}^{-1} = \begin{cases} \omega^2 \frac{m}{nq^2} & T > T_C \\ -2\omega^2 \frac{m}{nq^2} & T < T_C \end{cases} \qquad (4.104)$$

Temperature never enters these considerations because everything was done in the harmonic approximation and a phase transitions never happens. Indeed, anharmonicity is required for a phase transition and it is possible to account for that by assuming a temperature dependent volume of the medium. Again, anharmonicity causes thermal expansion of a medium. In first order of temperature, the volume can be expressed as $V = V_0 (1 + \zeta T)$ where ζ is the volume coefficient of expansion. Thus $n = \frac{N}{V} = \frac{N}{V_0 + \Delta V}$ with $\Delta V = V_0 \zeta T$. Since $\Delta V \ll V_0$ leads to $n \approx \frac{N}{V_0} - \frac{N}{V_0} \frac{\Delta V}{V_0}$. Hence $n = n_0 (1 - \zeta T)$. Thus ω^2 becomes with $\Delta n = n_0 \zeta T$ and $\Delta n \ll n_0$

$$\begin{aligned} \omega^2 &= \frac{2}{m} \left(-\eta + \frac{J_0}{2} - \frac{(n_0 - \Delta n) q^2}{2\varepsilon_0} \right) \\ &= \frac{q^2 n_0 \zeta}{m\varepsilon_0} (T - T_C) \\ T_C &= \frac{\varepsilon_0}{q^2 n_0 \zeta} \left(2\eta + \frac{q^2 n_0}{\varepsilon_0} - J_0 \right) \end{aligned} \qquad (4.105)$$

and $\frac{\omega^2}{n}$,

$$\begin{aligned} \frac{\omega^2}{n} &= \frac{2}{m (n_0 - \Delta n)} \left(-\eta + \frac{J_0}{2} - \frac{(n_0 - \Delta n) q^2}{2\varepsilon_0} \right) \\ &= \frac{(J_0 - 2\eta) \zeta}{m\varepsilon_0} (T - T_C^*) \\ T_C^* &= \frac{1}{\zeta (J_0 - 2\eta)} \left(2\eta + \frac{q^2 n_0}{\varepsilon_0} - J_0 \right) \end{aligned} \qquad (4.106)$$

Thus the relaxation time and relaxation strength for displacive phase transition exhibits a Curie Weiss behaviour given by,

$$\tau^{-1} = \begin{cases} \frac{q^2 n_0 \zeta \rho}{m^2 \varepsilon_0} (T - T_C) & T > T_C \\ 2 \frac{q^2 n_0 \zeta \rho}{m^2 \varepsilon_0} (T_C - T) & T < T_C \end{cases} \qquad (4.107)$$

$$\Delta\varepsilon_r^{-1} = \begin{cases} \frac{(J_0 - 2\eta)\zeta}{q^2 \varepsilon_0} (T - T_C^*) & T > T_C \\ 2 \frac{(J_0 - 2\eta)\zeta}{q^2 \varepsilon_0} (T_C^* - T) & T < T_C \end{cases} \qquad (4.108)$$

Both phase transition temperatures, T_C and T_C^* are not equal. This discrepancy is a consequence of the quasi harmonic approximation in addition with considering anharmonicity effects by thermal expansion behaviour. In order to resolve this dilemma, the shape parameter η must fulfill $\eta = \frac{1}{2} \left(J_0 - \frac{q^2 n_0}{\varepsilon_0} \right)$. Equation (4.105) reveals that the frequency of the zone centre phonon during a ferroelectric phase transition decreases (the phonon "*softens*") and vanishes at the critical temperature. This is the reason why the corresponding mode is called "*soft mode*". The softening of a mode is caused by the fact that its restoring force becomes very small and the crystal becomes unstable to such a motion, i.e. it is no longer dynamical

but is transformed into a static displacement.

Nota bene. The classical Curie-Weiss behaviour of the soft mode rely only on the assumption that the temperature dependence of the volume is linear with temperature and the coefficient of expansion is constant. Generally, the coefficient of expansion is defined as $\zeta = \frac{1}{V}\frac{dV}{dT}$ leading to $\ln V = \int \zeta dT + C$. Only for constant ζ the volume becomes $V = V_0 \exp(\zeta T) \approx V_0 (1 + \zeta T)$. Indeed, Kozlov et al. [137, 138] found a temperature behaviour of the relaxation time of a over damped soft mode in Rochelle salt as $(2\pi\tau)^{-1} \propto (T_C - T)^3$ in the low temperature phase. They showed that this is caused by a temperature dependent coefficient of expansion given by $\zeta = -0.0647 + 11.744t^2 - 14.814t^3 - 45.536t^4$ and by the absent of the linear term where $t = (T - T_C)/T$.

However, in the case of a displacive phase transition the corresponding relaxation of the order parameter slows down when the system approaches T_C and accelerates afterwards continuously.

# Dielectric Spectroscopy and analysis of permittivity spectra

5.1 Low frequency dielectric measurement

Measurements of the dielectric constant by the dielectric response, $\chi = \frac{1}{\varepsilon_0} \frac{\mathrm{d}P}{\mathrm{d}E} = (\varepsilon - 1)$ give valuable information about the ferroelectric phase transition phenomenon of that material. This can be done, e.g. by measuring the change of electric polarization upon the application of an electric field at different temperatures, $\chi_{static}\left(T\right) = \frac{1}{\varepsilon_0} \left.\frac{\mathrm{d}P}{\mathrm{d}E}\right|_T$. However, measuring the change of electric polarization at several temperatures with respect to the change of electric field is rather inconvenient since, apart from difficulties of measuring electric polarization, it will take a long time to study the ferroelectric phase transition behaviour. Alternatively, a fast and reliable method to measure the dielectric constant of an material is by measuring its impedance.

Accordingly, a time-varying electric field must be applied so that instead of a static response the dynamic dielectric response is measured. In addition, measuring the dynamic response provides much more information about the dielectric behaviour, e.g. the relaxation time of the order parameter, when a material undergoes a ferroelectric phase transition. To measure the dynamic response either the frequency domain or the time domain approach can be used. In the frequency domain approach the dielectric constant is measured at various frequencies of alternating excitation fields, whereas in the time domain approach a Fourier transform would be necessary to obtain the frequency dependent dielectric constant. Time domain spectroscopy is less time consuming than measurements in the frequency domain at very low frequencies (<10mHz) but has reduced accuracy.

For low frequency impedance measurements (<1MHz), the principle of dielectric measurement in the frequency domain is shown in Fig. 5.1. The sample is mounted between two electrodes (conveniently made of silver paste) forming a sample capacitor. In order to minimize the effects of fringing field, the thickness of this capacitor should be much less than the electrode size. A voltage with a constant amplitude and a certain frequency is applied to the sample. The applied voltage causes a current in the sample which will have the same frequency in the linear case. In addition, there will generally be a phase shift between the current and the voltage described by a phase angle (Fig.5.2).

The ratio between the peak value of the voltage, U_0, and the peak value of the current, I_0, and the phase angle, φ are determined by electric properties (permittivity and conductivity)
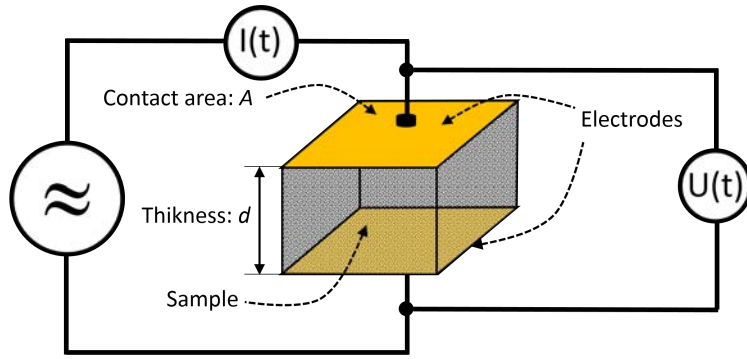
Figure 5.1: *Principle of dielectric measurement.* A four wire configuration is commonly used for measuring the sample impedance in order to eliminate additionally cable impedance contributions.
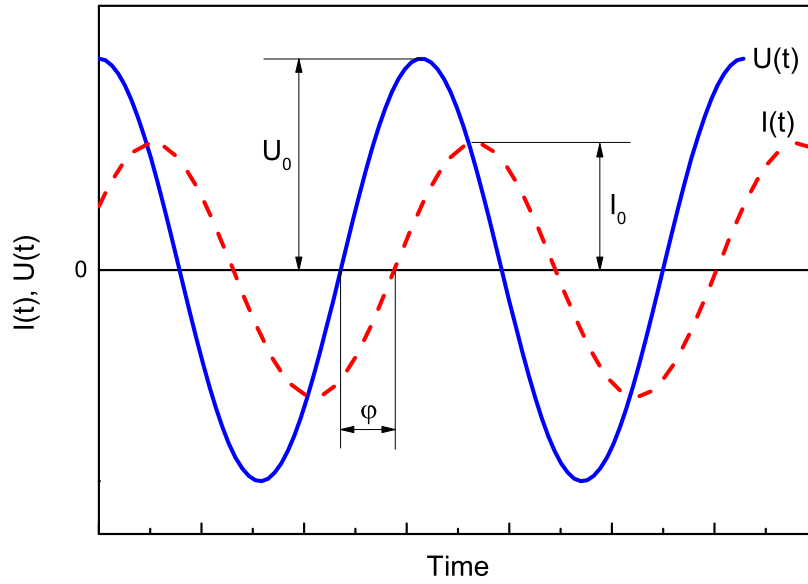
Figure 5.2: *Time dependent current and voltage signal.* Amplitude and phase relations between voltage (blue solid line) and current (red dashed line) of a sample at a given frequency.

of the material and by the sample geometry. In complex notation, the impedance is defined as the ratio between the time dependent voltage and the time dependent current as,

$$Z^*\left(\omega\right) = \frac{U_0\left(\omega\right)\exp\left[i\left(\omega t + \varphi_U\right)\right]}{I_0\left(\omega\right)\exp\left[i\left(\omega t + \varphi_I\right)\right]} = \frac{U_0\left(\omega\right)}{I_0\left(\omega\right)}\exp\left(i\varphi\right) = Z' + iZ'' \tag{5.1}$$

with $\varphi = \varphi_U - \varphi_I$. The capacity of the sample material is given by[1],

$$\frac{1}{i\omega C} = Z^* \tag{5.2}$$

The relative permittivity is related to the capacity by $C = \varepsilon_r\varepsilon_0\frac{A}{d}$ where A is the surface area of the electrodes and d is the thickness of the sample material. The vacuum permittivity is

---

[1] $U = \frac{Q}{C} \Rightarrow \frac{\mathrm{d}U}{\mathrm{d}t} = \frac{1}{C}\frac{\mathrm{d}Q}{\mathrm{d}t} \Rightarrow \frac{\mathrm{d}U}{\mathrm{d}t} = \frac{1}{C}I$. With $U = U_0\exp\left(i\omega t\right)$ follows, $I = i\omega C U_0\exp\left(i\omega t\right)$. Thus, $Z* = \frac{U}{I} = \frac{1}{i\omega C}$

given by ε_0 and the relative permittivity by ε_r. Thus with $C_0 = \varepsilon_0 \frac{A}{d}$ the complex permittivity of the sample material is given by[2],

$$\varepsilon^* = \varepsilon' - i\varepsilon'' = \frac{1}{C_0} \frac{1}{i\omega Z^*} \tag{5.3}$$

The real part, ε', describes the in phase response with the electric field, while the imaginary part, ε'', describes the out-of-phase response. For a pure ohmic resistor $Z^* = R = \varrho \frac{d}{A}$ and with Eq. (5.3) the permittivity becomes,

$$\varepsilon^* = \varepsilon' - i\varepsilon'' = -i \left(\frac{1}{\varepsilon_0 \omega \varrho} \right) = -i \left(\frac{\sigma}{\varepsilon_0 \omega} \right) \tag{5.4}$$

where ϱ is the resistivity and σ is the conductivity. The permittivity is purely imaginary in that case. That means, that the imaginary part of the complex permittivity is affected by the movement of free charges[3]. In general, at AC fields, free charges do not move arbitrarily far, but oscillate back and forth with the frequency of the field, whereas the bound charges[4] no longer come to rest at new equilibrium positions, but also oscillate at the field frequency determining the frequency behaviour of ε'. Thus both types of charges will contribute to an overall AC current and the distinction between free and bound charges blurs and is entirely a conventional one.

Hence, it is convenient to define a complex conductivity, $\sigma^* = \sigma' - i\sigma''$ in analogy to the complex permittivity. Therefore, with Eq. (5.4) the transformation rule between the permittivity and conductivity notation is given by $\sigma^* = i\varepsilon_0\omega\varepsilon^*$ with $\sigma' = \varepsilon_0\omega\varepsilon''$ and $\sigma'' = \varepsilon_0\omega\varepsilon'$. Both notation are just alternative representations of the dielectric properties of a material.

5.1.1 Interfacial effect: contact polarization

While the sample capacitor method in low frequency dielectric measurements and the underlying theory is rather simple, the analysis of a measured frequency dependent dielectric constant can be very complicated. In general, in addition to intrinsic phenomena also extrinsic effect can add up to the total permittivity.

In the low frequency regime it may be important (depending on the conductivity of the material under investigation) to consider interfacial polarization effects which originate from: i) the presence of electrons trapped with a finite lifetime in localized states near the interface [139], ii) space charge polarization effects due to the presence of mobile ions in the material which are virtually always present [140, 141, 142] iii) blocking layer with different density of charge carriers owing to band bending near the electrode-dielectric interfaces, causing charge injection from the electrode into the dielectric or vice versa charge depletion due to different

---

[2]Nota bene, ε^* has to be considered as the relative permittivity. According to literature the subscript r is omitted.

[3]Those that can move freely over arbitrary distances in respond to the DC field

[4]Those that are bound to equilibrium positions and only stretched to new equilibrium positions by the DC field

work functions of electrode and the dielectric material.

All these phenomena are summarized under the term "*Maxwell-Wagner polarization*" and can be basically modelled by a leaky capacitor in series with the bulk sample impedance [143] (Fig. 5.3).
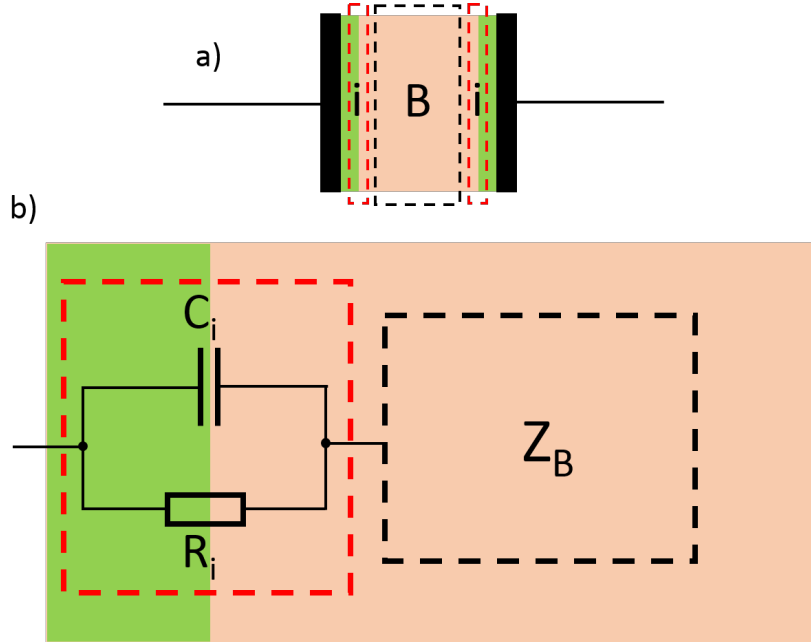
Figure 5.3: *Interfacial effects.* (a) Due to interfacial effects a double layer is formed near the two electrodes. (b) The double layer provokes a additionally capacitance and a resistance at the interface (green-beige) in series with the bulk impedance (beige)

The total impedance for such a configuration is given by,

$$Z_T^* = \underbrace{\frac{R_K}{1 + i\left(R_K C_K\right)\omega}}_{Z_K} + Z_B \tag{5.5}$$

where Z_B is the sample bulk impedance and Z_K is the contribution from the interface. With $\omega \gg (\tau_K)^{-1}$ and $\tau_K = R_K C_K$ where τ_K is the relaxation time, the impedance arising from the contacts vanishes and the measured impedance is equal to the sample impedance. On the other hand, if $\omega \ll (\tau_K)^{-1}$, then $Z_K = R_K$ and the total impedance is predominately governed by the interface resistance since R_K can take huge values. Hence, depending on τ_K intrinsic effects my be masked by interfacial effects. As it is evident, for very low conductive materials, interfacial polarization effects only arises at very low frequencies.

5.2   Linear response and dielectric relaxation

The time dependent response of an isotropic system following a disturbance with considering causality, locality and superposition principle can be described as,

$$R\left(t\right) = \int\limits_{-\infty}^{t} \mathrm{d}t' \chi\left(t - t'\right) F\left(t'\right) \tag{5.6}$$

where $R\left(t\right)$ is the response at time t, $F\left(t'\right)$ is the disturbance at time t' and $\chi\left(t - t'\right)$ is the response function dependent on the age, $t - t'$. Equation (5.6) means that the response at time t is the sum of all disturbances in the past multiplied with the response function at $t - t'$. Thus $\chi\left(t - t'\right)$ is a measure of how strong the disturbance at time t' contributes to the total response of the system at time t.

Basically, the response function decays exponentially with $\left(t - t'\right)$ so that a disturbance long time ago does not influence the present state of the system effectively.

With $t'' = t - t'$ Eq. (5.6) becomes,

$$R\left(t\right) = \int\limits_{0}^{\infty} \mathrm{d}t'' \chi\left(t''\right) F\left(t - t''\right) \tag{5.7}$$

In Fourier space Eq. (5.7) becomes,

$$\begin{aligned}
\underbrace{\int\limits_{-\infty}^{+\infty} \mathrm{d}\omega \exp\left(-i\omega t\right) R\left(\omega\right)}_{R(t)} &= \int\limits_{0}^{\infty} \mathrm{d}t'' \chi\left(t''\right) \underbrace{\int\limits_{-\infty}^{+\infty} \mathrm{d}\omega \exp\left[-i\omega\left(t - t''\right)\right] F\left(\omega\right)}_{F(t-t'')} \\
&= \int\limits_{0}^{\infty} \mathrm{d}t'' \chi\left(t''\right) \exp\left(i\omega t''\right) \int\limits_{-\infty}^{+\infty} \mathrm{d}\omega \exp\left(-i\omega t\right) F\left(\omega\right) \\
&= \int\limits_{-\infty}^{+\infty} \mathrm{d}\omega \chi\left(\omega\right) F\left(\omega\right) \exp\left(-i\omega t\right)
\end{aligned} \tag{5.8}$$

Thus in frequency space the response to a disturbance becomes,

$$R\left(\omega\right) = \chi\left(\omega\right) F\left(\omega\right) \tag{5.9}$$

with the frequency dependent response function given by the Laplace transformed response function with imaginary argument as,

$$\chi\left(\omega\right) = \int\limits_{0}^{\infty} \mathrm{d}t \chi\left(t\right) \exp\left(i\omega t\right) \tag{5.10}$$

A very important case study is the response to a heaviside step function since an arbitrary disturbance can be approximated by a series of successive elementary steps (Fig. 5.4.

For a steady input that is abruptly turned off ($\downarrow$) or on ($\uparrow$) at $t' = 0$, the disturbance is given by $F\left(t'\right) = F_0\Theta\left(-t'\right)$ respectively $F\left(t'\right) = F_0\Theta\left(t'\right)$ where $\Theta\left(t\right)$ is the heaviside step function and F_0 is the amplitude. Hence the response becomes,
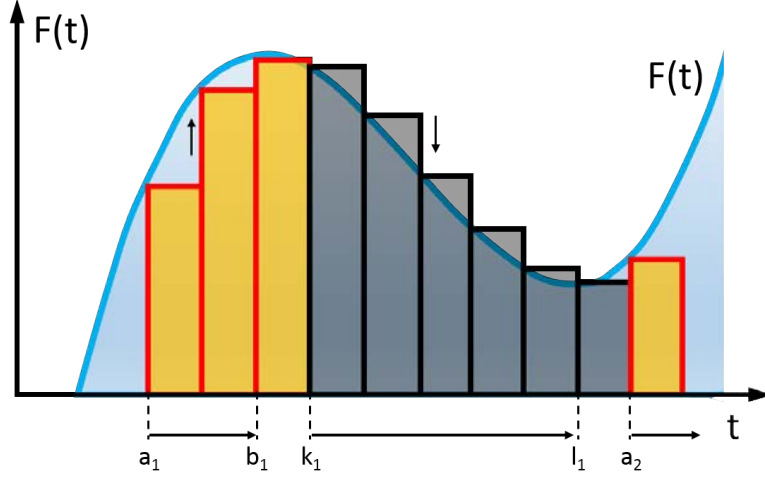
Figure 5.4: *Approximation of arbitrary disturbance.* A time-dependent disturbance can be build up from a succession of elementary steps. In the time interval $[a_i, b_i]$ the disturbance is monotonically increasing necessitating a monotonically increasing of the amplitude of the elementary steps (yellow) whereas it is contrary in the time interval $[k_i, l_i]$ (black)

$$R_{\Theta}(t) = \begin{cases} F_0 \int\limits_0^{\infty} dt'' \chi(t'') \, \Theta(t'' - t) = F_0 \int\limits_t^{\infty} dt'' \chi(t'') & \downarrow \\ F_0 \int\limits_0^{\infty} dt'' \chi(t'') \, \Theta(t - t'') = F_0 \int\limits_0^t dt'' \chi(t'') & \uparrow \end{cases} \qquad (5.11)$$

Thus the response function for a heaviside step input is given by,

$$\chi_{\Theta}(t) = \frac{1}{F_0} \begin{cases} -\dfrac{dR_{\Theta}(t)}{dt} & \downarrow \\ +\dfrac{dR_{\Theta}(t)}{dt} & \uparrow \end{cases} \qquad (5.12)$$

Therefore with Eq. (5.7) the general response of a system to a general disturbance is given by,

$$R(t) = \int\limits_0^{\infty} dt'' \chi_{\Theta}(t'') F(t - t'') = \frac{1}{F_0} \sum_i \begin{cases} -\int\limits_{a_i}^{b_i} dt'' \dfrac{dR_{\Theta}(t'')}{dt} F(t - t'') & \downarrow \\ +\int\limits_{k_i}^{l_i} dt'' \dfrac{dR_{\Theta}(t'')}{dt} F(t - t'') & \uparrow \end{cases} \qquad (5.13)$$

where in the time interval $[a_i, b_i]$ and $[k_i, l_i]$ the disturbance is monotonically decreasing

respectively increasing.

In dielectrics the disturbance is the time dependent electric field, $F(t) = E(t)$ and the response of the system is the electric polarization, $R(t) = P(t)$.

5.2.1 Debye function

In principle the total electric polarization is composed of polarization processes occurring on short and long time scales. On the one hand, processes taking place on short time scales can be considered to follow instantaneously an excitation field without any time lag, whereas on the other hand, a certain time exists to respond to an excitation fields for polarization processes taking place on long time scales. Hence the total electric polarization is given by,

$$P(t) = P_O(t) + P_\infty(t) \tag{5.14}$$

where $P_O(t)$ and $P_\infty(t)$ are the long and short time scale electric polarization contributions. Hence, with Eq. (5.7) the total electric polarization is given by,

$$P(t) = \underbrace{\int_0^\infty dt'' \chi_O(t'') E(t - t'')}_{P_O(t)} + \underbrace{\int_0^\infty dt'' \chi_\infty(t'') E(t - t'')}_{P_\infty(t)} \tag{5.15}$$

The most simple assumption for the long time scale electric polarization is that the change of the electric polarization is proportional to its actual value after the removal of the excitation field [144, 145]. Consequently,

$$\frac{dP_O}{dt} = -\frac{1}{\tau} P_O \tag{5.16}$$

where τ is the characteristic relaxation time. With $P_O(t = 0) = P_{O_0} = (P_{Equ} - P_\infty)$, Eq. (5.16) leads to an exponential decay for P_O as,

$$P_O(t) = (P_{Equ} - P_\infty) \exp\left(-\frac{t}{\tau}\right) \tag{5.17}$$

where P_{Equ} is the equilibrium electric polarization. Since $P_\infty(t)$ follows immediately an excitation field, the short scale polarization processes for an abruptly turned off excitation field are given by,

$$P_\infty(t) = P_\infty \Theta(-t) \tag{5.18}$$

For an abruptly turned on excitation field, the different polarization contribution are given by,

$$
\begin{aligned}
P_O(t) &= P_{Equ} - (P_{Equ} - P_\infty) \exp\left(-\frac{t}{\tau}\right) \\
P_\infty(t) &= P_\infty \Theta(t)
\end{aligned}
\tag{5.19}
$$

with $P_{Equ} = \varepsilon_0 \left(\varepsilon_{Equ} - 1\right) E_0$ and $P_{\infty} = \varepsilon_0 \left(\varepsilon_{\infty} - 1\right) E_0$ where E_0 is the excitation field, ε_{Equ} is the relative equilibrium permittivity and ε_{∞} is the relative permittivity from high frequency contributions, the response function becomes (Eq. 5.12),

$$\chi_O\left(t\right) = \begin{cases} \varepsilon_0 \left(\varepsilon_{Equ} - \varepsilon_{\infty}\right) \dfrac{1}{\tau} \exp\left(-\dfrac{t}{\tau}\right) & \downarrow \\[3mm] \varepsilon_0 \left(\varepsilon_{Equ} - \varepsilon_{\infty}\right) \dfrac{1}{\tau} \exp\left(-\dfrac{t}{\tau}\right) & \uparrow \end{cases} \tag{5.20}$$

$$\chi_{\infty}\left(t\right) = \begin{cases} \varepsilon_0 \left(\varepsilon_{\infty} - 1\right) \delta\left(t\right) & \downarrow \\[2mm] \varepsilon_0 \left(\varepsilon_{\infty} - 1\right) \delta\left(t\right) & \uparrow \end{cases} \tag{5.21}$$

where $\delta\left(t\right) = \frac{\mathrm{d}\Theta(t)}{\mathrm{d}t}$ is the delta function and considering the identity $\delta\left(-t\right) = \delta\left(t\right)$. Obviously, in both cases the response function is equal and thus it is not necessary to distinguish between increasing and decreasing excitation field. Thus the integrals in Eq. (5.15) can be readily evaluated. Consequently, knowing the response function of a heaviside step excitation, the respond to any arbitrary excitation field can be calculated. Particularly, the respond of the electric polarization for an harmonic excitation field, $E\left(t\right) = E_0 \cos\left(\omega t\right) = \Re\left[E_0 \exp\left(i\omega t\right)\right]$ becomes,

$$
\begin{aligned}
P\left(t\right) = \ & \Re\left\{\int_0^{\infty} \mathrm{d}t'' \varepsilon_0 \left(\varepsilon_{Equ} - \varepsilon_{\infty}\right) \frac{1}{\tau} \exp\left(-\frac{t''}{\tau}\right) E_0 \exp\left[i\omega\left(t - t''\right)\right]\right\} \\[2mm]
+ \ & \Re\left\{\int_0^{\infty} \mathrm{d}t'' \varepsilon_0 \left(\varepsilon_{\infty} - 1\right) \delta\left(t''\right) E_0 \exp\left[i\omega\left(t - t''\right)\right]\right\} \\[2mm]
= \ & \Re\left\{E_0 e^{i\omega t}\left[\varepsilon_0 \left(\varepsilon_{Equ} - \varepsilon_{\infty}\right) \frac{1}{\tau}\int_0^{\infty} \mathrm{d}t'' \exp\left[-\left(\frac{1}{\tau} + i\omega\right)t''\right] + \varepsilon_0 \left(\varepsilon_{\infty} - 1\right)\right]\right\} \\[2mm]
= \ & \Re\left\{\varepsilon_0 \underbrace{\left[\frac{\left(\varepsilon_{Equ} - \varepsilon_{\infty}\right)}{1 + i\tau\omega} + \left(\varepsilon_{\infty} - 1\right)\right]}_{\chi} \underbrace{E_0 \exp\left(i\omega t\right)}_{E(t)}\right\}
\end{aligned}
\tag{5.22}
$$

Thus with $\varepsilon_r = 1 + \chi$ the frequency dependent complex permittivity for a relaxation process becomes,

$$\varepsilon_r^* = \varepsilon_{\infty} + \frac{\left(\varepsilon_{Equ} - \varepsilon_{\infty}\right)}{1 + i\tau\omega} = \varepsilon_{\infty} + \frac{\Delta\varepsilon}{1 + i\tau\omega} \tag{5.23}$$

where $\Delta\varepsilon = \left(\varepsilon_{Equ} - \varepsilon_{\infty}\right)$. Nota bene, for harmonic excitation fields, the classification of the polarization mechanism into slow and fast processes depends on the measuring frequency. Thus in the case where the medium has several polarization mechanisms coexisting and not significantly interacting among themselves, the permittivity can be expressed as the sum of the contributions of the individual mechanisms as (5.24)[146, 147],

$$\varepsilon(\omega) = \varepsilon_0 \left[1 + \sum_l^N \chi_l(\omega) \right] \qquad (5.24)$$

In case of considering only relaxation processes, Eq. (5.24) can be written as,

$$\varepsilon(\omega) = \varepsilon_0 \left[\varepsilon_\infty + \sum_l^N \frac{\Delta\varepsilon_l}{1 + i\tau_l\omega} \right] \qquad (5.25)$$

where all high frequency contributions (resonance phenomena) are combined in ε_∞. With $\exp(i\omega t) = \cos(\omega t) + i\sin(\omega t)$, the electric polarization (Eq. 5.22) is given by,

$$P(t) = \left[\overbrace{\left(\frac{\Delta\varepsilon}{1 + (\tau\omega)^2} + \varepsilon_\infty \right)}^{\varepsilon'} - 1 \right] \underbrace{\varepsilon_0 E_0 \cos(\omega t)}_{\text{In phase with applied electric field}} + \underbrace{\left[\overbrace{\frac{\Delta\varepsilon\tau\omega}{1 + (\tau\omega)^2}}^{\varepsilon''} \right] \varepsilon_0 E_0 \sin(\omega t)}_{\text{Lag by } \pi/2} \qquad (5.26)$$

$$= \varepsilon_0 E_0 \sqrt{(\varepsilon' - 1)^2 + (\varepsilon'')^2} \cos(\omega t - \varphi)$$

where $\varepsilon_r^* = \varepsilon' - i\varepsilon''$ and φ is the loss angle given by $\tan\varphi = \frac{\varepsilon''}{\varepsilon' - 1}$. The component in phase with the applied field is the lossless component, while the component with $\frac{\pi}{2}$ out of phase is the loss component which represents the dielectric losses in the form of energy absorption. Dielectric losses show a maximum at $\omega = \tau^{-1}$. It is obvious that for $\omega \gg \tau^{-1}$ the electric polarization can not follow the field variation and the electric polarization is governed solely by high frequency contributions, $(\varepsilon_\infty - 1)$, which is in phase with the applied field (Fig. 5.5).

A Debye dielectric material, i.e. the time dependent polarization obeys the Debye equation (Eq. 5.16), can be modelled by an electric circuit [148] (Fig.5.6) with the impedance given by,
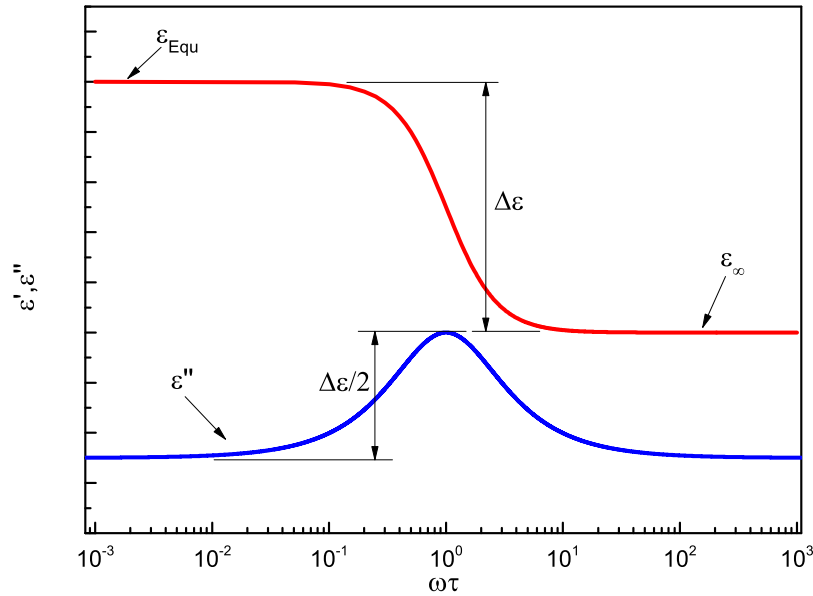
$$\frac{1}{Z_B^*} = i\omega \left(C_1 + \frac{C_2}{1 + iRC_2\omega} \right) \qquad (5.27)$$

With Eq. (5.3) the permittivity is given by,

$$\varepsilon^* = \frac{C_1}{C_0} + \frac{\frac{C_2}{C_0}}{1 + iRC_2\omega} \qquad (5.28)$$

With $\frac{C_1}{C_0} = \varepsilon_\infty$, $\frac{C_2}{C_0} = \Delta\varepsilon$ and $RC_2 = \tau$, Eq. (5.28) is identical with Eq. (5.23).

Hence, with Eq. (5.3) and Eq. (5.5) the total permittivity is given by,

Figure 5.5: *Frequency dependent permittivity for a Debye relaxation process.* At low frequencies of the excitation field ($\omega \ll \tau^{-1}$) the long time scale processes (e.g. orientation of dipoles) leading to an electric polarization can follow the excitation field without any time lag and the permittivity is equal to ε_{Equ}. By increasing the excitation frequency, the electric polarization can not longer follow the excitation immediately but with a certain time lag. Consequently, the electric polarization loses on strenght and energy dissipation takes place. This behaviour is characterized by a step-like decrease of the real part of the permittivity and an increase of the imaginary part. At frequencies $\omega \gg \tau^{-1}$ the long time scale processes fail to follow the excitation field and the permittivity is solely governed by the short time scale processes, ε_∞ .
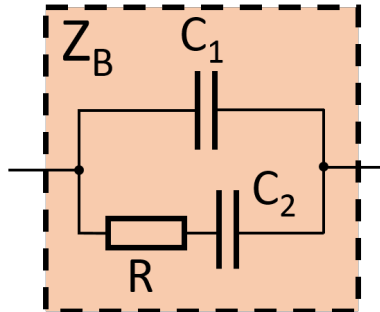
Figure 5.6: *Equivalent circuit for a Debye dielectric.* Nota bene, according to [149, 150], the problem of modelling the behaviour of an dielectric material by an electric circuit does not have a unique solution.

$$
\begin{aligned}
\varepsilon^* &= \frac{1}{i\omega C_0} \frac{1}{Z^*} \\
&= \frac{1}{i\omega C_0} \frac{1}{(Z_K + Z_B)} \\
&= \frac{1}{i\omega C_0} \frac{1}{\left(Z_K + \frac{1}{i\omega C_0} \frac{1}{\varepsilon^*_{Mat}}\right)} \\
&= \frac{1}{i\omega C_0 Z_K + \frac{1}{\varepsilon^*_{Mat}}}
\end{aligned}
\tag{5.29}
$$

where ε^*_{Mat} is the complex permittivity of the material. Usually, for the permittivity of the material, model functions are applied (discussed below) which describes the frequency behaviour of ε^*_{Mat} accurately.

5.2.1.1 Deviations from Debye behaviour

The Debye equation describes an ideal relaxation process of the electric polarization with one characteristic relaxation time. Generally, this is rarely the case and deviations from the Debye spectral shape are commonly observed and ascribed to a distribution of relaxation times. In fact, according to Eq. (4.53) each mode of the Fourier transformed order parameter field decays with a different relaxation time.

Consequently, the deviation of the Debye spectral shape is caused by fluctuations of the order parameter near the phase transition temperature (Fig. 5.7).

At temperatures well above the critical temperature, $T > T_C$, fluctuations of the electric polarization are only playing a minor role and in ideal consideration as depicted in Fig. 5.7. The average value of the coarse-grained electric polarization is equal to the total average value of the electric polarization, $\overline{P(x_i)} = \overline{P(x)} \ \forall x_i$. Thus, only the zero wavelength Fourier component ($q = 0$) exists in the Fourier transformed spectrum of the electric polarization field, $P(q) \propto \int P(x) \exp(iqx) \, dx$. Hence, only the relaxation time with $q = 0$ exists and no relaxation time distribution is present.

In the close vicinity to the phase transition temperature, critical fluctuations arises. Here $\overline{P(x_i)} \neq \overline{P(x)} \ \forall x_i$ and thus in turn the Fourier transformed spectrum of $P(x)$ consists of many different wave vectors leading to a distribution of relaxation times. Accordingly, this causes a deviation from the Debye spectral shape of a single relaxation process.

At very low temperatures, the average value of the coarse-grained electric polarization is again equal to the non zero total average value and thus in turn only the zero wavelength Fourier component exists in the Fourier transformed spectrum of $P(x)$ again.

Compared to a single Debye process, a distribution of relaxation times leads to a broadening of the dielectric function (Fig. 5.8).

Generally, a broadened relaxation processes can be described by a superposition of Debye-
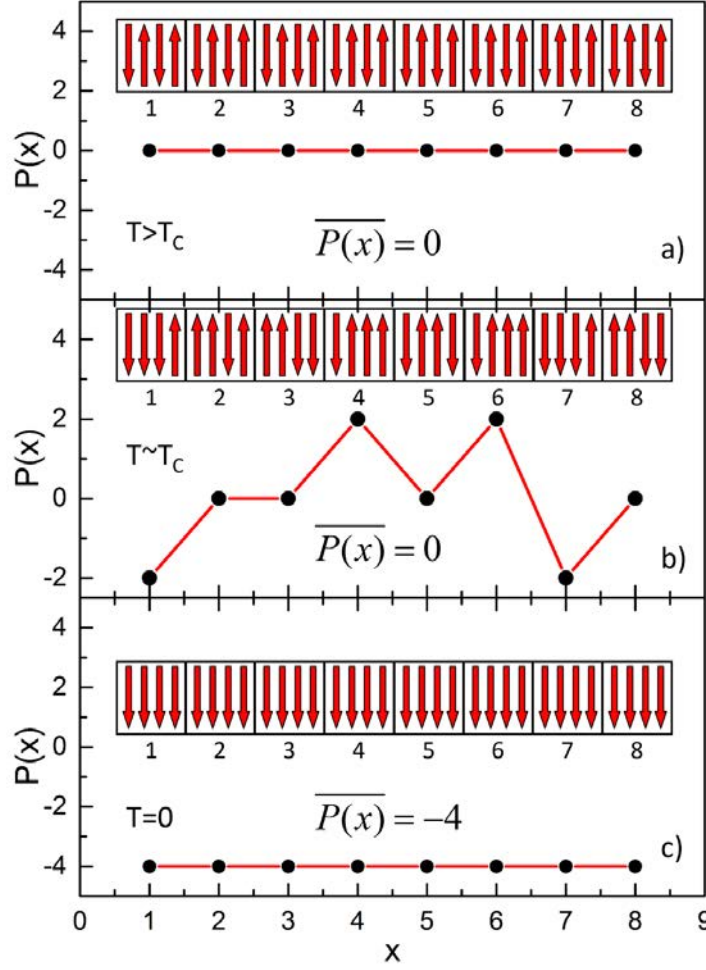
Figure 5.7: *Coarse-grained order parameter field in the pseudo-spin approxima-tion.* a) Electric polarization field at $T > T_C$. No fluctuation of the electric polarization is present. The inset depicts the corresponding pseudo spin distribution. b) Near the phase transition temperature critical fluctuation arises. c) At temperatures below the phase transition temperature the mean electric polarization is non-zero and no fluctuation of the electric polarization exists.

functions with different relaxation times [145, 151, 144, 148] as,[5]

$$\varepsilon' - i\varepsilon'' = \varepsilon_\infty + \Delta\varepsilon \int \frac{f(\tau)}{1 + i\omega\tau} d\tau \qquad (5.30)$$

where $f(\tau)$ is the relaxation time distribution function with $\int_0^\infty f(\tau) \, d\tau = 1$.

---

[5]Assuming that $\Delta\varepsilon(\tau_l)$ is the relaxation strength of one particular Debye process with a relaxation time, τ_l, contribution to the overall non Debye relaxation process (Fig. 5.8). Then the discrete relaxation time distribution function is defined as $f(\tau_l)\Delta\tau = \frac{\Delta\varepsilon(\tau_l)}{\Delta\varepsilon}$ where $\Delta\varepsilon = \sum_l \Delta\varepsilon(\tau_l)$. Thus, a relaxation process governed by a superposition of Debye-functions is given by $\varepsilon' + \varepsilon'' = \varepsilon_\infty + \sum_{\tau_l} \frac{\Delta\varepsilon(\tau_l)}{1+i\omega\tau_l} = \varepsilon_\infty + \Delta\varepsilon \sum_{\tau_l} \frac{f(\tau_l)\Delta\tau}{1+i\omega\tau_l}$. In the continuum limit it follows that $\varepsilon' + \varepsilon'' = \varepsilon_\infty + \Delta\varepsilon \int \frac{f(\tau)}{1+i\omega\tau} d\tau$
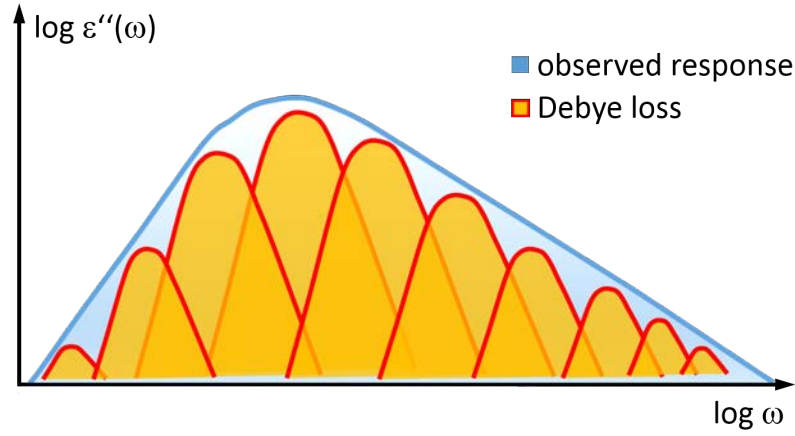
Figure 5.8: *Distribution of relaxation times.* A schematic representation of the significance of the existence of a distribution of relaxation times in the application to the interpretation of a non Debye loss peak in a dielectric material after Jonscher [146].

5.2.2   Model function for the analysis of dielectric spectra

Calculation of the relaxation time spectra from the experimentally-determined frequency dependent permittivity requires the inversion of Eq. (5.30). However, from a mathematical point of view this is an ill-conditioned problem, i.e. that small errors in the dielectric data result in much larger errors in the relaxation time distribution and special methods must be applied to solve this problem numerically [152, 153, 154, 155, 156].

More convenient, empirically model function have been developed to describe broadened and /or asymmetric loss peaks (ε'') . The most general model function was introduced by Havriliak and Negami [157, 158] as,

$$\varepsilon^*_{HN} = \varepsilon_\infty + \frac{\Delta\varepsilon}{\left[1 + (i\omega\tau)^{1-\alpha}\right]^\beta} \tag{5.31}$$

Here $\Delta\varepsilon$ is the relaxation strength, ε_∞ is the high frequency limit of the dielectric constant, τ is the characteristic relaxation time, α and β are the width and asymmetry parameters, respectively (Fig. 5.9). The dispersion and absorption spectra for the Havriliak-Negami function are [151],

$$\varepsilon'_{HN} = \varepsilon_\infty + \frac{\Delta\varepsilon \cos\left(\beta \arctan\left[\frac{\sin\left((1-\alpha)\frac{\pi}{2}\right)}{(\omega\tau)^{\alpha-1}+\cos\left((1-\alpha)\frac{\pi}{2}\right)}\right]\right)}{\left[1 + 2\left(\omega\tau\right)^{1-\alpha}\cos\left((1-\alpha)\frac{\pi}{2}\right) + (\omega\tau)^{2(1-\alpha)}\right]^{\frac{\beta}{2}}} \tag{5.32}$$

$$\varepsilon''_{HN} = \frac{\Delta\varepsilon \sin\left(\beta \arctan\left[\frac{\sin\left((1-\alpha)\frac{\pi}{2}\right)}{(\omega\tau)^{\alpha-1}+\cos\left((1-\alpha)\frac{\pi}{2}\right)}\right]\right)}{\left[1 + 2\left(\omega\tau\right)^{1-\alpha}\cos\left((1-\alpha)\frac{\pi}{2}\right) + (\omega\tau)^{2(1-\alpha)}\right]^{\frac{\beta}{2}}} \tag{5.33}$$

The characteristic relaxation time of the asymmetric Havriliak-Negami model function

does not coincide with the relaxation time which is related to the position of the maximal loss $(\tau = \omega_{max}^{-1})$ (Fig. 5.10) , but depends on the parameters α and β as [159, 160, 161],

$$\tau = \frac{1}{\omega_{max}} \left\{ \frac{\left[\sin \left(\frac{(1-\alpha)\pi}{2(1+\beta)} \right) \right]}{\left[\sin \left(\frac{(1-\alpha)\beta\pi}{2(1+\beta)} \right) \right]} \right\}^{\frac{1}{1-\alpha}} \tag{5.34}$$

whereas for the symmetric Havriliak-Negami model function $\tau = \omega_{max}^{-1}$ holds (Fig. 5.9).
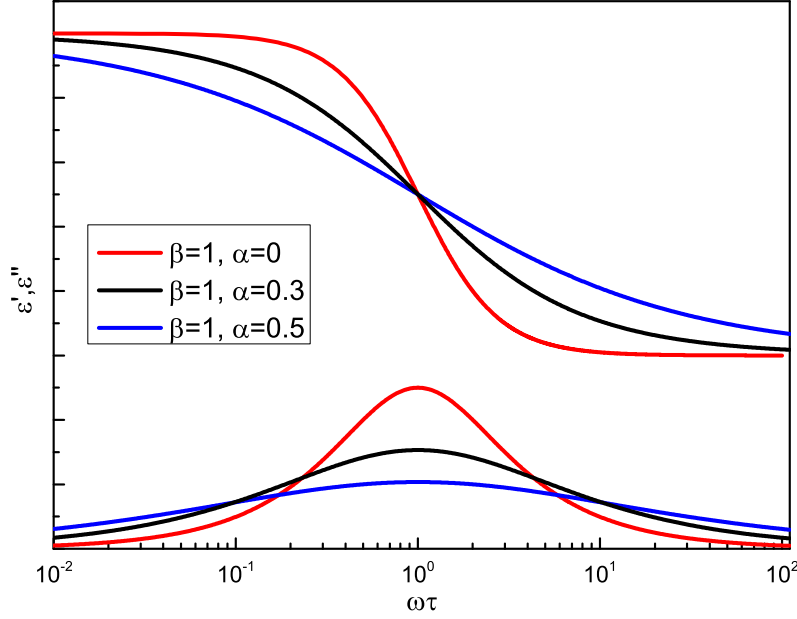
Figure 5.9: *Symmetric Havriliak-Negami model function for the complex permittivity.* The parameter α accounts for a symmetric broadening of the loss peak. For $\beta = 1$ the Havriliak-Negami model function is equal to the Cole-Cole model function.

The shape parameters, α and β, accounts for a broadened asymmetric loss peak (Fig. 5.9, 5.10) with power law characteristics for the low- and high-frequency asymptotic behaviour as $\omega^{1-\alpha}$ and $\omega^{-(1-\alpha)\beta}$ whereas the boundary conditions for the shape parameters are $0 \leq \alpha < 1$ and $0 < \beta \leq (1-\alpha)^{-1}$ respectively[6]. A simple Debye behaviour in Eq. (5.31) would corresponds to $\alpha = 0$ and $\beta = 1$.

The mean logarithmic relaxation time is related to the characteristic relaxation time by [162],

$$\langle \ln \tau_{HN} \rangle = \ln \tau + \frac{\psi(\beta) + Eu}{1 - \alpha} \tag{5.35}$$

where $\psi(\beta)$ is the digamma function and $Eu \approx 0.577$ is the Euler constant. The width of

---

[6]Since the loss peak is broader for the Havriliak-Negami function than the Debye peak, the asymptotic behaviour for $\omega \to 0$ in both cases must fulfil: $\omega^{1-\alpha} \leq \omega^1$. Thus $\alpha \geq 0$. With $\left. \frac{d\varepsilon''}{d\omega} \right|_{\omega \to 0} > 0$ follows that $\alpha < 1$. Hence, $0 \leq \alpha < 1$.

For $\omega \to \infty$ follows, $\omega^{-\beta(1-\alpha)} \leq \omega^{-1}$. Thus $\beta \leq (1-\alpha)^{-1}$. With $\left. \frac{d\varepsilon''}{d\omega} \right|_{\omega \to \infty} < 0$ follows that $\beta > 0$. Hence, $0 < \beta \leq (1-\alpha)^{-1}$.
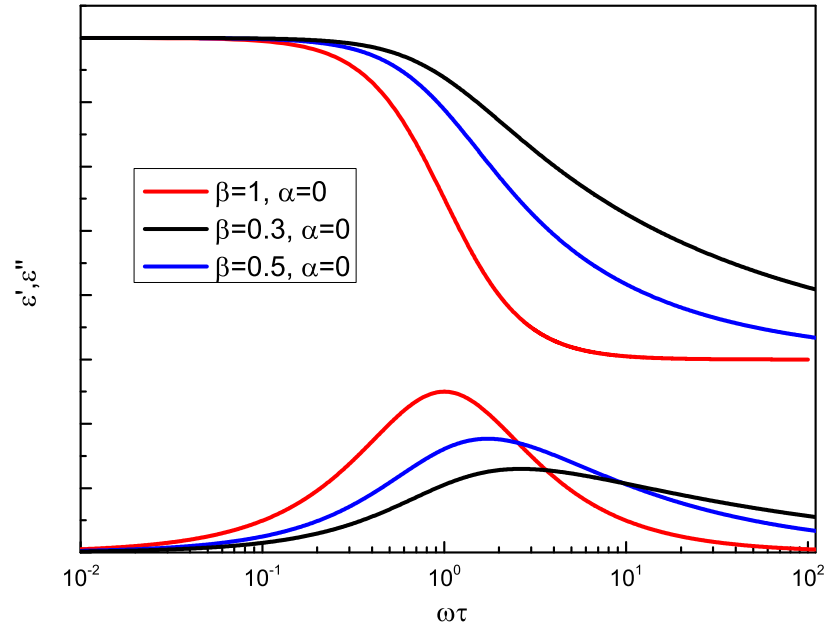
Figure 5.10: *Asymmetric Havriliak-Negami model function for the complex permittivity.* The parameter β accounts for an asymmetric broadening of the loss peak

a non-Debye relaxation is defined as the variance of the distribution of logarithmic relaxation times. For a Havriliak-Negami model function the width is given by [162],

$$
\begin{aligned}
\sigma^2 &= \langle (\ln \tau_{HN})^2 \rangle - \langle \ln \tau_{HN} \rangle^2 \\
&= \frac{\psi'(\beta)}{(1-\alpha)^2} + \frac{\pi^2}{6(1-\alpha)^2} - \frac{\pi^2}{3}
\end{aligned}
\tag{5.36}
$$

where $\psi'(\beta)$ is the trigamma function. There are some other macroscopic models proposed and used widely for data processing, e.g. Cole-Cole [163], Cole-Davidson [164, 165], Fuoss-Kirkwood [145, 166], Jonscher [146, 167] and so on.

CHAPTER 6

Magnetoelectric phase transition in DyMnO$_3$

In rare-earth manganites (RMnO$_3$) a non-collinear long range cycloidal spin order of the Mn-spins is present in the ferroelectric phase. Above the magnetoelectric phase transition temperature a collinear sinusoidally-modulated spin order is proposed. Based on results by magneto-capacitance and by dielectric spectroscopy, an experimental evidence is provided that the magnetoelectric phase transition in DyMnO$_3$ follows an order-disorder scenario and that a coupling between spin and charge degrees of freedom exists well above the magneto-electric phase transition. These results suggest the interpretation of the paraelectric sinusoidal phase in manganites as a dynamical equilibrium of magnetic cycloids with opposite chiralities. Additionally a free-energy model is provided describing the magnetoelectric phase transition of cycloidal magnetoelectric multiferroics. The model is based on the assumption of a double-well potential and it includes the symmetry-allowed terms up to the second order.

6.1   Magnetic and dielectric phases of DyMnO$_3$

DyMnO$_3$ single crystals were used in this work grown in Ar flow by a floating-zone method with radiation heating [168, 169]. Terahertz properties of the samples from the same batch have been presented previously [170, 171]. The complex dielectric constant was measured for electric field along the crystallographic **a**-axis at a constant frequency of 10 Hz (quasi static) using a frequency response analyzer in several magnetic fields between 0T and 14T and with **B**∥**b**-axis. An anomaly of the real dielectric constant is observed shifting to higher temperatures with increasing magnetic field. For magnetic field $B > 6$T the anomaly shifts back to lower temperatures (Fig. 6.1).

The shape of that anomaly is depicted in more detail in Fig. 6.2.
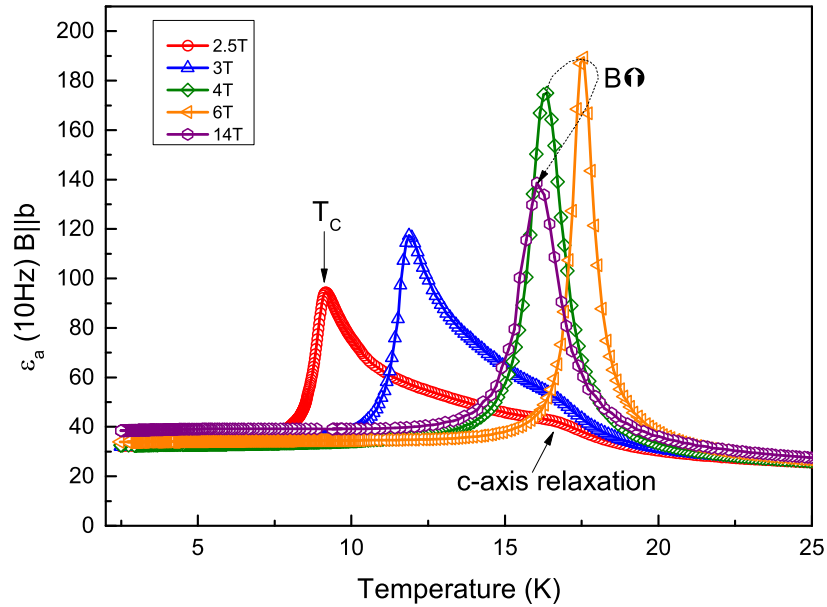
Here at low magnetic fields the peak structure shows a well distinct asymmetric divergency behaviour with a jump-like decrease of the quasi static permittivity at T_C. This is a hallmark feature of a first order phase transition where the order parameter (electric polarization) exhibits a step like change[1] at T_C [136]. Indeed it has been shown, that for $B < 4$T a step

---

[1]The free energy near T_C is given by, $F = F_0 + \frac{C}{2}(T - T_C)P^2 + \frac{D}{4}P^4 + \ldots$. Thus $\varepsilon \propto \chi^{-1} = \frac{\partial^2 F}{\partial P^2} = C(T - T_C) + 3DP^2 + \ldots$. Let assume $P^2 = A\Theta(T_C - T) + B(T_C - T)$ where $\Theta(T_C - T)$ is the heaviside function. Thus for $T > T_C$, $\chi^{-1} = C(T - T_C)$ and for $T < T_C$, $\chi^{-1} = -C(T_C - T) + 3DB(T_C - T) + 3A\Theta(T_C - T) = (3DB - C)(T_C - T) + 3A$. Therefore, $\chi_{T>T_C}(T = T_C) = \infty$ and $\chi_{T<T_C}(T = T_C) = \frac{1}{3A}$
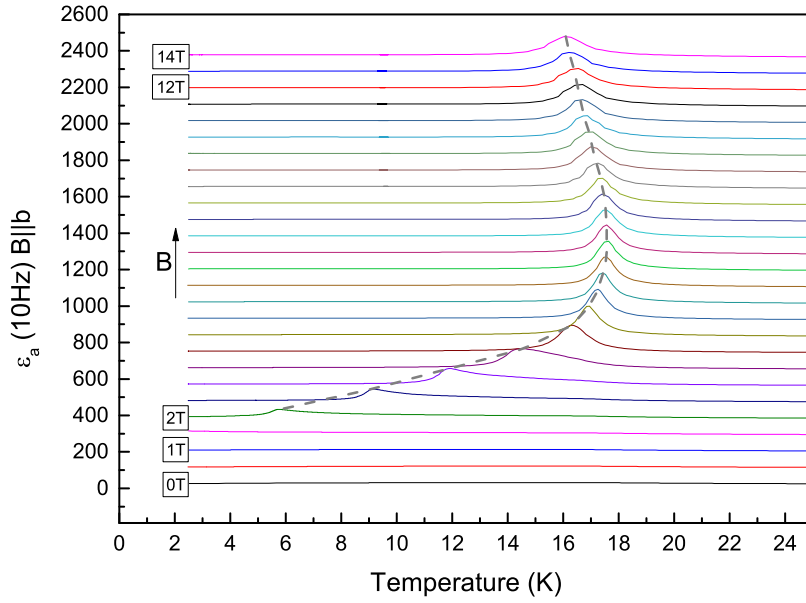
Figure 6.1: *Dielectric constant of DyMnO₃.* Grey dashed line indicates the trajectory of the dielectric constant anomaly as a function of magnetic field and temperature.


Figure 6.2: *Temperature profile of the dielectric constant.* With increasing magnetic fields the peak of the anomaly is shifting towards higher temperatures (grey dashed line). Additionally, the peak shape is asymmetric at low magnetic fields probably indicating a first-order ferroelectric phase transition

like increase of the electric polarization along the **a**-axis exists accompanied with a step like decrease of the electric polarization along **c**-axis at T_C [26, 64, 172, 173]. Consequently, a magnetic field **B**∥**b** induces an electric polarization flop from **P**∥**c** to **P**∥**a**. This behaviour is attributed to the flop of the spin cycloidal basal plane from bc to ab. At higher magnetic fields, $B \geqq 4$T, the shape of the peak becomes more symmetric and no jump like change of the quasi static permittivity is observed below T_C. This is a hallmark feature for a second order phase transition, where the order parameter increases continuously below T_C. Consequently, at $B \approx 4$T a tricritical point exist where a phase boundary line of first order transition intersect a phase boundary line of second order phase transition.

Additionally, the magnitude of the peak increases with increasing magnetic field and for $B \gtrsim 6$T it decreases again. Thus, it might be that the correlation length changes correspondingly (Eq. 4.19). Furthermore, the kink in ε_a at low magnetic fields is observed denoted by an arrow around 17K in Fig. (6.2). This feature reflects the ordering process along the **c**-axis. This kink is attributed to a misalignment of the crystal.

As a summary of dielectric experiments, figure 6.3 depicts the dielectric phase diagram of DyMnO$_3$ in magnetic filed along the **b**-axis.
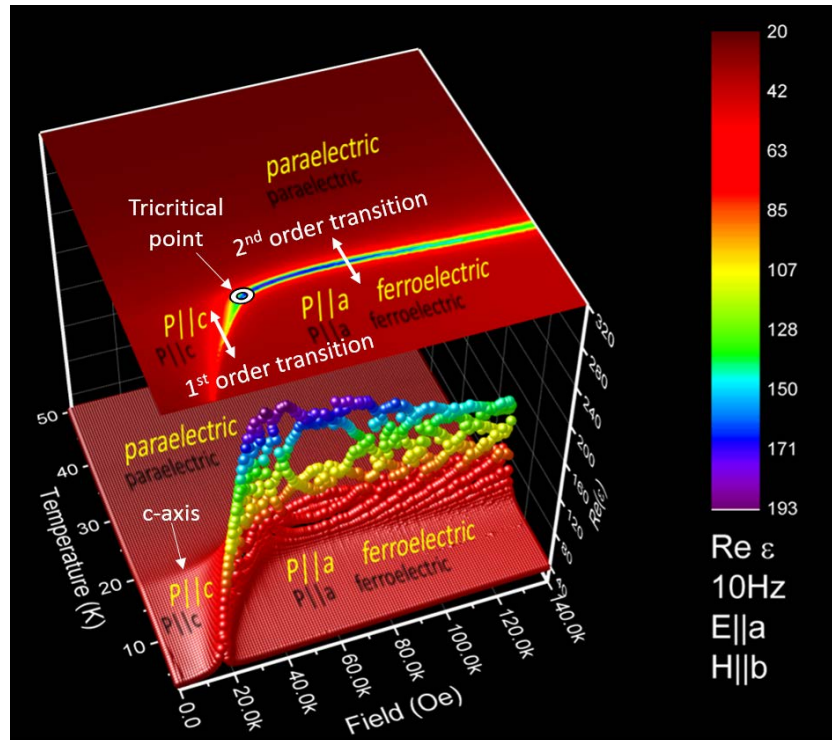
Figure 6.3: *Dielectric phase diagram of DyMnO$_3$.* At higher magnetic fields and low temperatures a ferroelectric state with an electric polarization pointing along the **a**-axis exists (**P**∥**a**). At lower magnetic fields the electric polarization points along the **c**-axis (**P**∥**c**). The transition from the paraelectric to the **P**∥**a** state is of second order whereas the transition from the **P**∥**c** to **P**∥**a** state is of first order. Additionally due to misalignment, the phase boundary between the paraelectric and ferroelectric **P**∥**c** state is also observed.

The divergent behaviour of the dielectric constant at certain temperatures and magnetic

fields indicates a phase transition from one dielectric phase to another. According to Kimura et al. [26] three regions of dielectric phases exists, (i) a paraelectric phase in the range $T_C < T < T_N$ where T_C denotes the ferroelectric transition temperature and T_N is the Neel temperature at which an antiferromagnetic order emerges, (ii) a ferroelectric phase with a static electric polarization along the crystallographic **c**-axis below T_C, and (iii) a ferroelectric phase with a static electric polarization along the crystallographic **a**-axis. Since $\mathrm{DyMnO_3}$ belongs to the material class of multiferroic rare-earth manganites $\mathrm{RMnO_3}$ (R=Gd, Tb, Dy, Eu/Y) with orthorhombically distorted perovskite structure and with strongly coupled antiferromagnetic and ferroelectric properties, the magnetic phases are of great significance.

In $\mathrm{TbMnO_3}$ Kenzelmann et al. [28] have analysed more than 900 first-order magnetic Bragg reflections obtained by neutron diffraction experiments.It has been proposed that in the paraelectric phase the magnetization, **M**, of the Mn-sublattice can be refined as a longitudinal sinusoidal modulation of the form shown in (Fig. 6.4) and repectively by,

$$
\begin{aligned}
M_a &= 0 \\
M_b &= M_{b,0} \cos\left(\mathbf{k}_{Mn}\mathbf{x}\right) \\
M_c &= 0
\end{aligned}
\tag{6.1}
$$

Here $M_{b,0} = 2.9\mu_B$ and $\mathbf{k}_{Mn}||\mathbf{b}$ is the magnetic modulation vector. Additionally, this assumption is confirmed by Mannix et al. [174] and Wilkins et al. [175] by x-ray scattering experiments on $\mathrm{TbMnO_3}$. However, both x-ray experiments show a small component of the magnetic moment aligned with the **c**-axis.

Within the ferroelectric phase with **P**||**c** the Mn-spin order changes. One observes a cycloidal structure with the magnetic moments confined to the **bc**-plane and rotating around the **a**-axis which may be described as,

$$
\begin{aligned}
M_a &= 0 \\
M_b &= M_{b,0} \cos\left(\mathbf{k}_{Mn}\mathbf{x}\right) \\
M_c &= M_{c,0} \sin\left(\mathbf{k}_{Mn}\mathbf{x}\right)
\end{aligned}
\tag{6.2}
$$

where $M_{b,0} = 3.9\mu_B$ and $M_{c,0} = 2.8\mu_B$, i.e. an elliptical spiral with the long axis of the ellipse close to the **b**-axis. In the ferroelectric phase with **P**||**a** the basal plane of the spin cycloid is rotated by 90° around the **b**-axis, i.e.

$$
\begin{aligned}
M_a &= M_{a,0} \sin\left(\mathbf{k}_{Mn}\mathbf{x}\right) \\
M_b &= M_{b,0} \cos\left(\mathbf{k}_{Mn}\mathbf{x}\right) \\
M_c &= 0
\end{aligned}
\tag{6.3}
$$

Neutron diffraction experiments clarifying the magnetic structure of the Mn-spins in $\mathrm{DyMnO_3}$ are very difficult to carry out due to a high absorption of neutrons and currently no publications are available addressing that issue.

Since similar phase diagrams have been reported for the closely related rare-earth manganates $\mathrm{RMnO_3}$ (R=Gd, Tb, Dy, Eu/Y) [26, 176], it may be expected that the magnetic structure
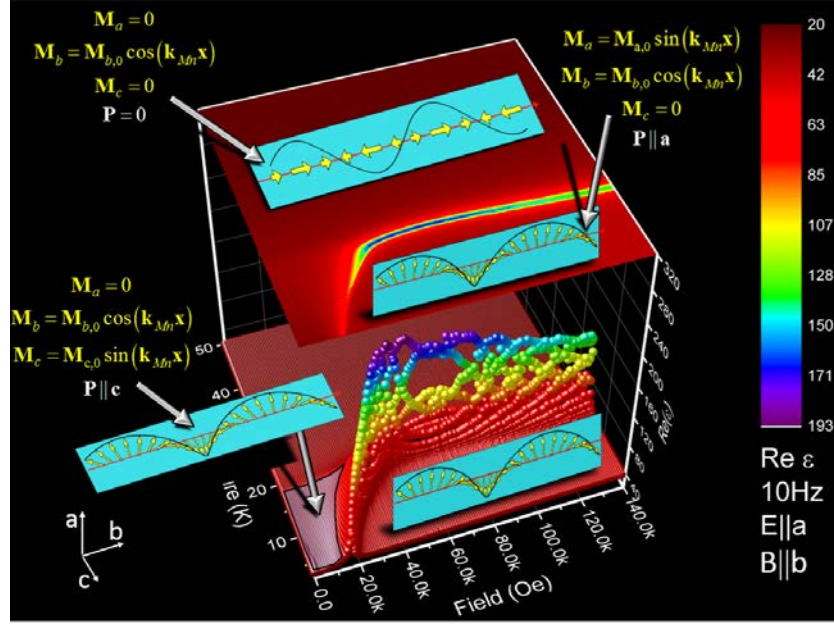
Figure 6.4: *Magnetic phase diagram of DyMnO₃.* In the paraelectric state the Mn-spins (yellow arrows) are sinusoidal modulated along the **b**-axis generating a spin density wave. In the **P**||**a** region the Mn-spins are cycloidal ordered in the *ab*-plane whereas in the**P**||**c** state the Mn-spins are cycloidal ordered in the *bc*-plane.

in $DyMnO_3$ is identical to that of $TbMnO_3$ in the paraelectric state as well as in the ferroelectric phase and the unique cycloidal magnetic ordering in the ferroelectric phase in any $RMnO_3$ (R=Gd, Tb, Dy, Eu/Y) is assigned to the Mn-3d spins [26, 28, 64, 177, 174, 178, 179]. The cycloidal order is a consequence of spin frustration (discussed in chapter 3) caused by $GdFeO_3 - like$ distortion of the MnO_6 octaedra (this will be discussed in chapter 6.1.1).

It is generally accepted that the ferroelectric polarization in $DyMnO_3$ is induced by a cycloidal magnetic order [28, 31, 180] through the IDM interaction (Eq. 3.14) [4, 63, 70, 74] and it can be written as (Eq. 3.17),

$$P = \sum_{i,j} K e_{i,j} \times (S_i \times S_j) \tag{6.4}$$

where $e_{i,j}$ denotes the unit vector connecting the spins S_i and S_j, K is a constant representing the exchange interaction and the spin-orbit interaction. Accordingly, the electric polarization, P, is intimately linked to the chirality of the magnetic cycloid (clockwise respectively counter-clockwise cycloidal magnetic ordering), that is, changing the direction of $+P \rightarrow -P$ implies changing the rotation (chirality) of the magnetic cycloid. This was demonstrated by the asymmetry in the scattering of left-handed and right-handed circularly-polarized x-rays by non-resonant magnetic x-ray diffraction for closely similar compound $TbMnO_3$ [181].

In addition, the ordering of the Dy-4f moments in $DyMnO_3$ is also of interest [182]. Although it is the magnetic structure of the Mn subsystem that determines the emergence of ferroelectricity in rare-earth manganites [183], the mutual coupling of the Mn-3d and Dy-4f moments and, consequently, the ordering of the 4f moments in $DyMnO_3$ causes a particular

large polarization observed in this material [184, 185].

6.1.1 GdFeO₃-like distortion and magnetic frustration in DyMnO₃

DyMnO₃ belongs to the crystal class of the Perovskites (ABX_3) with Dy^{3+} on the A-site, Mn^{3+} on the B-site and O^{2-} on the X-site. The magnetic frustration phenomenon of the Mn-3d spins is based on a peculiar arrangement of the O^{2-}-ion in the unit cell caused by a size mismatch of the ionic radii of the Dy^{3+}-ion and Mn^{3+}-ion. The ideal Perovskite structure has a cubic unit cell and consist of corner-sharing MnO_6 octahedra whereas the $R = Dy$-ion occupies the space between these octahedra (Fig. 6.5) . The lattice constant is determined by the side lenght and thus in turn related to the ionic radii via $a = L = 2\,(r_{Mn} + r_O)$ or via the diagonal by, $a = \left(\sqrt{2}\right)^{-1} D = \left(\sqrt{2}\right)^{-1} 2\,(r_R + r_O)$ respectively. For an ideal Perovskite structure the Goldschmidt's tolerance factor [186] given by,

$$t = \frac{L}{\left(\sqrt{2}\right)^{-1} D} = \frac{(r_R + r_O)}{\sqrt{2}\,(r_{Mn} + r_O)} \tag{6.5}$$

is equal to $t = 1.00$. However, the Dy-ion is smaller than the ideal value leading to $t < 1$. In that case the MnO_6 octahedra tilts around [110] and rotates around [001] of the cubic Perovskite (Fig. 6.6). Consequently, the cubic symmetry is broken and an orthorhombic structure with space group *Pbnm* is obtained (Fig.6.7).

This distortion from the ideal cubic Perovskite structure is called $GdFeO_3-like$ distortion. The orthorhombic unit cell is formed by doubling the **c**-axis and taking the two diagonals of the *ab*-plane as new crystallographic axes. This new unit cell contains 20 atoms (4xDy, 4xMn, 12xO) accordingly where a=5.279Å, b=5.834Å and c=7.378Å [187]. Additionally the MnO_6 octahedra is stretched along the **a**-axis and shortened along **b**-axis of the cubic unit cell due to the Jahn-Teller effect [188] caused by the interaction of Mn-3d electrons with the crystal field (crystal field splitting) of the surrounding oxygen octahedra. Since each oxygen atom is a shared vertex of two MnO_6 octahedra a stretching along the **a**-axis and shortening along **b**-axis of one octahedra leads to a opposite Jahn-Teller distortion i.e. a shortening along the **a**-axis and a stretching along the **b**-axis of the neighbouring octahedra (Fig.6.8). This collective distortions of the MnO_6 octahedra are called cooperative Jahn-Teller effect. From neutron diffraction study the long bond (Mn(4)-O(3)) is equal to 2.22Å and the short bond (Mn(4)-O(1)) is 1.90Å [187].

Furthermore, due to the crystal-field splitting the coupling of the orbital magnetic moment and the spin is broken up, so that the total magnetic moment is no longer influenced by the total angular momentum. Hence, the magnetic moment of the Mn^{3+} ions are solely determined by the spin and the contribution of the orbital motion to the magnetic moment diminishes (quenching of the orbital momentum).

The Pbnm structure is inversion symmetric with inversion centre at the position of the Mn-ions in the unit cell [189, 190]. Consequently, the existence of the linear magnetoelectric effect requires the broken space inversion symmetry of the magnetic order. As will be shown below, due to magnetic frustration a cycloidal magnetic order which breaks the space inversion

symmetry exists and thus the linear magnetoelectric effect is allowed in $DyMnO_3$.

6.1.1.1 Magnetic interactions

Magnetic order in $DyMnO_3$ is determined by super-exchange interactions. In contrast to direct exchange that arises from the overlap of the electronic orbitals of two adjacent magnetic ions, super-exchange is an indirect coupling of magnetic moments mediated by a intermediate diamagnetic ligand ion through virtual electron transfer (hopping) from the ligand to the magnetic ion. In $DyMnO_3$ the virtual hopping of electrons takes place between Mn-O-Mn respectively between Mn-O-O-Mn bonds.
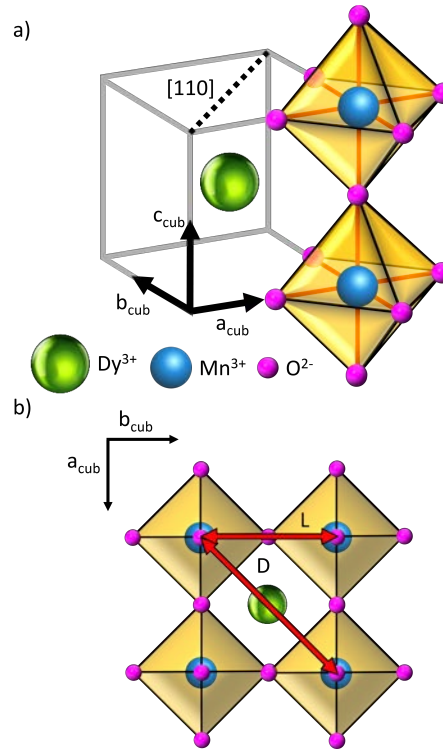

Figure 6.5: *Ideal Perovskite structure with cubic unit cell.* (a) Isometric projection of the ideal Perovskite structure. The green sphere represents the A-ion, the blue spheres represent the B-ion and the magenta spheres represent the X-ion. Corner-sharing MnO_6 octahedra and [110] axis are visible. (b) Top view of the ideal Perovskite structure. Red arrows represent the cube edge respectively the face diagonal of the cube.

The exchange interaction in the *ab*-plane between the nearest neighbour (NN) Mn spins (Mn-O-Mn) is ferromagnetic according to the Goodenough-Kanamori-Anderson rules [78] since the hopping occures between a filled and an empty orbital of the Mn ions.

The next nearest neighbour (NNN) exchange interaction between Mn spins (Mn-O-O-Mn) is antiferromagnetic since it occures between two filled orbitals of the Mn ions. It is much weaker than the Mn-O-Mn interaction. Thus, in the ideal perovskite structure, the NN interaction dominates and a ferromagnetic alignment of the Mn spins exists.

As the $GdFeO_3 - like$ distortion of perovskite structure increases, the distance between one pair of the opposite oxygen atoms in the *ab*-MnO_2 planes decreases (O(2)-O(3)), while
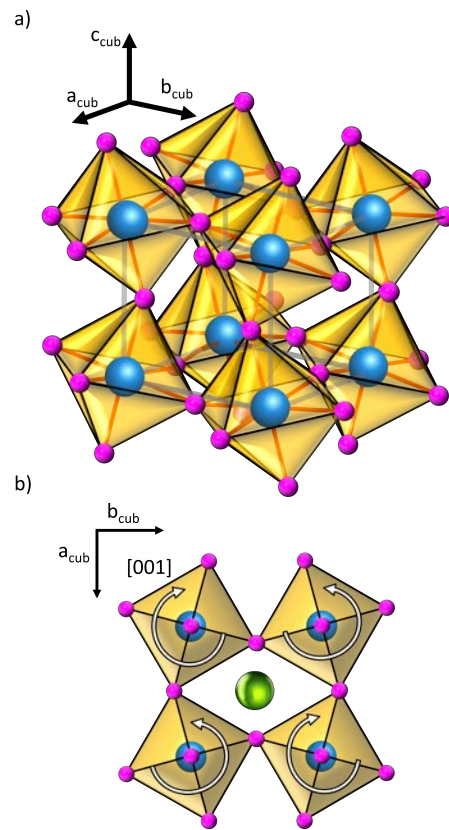
Figure 6.6: *Tilting and rotation of* MnO_6 *octahedra.* (a) Tilting of MnO_6 octa-
hedra. (b) Rotation of MnO_6 octahedra.
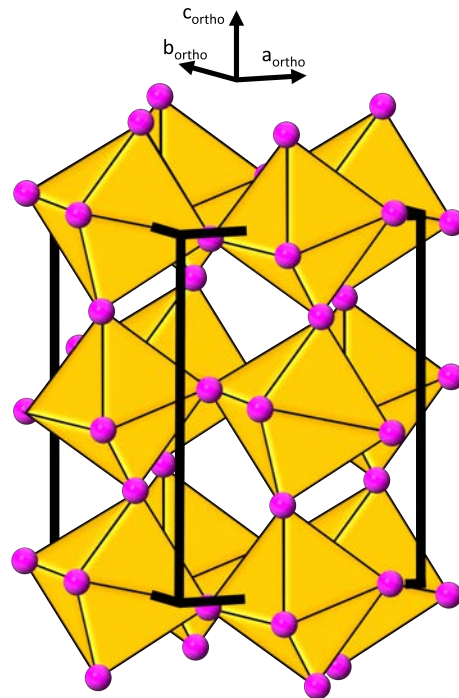
Figure 6.7: *Orthorhombic Pbnm structure of the unit cell.* The tilt and rotation of
the MnO_6 octahedra is visible ($GdFeO_3 - like$ distortion)
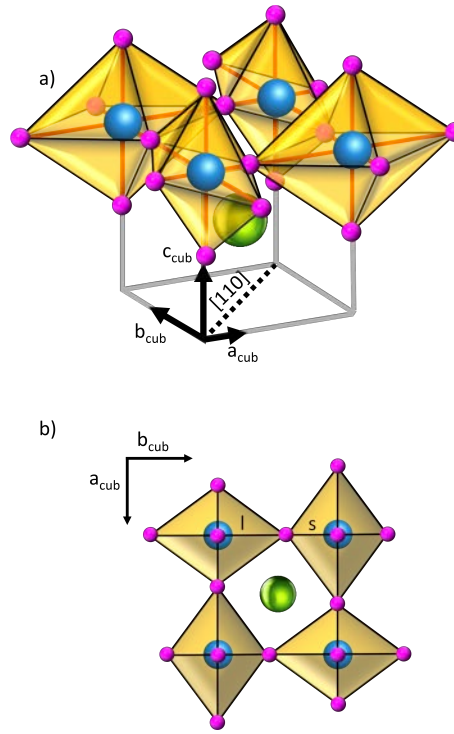
Figure 6.8: *Jahn-Teller distortion of the* MnO$_6$ *octahedra.* The MnO$_6$ octahedra is stretched respectively shortened an the *ab*-plane leading to a long and short Mn-O bond

for the other pair increases (O(1)-O(4)). This leads to a significant AFM NNN exchange interaction which is much stronger along the **b**-axis (Mn(1)-O(3)-O(2)-Mn(4)) than along the **a**-axis (Mn(2)-O(2)-O(3)-Mn(3)).

Therefore, the magnetic system in RMnO$_3$ is heavily frustrated leading to a cycloidal magnetic order with a magnetic modulation vector parallel to the **b**-axis ($\mathbf{k}_{Mn}||\mathbf{b}$). As a results of IDM interaction the O^{2-} ions will be displaced along the Δx-direction.

6.2 Classification of magnetoelectric phase transitions in - DyMnO$_3$

DyMnO$_3$ is a ferroelectric material with a direct one-to-one correlation between the position of of the O^{2-} ion and the angle between the neighbouring Mn^{3+} spins which exists due to IDM interaction. Consequently, for the two limiting cases (displacive or order-disorder transitions) the magnetic structure formed by the Mn^{3+} spins must take a special form and is not independent from the dielectric state. Thus, the spin degrees of freedom and the charge degrees of freedom are coupled in this material. Hence, for the magnetoelectric phase transition following conclusions may be drawn.
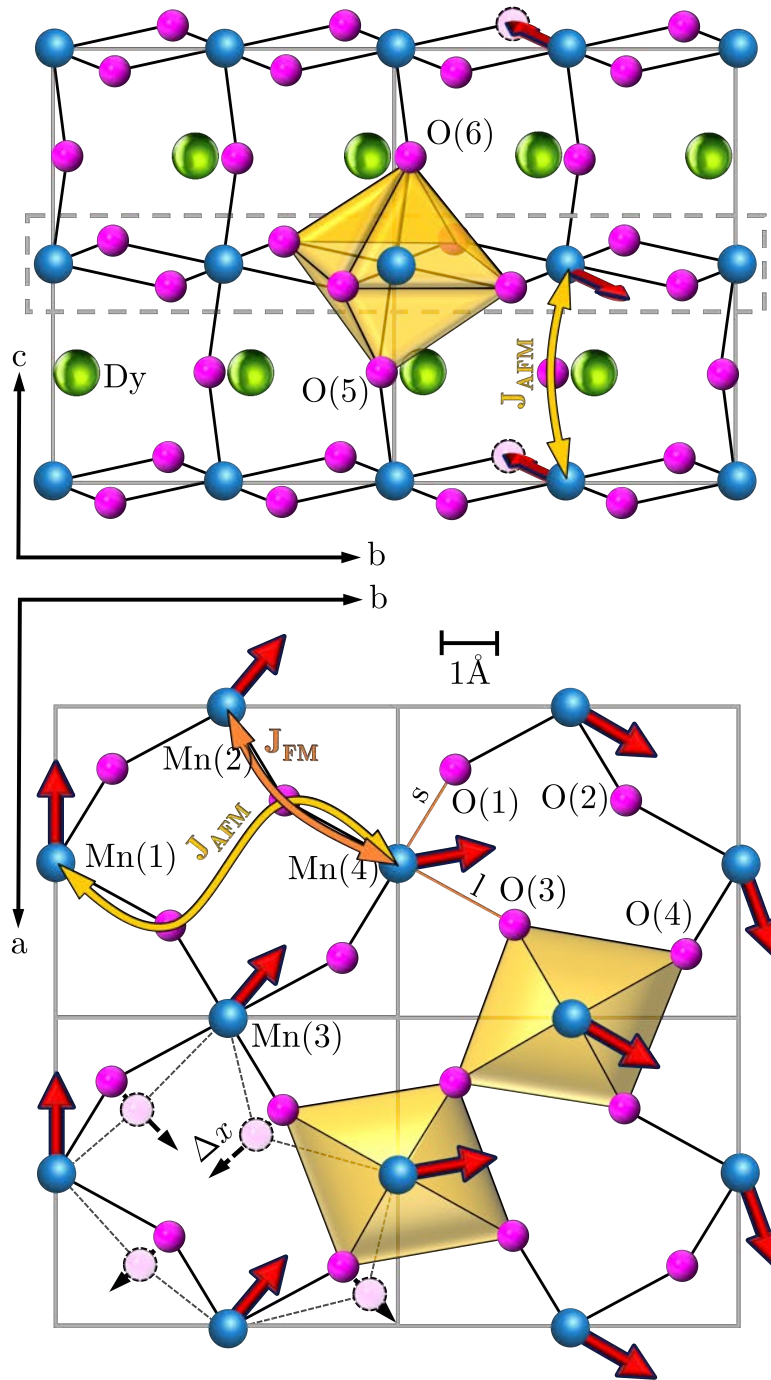
Figure 6.9: *Real crystal structure of the orthorhombic rare earth manganite* $DyMnO_3$. (a) bc-plane . Grey dashed lines mark one MnO_2 plane. Tilted and rotated MnO_6 octahedra are depicted. Red arrows represent Mn-3d total spins. (b) MnO_2 plane. Grey lines mark the boarder of the unit cell. Jahn-Teller distorted MnO_6 octahedra are visible. Yellow and orange arrows represents (AFM) respectively (FM) super-exchange interaction between NN and NNN Mn ions. Black dashed lines represents direction of displaced O-ion due to IDM. Two neighbouring MnO_2 planes differ in the position of the oxygen ion along the **c**-axis and in the direction of the Mn-spins (180° rotation) leading to the same position of the Mn and O-ions and the same chirality of the spin cycloide in the ab-plane.

6.2.1 Displacive-type magnetoelectric phase transition

Above the magnetoelectric transition temperature, the O^{2-} ions are not displaced to one side of the local double well potential thus in turn no net macroscopic electric polarization is generated (Fig.6.10).

According to IDM interaction, the neighbouring Mn^{3+} spins must align collinearly ($S_i \times S_{i+1} = 0$). Below the transition temperature the mean positions of all O^{2-}ions are displaced by the same small amount to one side of the origin, and the magnitude of this displacement increases on further cooling. Hence, at the transition temperature a macroscopic electric polarization arises and grows towards its maximum as $T \to 0$.

Again, due to IDM, the spins must not align collinearly in that phase ($S_i \times S_{i+1} \neq 0$). Both spin structures are in agreement with the proposed spin structure in TbMnO$_3$ [28]. Since DyMnO$_3$ is closely related to TbMnO$_3$, it should show the characteristics of a displacive phase transition at the magnetoelectric phase transition. Additionally, as $T \to 0$, the angle between neighbouring spins must increase. Consequently, the magnetic wave vector, $\mathbf{k}_{Mn}$, increases as $T \to 0$.

6.2.2 Order-Disorder type magnetoelectric phase transition

Even at temperatures well above the transition temperature, the O^{2-} ions will reside in one or other of the two wells, albeit with a random occupancy. Consequently, no macroscopic electric polarization is generated (Fig.6.11).

Due to IDM interactions, the neighbouring Mn^{3+} spins are not collinear ($S_i \times S_{i+1} \neq 0$) with a constant rotation angle between the spins, $\varphi = \pm\varphi_0$.

On cooling toward the transition temperature, $T > T_C$, the effects of interactions become more significant and a degree of short-range order in both magnetic and dielectric structures due to IDM interactions is established, i.e. an electric polarization exists on a mesoscopic scale but still on a macroscopic scale the electric polarization is zero. However, the spatial range of this short-range order grows on cooling toward T_C.

Below the transition temperature, $T < T_C$, the probability is larger that one side of the double-well potential (in this case the left-hand side) will be occupied. A long-range order is established (magnetic and dielectric) and, accordingly, a macroscopic electric polarization appears. However, there is also a significant probability that some atoms will occupy the alternative potential well.

At very low temperatures, $T \ll T_C$, most of the O^{2-} ions occupy the same side of the double-well potential. Thus, the electric polarization reaches its maximum.

Therefore, the electric polarization in the ferroelectric phase in DyMnO$_3$ is proportional to the difference of the number of clockwise and counter-clockwise rotating pair of neighbouring Mn^{3+} spins, i.e. it is proportional to the difference between opposite chiralities of Mn^{3+} spin pairs.
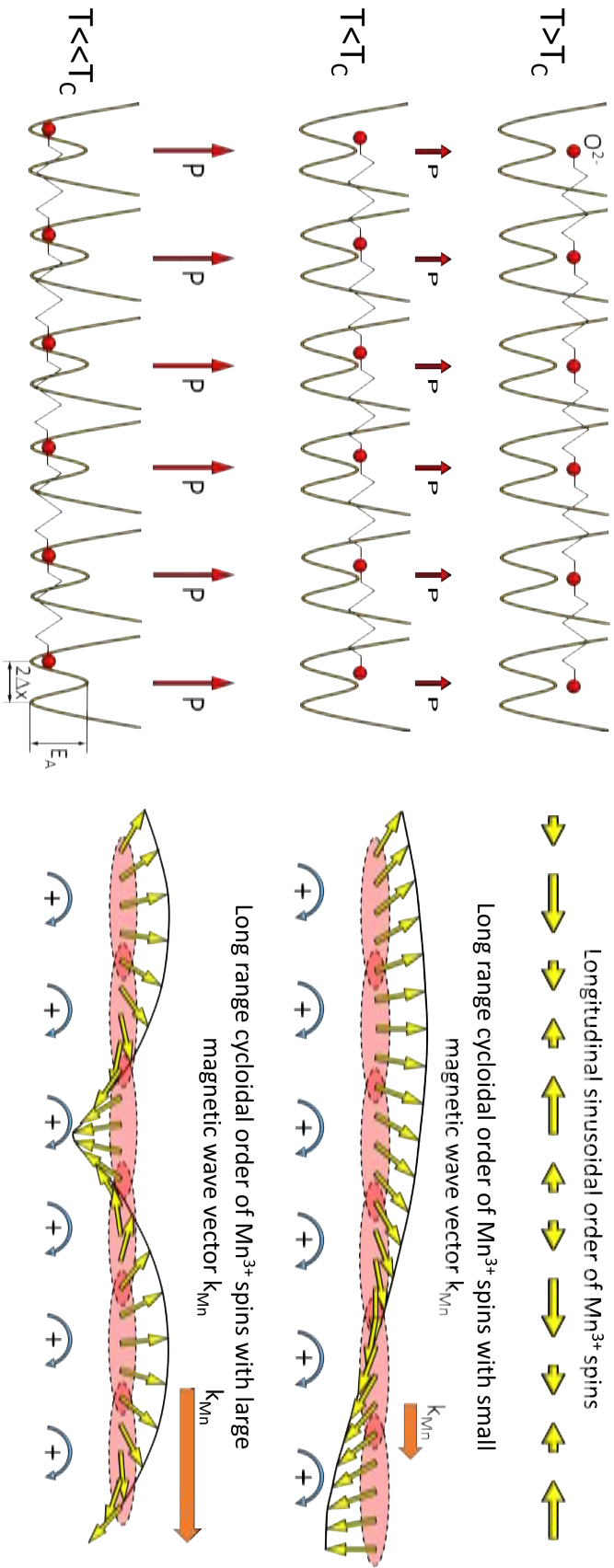
Figure 6.10: *Magnetoelectric phase transition of the displacive type.* Above the phase transition temperature ($T > T_C$) a longitudinal sinusoidal modulated spin structure of the Mn^{3+} spins is proposed. Accordingly, the O^{2-} ions are not displaced to one side of the origin. Below T_C, all O^{2-} ions are displaced to one side of the origin with increasing displacement as $T \to 0$. As a result, a cycloidal magnetic order emerges due to IDM interaction with increasing magnetic wave vector on further cooling.
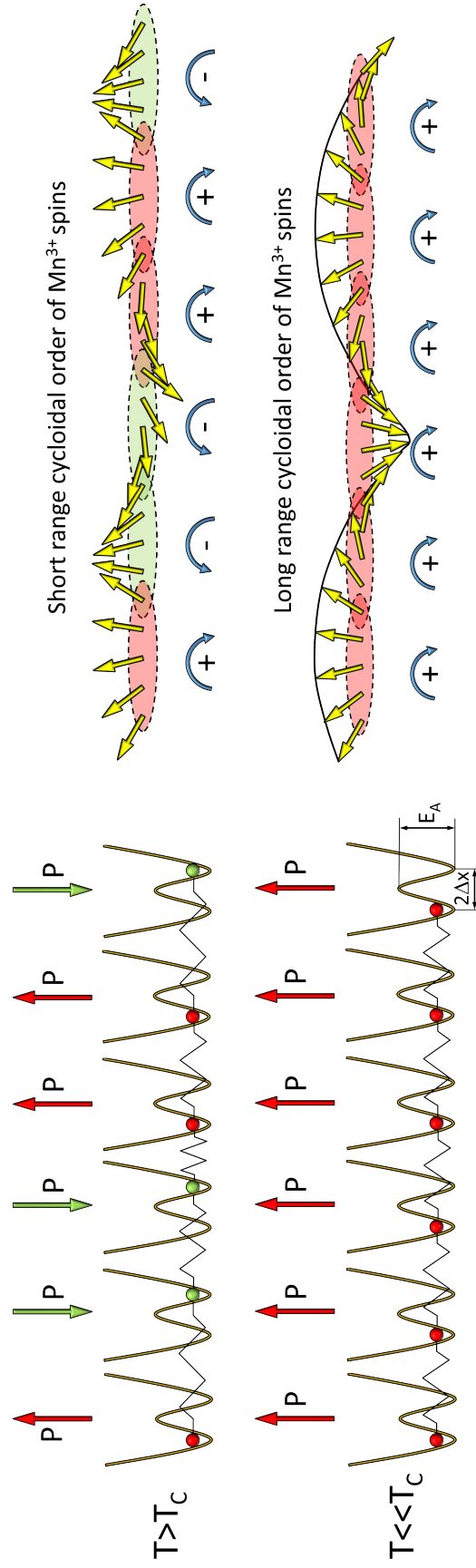
Figure 6.11: *Order-Disorder type magnetoelectric phase transition.* Above the magnetoelectric phase transition temperature ($T > T_C$) a short range order of the O^{2-} ions exist. Accordingly, a short range cycloidal order of the Mn^{3+} spins must exist due to IDM interaction. By further cooling below T_C, the correlation length increases. Thus in turn, all O^{2-} ions will be displaced finally to one side of the origin. Consequently, a long range cycloidal magnetic order emerges due to IDM interaction at $T = T_C$ with increasing order length on further cooling.

6.3   Experimental investigation of the magnetoelectric phase transition in DyMnO$_3$

In recent experimental studies [32, 33] it was found, that a non-zero dielectric contribution of electromagnon in the longitudinal sinusoidal ordered spin phase of Mn^{3+} ions exists. According to the commonly accepted mechanism of the electromagnon [34, 35], the majority of the spectral weight of this mode originates from exchange striction mechanism and can only exist in magnetic phases with non-collinear spin arrangement.

Consequently, the collinear sinusoidally-modulated spin phase contradicts this experimental facts.[2]. As will be shown below, present results support the idea, that the sinusoidal phase must be represented as a dynamical mixture of cycloidal phases with opposite polarities.

In order to solve that dilemma, the dielectric dynamics near the magnetoelectric phase transition, i.e. from the paralectric, $P = 0$, to the ferroelectric, $\mathbf{P} \parallel \mathbf{a}$, state were studied by the dielectric response of $DyMnO_3$ in the broadband radio-wave frequency regime. Complex dielectric permittivity was measured for electric field along the crystallographic $\mathbf{a}$-axis in the frequency range 0.1Hz-1MHz using a frequency response analyzer in magnetic fields 0-14 T and with $\mathbf{B} \parallel \mathbf{b}$-axis.

The spectrum of the dielectric constant at temperatures close to the critical temperature of the paraelectric-ferroelectric phase transition (white dashed boxes in Fig.6.12) were studied with an increment of $\Delta T = 0.1$K by using a Physical Property Measurement System (PPMS). Silver paint contacts were applied to the sample forming a capacitor.

6.3.1   Results

Detailed permittivity measurements in the frequency domain where carried out at magnetic fields of 4T,10T and 12T and at several temperatures near the magnetoelectric phase transition corresponding to the transition from the paraelectric to the $\mathbf{P} \parallel \mathbf{a}$-axis ferroelectric phase.

A well pronounced absorption is observed in the vicinity of T_C and it is accompanied by a dispersion of the permittivity revealing a relaxational response to the applied electric field as demonstrated in Fig. 6.13.

The spectra below the megahertz range are dominated by two relaxation processes. Only a wing of the high-frequency relaxation is seen in the spectra because the characteristic frequency of this mode is far above 1MHz. According to previous dielectric studies, the high-frequency mode can be attributed to the relaxation of the domain walls [191, 192] in $DyMnO_3$.

Figure 6.14 shows typical dielectric spectra of $DyMnO_3$ close to the ferroelectric transition temperature $T_C \approx 18$K.

In the following we concentrate the analysis on an absorption peak observed for frequencies below 1 kHz. As seen already in the spectra in Fig.6.14, this peak grows in magnitude with decreasing temperature, reaches a maximum value at T_C, and decreases again after

---

[2]The sinusoidal modulated spin phase describes only the time averaged value of the spin. Thus, the picture of a sinusoidal spin structure breaks down on a short time scale.
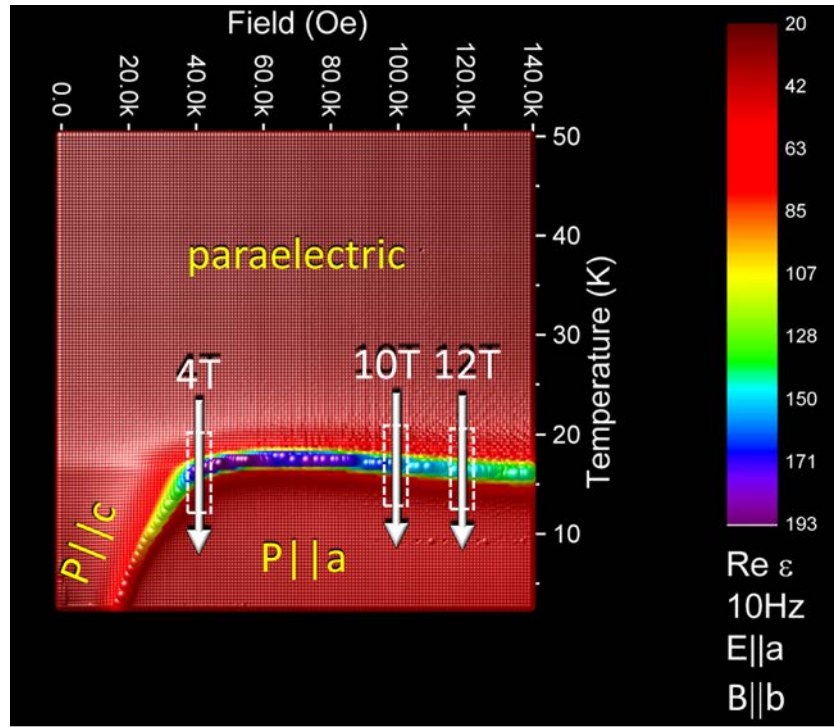
Figure 6.12: *Phase diagramm with dielectric experimental procedure.* The frequency dependent permittivity was measured in the close vicinity of the magnetoelectric phase transition at ,magnetic fields of 4T, 10T and 12T

passing the critical temperature. The observed dielectric relaxation is slightly asymmetrical with broadening towards low-frequencies.

To obtain quantitative information of the origin of the low-frequency mode the spectra were fitted to the phenomenological Havriliak-Negami equation[3], Eq.(5.31). Since the symmetric Cole-Cole function, Eq.(5.31) given by $\beta = 1$, is intensively used as a fitting function to describe permittivity data of conventional materials as well as magnetoelectric materials [30, 193], it is demonstrated by the dashed line in Fig. (6.14) for the $T = 16K$ data, that the symmetric Cole-Cole function results in a worse fit to the data compared to the Havriliak-Negami expression. Therefore, the subsequent analysis within the present work has been done according to Eq.(5.31). Most probably, a fitting procedure using the Cole-Cole function would lead to qualitatively similar behaviour of the relaxation time and dielectric strength. In doing so, one can extract the fundamental properties of the relaxation process as a function of temperature at several magnetic fields, i.e. the relaxation time and relaxation strength, and particularly, the behaviour of that quantities near a phase transition.

---

[3]To obey the constraints for the shape parameters during the fitting procedure it is better to use $n = 1 - \alpha$ and $m = (1 - \alpha)\,\beta$. Thus the Havriliak-Negami function is given by, $\varepsilon^*_{HN} = \varepsilon_\infty + \frac{\Delta\varepsilon}{[1+(i\omega\tau)^n]^{\frac{m}{n}}}$. Hence, the boundary conditions are independent from each other and are given by, $0 < n \leq 1$ and $0 < m \leq 1$.
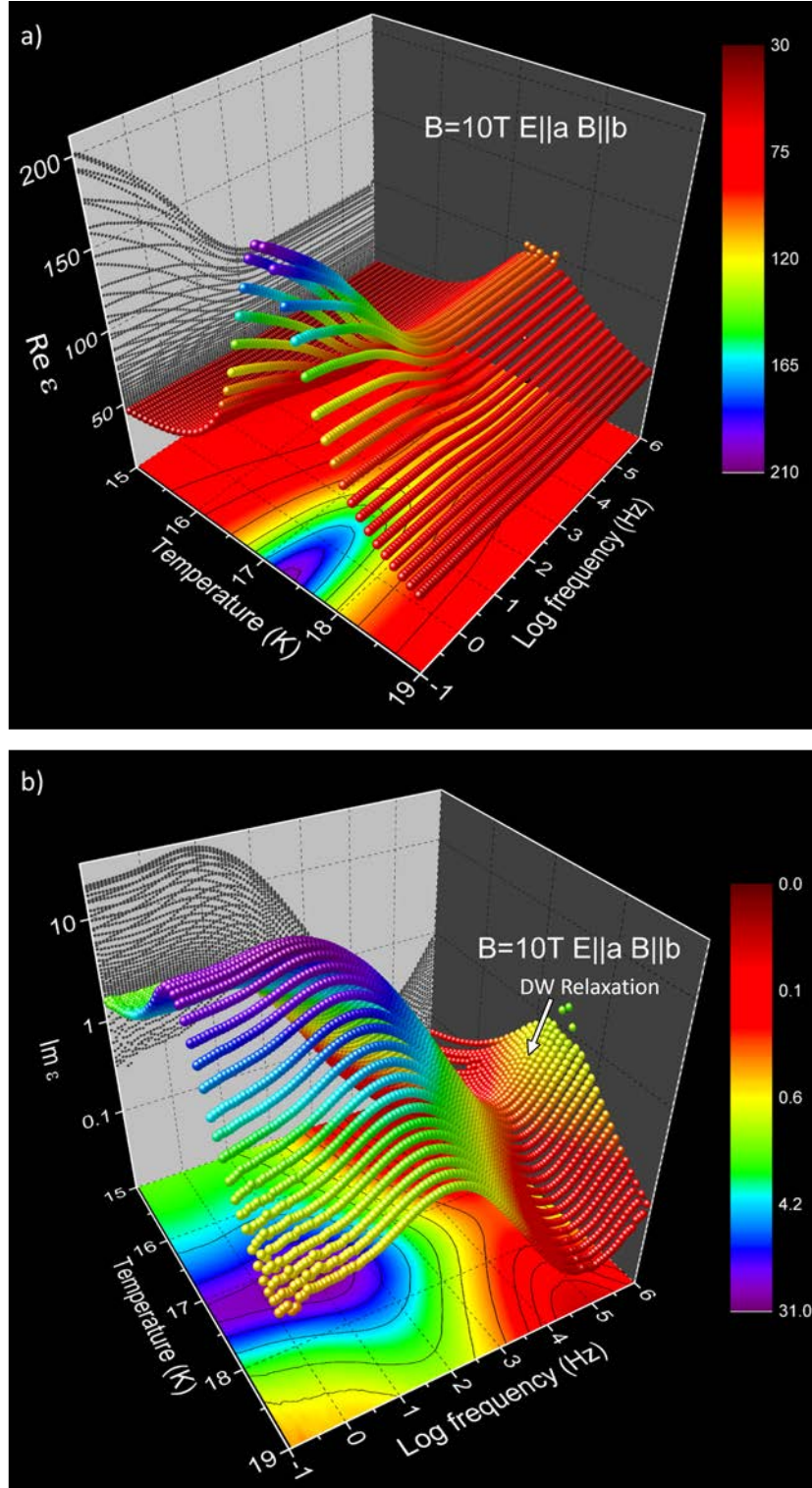
Figure 6.13: *Low frequency relaxation at the magnetoelectric phase transition.* Absorption (top) and dispersion (bottom) phenomena in the vicinity of the paraelectric to ferroelectric phase transition at a magnetic field of $\mu_0 H = 10\text{T}$
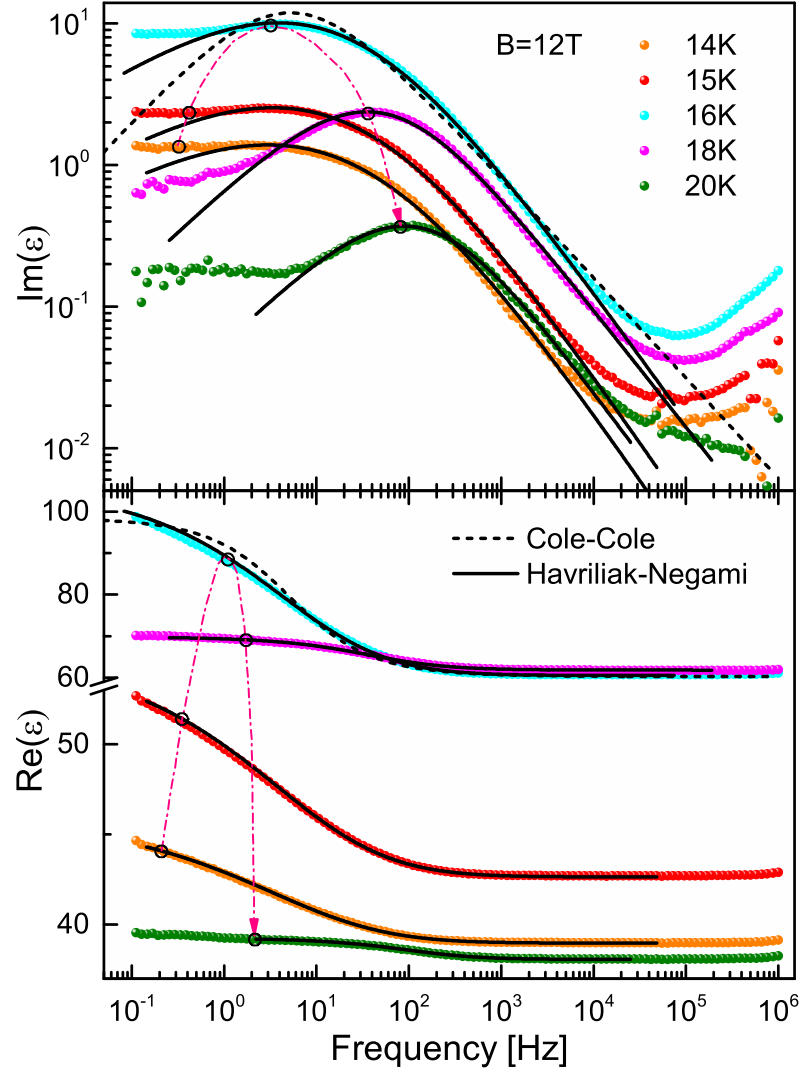
Figure 6.14: *Spectrum of the dielectric permittivity in a magnetic field of $\mu_0 H = 12T$.* Typical frequency dependence of the dielectric constant, Re(ε), and dielectric loss, Im(ε), at several temperatures above ($T = 18$K, $T = 20K$) and below ($T = 14K$, $T = 15K$, $T = 16K$) the critical temperature, $T_C \approx 17$K (at 12T). Black solids lines represents the fit according to the Havriliak-Negami relaxation function, Eq. (5.31). The dashed black line shows the fit according to the Cole-Cole equation, Eq.~(\ref{eqCC}). Dash-dotted lines with open circles schematically indicate the position of the spectra with increasing temperature.

6.3.1.1 Relaxation time

The inverse relaxation time of the low frequency mode obtained from the spectral analysis of dielectric permittivity is shown in Fig.6.15.
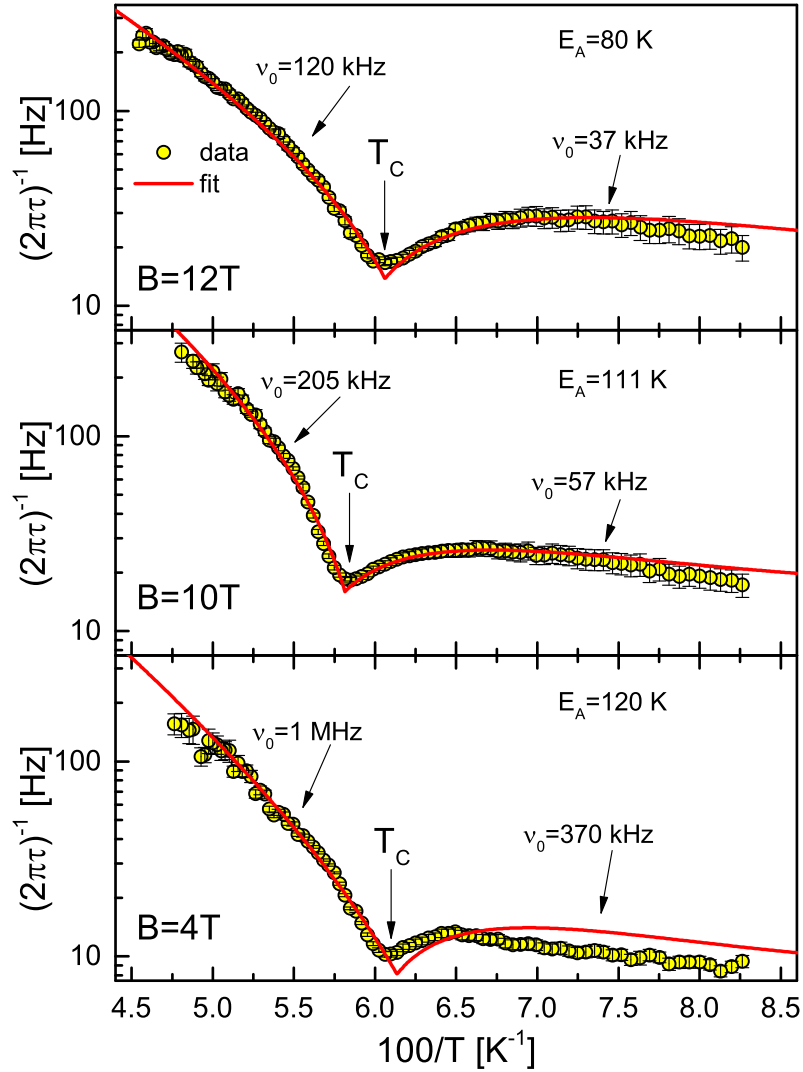
Figure 6.15: *Inverse relaxation time.* Inverse mean relaxation time along the **a**-axis of the low frequency mode as a function of temperature for different magnetic fields **B∥b**-axis. The yellow symbols are obtained by the spectral analysis procedure and the red solid line corresponds to the order-disorder fit function according to Eq.(4.96)

On cooling from the paraelectric phase the inverse relaxation time decreases toward $T_C \sim$ 16.5K. Below T_C, $1/\tau$ shows a broad characteristic maximum and decreases again for low temperatures. Qualitatively, the temperature behaviour of the relaxation time can be explained as a superposition of two processes: (i) Activated behaviour with a characteristic energy of $E_A \sim 100$K and (ii) Critical slowing down of the relaxation in the vicinity of T_C. This observation is typical for order-disorder phase transitions involving shallow double well potentials [119, 134, 135].

Both processes determining the temperature evolution of the relaxation time are qualitatively well captured within the present simple order-disorder model (Eq.4.96). The temperature activated behaviour, expressed by the exponential factor in Eq.(4.96), prevails for temperatures far from T_C and, therefore, causes an overall decrease of the relaxation time for decreasing temperature.

Because of that, the displacive model (Eq.4.107) is not able to describe this behaviour for $T < T_C$ which actually shows a pure Curie-Weiss like behaviour of the relaxation time without a superimposed temperature activated behaviour. Hence, the observed temperature activated behaviour is not captured by the displacive limit. Consequently, the magnetoelectric phase transition in DyMnO$_3$ does not belong to the displacive type ferroelectric phase transition.

Qualitatively similar behaviour of the relaxation time was found [30] for a **c**-axis relaxation (**E**∥**c**) in DyMnO$_3$ for a transition to a bc-cycloidal magnetic ordering. The **P**∥**c**-axis state is achieved in DyMnO$_3$ for cooling in zero external magnetic field. It seem to be plausible that the **c**-axis relaxation in multiferroic manganites may be explained by the present order-disorder model model as well.

In case of inverse relaxation time the suggested model gives a qualitative explanation of the observed data. Equation (4.96) contains two temperature-dependent factors, Arrhenius term $\exp(-E_A/(k_B T))$ and the critical-slowing term $\nu_0(T-T_C)/T$. These two terms qualitatively explain the temperature dependence of the relaxation time close to phase transition. In order to obtain reasonable fits to the critical behaviour of the relaxation time, different values of the attempt frequency above and below T_C have been used and a temperature independent constant was added to Eq.(4.96). The distribution of relaxation times may play an role to explain that feature.

According to Eqs.(4.40),(4.43),(4.85), the ratio of $E_A/k_B T_C \sim 5$ is a further evidence of an order-disorder type phase transition which is totally in contrast to a displacive type where $E_A/k_B T_C \ll 1$ should holds. Furthermore, $E_A/k_B \sim 100$K corresponds well to a characteristic energy of the magnetic order as determined by Néel temperature of $T_N \sim 39$K [194].

Additionally, Fig.(6.16) shows the width of the low-frequency dielectric relaxation in DyMnO$_3$, obtained via Eq.(5.36). The increase of the characteristic width below $T_C \sim 18$K is clearly seen. In the ordered magnetic state, the effective length of the elementary cycloids increases thus leading to broader length distribution. Most probably, this also leads to the observed broadening of the dielectric relaxation.

In present work the higher-frequency relaxation attributed to the domain wall motions are not considered. Compared to fluctuations on the atomic level, ferroelectric domains are typically of μm size and they are responsible for the high-frequency dielectric relaxation [1, 191, 192]. Further two arguments are in favour of nano-size origin of the relaxation discussed here: (i) the low frequency relaxation (Fig.6.14) is well pronounced below and above T_C, and (ii) no signature of thermally activated creep motion of domain walls is evident in the Cole-Cole plots (Fig.6.17).
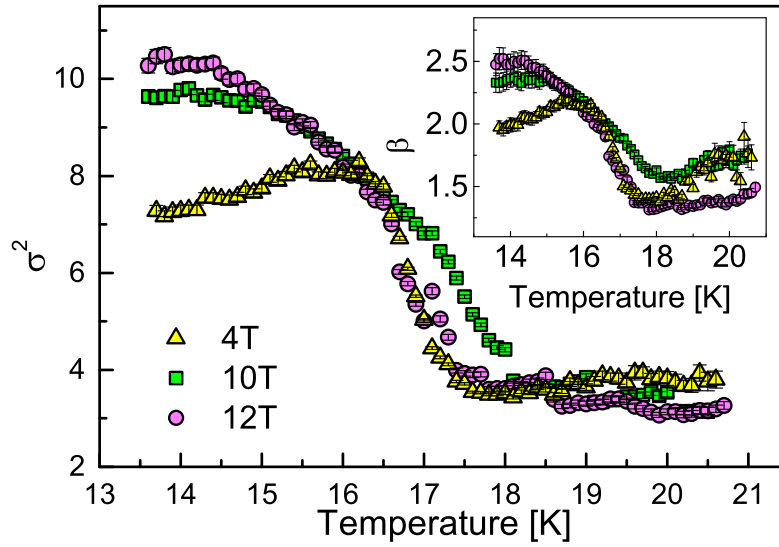
Figure 6.16: *Relaxation width of low frequency mode in* DyMnO₃. Width and asymmetry (inset) of the low-frequency dielectric relaxation.
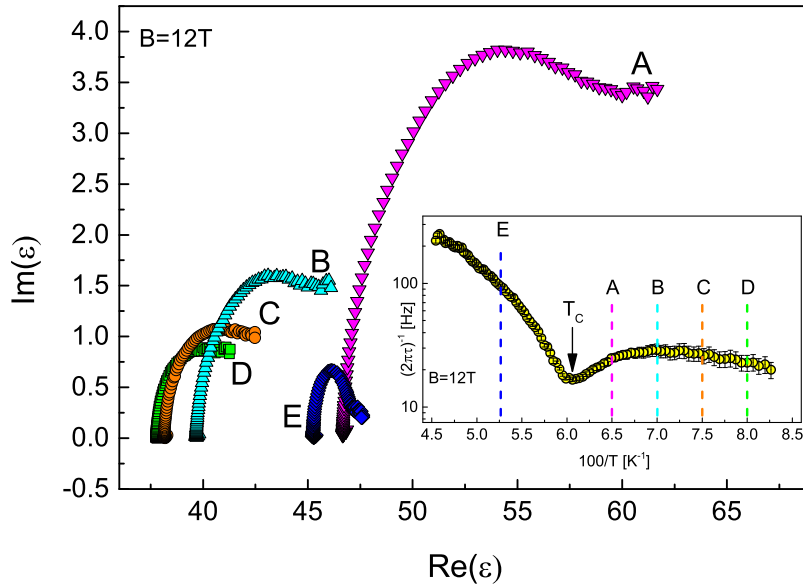

Figure 6.17: *Cole-Cole plots of low frequency relaxation.* A circularshape of the relaxation curves is clearly observed in a broad temperature range above and below T_C.

In the latter case a linear relationship between the imaginary and real part of the permittivity with $\text{Im}(\varepsilon) \propto \tan(\pi\beta/2) \cdot \text{Re}(\varepsilon)$ and $0 < \beta < 1$ will be expected [195, 196, 197].

6.3.1.2 Relaxation strength

The temperature dependence of the inverse relaxation strength of the low frequency mode is presented in Fig.(6.18).
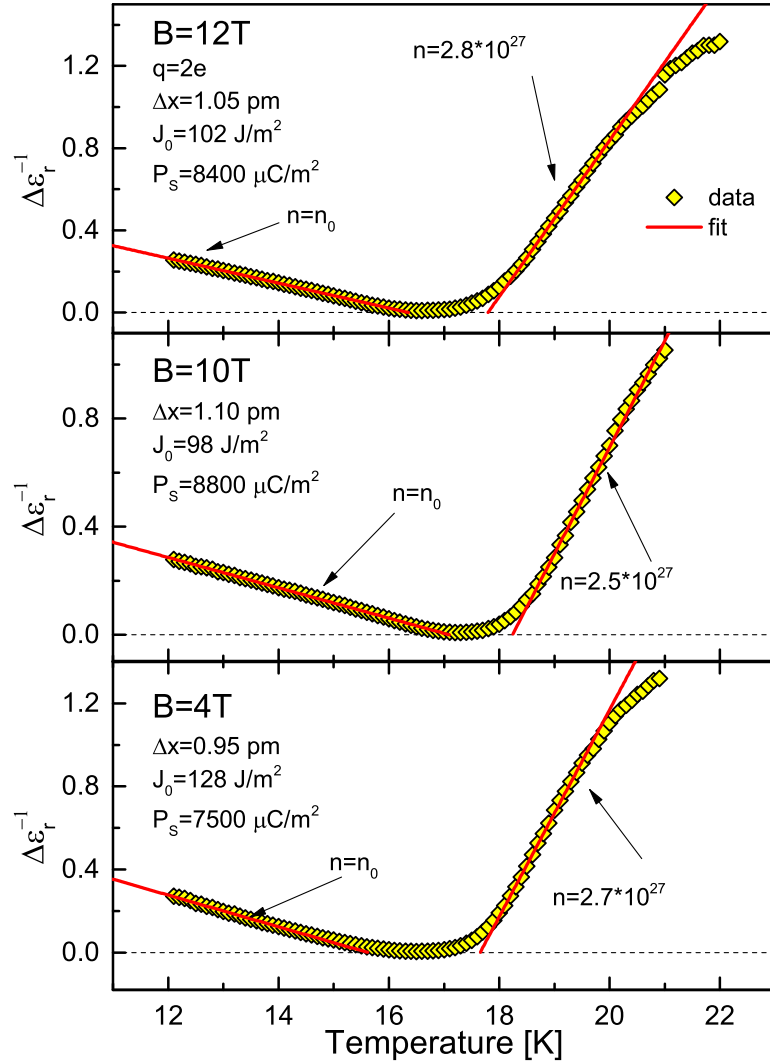
Figure 6.18: *Inverse Relaxation Strength.* For $T < T_C$, n and q are known thus in turn the displacement, Δx, is determined from the fits. For $T > T_C$, q and Δx are assumed to be constant thus the dipol density, n, must change.

Dielectric permittivity diverges as the temperature approaches T_C. At the magnetoelectric transition temperature DyMnO₃ undergoes a phase transition accompanied by a minimum in $\Delta\varepsilon_r^{-1}$ at T_C. As predicted by Eq. (4.97), close to the phase transition, $\Delta\varepsilon_r^{-1}(T)$ shows the regions of linear dependence. In addition, in the close vicinity of T_C, $\Delta\varepsilon_r^{-1}(T)$ reveals a distinct deviation from the linear temperature dependence which is associated by considerable

fluctuations[4] of the order parameter (electric polarization) very close to T_C. In that narrow temperature region, $\Delta\varepsilon_r^{-1}(T)$ shows a power law behaviour shown in Fig. 6.19. Here, an analysis using the formalism of critical exponents, $\Delta\varepsilon_r^{-1} \propto |T - T_C|^\gamma$ was carried out.
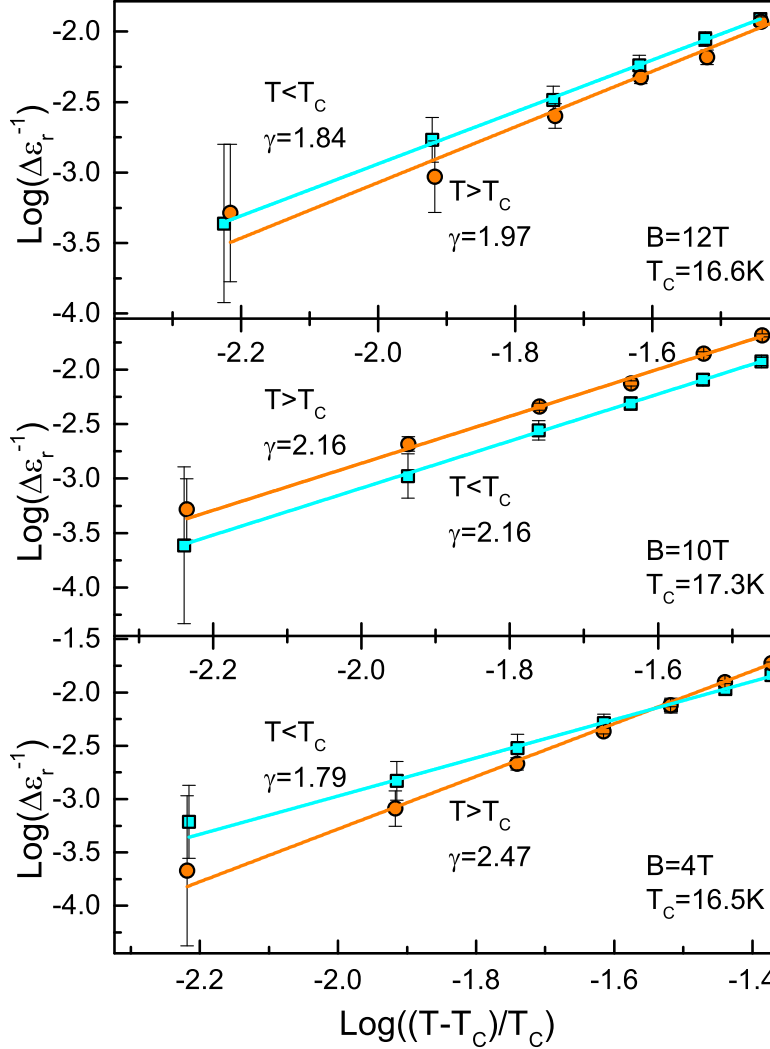
Figure 6.19: *Critical exponents close to T_C. The inverse of the relaxation strength of the low frequency mode follows a critical behaviour based on the formalism of critical exponents.*

As a result, the critical exponents are almost equal below and above T_C which is in accordance with the scaling law hypothesis [198] except for the case of $B \approx 4T$. This might be caused by a transition near the tricritical point. As discussed above, the tricritical point is at ~4T. Additionally, the values of the critical exponents are much larger than 1. Thus critical fluctuations very close to T_C play much more prominent role as for e.g. in itinerant ferromagnets, such as Ni, where the critical exponent is equal to 1.32 or in a uni-axial ferroelectric, such as TGS (triglycine sulphate) where $\gamma = 1$ [134]. This might be caused by a coupling of critical fluctuations of the electric polarization to the critical fluctuations of the magnetization

---

[4]usually denoted as "*critical fluctuations*"

since charge and spin degrees of freedom are coupled in DyMnO$_3$.

The electric dipole moment is generated by the displacements of the O^{2-} ions and only the ions labeled as O(1),O(2),O(3),O(4) in Fig. 6.9 generate a static electric polarization along the **a**-axis. Therefore, an electric dipole density in DyMnO$_3$ equal to $2/3$ of the full density of O^{2-} ions in the unit cell, $n_{O^{2-}} = n_0 \sim 3.5 \cdot 10^{28} m^{-3}$, and a charge of $q = 2e$, where e is the elementary charge are assumed. According to Eq. (4.97), the slope of $\Delta\varepsilon_r^{-1}$ is inversely proportional to $n(q\Delta x)^2 = 2P_s^2/n$ with static electric polarization along the **a**-axis, $P_s = nq\Delta x/\sqrt{2}$. The factor $\sqrt{2}$ appears due to 45° degree misalignment between the oxygen displacement and the **a**-axis (Fig. 6.9). Hence, from the slopes of $\Delta\varepsilon_r^{-1}$ for $T < T_C$, the static electric polarization is directly estimated. The microscopic parameters of the model, Δx and J_0 are obtained from the values of the static polarization and from $J_0 = k_B T_C/(\Delta x)^2$ (Eq. 4.80). These parameters are given in Fig. (6.18). Taking into account the simplicity of the model, the obtained values of the electric polarization agree reasonably well with directly measured data [26] where $P \sim 2000\mu C/m^2$. In addition, the obtained coupling constant coincide with the classical electric dipole energy in the Mn-O-Mn chains along the **b**-axis $J_0 \sim (q^2/2\pi\varepsilon_0)/(l^2+s^2)^{3/2} \sim 70 J/m^2$ (Fig. 6.9) with l and s being the long and short bond distances.

Near T_C the high frequency contributions, ε_∞, exhibits also a critical behaviour (Fig. 6.20).
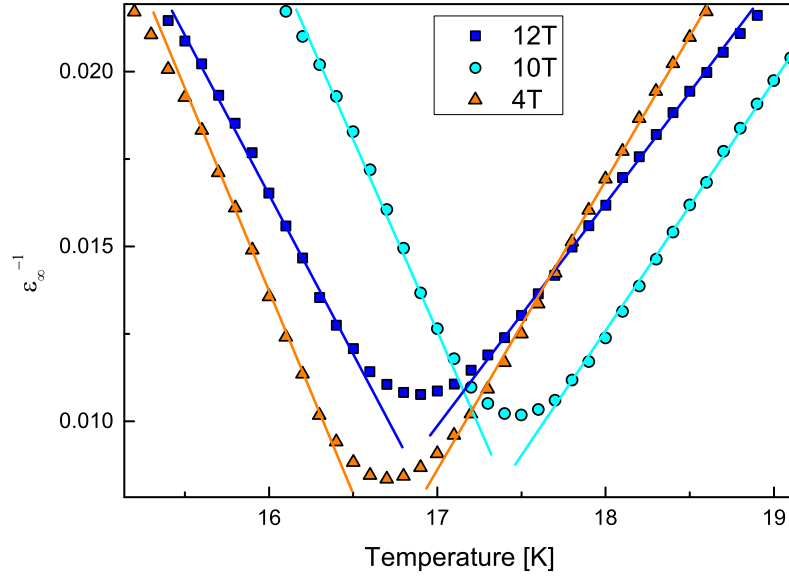
Figure 6.20: *Temperature characteristics of the high frequency contribution.* A Curie-Weiss behaviour of the high frequency contributions is observed at the magnetoelectric phase transition.

Thus high frequency contributions near the phase transition from the paraelectric to the ferroelectric **P** ∥ **a** state play also an important role.

6.3.2 Discussion

In magnetoelectric materials the electric polarization is directly linked to the magnetic structure. In order to describe this phenomenon, Smolenskii [199] introduced a bi-quadratic term ($F \propto \gamma P^2 M^2$, magnetodielectric effect) into the free energy which accounts for the coupling between magnetization and electric polarization.

Bi-quadratic terms are invariant to all symmetry operations and thus they are allowed in any material with coupled spin and charge degrees of freedom. Since the dielectric susceptibility is determined by taking the second derivative of the free energy with respect to the polarization, the dielectric constant will be proportional to the square of the order parameter, $\varepsilon \propto M^2$ [200]].

Describing the magnetodielectric effects in antiferromagnetic materials, the expression $F \propto \gamma P^2 M^2$ is not sufficient since the magnetization, M, remains zero in the ordered phase. In such a case, M is replaced by the antiferromagnetic vector, $L = M_1 - M_2$. Here M_1 and M_2 are the magnetizations of two antiferromagnetic subsystems.

Within a more general model, Lawes et al. [52, 201] proposed the coupling of the polarization to the q-dependent magnetic correlation function $\langle M_q M_{-q} \rangle$. This coupling leads to a magnetodielectric term in the free energy $F \propto \sum_q g(q) P^2 \langle M_q M_{-q} \rangle$, where $g(q)$ is a q-dependent coupling constant. The q-dependence of the free energy via a spin-spin correlation function enables to apply it to very general forms of magnetic order, including ferromagnetic (FM) and antiferromagnetic (AFM) transitions. In order to obtain a microscopic theory for $g(q)$ in systems with a strong spin-lattice interaction, the coupling between the polarization and the spin correlations arises from the coupling of magnetic fluctuations to the optical phonons. That is, the spin correlations perturb the optical phonon frequencies which in turn shift the dielectric constant through the spectral weight transfer and the Lyddane-Sachs-Teller relation. The model determines the coupling $g(q)$ by expanding the exchange integral of neighbouring spins in terms of the normal coordinates for the phonons. Physically, this procedure corresponds to a coupling between the magnetic correlation function and atomic displacements.

In multiferroic rare earth manganites, $RMnO_3$, the electric polarization is directly linked to the chirality of the magnetic cycloid [4, 63]. Based on this fact, it is proposed that the polarization in the ferroelectric phase in $DyMnO_3$ is proportional to the difference of opposite chiralities of Mn^{3+} magnetic cycloids. Here an order-disorder type phase transition between paraelectric and ferroelectric states is proposed. Similarly, it is demonstrated that in the triangular lattice antiferromagnet $RbFe(MoO_4)$ a proportionality between polarization in the multiferroic phase and the chirality difference of the magnetic structure exists. [202]. Hence, the electric polarization is nonzero as long as the net chirality is nonzero.

Thus, the following assumptions for the magnetoelectric phase transition in $DyMnO_3$ are imposed (Fig.6.21).

(i) A disorder between clockwise and counter-clockwise ab-cycloidal order of the Mn^{3+} magnetic moments is assumed.

(ii) The electric dipole moments are associated with the displacement of the O^{2-} ions due
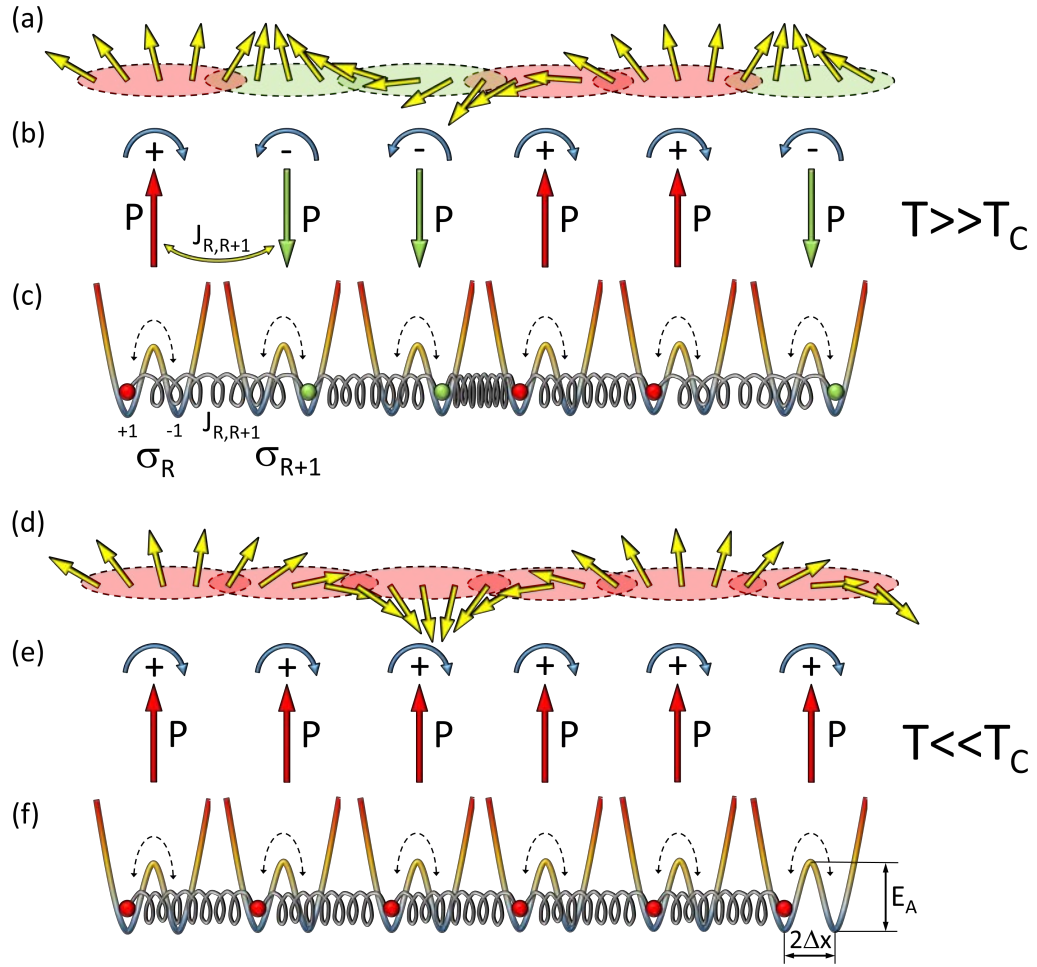
Figure 6.21: *Order-Disorder Model.* (a) Short range cycloidal order of the Mn^{3+} magnetic moments for $T > T_C$. (b) According to the IDM interaction, electric dipoles associated with the O^{2-} ions are generated by the canting of neighbouring spins leading to a mesoscopic electric polarization (red and green zones). However, the macroscopic electric polarization is zero for $T > T_C$. Each electric dipole interacts with neighbouring electric dipoles. (c) Ising type pseudo spins in local double-well potential separating energetically the clockwise ab-cycloidal and the counter-clockwise ab-cycloidal order of the Mn^{3+} magnetic moments. Each pseudo spin is in a local double-well potential and interacts with neighbouring pseudo spins by harmonic forces, represented as springs. Each pseudo spin generates a electric dipole moment of $\mu_R = \sigma_R q\Delta x$. Although the microscopic mechanism of the magnetoelectric coupling is more complex, within present simple model it is represented as an interaction between neighbouring pseudo spins via harmonic forces. (d) Long range cycloidal order of the Mn^{3+} magnetic moments for $T \ll T_C$ and leading to (e) non-zero macroscopic polarization. (f) At low temperatures most of the pseudo spins occupy the same side of the double-well potential.

to inverse DM interaction [4, 63].

(iii) The direction of the electric dipoles depend on the chirality of the magnetic order.

(iv) Two possible direction of the electric dipoles are energetically separated by an energy barrier.

(v) Similar to Lawes et al. [52, 201] a coupling of the magnetic correlation function and the correlation of O^{2-} atomic displacements is proposed. Thus it is assume that the ordering of the magnetic sublattice can be described by the ordering process of the O^{2-} ions.

6.3.2.1   Model deviations

The present simple order-disorder model qualitatively resembles the temperature evolution of the relaxation strenght and particularly the relaxation time very well. The temperature activated behaviour as predicted by the model and expressed by the exponential factor is well observed in the experimental obtained relaxation time temperature profile.

However, it is evident that the temperature dependence of the inverse relaxation strength becomes steeper in the paraelectric phase, $T > T_C$, although the model predicts an opposite behaviour if constant values of the microscopic parameters q, Δx and n are assumed. Two possible explanations for this behaviour are suggested and they are discussed below.

#### 6.3.2.1.1   Non-constant electric dipole density

From Fig. 6.14 it is evident, that a second relaxation follows after the low frequency mode with increasing frequency. It was shown that this mode arises at the phase transition from the $\mathbf{P} \parallel \mathbf{c}$ to $\mathbf{P} \parallel \mathbf{a}$ ferroelectric state and is associated with multiferroic domain wall relaxation between $\mathbf{P} \parallel \mathbf{c}$ and $\mathbf{P} \parallel \mathbf{a}$ domains [191].

This mode is clearly observed far away from the phase boundary between $P = 0$ to $\mathbf{P} \parallel \mathbf{a}$ (Fig.6.13), well pronounced in the vicinity of the phase transition boundary line, and increases in magnitude when approaching T_C (Fig. 6.20). Therefore, it is suggested, that this mode is associated with an ordering process between bc-cycloidal and ab-cycloidal short range order of the Mn^{3+} magnetic moments, insted of multiferroic domain wall relaxational motion.

This provokes an ordering process due to IDM between $\mathbf{p}||\mathbf{a}$ and $\mathbf{p}||\mathbf{c}$ local electric dipoles and thus in turn causes the divergency like decrease of ε_∞^{-1} in (Fig. 6.20) since the correlation length of fluctuations between bc-cycloidal and ab-cycloidal short range order of the Mn^{3+} magnetic moments increases towards T_C (Eq. 4.19). Hence, the electric dipole density will increase by approaching T_C (Fig. 6.22).

Accordingly, a more complicated potential in the single ion φ^4 model must be introduced similar to Mexican hat potential with four minima in the energy instead of a double well potential (Fig.6.23).

It is evident that the energy barrier between next neighbouring equilibria, E_B, is always smaller than between next nearest neighbouring equilibria, E_A, in such a potential landscape. Since the frequency of occurrence of a flip of the local electric dipol between $\mathbf{p}||\mathbf{a}_+ \leftrightarrow \mathbf{p}||\mathbf{a}_-$, $\mathbf{p}||\mathbf{c}_+ \leftrightarrow \mathbf{p}||\mathbf{c}_-$ and $\mathbf{p}||\mathbf{a}_\pm \leftrightarrow \mathbf{p}||\mathbf{c}_\pm$ is temperature activated, the relaxation dynamics between $\mathbf{p}||\mathbf{a}_\pm \leftrightarrow \mathbf{p}||\mathbf{c}_\pm$ is faster than between $\mathbf{p}||\mathbf{a}_+ \leftrightarrow \mathbf{p}||\mathbf{a}_-$ and $\mathbf{p}||\mathbf{c}_+ \leftrightarrow \mathbf{p}||\mathbf{c}_-$
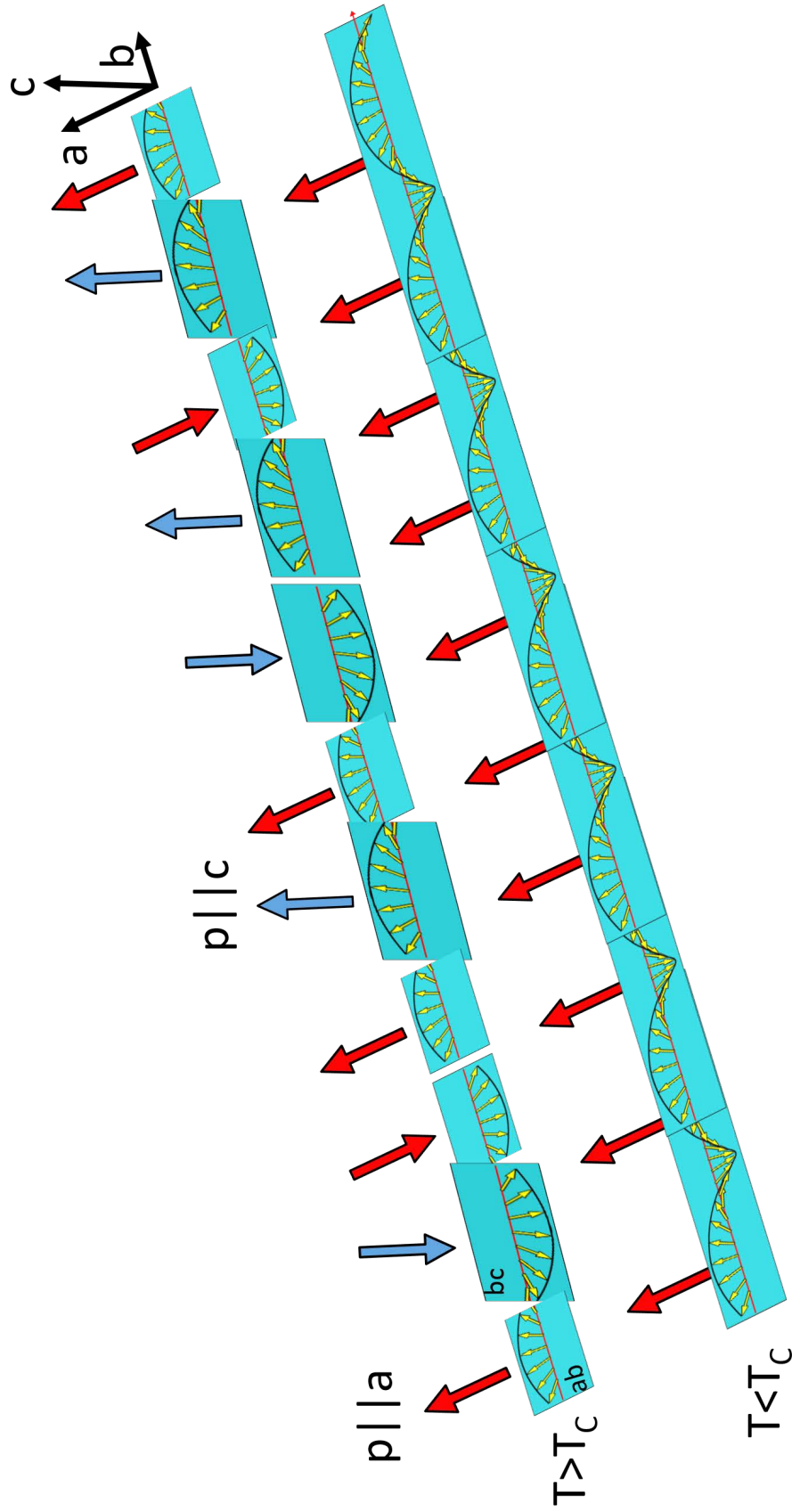
Figure 6.22: *Ordering process between bc-cycloidal and ab-cycloidal short range order of* Mn^{3+} *spins.* Above the magnetoelectric phase transition temperature ($T > T_C$) a mixture of bc-cycloidal and ab-cycloidal short range order of Mn^{3+} spins exist. Lowering the temperature towards T_C the number of ab-cycloidal regions increases to the expense of bc-cycloidal regions thus the number of $\mathbf{p}\|\mathbf{a}$ dipoles increase.
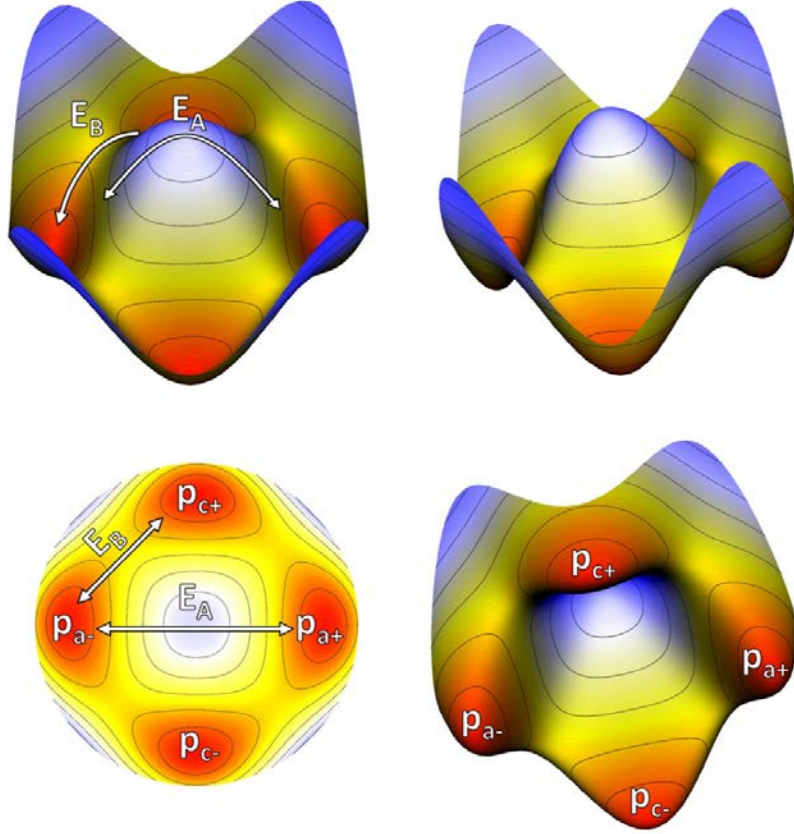
Figure 6.23: *Mexican hat potential with 4 minima.* Local electric dipoles can flip between four different states separated by a characteristic energy barrier.

However, to obtain reasonable fits to the critical behaviour of the relaxation time and the relaxation strength, different values of the attempt frequency respectively the dipol density above and below T_C must be assumed. To explain this behaviour, solely changes in the effective dipole density at the phase transition is not sufficient. Evidently, the variation of the attempt frequency across the transition cannot be explained.

6.3.2.1.2   Free Energy near T_C including magnetoelectric coupling

The double-well model may be improved including additional terms to the free energy. In fact this approach is even more general, as it includes all symmetry-allowed coupling terms between the dielectric and magnetic order parameters.

Accounting free energy contributions arising from the linear (Eq. 2.50) and non-linear ($F_{DE} = \sum_{i=2} \sum_{j=1}^{j<2i} \eta_i P^j M^{(2i-j)}$) magnetoelectric coupling, following elementary free energy expansion near T_C is proposed,

$$F^* = \underbrace{\sum_i a_i P^{2i} - gEP}_{F_P} + \underbrace{\frac{\mu_0}{\varepsilon_0 \chi_E \chi_M} \gamma PM}_{F_{ME}} + \underbrace{\sum_{i=2}^{} \sum_{j=1}^{j<2i} \eta_{ij} P^j M^{(2i-j)}}_{F_{MDE}} + \underbrace{\sum_i A_i M^{2i}}_{F_M} \quad (6.6)$$

where F_P is the pure free energy contribution originating from the ferroelectric subsystem (energy associated with electric dipole-dipole interaction and dipole-field interaction), F_{ME} is the free energy associated with the linear magnetoelectric effect, F_{MDE} is the non-linear magnetoelectric free energy caused by magnetodielectric effects and F_M is the pure magnetic free energy originating from spin interaction energy. M has to be understood as the amplitude of the transverse component of the spin-cycloidal, $S = (0, M\cos qy, M\sin qy)$. Only even powers in the non linear magnetoelectric free energy contribution are always allowed by symmetry. However, the bilinear term and terms with odd powers in P or M are only allowed in systems in which the magnetic structure breaks the spatial inversion symmetry. Due to the one to one relationship between displacement of charge and angle between two neighbouring spins caused by IDM, distinguishing whether M is the primary order parameter and P emerges as a secondary one (due to order in magnetic subsystem) or P is the primary order parameter and M emerges as a secondary one (due to order in dielectric subsystem), is not possible. Thus again, according to assumption (v) of the magnetoelectric phase transition, P is the primary order parameter and M emerges as a secondary one. This is confirmed by the fact, that the static electric polarization follows a power law as, $P \propto (T_C - T)^{1/2}$ [26]. According to Strukov and Levanyuk [203] this temperature dependence is in accordance with the temperature behaviour of the order parameter of a proper ferroelectric phase transition where P is the order parameter[5].

The strength of the bilinear coupling between P and M depends not only on the magnetoelectric susceptibility, but also on the inverse of the electric and magnetic susceptibilities given by $\chi^E \propto \left(\frac{d^2F}{dP^2}\right)^{-1}$ and $\chi^M \propto \left(\frac{d^2F}{dM^2}\right)^{-1}$. Additionally, the coefficient determining the strength of the bilinear coupling is not constant but depends on temperature and vanishes when the material becomes ferroelectric since $\chi^E \chi^M \to \infty$ if $T \to T_C$.

Thus, to study the effect on magnetoelectric coupling on the temperature behaviour of the electric susceptibility further simplification is made. Hence, the free energy may be written as,

$$F^* = \underbrace{\sum_i a_i P^{2i} - gEP}_{F_P} - \underbrace{\tilde{\gamma} PM}_{F_{ME}} + \underbrace{\sum_{i=2}^{} \sum_{j=1}^{j<2i} \eta_{ij} P^j M^{(2i-j)}}_{F_{MDE}} + \underbrace{\sum_i A_i M^{2i}}_{F_M} \quad (6.7)$$

where $\tilde{\gamma}$ is a constant. To simplicity further, only such terms should be introduced in the free energy which are essential to explain the temperature dependence of the electric susceptibility in case of a magnetoelectric phase transition. From the stability criteria ($\frac{\partial F^*}{\partial P} =$

---

[5]For improper ferroelectric phase transitions where P emerges as a secondary order parameter, the electric polarization shows a unusual temperature dependence differing from $P \propto (T_C - T)^{1/2}$

$0 \wedge \frac{\partial F^*}{\partial M} = 0$) it follows that ($E = 0$),

$$
\text{I)} \sum_i 2ia_i P^{(2i-1)} - \tilde{\gamma}M + \sum_{i=2} \sum_{j=1}^{j<2i} \eta_{ij} j P^{(j-1)} M^{(2i-j)} \quad = \quad 0
$$

$$
\text{II)} -\tilde{\gamma}P + \sum_{i=2} \sum_{j=1}^{j<2i} \eta_{ij} (2i-j) P^j M^{(2i-j-1)} + \sum_i 2iA_i M^{(2i-1)} \quad = \quad 0
$$

(6.8)

The electric susceptibility becomes with $\left(\chi^E\right)^{-1} = \varepsilon_0 \frac{1}{g} \frac{\partial^2 F^*}{\partial P^2}$,

$$
\left(\chi^E\right)^{-1} = \varepsilon_0 \frac{1}{g} \left[\sum_i 2i(2i-1) a_i P^{(2i-2)} + \sum_{i=2} \sum_{j=1}^{j<2i} \eta_{ij} j (j-1) P^{(j-2)} M^{(2i-j)} \right] \quad (6.9)
$$

Nota bene, the linear magnetoelectric coupling does not contribute to the electric susceptibility at all. Consequently, if it is necessary to account for the magnetoelectric properties of a system, then it is essential to consider non-linear coupling between P and M. Furthermore, for simplicity, only the bi-quadratic contribution of the non-linear magnetoelectric free energy is considered since (i) it is always allowed by symmetry and (ii) higher order non-linear coupling is supposed to be much weaker than the bi-quadratic contribution. Additionally, since M emerges as a secondary order parameter, it is sufficient to consider only the first term in the magnetic free energy contribution[6]. Thus the simplest total free energy for a megnetoelectric medium is proposed to be,

$$
F^* = \underbrace{aP^2 + bP^4 - gEP}_{F_P} - \underbrace{\tilde{\gamma}PM}_{F_{ME}} + \underbrace{\eta P^2 M^2}_{F_{MDE}} + \underbrace{AM^2}_{F_M} \quad (6.10)
$$

where $\eta > 0$ and $A > 0$. According to symmetry arguments, γ is zero above T_C and otherwise $\gamma > 0$. In case of a order-disorder transition $a = \frac{J_0}{2nq^2}\left(\frac{T-T_C}{T}\right)$, $b = \frac{(\Delta x)^4 J_0^4}{12n^3 q^4 k_B^3 T^3}$, $g = \frac{(\Delta x)^2 J_0}{k_B T}$.

The stability criteria becomes,

$$
\text{I)} \quad 2aP_0 + 4bP_0^3 + 2\eta P_0 M_0^2 - \tilde{\gamma}M_0 = \quad 0
$$

$$
\text{II)} \qquad 2AM_0 + 2\eta P_0^2 M_0 - \tilde{\gamma}P_0 = \quad 0
$$

(6.11)

From the second equation in Eq. (6.11) it follows that $M_0 = \frac{\tilde{\gamma}P_0}{2\eta P_0^2 + 2A}$. Near T_C, $P_0 \to 0$ (additionally, it is also reasonable to assume $\eta \ll \tilde{\gamma}$) thus the magnetic order parameter is given by,

$$
M_0 \approx \frac{\tilde{\gamma}}{2A} P_0 \quad (6.12)
$$

The electric susceptibility becomes with Eq. (6.12),

---

[6]The M^4 term which is usually needed to describe second order magnetic phase transition is not necessary here since M is triggered by the onset of P

$$\left(\chi^E\right)^{-1} = \varepsilon_0 \frac{1}{g} \left(2a + 12bP_0^2 + \frac{\tilde{\gamma}^2 \eta}{2A^2} P_0^2\right) \tag{6.13}$$

From the first equation in Eq. (6.11) and with Eq. (6.12) the polarization for $T < T_C$ is given by,

$$P_0^2 = \frac{-4a + \frac{\tilde{\gamma}^2}{A}}{8b + \frac{\tilde{\gamma}^2 \eta}{A^2}} \tag{6.14}$$

Hence, the electric susceptibility for $T < T_C$ becomes[7] with Eq. (6.14)

$$\left(\chi^E\right)^{-1} = \varepsilon_0 \left[-4\frac{a}{g}\Lambda + \frac{\tilde{\gamma}^2}{2gA} \left(1 + 2\Lambda\right)\right] \tag{6.15}$$

with,

$$\Lambda = \frac{1}{1 + \frac{\tilde{\gamma}^2 \eta}{8A^2 b}} \tag{6.16}$$

If $\tilde{\gamma}^2 \ll 2gA$ the static electric susceptibility becomes,

$$\left(\chi^E\right)^{-1} = \begin{cases} 2\frac{a}{g}\varepsilon_0 & T > T_C \\ -4\frac{a}{g}\varepsilon_0\Lambda & T < T_C \end{cases} \tag{6.17}$$

and the relaxation time becomes with Eq. (4.63),

$$\tau^{-1} = \begin{cases} 2a\Gamma & T > T_C \\ -4a\Gamma\Lambda & T < T_C \end{cases} \tag{6.18}$$

Hence, the ratio of slopes is not necessarily 2 as predicted in Eq. (4.66) but depends on the parameter Λ. Since the variables a, g, and Γ characterize the order parameter dynamics in case of a proper ferroelectric phase transition (no coupling of P with a secondary order parameter), they can be easily determined (see chapters 4.3, 4.4 and 4.5)

Thus, with Eq. (4.96) and Eq. (4.97), in case of an order-disorder type magnetoelectric phase transition, the relaxation strength and relaxation time becomes,

$$\Delta\varepsilon_r^{-1} = \begin{cases} \frac{\varepsilon_0 k_B}{nq^2(\Delta x)^2}\left(T - T_C\right) & T > T_C \\ 2\Lambda\frac{\varepsilon_0 k_B}{nq^2(\Delta x)^2}\left(T_C - T\right) & T < T_C \end{cases} \tag{6.19}$$

---

[7]Inserting Eq. (6.14) into Eq. (6.13) leads to,
$\left(\chi^E\right)^{-1} = \varepsilon_0 \left(-4\frac{a}{g}\frac{A^3 b}{A^3 b + \frac{1}{8}A\tilde{\gamma}^2\eta} + \frac{3}{2g}\frac{A^2 b\tilde{\gamma}^2}{A^3 b + \frac{1}{8}A\tilde{\gamma}^2\eta} + \frac{1}{16g}\frac{\tilde{\gamma}^4\eta}{A^3 b + \frac{1}{8}A\tilde{\gamma}^2\eta}\right)$. With $\Lambda = \frac{A^3 b}{A^3 b + \frac{1}{8}A\tilde{\gamma}^2\eta} = \frac{1}{1 + \frac{1}{8}\frac{\tilde{\gamma}^2\eta}{A^2 b}}$

follows,

$\left(\chi^E\right)^{-1} = \varepsilon_0 \left(-4\frac{a}{g}\Lambda + \frac{3}{2g}\Lambda\frac{\tilde{\gamma}^2}{A} + \frac{1}{16g}\Lambda\frac{\tilde{\gamma}^4\eta}{A^3 b} = -4\frac{a}{g}\Lambda + \frac{3}{2g}\Lambda\frac{\tilde{\gamma}^2}{A} + \frac{1}{16g}\Lambda\frac{\tilde{\gamma}^2\eta}{A^2}\frac{\tilde{\gamma}^2}{Ab}\right)$. Now,

$\Lambda = \frac{1}{1 + \frac{1}{8}\frac{\tilde{\gamma}^2\eta}{A^2 b}} \Rightarrow \Lambda + \Lambda\frac{1}{8}\frac{\tilde{\gamma}^2\eta}{A^2 b} = 1 \Rightarrow \frac{\tilde{\gamma}^2\eta}{A^2} = 8b\left(\frac{1}{\Lambda} - 1\right)$. Hence,

$\left(\chi^E\right)^{-1} = \varepsilon_0 \left(-4\frac{a}{g}\Lambda + \frac{3}{2g}\Lambda\frac{\tilde{\gamma}^2}{A} + \frac{1}{16g}\Lambda 8b\left(\frac{1}{\Lambda} - 1\right)\frac{\tilde{\gamma}^2}{Ab}\right) \Rightarrow \left(\chi^E\right)^{-1} =$

$\varepsilon_0 \left(-4\frac{a}{g}\Lambda + \frac{3}{2g}\Lambda\frac{\tilde{\gamma}^2}{A} + \frac{1}{2g}\left(1 - \Lambda\right)\frac{\tilde{\gamma}^2}{A}\right) \Rightarrow \left(\chi^E\right)^{-1} = \varepsilon_0 \left(-4\frac{a}{g}\Lambda + \frac{\tilde{\gamma}^2}{2gA}\left(3\Lambda + 1 - \Lambda\right)\right) =$

$\varepsilon_0 \left(-4\frac{a}{g}\Lambda + \frac{\tilde{\gamma}^2}{2gA}\left(2\Lambda + 1\right)\right)$

$$(2\pi\tau)^{-1} = \begin{cases} \left[\frac{\nu_0}{\pi} \left(\frac{T-T_C}{T} \right) \exp\left(-\frac{E_A}{k_B T} \right) \right] & T > T_C \\ 2\Lambda \left[\frac{\nu_0}{\pi} \left(\frac{T_C-T}{T} \right) \exp\left(-\frac{E_A}{k_B T} \right) \right] & T < T_C \end{cases} \tag{6.20}$$

It is clear, that adding explicitly the magnetoelectric terms into the free energy leads to a slope correction of the relaxation strength and of the relaxation time below the phase transition. Therefore, no changes in the effective dipole density and in the attempt frequency across the transition is necessary. However, fitting the relaxation time and the relaxation strength with the same slope correction factor, Λ, does not lead to satisfactory fits. Consequently, a variation of the dipole density is still assumed whereas the attempt frequency is held constant.

Accordingly, the new values for the displacement of O^{2-} in the low temperature phase, the dipole density in the high temperature phase and the static electric polarization becomes, $\Delta x_{ME} = \Delta x \sqrt{\Lambda}$, $n_{ME} = n\Lambda^{-1}$ and $P_{ME} = P\sqrt{\Lambda}$. With $\Lambda\nu_0 = \nu_0^*$ where ν_0^* is equal to the attempt frequency below T_C and ν_0 is the high temperature attempt frequency obtained by the fit of the relaxation time without considering magnetoelectric coupling explicitly in the free energy, the new values becomes with $\Lambda = \frac{\nu_0^*}{\nu_0}$ for $B = 10T$: $\Delta x_{ME} = 0.58$pm, $n_{ME} = 9E27$, $P_{ME} = 4640\mu C/m^2$ and for $B = 12T$: $\Delta x_{ME} = 0.58$pm, $n_{ME} = 9.1E27$, $P_{ME} = 4660\mu C/m^2$.

Nevertheless both approaches leads to a perfect agreement of the observed temperature characteristics of the relaxation time and of the dielectric strength in the vicinity of the magnetoelectric phase transition.

6.4   Magnetocapacitance

In a magnetoelectric multiferroic material, magnetic order is coupled to polarization and thus to the dielectric constant as well. Since magnetic field affects the magnetic ordering, the field also indirectly alters the dielectric constant of magnetoelectric multiferroics. In other words, perturbation of the magnetic structure due to magnetic field couples to the dielectric constant. This is the so called magnetodielectric or magnetocapacitance effect, which has been reported for a wide range of materials[200, 204, 205, 206, 207, 208, 209]. The magnetocapacitance has been measured at several temperatures above T_C as a function of magnetic field (often referred as magnetocapacitance, $[\varepsilon(H) - \varepsilon(H=0)]/\varepsilon(H=0)$) (Fig. 6.24).

A clear dependence of the dielectric constant on magnetic field is observed well above T_C (Fig. 6.24). Even at $T = 50$K, the relationship between the dielectric constant and magnetic field is well pronounced. Therefore, it is evident, that a coupling between spin and charge degrees of freedom is present not only in the low temperature but also in the high temperature phase. The coupling phenomenon can be derived by considering the electromagnetic free energy.

According to Eq.(2.27),the electromagnetic free energy including the free space contribution is given by,
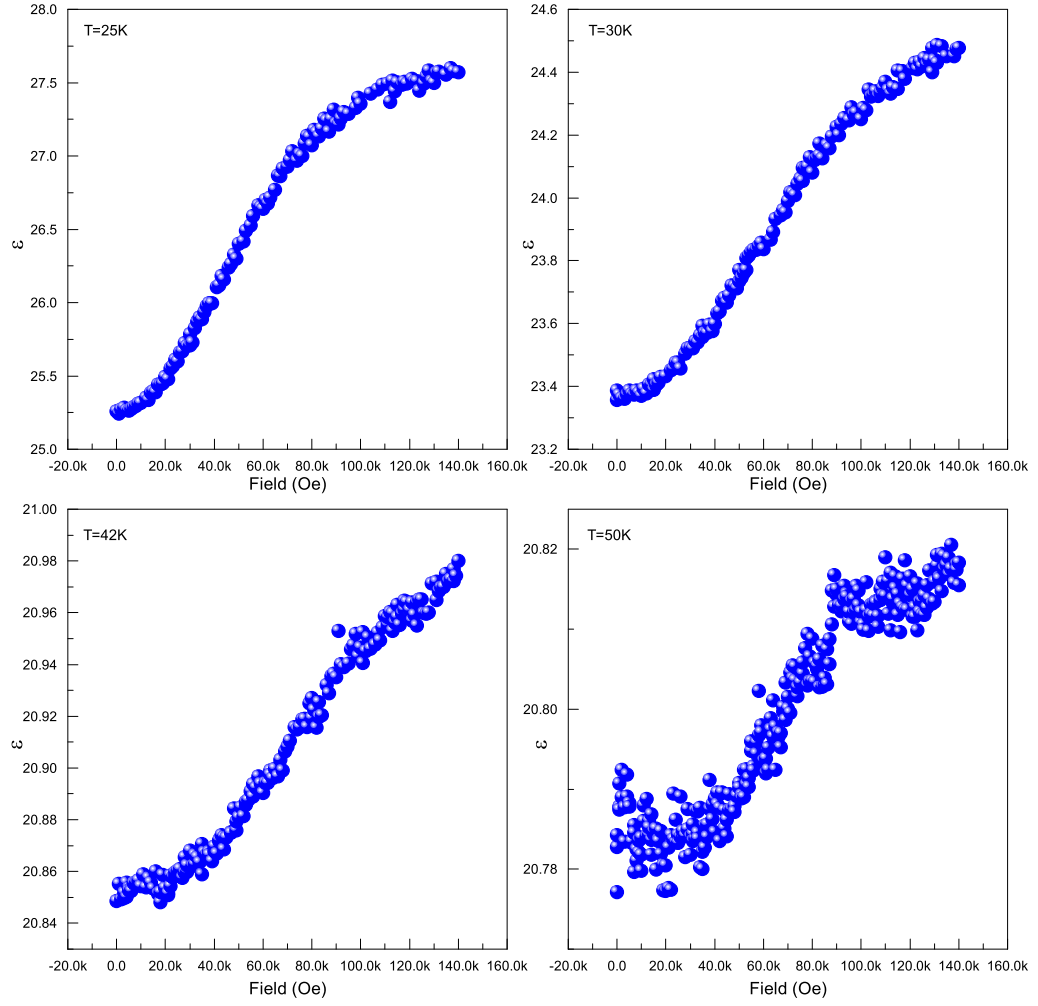
Figure 6.24: *Magnetocapacitance in DyMnO₃ at* 10Hz. For temperatures between 2K and 50K the dielectric constant measured at 10Hz exhibits a significant dependence on a magnetic field. Even well above the ferroelectric phase transition temperature the dielectric constant shows an excellent agreement with Eq. (6.23) .

$$F_{EM} = -\int\limits_{V} \left(\frac{1}{2}\varepsilon E^2 + \frac{1}{2}\mu H^2 + \gamma HE + \dots \right) \mathrm{d}\tau \tag{6.21}$$

In order to consider magnetodielectric effects, higher order coupling terms have to be introduced in Eq. (6.21). Since the permittivity is given by $\varepsilon = \frac{\mathrm{d}^2 F_{EM}}{\mathrm{d}E^2}$, only coupling terms proportional to E^2 contributes to the permittivity. Furthermore, coupling terms with even powers are always allowed apart from symmetry considerations. Therefore, the electromagnetic free energy for a magnetoelectric material may be written as,

$$
\begin{aligned}
F_{EM} = \quad & -\int_V \left(\frac{1}{2}\varepsilon E^2 + \frac{1}{2}\mu H^2 + \gamma HE + \frac{1}{2}\kappa H^2 E^2 + \dots \right) \mathrm{d}\tau \\
= \quad & -\int_V \frac{1}{2} \left\{ \left(\underbrace{\varepsilon + \kappa H^2}_{\varepsilon_T} \right) E^2 + \mu H^2 + 2\gamma HE + \dots \right\} \mathrm{d}\tau
\end{aligned}
\tag{6.22}
$$

where κ is the magnetodielectric parameter. With $\varepsilon_T = -\frac{\partial^2 F_{EM}}{\partial E^2}$ the total permittivity is given by,

$$
\varepsilon_T = \varepsilon + \kappa H^2 \Rightarrow \frac{\varepsilon_T}{\varepsilon_0} = \frac{\varepsilon}{\varepsilon_0} + \frac{\kappa}{\varepsilon_0} H^2
\tag{6.23}
$$

In order to obtain quantitative information of the temperature dependence of the magnetodielectric parameter, the measured permittivity as a function of magnetic field at several temperatures above T_C was fitted to the Eq. (6.23) (Fig. 6.25). A good agreement between Eq.(6.23) and the measured isothermal dielectric constant is obtained. However, notable deviations at higher fields are observed (Fig. 6.24). From that, it is evident that at higher magnetic fields, higher order non-linear coupling terms must considered in the free energy.

The magnetodielectric parameter as a function of temperature obtained from magnetic field analysis is shown in Fig. (6.26). On cooling from the paraelectric state the magnetodielectric parameter increases toward T_C revealing a divergent behaviour at $T = T_C$.

On a semi-logarithmic scale the temperature characteristic of κ^{-1} reveals a exponential temperature dependent behaviour at higher temperatures (well above the phase transition temperature) whereas on a double-logarithmic scale, the inverse magnetodielectric parameter exhibits a power law behaviour at temperatures close to T_C, $\kappa^{-1} \propto (T - T_C)^\alpha$ with $\alpha \approx 2.2$ Fig. (6.27).

Catalan et al.[210] has shown, that magnetocapacitance phenomenon can exist in materials that are not necessarily multiferroic. As it is shown in chapter 5, usually the material under investigation is placed in between two sample electrodes forming a sample capacitor in order to measure the dielectric response in the radio wave frequency regime. As a result, a layer near the electrode interface exist with a different density of charge carriers and hence with different resistivity than that of the core leading to interfacial polarization effects. This effect has been documented in several oxide materials, including manganites [211, 209, 212], and may happen not only at dielectric electrode interfaces but also at grain boundaries in ceramics [213] and interslab interfaces in superlattices [214, 210] leading to a MW-relaxation contribution at low frequencies.

If the resistance of the interfacial layer, R_i, is changed by a magnetic field, so will the measured permittivity (Fig. 6.28). Magnetoresistance MR combined with the Maxwell-Wagner effect thus provides a mechanism for magnetocapacitance in materials that are not necessarily multiferroic.

In order to verify the nature of the magnetodielectric effect in $\mathrm{DyMnO_3}$ the isothermal dielectric constant as a function of magnetic field was measured at 100kHz (Fig. 6.29).

Basically, MW relaxation plays only an important role at low frequencies. Thus, if mag-
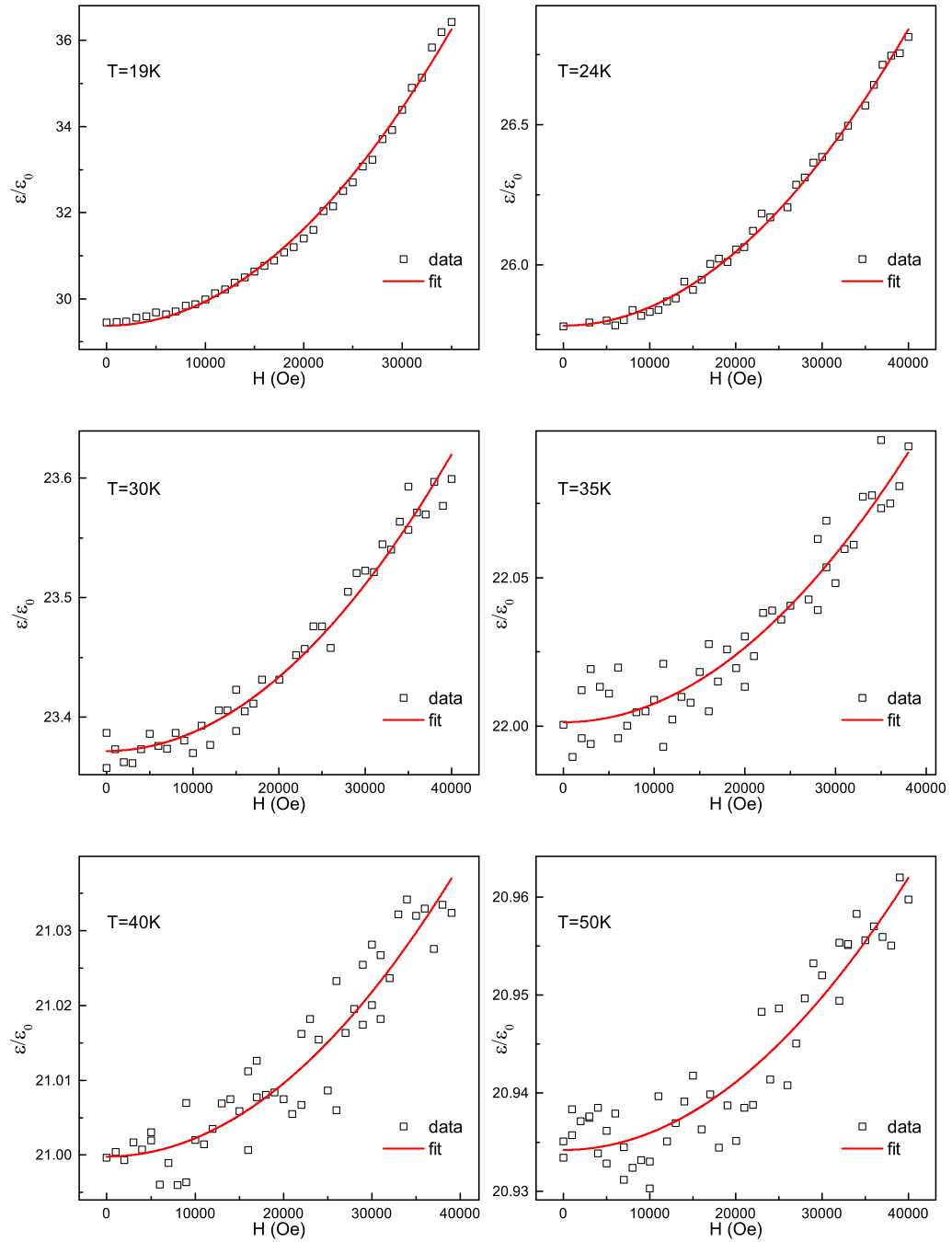
Figure 6.25: *Magnetic field dependent permittivity for $T > T_C$.* Typical magnetic field dependence of the dielectric constant at several temperatures above the critical temperature. Red solid lines represents the fit according to Eq. (6.23)
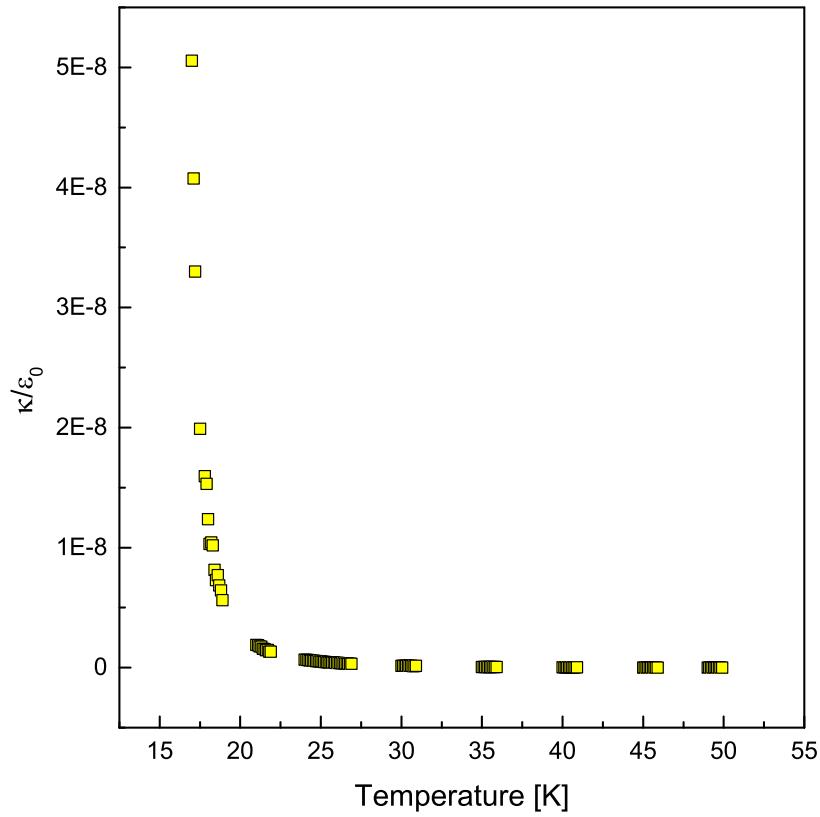
Figure 6.26: *Critical behaviour of the magnetodielectric parameter.* The yellow
are obtained by a fit procedure of the magnetic field dependent
dielectric constant according to Eq. (6.23).

netodielectric phenomenon due to MW relaxation exists, the magnetodielectric effect should
vanish at high frequencys. However, Fig.6.29 depicts a dependence of the dielectric constant
on magnetic field, even at at frequency of 100kHz above and below T_C. Hence, it is suggested,
that the magnetodielectric phenomenon in $DyMnO_3$ is intrinsic and caused by coupling of
spin and charge degrees of freedom.
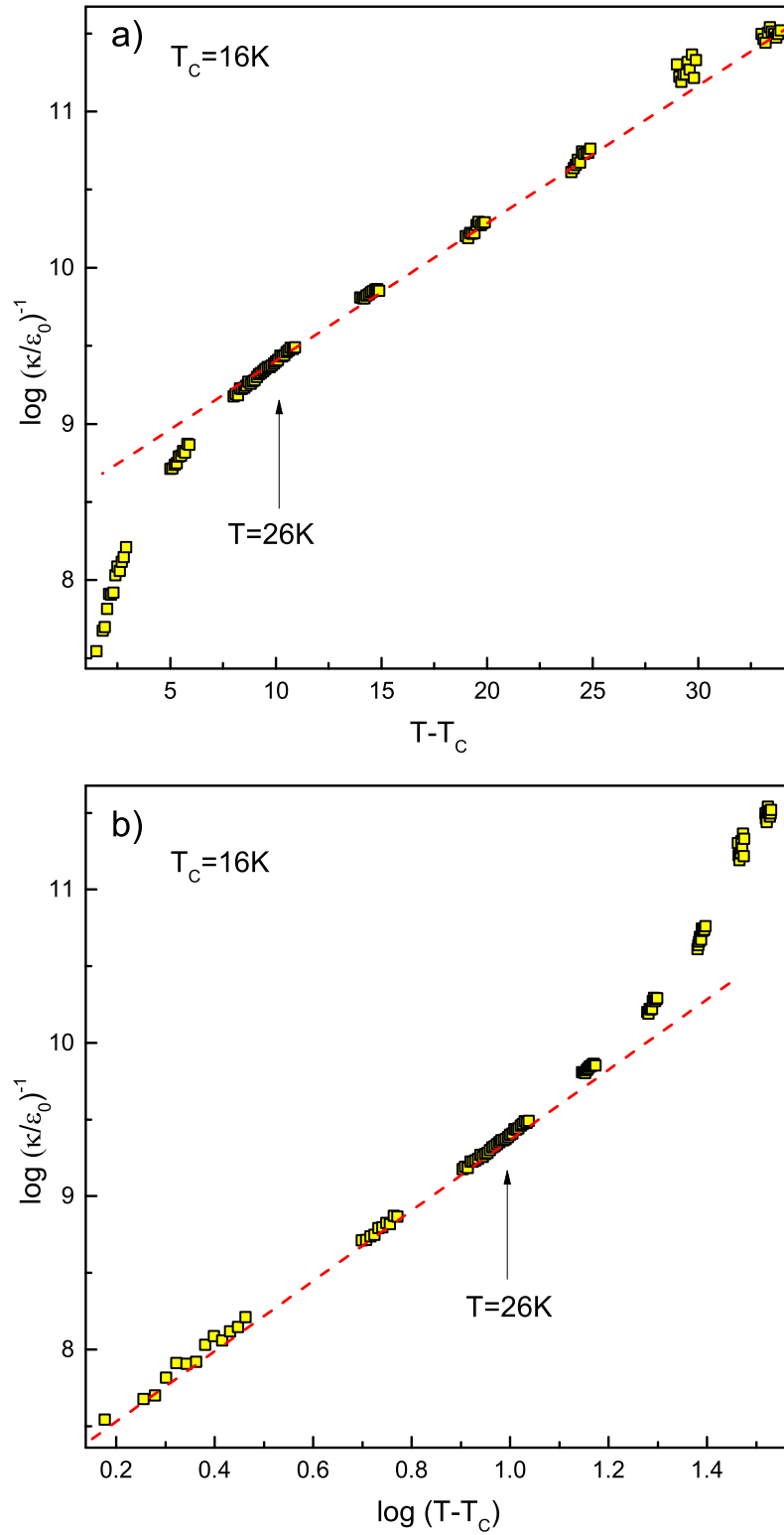
Figure 6.27: *Temperature characteristics of the magnetodielectric parameter.* a) On a semi-logarithmic scale, the inverse magnetodielectric parameter exhibits a exponential temperature dependent behaviour at higher temperatures. b) The inverse of the magnetodielectric parameter is plotted on a double-logarithmic scale. It is evident that at temperatures close to the phase transition temperature κ^{-1} fllollows a power law with respect to the temperature. The red dashed line is a guide to the eyes.
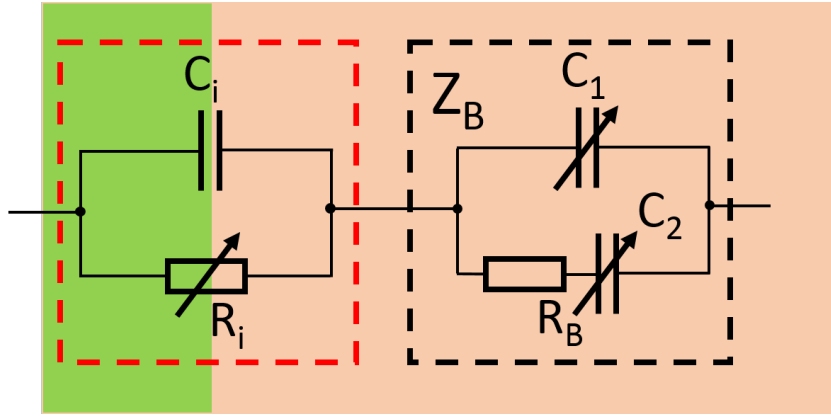
Figure 6.28: *Magneto-sensitive interfacial effects.* If the resistance of the interfacial layer changes with magnetic field, the intrinsic magnetocapacitance behaviour may be masked by the extrinsic magnetoresistance effect at low frequencies.
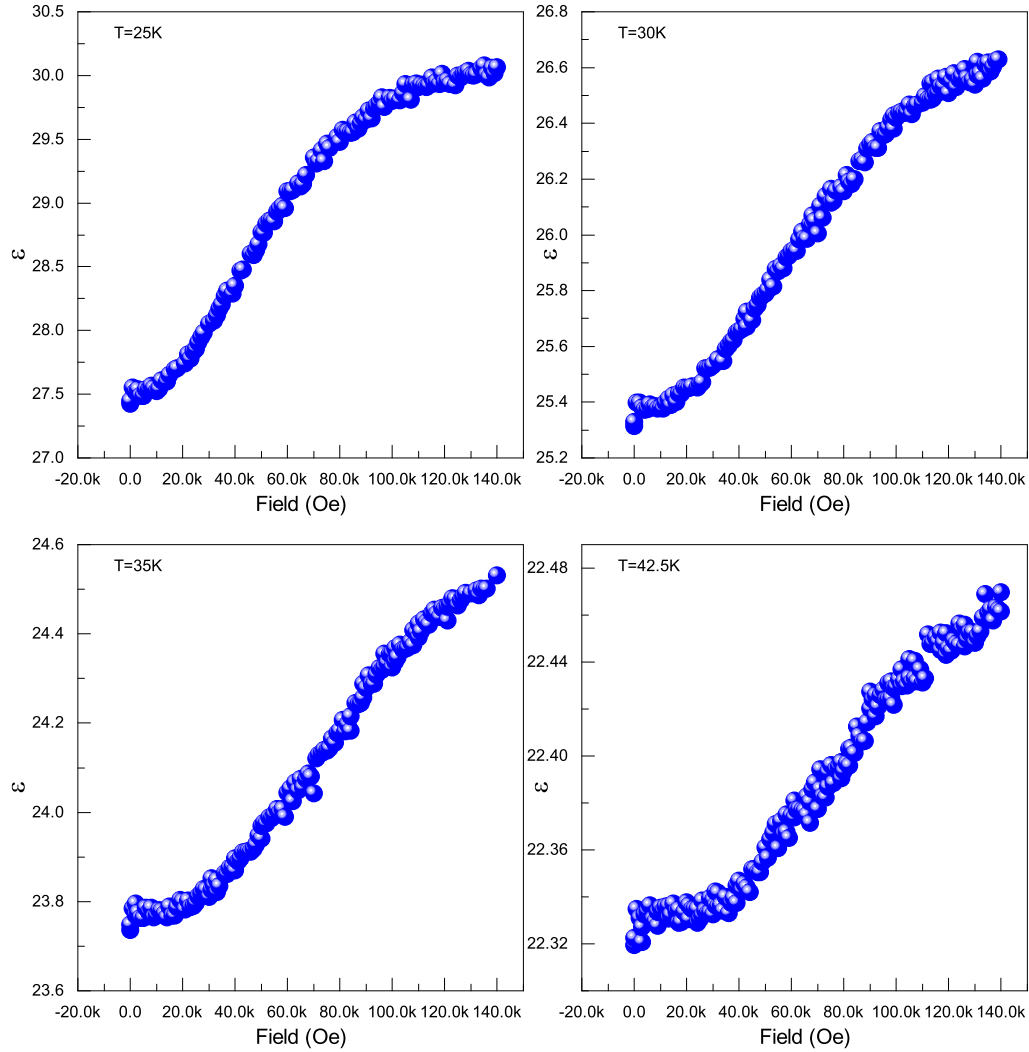
Figure 6.29: *Magnetocapacitance in DyMnO₃ at 100kHz.* For temperatures between 2K and 50K the dielectric constant measured at 100kHz exhibits also significant dependence on a magnetic field. Hence, a Maxwell-Wagner effect causing this behaviour can be excluded.

CHAPTER 7

Conclusion

This work presents the results of the dielectric study of single crystal $DyMnO_3$ with orthorhombically distorted perovskite structure. Electric field was applied along the crystallographic **a**-axis with magnetic field applied along the **b**-axis. The dielectric constant exhibits a distinct magnetic field dependent anomalous behaviour at the ferroelectric phase transition caused by a coupling between spin and charge degrees of freedom. In the vicinity at the transition from the non-polarized to the polarized state, i.e. from $\mathbf{P} = 0$ to $\mathbf{P}||a$, a low-frequency relaxation mode is observed in dielectric properties and it reveals critical behaviour at the ferroelectric transition temperature, $T_C \sim 18K$. Accordingly, this low frequency relaxation can be associated with the order parameter dynamics at the ferroelectric phase transition in $DyMnO_3$.

The analysis of the low-frequency dielectric relaxation demonstrates an overlap of two processes: critical dynamics close to T_C and activation behaviour in the broader frequency range. This observation may be reasonably explained using a simple model of an order-disorder phase transition with a double well potential.

This potential reflects a dynamical switching between cycloids of the opposite chirality and correlates well with known physical properties of $DyMnO_3$. Thus, the characteristic energies of magnetic ordering and the value of the static electric polarization are in agreement with known values.

Combining present results with several other experiments on multiferroics the paramagnetic sinusoidal phase should be explained as a dynamical equilibrium between the clockwise and counterclockwise cycloidal magnetic orders. The short range order in the paraelectric phase is transformed to a long-range cycloid at the ferroelectric transition temperature. In addition to the dielectric results, this hypothesis resolve several experimental constraints which contradicted the concept of static sinusoidally modulated magnetic phase.

Furthermore, accounting free energy contributions caused by magnetoelectric coupling between the dielectric and magnetic sub-system, it can be shown, that the slope ratio of the electric susceptibility does not necessarily follow Landau behaviour. Nevertheless, the results suggest a variation of the dipole density during the magnetoelectric phase transition. This assumption is confirmed by the fact, that a second relaxation process appears revealing a divergency like behaviour near T_C. This can be associated with an ordering process between bc-cycloidal and ab-cycloidal short range order of the Mn^{3+} magnetic moments.

APPENDIX A

Electric Polarization in cycloidal spin magnets

A.1   Phenomenological Description

For the sake of simplicity it is assumed, that the propagation vector,$\mathbf{Q}$, of the spin cycloid lies parallel to one of the principal planes (xy-plane,xz-plane, yz-plane), i.e. the rotation axis of the spins is perpendicular to one of the prinicpal planes. Thus for CCW rotation,

$$Plane: xy \quad Rotation\,axis: z \quad \mathbf{M}_{xy} = \begin{pmatrix} M\cos\left(Q_x x + Q_y y\right) \\ M\sin\left(Q_x x + Q_y y\right) \\ 0 \end{pmatrix} \tag{A.1}$$

$$Plane: zx \quad Rotation\,axis: y \quad \mathbf{M}_{zx} = \begin{pmatrix} M\sin\left(Q_x x + Q_z z\right) \\ 0 \\ M\cos\left(Q_x x + Q_z z\right) \end{pmatrix} \tag{A.2}$$

$$Plane: yz \quad Rotation\,axis: x \quad \mathbf{M}_{yz} = \begin{pmatrix} 0 \\ M\cos\left(Q_y y + Q_z z\right) \\ M\sin\left(Q_y y + Q_z z\right) \end{pmatrix} \tag{A.3}$$

The electric polarization is given by $\mathbf{P} = \chi^E \lambda \left[\left(\mathbf{M}\cdot\nabla\right)\mathbf{M} - \mathbf{M}\left(\nabla\cdot\mathbf{M}\right)\right]$. Therefore,

$$\mathbf{P} = \chi^E \lambda \begin{pmatrix} \cancel{M_x \partial_x M_x} + M_y \partial_y M_x + M_z \partial_z M_x - \cancel{M_x \partial_x M_x} - M_x \partial_y M_y - M_x \partial_z M_z \\ M_x \partial_x M_y + \cancel{M_y \partial_y M_y} + M_z \partial_z M_y - M_y \partial_x M_x - \cancel{M_y \partial_y M_y} - M_y \partial_z M_z \\ M_x \partial_x M_z + M_y \partial_y M_z + \cancel{M_z \partial_z M_z} - M_z \partial_x M_x - M_z \partial_y M_y - \cancel{M_z \partial_z M_z} \end{pmatrix} \tag{A.4}$$

$Plane: xy$ $\qquad$ $Rotation\, axis: z$

$$\mathbf{P}_{xy} = \chi^E \lambda \begin{pmatrix} M_y \partial_y M_x - M_x \partial_y M_y \\ M_x \partial_x M_y - M_y \partial_x M_x \\ 0 \end{pmatrix}$$

$$= \chi^E \lambda \begin{pmatrix} -M^2 Q_y \sin^2 (Q_x x + Q_y y) - M^2 Q_y \cos^2 (Q_x x + Q_y y) \\ +M^2 Q_x \cos^2 (Q_x x + Q_y y) + M^2 Q_x \sin^2 (Q_x x + Q_y y) \\ 0 \end{pmatrix}$$

$$= \chi^E \lambda M^2 \begin{pmatrix} -Q_y \\ +Q_x \\ 0 \end{pmatrix}$$

$$= \chi^E \lambda M^2 \begin{pmatrix} 0 \\ 0 \\ 1 \end{pmatrix} \times \begin{pmatrix} Q_x \\ Q_y \\ Q_z \end{pmatrix}$$

$$= \chi^E \lambda M^2 \left(\mathbf{e_z} \times \mathbf{Q} \right)$$

$$(A.5)$$

$Plane: zx$ $\qquad$ $Rotation\, axis: y$

$$\mathbf{P}_{zx} = \chi^E \lambda \begin{pmatrix} M_z \partial_z M_x - M_x \partial_z M_z \\ 0 \\ M_x \partial_x M_z - M_z \partial_x M_x \end{pmatrix}$$

$$= \chi^E \lambda \begin{pmatrix} +M^2 Q_z \sin^2 (Q_x x + Q_z z) + M^2 Q_z \cos^2 (Q_x x + Q_z z) \\ 0 \\ -M^2 Q_x \cos^2 (Q_x x + Q_z z) - M^2 Q_x \sin^2 (Q_x x + Q_z z) \end{pmatrix}$$

$$= \chi^E \lambda M^2 \begin{pmatrix} +Q_z \\ 0 \\ -Q_x \end{pmatrix}$$

$$= \chi^E \lambda M^2 \begin{pmatrix} 0 \\ 1 \\ 0 \end{pmatrix} \times \begin{pmatrix} Q_x \\ Q_y \\ Q_z \end{pmatrix}$$

$$= \chi^E \lambda M^2 \left(\mathbf{e_y} \times \mathbf{Q} \right)$$

$$(A.6)$$

$$Plane : yz \qquad\qquad Rotation\,axis : x$$

$$\mathbf{P}_{yz} = \qquad \chi^E \lambda \begin{pmatrix} 0 \\ M_z \partial_z M_y - M_y \partial_z M_z \\ M_y \partial_y M_z - M_z \partial_y M_y \end{pmatrix}$$

$$= \qquad \chi^E \lambda \begin{pmatrix} 0 \\ -M^2 Q_z \sin^2\left(Q_y y + Q_z z\right) - M^2 Q_z \cos^2\left(Q_y y + Q_z z\right) \\ +M^2 Q_y \cos^2\left(Q_y y + Q_z z\right) + M^2 Q_y \sin^2\left(Q_y y + Q_z z\right) \end{pmatrix}$$

$$= \chi^E \lambda M^2 \begin{pmatrix} 0 \\ -Q_z \\ +Q_y \end{pmatrix}$$

$$= \chi^E \lambda M^2 \begin{pmatrix} 1 \\ 0 \\ 0 \end{pmatrix} \times \begin{pmatrix} Q_x \\ Q_y \\ Q_z \end{pmatrix}$$

$$= \chi^E \lambda M^2 \left(\mathbf{e_x} \times \mathbf{Q}\right)$$

$$(A.7)$$

References

[1] M. Fiebig. Revival of the magnetoelectric effect. *J. Phys. D: Appl. Phys.*, 38(8):R123, 2005.

[2] R. Ramesh and N. A. Spaldin. Multiferroics: progress and prospects in thin films. *Nat. Mater.*, 6(1):21, Jan 2007.

[3] Yoshinori Tokura. Multiferroics as quantum electromagnets. *Science*, 312(5779):1481, 2006.

[4] Sang-Wook Cheong and Maxim Mostovoy. Multiferroics: a magnetic twist for ferroelectricity. *Nat. Mater.*, 6(1):13, Jan 2007.

[5] N. A. Spaldin and M. Fiebig. The renaissance of magnetoelectric multiferroics. *Science*, 309(5733):391–392, 2005.

[6] W. Eerenstein, N. D. Mathur, and J. F. Scott. Multiferroic and magnetoelectric materials. *Nature*, 442(7104):759, Aug 2006.

[7] J. Akerman. Toward a universal memory. *Science*, 308(5721):508–510, Apr 22 2005.

[8] Stuart S. P. Parkin, Masamitsu Hayashi, and Luc Thomas. Magnetic domain-wall racetrack memory. *Science*, 320(5873):190–194, Apr 11 2008.

[9] P. Borisov, A. Hochstrat, X. Chen, W. Kleemann, and C. Binek. Magnetoelectric switching of exchange bias. *Physical Review Letters*, 94(11), Mar 25 2005.

[10] C. Binek, P. Borisov, X. Chen, A. Hochstrat, S. Sahoo, and W. Kleemann. Perpendicular exchange bias and its control by magnetic, stress and electric fields. *European Physical Journal B*, 45(2), 2005.

[11] C. Binek and B. Doudin. Magnetoelectronics with magnetoelectrics. *Journal Of Physics-Condensed Matter*, 17(2):L39–L44, Jan 19 2005.

[12] D. Lebeugle, A. Mougin, M. Viret, D. Colson, and L. Ranno. Electric Field Switching of the Magnetic Anisotropy of a Ferromagnetic Layer Exchange Coupled to the Multiferroic Compound $BiFeO_3$. *Physical Review Letters*, 103(25), Dec 18 2009.

[13] D. Lebeugle, A. Mougin, M. Viret, D. Colson, J. Allibe, H. Bea, E. Jacquet, C. Deranlot, M. Bibes, and A. Barthelemy. Exchange coupling with the multiferroic compound $BiFeO_3$ in antiferromagnetic multidomain films and single-domain crystals. *Physical Review B*, 81(13), Apr 1 2010.

[14] D. Lebeugle, D. Colson, A. Forget, M. Viret, A. M. Bataille, and A. Gukasov. Electric-field-induced spin flop in $BiFeO_3$ single crystals at room temperature. *Physical Review Letters*, 100(22), Jun 6 2008.

[15] D. Lebeugle, D. Colson, A. Forget, M. Viret, P. Bonville, J. F. Marucco, and S. Fusil. Room-temperature coexistence of large electric polarization and magnetic order in $BiFeO_3$ single crystals. *Physical Review B*, 76(2), Juli 2007.

[16] Ying-Hao Chu, Lane W. Martin, Mikel B. Holcomb, Martin Gajek, Shu-Jen Han, Qing He, Nina Balke, Chan-Ho Yang, Donkoun Lee, Wei Hu, Qian Zhan, Pei-Ling Yang, Arantxa Fraile-Rodriguez, Andreas Scholl, Shan X. Wang, and R. Ramesh. Electric-field control of local ferromagnetism using a magnetoelectric multiferroic. *Nature Materials*, 7(6):478–482, Juni 2008.

[17] A. M. Kadomtseva, Yu. F. Popov, G. P. Vorob'ev, N. V. Kostyuchenko, A. I. Popov, A. A. Mukhin, V. Yu. Ivanov, L. N. Bezmaternykh, I. A. Gudim, V. L. Temerov, A. P. Pyatakov, and A. K. Zvezdin. High-temperature magnetoelectricity of terbium aluminum borate: The role of excited states of the rare-earth ion. *Physical Review B*, 89(1), Jan 21 2014.

[18] A. M. Kadomtseva, Yu. F. Popov, G. P. Vorob'ev, A. P. Pyatakov, S. S. Krotov, K. I. Kamilov, V. Yu. Ivanov, A. A. Mukhin, A. K. Zvezdin, A. M. Kuz'menko, L. N. Bezmaternykh, I. A. Gudim, and V. L. Temerov. Magnetoelectric and magnetoelastic properties of rare-earth ferroborates. *Low Temperature Physics*, 36(6):511–521, 2010.

[19] A. M. Kadomtseva, Yu. F. Popov, A. P. Pyatakov, G. P. Vorob'ev, A. K. Zvezdin, and D. Viehland. Phase transitions in multiferroic $BiFeO_3$ crystals, thin-layers, and ceramics: enduring potential for a single phase, room-temperature magnetoelectric 'holy grail'. *Phase Transitions*, 79(12), 2006.

[20] T. Zhao, A. Scholl, F. Zavaliche, K. Lee, M. Barry, A. Doran, M. P. Cruz, Y. H. Chu, C. Ederer, N. A. Spaldin, R. R. Das, D. M. Kim, S. H. Baek, C. B. Eom, and R. Ramesh. Electrical control of antiferromagnetic domains in multiferroic $BiFeO_3$ films at room temperature. *Nat. Mater.*, 5(10):823–829, Oct 2006.

[21] S. Rayaprol, S. Mukherjee, S. D. Kaushik, S. Matteppanavar, and B. Angadi. Electric field-induced tuning of magnetism in $PbFe_{0.5}Nb_{0.5}O_3$ at room temperature. *Journal Of Applied Physics*, 118(5), Aug 7 2015.

[22] Y. Q. Xiong, W. P. Zhou, Q. Li, Q. Q. Cao, T. Tang, D. H. Wang, and Y. W. Du. Electric field modification of magnetism in $Au/La_{2/3}Ba_{1/3}MnO_3/Pt$ device. *Scientific Reports*, 5, Aug 4 2015.

[23] C. Tannous and J. Gieraltowski. Electronic control of magnonic and spintronic devices. *Journal Of Materials Science-Materials In Electronics*, 26(7, SI):4675–4682, Jul 2015.

[24] Fumihiro Matsukura, Yoshinori Tokura, and Hideo Ohno. Control of magnetism by electric fields. *Nature Nanotechnology*, 10(3):209–220, Mar 15 2015.

[25] Shipeng Shen, Yisheng Chai, and Young Sun. Nonvolatile electric-field control of magnetization in a Y-type hexaferrite. *Scientific Reports*, 5, Feb 5 2015.

[26] T. Kimura, G. Lawes, T. Goto, Y. Tokura, and A. P. Ramirez. Magnetoelectric phase diagrams of orthorhombic $RMnO_3$ (R=Gd, Tb, and Dy). *Phys. Rev. B*, 71(22):224425, Jun 2005.

[27] J. Hemberger, F. Schrettle, A. Pimenov, P. Lunkenheimer, V. Yu. Ivanov, A. A. Mukhin, A. M. Balbashov, and A. Loidl. Multiferroic phases of $Eu_{1-x}Y_xMnO_3$. *Phys. Rev. B*, 75:035118, Jan 2007.

[28] M. Kenzelmann, A. B. Harris, S. Jonas, C. Broholm, J. Schefer, S. B. Kim, C. L. Zhang, S.-W. Cheong, O. P. Vajk, and J. W. Lynn. Magnetic inversion symmetry breaking and ferroelectricity in $TbMnO_3$. *Phys. Rev. Lett.*, 95(8):087206, Aug 2005.

[29] Masahito Mochizuki and Nobuo Furukawa. Microscopic model and phase diagrams of the multiferroic perovskite manganites. *Phys. Rev. B*, 80:134416, Oct 2009.

[30] F. Schrettle, P. Lunkenheimer, J. Hemberger, V. Yu. Ivanov, A. A. Mukhin, A. M. Balbashov, and A. Loidl. Relaxations as key to the magnetocapacitive effects in the perovskite manganites. *Phys. Rev. Lett.*, 102(20):207208, May 2009.

[31] T. Arima, A. Tokunaga, T. Goto, H. Kimura, Y. Noda, and Y. Tokura. Collinear to spiral spin transformation without changing the modulation wavelength upon ferroelectric transition in $Tb_{1-x}Dy_xMnO_3$. *Phys. Rev. Lett.*, 96:097202, Mar 2006.

[32] A. Pimenov, A. M. Shuvaev, A. A. Mukhin, and A. Loidl. Electromagnons in multiferroic manganites. *J. Phys.: Condens. Matter*, 20(43):434209, 2008.

[33] A. Pimenov, A. Loidl, A. A. Mukhin, V. D. Travkin, V. Yu. Ivanov, and A. M. Balbashov. Terahertz spectroscopy of electromagnons in $Eu_{1-x}Y_xMnO_3$. *Phys. Rev. B*, 77(1):014438, 2008.

[34] R. Valdes Aguilar, M. Mostovoy, A. B. Sushkov, C. L. Zhang, Y. J. Choi, S-W. Cheong, and H. D. Drew. Origin of electromagnon excitations in multiferroic $RMnO_3$. *Phys. Rev. Lett.*, 102(4):047203, 2009.

[35] J. S. Lee, N. Kida, S. Miyahara, Y. Takahashi, Y. Yamasaki, R. Shimano, N. Furukawa, and Y. Tokura. Systematics of electromagnons in the spiral spin-ordered states of $RMnO_3$. *Phys. Rev. B*, 79(18):180403, 2009.

[36] V. Cuartero, J. Blasco, J. A. Rodriguez-Velamazan, J. Garcia, G. Subias, C. Ritter, J. Stankiewicz, and L. Canadillas-Delgado. Effects of Al substitution on the multiferroic properties of $TbMnO_3$. *Phys. Rev. B*, 86:104413, Sep 2012.

[37] K. Taniguchi, N. Abe, S. Ohtani, and T. Arima. Magnetoelectric memory effect of the nonpolar phase with collinear spin structure in multiferroic $MnWO_4$. *Phys. Rev. Lett.*, 102:147201, Apr 2009.

[38] L. D. Landau and E. M. Lifshitz. *Electrodynamics of Continuous Media, Second Edition: Volume 8 (Course of Theoretical Physics 8)*. Butterworth-Heinemann, Oxford, 2nd edition, Dec 1979.

[39] D. N. Astrov. *J.Exptl.Teor.Fiz. 38, 984, Sov. Phys. JETP*, 11:708, 1960.

[40] V. J. Folen, G. T. Rado, and E. W. Stalder. Anisotropy of the magnetoelectric effect in Cr_2O_3. *Phys. Rev. Lett.*, 6:607−608, Jun 1961.

[41] David J. Griffiths. *Introduction to Electrodynamics*. Prentice Hall International, Essex, 4th edition, Jul 2013.

[42] W. F. Brown, R. M. Hornreich, and S. Shtrikman. Upper bound on the magnetoelectric susceptibility. *Phys. Rev.*, 168(2):574, Apr 1968.

[43] A. N. Vasiliev and E. A. Popova. Rare-earth ferroborates $RFe_3(BO_3)_4$. *Low Temp. Phys.*, 32(8):735–747, 2006.

[44] K.-C. Liang, R. P. Chaudhury, B. Lorenz, Y. Y. Sun, L. N. Bezmaternykh, V. L. Temerov, and C. W. Chu. Giant magnetoelectric effect in $HoAl_3(BO_3)_4$. *Phys. Rev. B*, 83:180417, May 2011.

[45] A. A. Mukhin, G. P. Vorob'ev, V. Yu. Ivanov, A. M. Kadomtseva, A. S. Narizhnaya, A. M. Kuz'menko, Yu. F. Popov, L. N. Bezmaternykh, and I. A. Gudim. Colossal magnetodielectric effect in $SmFe_3(BO_3)_4$ multiferroic. *JETP Lett.*, 93(5):275–281, 2011.

[46] R. P. Chaudhury, F. Yen, B. Lorenz, Y. Y. Sun, L. N. Bezmaternykh, V. L. Temerov, and C. W. Chu. Magnetoelectric effect and spontaneous polarization in $HoFe_3(BO_3)_4$ and $Ho_{0.5}Nd_{0.5}Fe_3(BO_3)_4$. *Phys. Rev. B*, 80:104424, Sep 2009.

[47] A. M. Kuzmenko, A. Shuvaev, V. Dziom, Anna Pimenov, M. Schiebl, A. A. Mukhin, V. Yu. Ivanov, L. N. Bezmaternykh, and A. Pimenov. Giant gigahertz optical activity in multiferroic ferroborate. *Phys. Rev. B*, 89:174407, May 2014.

[48] F. E. Neumann. *Vorlesungen über die Theorie der Elastizität der festen Körper und des Lichtäthers*. Teubner-Verlag, 1885.

[49] M. El-Batanouny. *Symmetry and Condensed Matter Physics: A Computational Approach*. Cambridge University Press, 2008.

[50] T. Kimura, S. Kawamoto, I. Yamada, M. Azuma, M. Takano, and Y. Tokura. Magnetocapacitance effect in multiferroic $BiMnO_3$. *Phys. Rev. B*, 67:180401, May 2003.

[51] T. Katsufuji, S. Mori, M. Masaki, Y. Moritomo, N. Yamamoto, and H. Takagi. Dielectric and magnetic anomalies and spin frustration in hexagonal $RMnO_3$(R=Y,Yb, and Lu). *Phys. Rev. B*, 64:104419, Aug 2001.

[52] G. Lawes, A. P. Ramirez, C. M. Varma, and M. A. Subramanian. Magnetodielectric effects from spin fluctuations in isostructural ferromagnetic and antiferromagnetic systems. *Phys. Rev. Lett.*, 91:257208, Dec 2003.

[53] R. Muralidharan, T.-H. Jang, C.-H. Yang, Y. H. Jeong, and T. Y. Koo. Magnetic control of spin reorientation and magnetodielectric effect below the spin compensation temperature in $TmFeO_3$. *Applied Physics Letters*, 90(1), 2007.

[54] Mohindar S. Seehra and R. E. Helmick. Anomalous changes in the dielectric constants of MnF_2 near its Néel temperature. *Journal of Applied Physics*, 55(6):2330–2332, 1984.

[55] Mohindar S. Seehra and Ronald E. Helmick. Dielectric anomaly in MnO near the magnetic phase transition. *Phys. Rev. B*, 24:5098–5102, Nov 1981.

[56] R. Tackett, G. Lawes, B. C. Melot, M. Grossman, E. S. Toberer, and R. Seshadri. Magnetodielectric coupling in Mn_3O_4. *Phys. Rev. B*, 76:024409, Jul 2007.

[57] N. Hur, S. Park, S. Guha, A. Borissov, V. Kiryukhin, and S.-W. Cheong. Low-field magnetodielectric effect in terbium iron garnets. *Applied Physics Letters*, 87(4), 2005.

[58] Masafumi Saito, Ryuji Higashinaka, and Yoshiteru Maeno. Magnetodielectric response of the spin-ice $Dy_2Ti_2O_7$. *Phys. Rev. B*, 72:144422, Oct 2005.

[59] T. Katsufuji and H. Takagi. Magnetocapacitance and spin fluctuations in the geometrically frustrated magnets $R_2Ti_2O_7$ (R=Rareearth). *Phys. Rev. B*, 69:064422, Feb 2004.

[60] Takehito Suzuki, Yuki Aikawa, and Takuro Katsufuji. Magnetocapacitance in Geometrically Frustrated Magnet $ZnFe_2O_4$. *Journal of the Physical Society of Japan*, 74(3):863–866, 2005.

[61] Robert E. Newnham. *Properties of Materials: Anisotropy, Symmetry, Structure.* Oxford University Press, Oxford, 1st edition, Jan 2005.

[62] L.D. Landau and E.M. Lifshitz. *Electrodynamics of Continuous Media.* Course of Theoretical Physics. Pergamon Press, 1975.

[63] M. Mostovoy. Ferroelectricity in spiral magnets. *Phys. Rev. Lett.*, 96(6):067601, 2006.

[64] T. Kimura, T. Goto, H. Shintani, K. Ishizaka, T. Arima, and Y. Tokura. Magnetic control of ferroelectric polarization. *Nature*, 426(6962):55, Nov 2003.

[65] G. Lawes, M. Kenzelmann, N. Rogado, K. H. Kim, G. A. Jorge, R. J. Cava, A. Aharony, O. Entin-Wohlman, A. B. Harris, T. Yildirim, Q. Z. Huang, S. Park, C. Broholm, and A. P. Ramirez. Competing Magnetic Phases on a Kagomé Staircase. *Phys. Rev. Lett.*, 93:247201, Dec 2004.

[66] K. Taniguchi, N. Abe, T. Takenobu, Y. Iwasa, and T. Arima. Ferroelectric Polarization Flop in a Frustrated Magnet $MnWO_4$ Induced by a Magnetic Field. *Phys. Rev. Lett.*, 97:097203, Aug 2006.

[67] O. Heyer, N. Hollmann, I. Klassen, S. Jodlauk, L. Bohatý, B. Becker, J. A. Mydosh, T. Lorenz, and D. Khomskii. A new multiferroic material: $MnWO_4$. *Journal of Physics: Condensed Matter*, 18(39):L471, 2006.

[68] A. H. Arkenbout, T. T. M. Palstra, T. Siegrist, and T. Kimura. Ferroelectricity in the cycloidal spiral magnetic phase of $MnWo_4$. *Phys. Rev. B*, 74:184431, Nov 2006.

[69] S. Jodlauk, P. Becker, J. A. Mydosh, D. I. Khomskii, T. Lorenz, S. V. Streltsov, D. C. Hezel, and L. Bohatý. Pyroxenes: a new class of multiferroics. *Journal of Physics: Condensed Matter*, 19(43):432201, 2007.

[70] H. Katsura, N. Nagaosa, and A. V. Balatsky. Spin current and magnetoelectric effect in noncollinear magnets. *Phys. Rev. Lett.*, 95(5):057205, Jul 2005.

[71] Patrick Bruno and Vitalii K. Dugaev. Equilibrium spin currents and the magnetoelectric effect in magnetic nanostructures. *Phys. Rev. B*, 72:241302, Dec 2005.

[72] Jiangping Hu. Microscopic origin of magnetoelectric coupling in noncollinear multiferroics. *Phys. Rev. Lett.*, 100:077202, Feb 2008.

[73] S. Picozzi, K. Yamauchi, B. Sanyal, I. A. Sergienko, and E. Dagotto. Dual nature of improper ferroelectricity in a magnetoelectric multiferroic. *Phys. Rev. Lett.*, 99:227201, Nov 2007.

[74] I. A. Sergienko and E. Dagotto. Role of the Dzyaloshinskii-Moriya interaction in multiferroic perovskites. *Phys. Rev. B*, 73(9):094434, 2006.

[75] Qichang Li, Shuai Dong, and J.-M. Liu. Multiferroic response and clamped domain structure in a two-dimensional spiral magnet: Monte carlo simulation. *Phys. Rev. B*, 77:054442, Feb 2008.

[76] I. E. Dzyaloshinskii. Theory Of Helicoidal Structures In Antiferromagnets. 1. Nonmetals. *Soviet Physics Jetp-USSR*, 19(4):960–971, 1964.

[77] T. Moriya. Anisotropic superexchange interaction and weak ferromagnetism. *Phys. Rev.*, 120:91, Oct 1960.

[78] J. B. Goodenough. *Magnetism and the Chemical Bond.* John Wiley and Sons, New York-London, 1st edition, Jan 1963.

[79] S-W. Cheong, J. D. Thompson, and Z. Fisk. Metamagnetism in La_2CuO_4. *Phys. Rev. B*, 39:4395–4398, Mar 1989.

[80] L. C. Chapon, G. R. Blake, M. J. Gutmann, S. Park, N. Hur, P. G. Radaelli, and S-W. Cheong. Structural Anomalies and Multiferroic Behavior in Magnetically Frustrated $TbMn_2O_5$. *Phys. Rev. Lett.*, 93:177402, Oct 2004.

[81] L. C. Chapon, P. G. Radaelli, G. R. Blake, S. Park, and S.-W. Cheong. Ferroelectricity Induced by Acentric Spin-Density Waves in YMn_2O_5. *Phys. Rev. Lett.*, 96:097601, Mar 2006.

[82] G. R. Blake, L. C. Chapon, P. G. Radaelli, S. Park, N. Hur, S-W. Cheong, and J. Rodriguez-Carvajal. Spin structure and magnetic frustration in multiferroic RMn_2O_5 (R=Tb, Ho, Dy). *Phys. Rev. B*, 71:214402, Jun 2005.

[83] Gianluca Giovannetti and Jeroen van den Brink. Electronic Correlations Decimate the Ferroelectric Polarization of Multiferroic $HoMn_2O_5$. *Phys. Rev. Lett.*, 100:227603, Jun 2008.

[84] Chenglong Jia, Shigeki Onoda, Naoto Nagaosa, and Jung Hoon Han. Microscopic theory of spin-polarization coupling in multiferroic transition metal oxides. *Phys. Rev. B*, 76:144424, Oct 2007.

[85] H. J. Xiang, Su-Huai Wei, M.-H. Whangbo, and Juarez L. F. Da Silva. Spin-Orbit Coupling and Ion Displacements in Multiferroic $TbMnO_3$. *Phys. Rev. Lett.*, 101:037209, Jul 2008.

[86] Andrei Malashevich and David Vanderbilt. First Principles Study of Improper Ferroelectricity in $TbMnO_3$. *Phys. Rev. Lett.*, 101:037210, Jul 2008.

[87] Michael E. Fisher and Walter Selke. Infinitely many commensurate phases in a simple ising model. *Phys. Rev. Lett.*, 44:1502–1505, Jun 1980.

[88] Y. J. Choi, H. T. Yi, S. Lee, Q. Huang, V. Kiryukhin, and S.-W. Cheong. Ferroelectricity in an ising chain magnet. *Phys. Rev. Lett.*, 100:047601, Jan 2008.

[89] P. C. Canfield, J. D. Thompson, S-W. Cheong, and L. W. Rupp. Extraordinary pressure dependence of the metal-to-insulator transition in the charge-transfer compounds $NdNiO_3$ and $PrNiO_3$. *Phys. Rev. B*, 47:12357–12360, May 1993.

[90] A. Pimenov, A. A. Mukhin, V. Yu. Ivanov, V. D. Travkin, A. M. Balbashov, and A. Loidl. Possible evidence for electromagnons in multiferroic manganites. *Nat. Phys.*, 2(2):97, Feb 2006.

[91] A. B. Sushkov, R. Valdes Aguilar, S. Park, S-W. Cheong, and H. D. Drew. Electromagnons in Multiferroic YMn_2O_5 and $TbMn_2O_5$. *Phys. Rev. Lett.*, 98(2):027202, 2007.

[92] A. Pimenov, T. Rudolf, F. Mayr, A. Loidl, A. A. Mukhin, and A. M. Balbashov. Coupling of phonons and electromagnons in $GdMnO_3$. *Phys. Rev. B*, 74(10):100403, Sep 2006.

[93] R. Valdes Aguilar, A. B. Sushkov, C. L. Zhang, Y. J. Choi, S.-W. Cheong, and H. D. Drew. Colossal magnon-phonon coupling in multiferroic $Eu_{0.75}Y_{0.25}MnO_3$. *Phys. Rev. B*, 76(6):060404, 2007.

[94] A. Pimenov, A. Loidl, A. A. Mukhin, V. D. Travkin, V. Yu. Ivanov, and A. M. Balbashov. Terahertz spectroscopy of electromagnons in $Eu_{1-x}Y_xMnO_3$. *Phys. Rev. B*, 77:014438, Jan 2008.

[95] N. Kida, Y. Ikebe, Y. Takahashi, J. P. He, Y. Kaneko, Y. Yamasaki, R. Shimano, T. Arima, N. Nagaosa, and Y. Tokura. Electrically driven spin excitation in the ferroelectric magnet $DyMnO_3$. *Phys. Rev. B*, 78(10):104414, 2008.

[96] Noriaki Kida, Yuichi Yamasaki, Ryo Shimano, Takahisa Arima, and Yoshinori Tokura. Electric-Dipole Active Two-Magnon Excitation in ab Spiral Spin Phase of a Ferroelectric Magnet $Gd_{0.7}Tb_{0.3}MnO_3$. *J. Phys. Soc. Jpn.*, 77(12):123704, 2008.

[97] Y. Takahashi, N. Kida, Y. Yamasaki, J. Fujioka, T. Arima, R. Shimano, S. Miyahara, M. Mochizuki, N. Furukawa, and Y. Tokura. Evidence for an Electric-Dipole Active Continuum Band of Spin Excitations in Multiferroic $TbMnO_3$. *Phys. Rev. Lett.*, 101(18):187201, 2008.

[98] R. Blinc and B. Žekš. *Soft modes in ferroelectrics and antiferroelectrics*. North-Holland Publishing, Amsterdam, 1974.

[99] B. A. Strukov and A. P. Levanyuk. *Ferroelectric Phenomena in Crystals*. Springer, Berlin, 1998.

[100] Martin T. Dove. *Introduction to Lattice Dynamics*. Cambridge University Press, 2005.

[101] M. Kardar. *Statistical Physics of Fields*. Cambridge University Press, 1st edition, Jun 2007.

[102] M. Le Bellac, F. Mortessagne, and G. G. Batrouni. *Equilibrium and Non-Equilibrium Statistical Thermodynamics*. Cambridge University Press, 2010.

[103] Mahdi Sanati and Avadh Saxena. Landau theory of domain walls for one-dimensional asymmetric potentials. *American Journal of Physics*, 71(10):1005–1012, 2003.

[104] L. Landau. The theory of phase transitions. *Nature*, 138:840–841, Jul-Dec 1936.

[105] A.F. Devonshire. Theory of barium titanate .1. *Phil. Mag.*, 40(309):1040–1063, 1949.

[106] A.F. Devonshire. Theory of barium titanate .2. *Phil. Mag.*, 42(333):1065–1079, 1951.

[107] A.F. Devonshire. Theory of ferroelectrics. *Advan. Phys.*, 3(10):85–130, 1954.

[108] Joon Chang Lee. *Thermal Physics: Entropy and Free Energies*. World Scientific Pub Co, 2nd edition, Mar 2011.

[109] Fließbach T. *Statistische Physik: Lehrbuch zur Theoretischen Physik IV*. Spektrum akademischer Verlag, 5th edition, Mar 2010.

[110] H. Nishimori and G. Ortiz. *Elements of Phase Transitions and Critical Phenomena*. Oxford University Press, 1nd edition, Jan 2011.

[111] A. D. Bruce and R. A. Cowley. *Structural Phase Transitions*. Taylor and Frencis, 1nd edition, Jan 1981.

[112] A. P. Giddy, M. T. Dove, and V. Heine. What do landau free-energies really look like for structural phase-transitions. *J. Phys. Cond. Matter*, 1(44):8327–8335, Nov 6 1989.

[113] E. K. H. Salje. Crystallography And Structural Phase-Transitions, An Introduction. *Acta Cryst. A*, 47(5):453–&, Sep 1 1991.

[114] S. Padlewski, A. K. Evans, C. Ayling, and V. Heine. Crossover between displacive and order-disorder behavior in the phi-4 model. *J. Phys. Cond. Matter*, 4(21):4895–4908, May 25 1992.

[115] S. Radescu, I. Etxebarria, and J. M. Perezmato. The Landau Free-Energy Of The 3-Dimensional Phi(4) Model In Wide Temperature Intervals. *J. Phys. Cond. Matter*, 7(3):585–595, Jan 16 1995.

[116] M. T. Dove. Theory of displacive phase transitions in minerals. *Am. Mineralogist*, 82(3-4):213–244, 1997.

[117] A. D. Bruce and R. A. Cowley. Structural phase transitions. *Taylor and Frencis, London*, 2007.

[118] J. F. Scott. Soft-mode spectroscopy: Experimental studies of structural phase transitions. *Rev. Mod. Phys.*, 46(1):83, Jan 1974.

[119] M. E. Lines and A. M. Glass. *Principles and Applications of Ferrorelectrics and Related Phenomena*. Oxford University Press, Oxford, 1st edition, Okt 1977.

[120] S. Ghose. Lattice dynamics, phase transitions and soft modes. *American Review in Mineralogy*, 14:127–163, 1985.

[121] Martin T. Dove. *Introduction to Lattice Dynamics*. Cambridge University Press, 1nd edition, Oct 2005.

[122] P. C. Hohenberg and B. I. Halperin. Theory of dynamic critical phenomena. *Rev. Mod. Phys.*, 49:435–479, Jul 1977.

[123] U. C. Täuber. *Critical Dynamics: A Field Theory Approach to Equilibrium and Non-Equilibrium Scaling Behaviour*. Cambridge University Press, 1nd edition, Apr 2014.

[124] L. D. Landau and E. M. Lifshitz. *Statistical Physics, Third Edition, Part 1: Volume 5 (Course of Theoretical Physics, Volume 5)*. Butterworth-Heinemann, Oxford, 3st edition, Dec 1975.

[125] J.-G. Caputo, E. V. Kazantseva, and A. I. Maimistov. Electromagnetically induced switching of ferroelectric thin films. *Phys. Rev. B*, 75:014113, Jan 2007.

[126] A. Widom, S. Sivasubramanian, C. Vittoria, S. Yoon, and Y. N. Srivastava. Resonance damping in ferromagnets and ferroelectrics. *Phys. Rev. B*, 81:212402, Jun 2010.

[127] B. B. Lavrencic and J. F. Scott. Dynamical model for the polar-incommensurate transition in $BaMnF_4$. *Phys. Rev. B*, 24:2711–2717, Sep 1981.

[128] V. P. Mineev. Magnetic relaxation in uranium ferromagnetic superconductors. *Phys. Rev. B*, 88:224408, Dec 2013.

[129] A. Starkov and I. Starkov. Asymptotic Description of the Time and Temperature Hysteresis in the Framework of Landau-Khalatnikov Equation. *Ferroelectrics*, 461(1, SI):50–60, Mar 12 2014.

[130] V. Fridkin, M. Kuehn, and H. Kliem. The Weiss model and the Landau-Khalatnikov model for the switching of ferroelectrics. *Physica B-Condensed Matter*, 407(12):2211–2214, Jun 15 2012.

[131] W. P. Mason. Theory of the ferroelectric effect and clamped dielectric constant of rochelle salt. *Phys. Rev.*, 72:854–865, Nov 1947.

[132] P. M. Chaikin and T. C. Lubensky. *Principles of Condensed Matter Physics*. Cambridge University Press, 2000.

[133] J.M. Yeomans. *Statistical Mechanics of Phase Transitions*. Oxford University Press, 1993.

[134] J. A. Gonzalo. *Effective Field Approach to Phase transitions and Some Applications to Ferroelectrics*. World Scientific, Ney Jersey, 2st edition, Okt 2006.

[135] D. Staresinic, K. Biljakovic, P. Lunkenheimer, and A. Loidl. Slowing down of the relaxational dynamics at the ferroelectric phase transition in one-dimensional $(TMTTF)_2AsF_6$. *Solid State Communications*, 137(5):241 – 245, 2006.

[136] G. Burns. *Solid State Physics*. Academic Press, 1nd edition, Aug 1985.

[137] G. Kozlov, E. Kryukova, S. Lebedev, and A. Sobyanin. Double Critical-Points And Points Of Extremal Susceptibility In Rochelle Salt. *Ferroelectrics*, 80:881–884, 1988.

[138] G. V. Kozlov and A. A. Volkov. Coherent source submillimeter wave spectroscopy. In G. Grüner, editor, *Millimeter and Submillimeter Wave Spectroscopy of Solids*, page 51. Springer, Berlin, 1998.

[139] J. Halbritter. Electric Surface Impedance. *Zeitschrift Fur Physik B-Condensed Matter*, 31(1):19–37, 1978.

[140] S. Senturia and N. Sheppard. Dielectric Analysis Of Thermoset Cure. *Advances In Polymer Science*, 80:1–47, 1986.

[141] D. Day, T. Lewis, H. Lee, and S. Senturia. The Role Of Boundary-Layer Capacitance At Blocking Electrodes In The Interpretation Of Dielectric Cure Data In Adhesives. *Journal Of Adhesion*, 18(1):73–90, 1985.

[142] J. Johnson and R. Cole. Dielectric Polarization Of Liquid And Solid Formic Acid. *Journal Of The American Chemical Society*, 73(10):4536–4540, 1951.

[143] E. Barsoukov and J. R. Macdonald. *Impedance Spectroscopy*. Wiley, 2005.

[144] H. Fröhlich. *Theory of dielectrics*. Oxford University Press, 1958.

[145] C.J.F. Bottcher. *Theory of Electric Polarization, Vol.2: Dielectrics in Time-Dependent Fields*. Elsevier Science, 1980.

[146] A.K. Jonscher. *Dielectric Relaxation in Solids*. Chelsea Dielectrics Press Ltd, 1983.

[147] M. Fox. *Optical Properties of Solids*. Oxford University Press, 2010.

[148] B. K. P. Scaife. *Principle of Dielectrics*. Oxford University Press, 1989.

[149] E. S. Guillemin. *The mathematics of Circuit Analysis*. Chapman Hall, 1949.

[150] F.K. Kuo. *Network Analysis and Synthesis*. Wiley, 1966.

[151] A. Schönhals F. Kremer. *Broadband Dielectric Spectroscopy*. Springer, London, 1nd edition, Dec 2002.

[152] J. Honerkamp and J. Weese. Determination Of The Relaxation Spectrum By A Regularization Method. *Macromolecules*, 22(11):4372–4377, Nov 1989.

[153] J. Weese. A Reliable And Fast Method For The Solution Of Fredholm Integral-Equations Of The 1st Kind Based On Tikhonov Regularization. *Computer Physics Communications*, 69(1):99–111, Feb 1992.

[154] H. Schäfer, E. Sternin, R. Stannarius, M. Arndt, and F. Kremer. Novel approach to the analysis of broadband dielectric spectra. *Physical Review Letters*, 76(12):2177–2180, Mar 18 1996.

[155] H. Schäfer and H. Bauch. Determination Of Local Polarization Distributions By H-1 Endor Line-Shape Analysis. *Physics Letters A*, 199(1-2):93–98, Mar 20 1995.

[156] H. Schäfer and R. Stannarius. Computation Of Orientational Distributions Of Partially Ordered Samples From Nmr-Spectra. *Journal Of Magnetic Resonance Series B*, 106(1):14–23, Jan 1995.

[157] S. Havriliak and S. Negami. A Complex Plane Analysis Of Alpha-Dispersions In Some Polymer Systems. *Journal Of Polymer Science Part C-Polymer Symposium*, (14PC):99–&, 1966.

[158] S. Havriliak and S. Negami. A Complex Plane Representation Of Dielectric And Mechanical Relaxation Processes In Some Polymers. *Polymer*, 8(4):161–&, 1967.

[159] R. Diaz-Calleja. Comment on the maximum in the loss permittivity for the Havriliak-Negami equation. *Macromolecules*, 33(24):8924, Nov 28 2000.

[160] A. Boersma, J. van Turnhout, and M. Wubbenhorst. Dielectric characterization of a thermotropic liquid crystalline copolyesteramide: 1. Relaxation peak assignment. *Macromolecules*, 31(21):7453–7460, Oct 20 1998.

[161] K. Schroter, R. Unger, S. Reissig, F. Garwe, S. Kahle, M. Beiner, and E. Donth. Dielectric spectroscopy in the alpha beta splitting region of glass transition in poly(ethyl methacrylate) and poly(n-butyl methacrylate): Different evaluation methods and experimental conditions. *Macromolecules*, 31(25):8966–8972, Dec 15 1998.

[162] Reiner Zorn. Logarithmic moments of relaxation time distributions. *The Journal of Chemical Physics*, 116(8):3204–3209, 2002.

[163] K. S. Cole and R. H. Cole. Dispersion and absorption in dielectrics I. Alternating current characteristics. *Journal Of Chemical Physics*, 9(4):341–351, Apr 1941.

[164] D. W. Davidson and R. H. Cole. Dielectric Relaxation In Glycerine. *Journal Of Chemical Physics*, 18(10):1417, 1950.

[165] D. W. Davidson and R. H. Cole. Dielectric Relaxation In Glycerol, Propylene Glycol, And Normal-Propanol. *Journal Of Chemical Physics*, 19(12):1484–1490, 1951.

[166] N. Hill, W.E. Vaughan, A.H. Price, and M. Davies. *Dielectric Propertiess and Molecular Behaviour.* Van Nostrand, London, 1989.

[167] A. K. Jonscher. Limiting losses in dielectrics. *IEEE Transactions On Dielectrics And Electrical Insulation*, 8(3):345–351, Jun 2001. 6th International Conference on Dielectrics and Related Phenomena, Spala, Poland, Sep 06-10, 2000.

[168] A. M. Balbashov, S. G. Karabashev, Ya. M. Mukovskiy, and S. A. Zverkov. Growth and giant magnetoresistance effect in La-Ca-Mn-O and La-Sr-Mn-O single crystals. *Journal of Crystal Growth*, 167(1-2):365, Sep 1996.

[169] Takanori Mori, Katsuyuki Aoki, Naoki Kamegashira, Toetsu Shishido, and Tsuguo Fukuda. Crystal structure of DyMnO$_3$. *Materials Letters*, 42(6):387 – 389, 2000.

[170] A. M. Shuvaev, J. Hemberger, D. Niermann, F. Schrettle, A. Loidl, V. Yu. Ivanov, V. D. Travkin, A. A. Mukhin, and A. Pimenov. Soft-mode behavior of electromagnons in multiferroic manganite. *Phys. Rev. B*, 82:174417, Nov 2010.

[171] A. Shuvaev, V. Dziom, Anna Pimenov, M. Schiebl, A. A. Mukhin, A. C. Komarek, T. Finger, M. Braden, and A. Pimenov. Electric field control of terahertz polarization in a multiferroic manganite with electromagnons. *Phys. Rev. Lett.*, 111:227201, Nov 2013.

[172] N. Aliouane, D. N. Argyriou, J. Strempfer, I. Zegkinoglou, S. Landsgesell, and M. v. Zimmermann. Field-induced linear magnetoelastic coupling in multiferroic TbMnO$_3$. *Phys. Rev. B*, 73(2):020102, 2006.

[173] J. Strempfer, B. Bohnenbuck, M. Mostovoy, N. Aliouane, D. N. Argyriou, F. Schrettle, J. Hemberger, A. Krimmel, and M. v. Zimmermann. Absence of commensurate ordering at the polarization flop transition in multiferroic DyMnO$_3$. *Phys. Rev. B*, 75:212402, Jun 2007.

[174] D. Mannix, D. F. McMorrow, R. A. Ewings, A. T. Boothroyd, D. Prabhakaran, Y. Joly, B. Janousova, C. Mazzoli, L. Paolasini, and S. B. Wilkins. X-ray scattering study of the order parameters in multiferroic TbMnO$_3$. *Phys. Rev. B*, 76:184420, Nov 2007.

[175] S. B. Wilkins, T. R. Forrest, T. A. W. Beale, S. R. Bland, H. C. Walker, D. Mannix, F. Yakhou, D. Prabhakaran, A. T. Boothroyd, J. P. Hill, P. D. Hatton, and D. F. McMorrow. Nature of the magnetic order and origin of induced ferroelectricity in TbMnO$_3$. *Phys. Rev. Lett.*, 103:207602, Nov 2009.

[176] J. Baier, D. Meier, K. Berggold, J. Hemberger, A. Balbashov, J. A. Mydosh, and T. Lorenz. Hysteresis effects in the phase diagram of multiferroic GdMnO$_3$. *Phys. Rev. B*, 73:100402, Mar 2006.

[177] J. Voigt, J. Persson, J. W. Kim, G. Bihlmayer, and Th. Brückel. Strong coupling between the spin polarization of Mn and Tb in multiferroic TbMnO$_3$ determined by x-ray resonance exchange scattering. *Phys. Rev. B*, 76:104431, Sep 2007.

[178] T. Goto, T. Kimura, G. Lawes, A. P. Ramirez, and Y. Tokura. Ferroelectricity and giant magnetocapacitance in perovskite rare-earth manganites. *Phys. Rev. Lett.*, 92(25):257201, Jun 2004.

[179] T. Kimura, S. Ishihara, H. Shintani, T. Arima, K. T. Takahashi, K. Ishizaka, and Y. Tokura. Distorted perovskite with e_g^1 configuration as a frustrated spin system. *Phys. Rev. B*, 68(6):060403, Aug 2003.

[180] M. Mochizuki and N. Furukawa. Microscopic model and phase diagrams of the multiferroic perovskite manganites. *Phys. Rev. B*, 80:134416, Oct 2009.

[181] F. Fabrizi, H. C. Walker, L. Paolasini, F. de Bergevin, A. T. Boothroyd, D. Prabhakaran, and D. F. McMorrow. Circularly polarized X rays as a probe of noncollinear magnetic order in multiferroic TbMnO$_3$. *Phys. Rev. Lett.*, 102:237205, Jun 2009.

[182] O. Prokhnenko, R. Feyerherm, E. Dudzik, S. Landsgesell, N. Aliouane, L. C. Chapon, and D. N. Argyriou. Enhanced ferroelectric polarization by induced dy spin order in multiferroic DyMnO$_3$. *Phys. Rev. Lett.*, 98:057206, Feb 2007.

[183] O. Prokhnenko, R. Feyerherm, M. Mostovoy, N. Aliouane, E. Dudzik, A. U. B. Wolter, A. Maljuk, and D. N. Argyriou. Coupling of frustrated ising spins to the magnetic cycloid in multiferroic TbMnO$_3$. *Phys. Rev. Lett.*, 99:177206, Oct 2007.

[184] N. Aliouane, O. Prokhnenko, R. Feyerherm, M. Mostovoy, J. Strempfer, K. Habicht, K. C. Rule, E. Dudzik, A. U. B. Wolter, A. Maljuk, and D. N. Argyriou. Magnetic order and

ferroelectricity in RMnO$_3$ multiferroic manganites: coupling between R- and Mn-spins. *J. Phys.: Cond. Matter*, 20(43), Oct 29 2008.

[185] E. Schierle, V. Soltwisch, D. Schmitz, R. Feyerherm, A. Maljuk, F. Yokaichiya, D. N. Argyriou, and E. Weschke. Cycloidal order of 4f moments as a probe of chiral domains in DyMnO$_3$. *Phys. Rev. Lett.*, 105:167207, Oct 2010.

[186] M. Johnsson and P. Lemmens. Crystallography and chemistry of perovskites. In H. Kronmüller and S. Perkin, editors, *Handbook of Magnetism and Advanced Magnetic Materials*, page 3064. John Wiley, Chichester, UK, 2006.

[187] Alonso, J. A. and Martinez-Lope, M. J. and Casais, M. T. and Fernandez-Diaz, M. T. Evolution of the Jahn-Teller Distortion of MnO_6 Octahedra in $RMnO_6$ Perovskites (R=Pr, Nd, Dy, Tb, Ho, Er, Y): A Neutron Diffraction Study. *Inorganic Chemistry*, 39(5):917–923, 2000. PMID: 12526369.

[188] H. A. Jahn and E. Teller. Stability of polyatomic molecules in degenerate electronic states. i. orbital degeneracy. *Proceedings of the Royal Society of London A: Mathematical, Physical and Engineering Sciences*, 161(905):220–235, 1937.

[189] M. Ahsan Zeb and Hae-Young Kee. Interplay between spin-orbit coupling and hubbard interaction in sriro$_3$ and related *Pbnm* perovskite oxides. *Phys. Rev. B*, 86:085149, Aug 2012.

[190] Jean-Michel Carter, V. Vijay Shankar, M. Ahsan Zeb, and Hae-Young Kee. Semimetal and topological insulator in perovskite iridates. *Phys. Rev. B*, 85:115105, Mar 2012.

[191] F. Kagawa, M. Mochizuki, Y. Onose, H. Murakawa, Y. Kaneko, N. Furukawa, and Y. Tokura. Dynamics of multiferroic domain wall in spin-cycloidal ferroelectric DyMnO$_3$. *Phys. Rev. Lett.*, 102(5):057604, Feb 2009.

[192] F. Kagawa, Y. Onose, Y. Kaneko, and Y. Tokura. Relaxation dynamics of multiferroic domain walls in DyMnO$_3$ with cycloidal spin order. *Phys. Rev. B*, 83:054413, Feb 2011.

[193] D. Niermann, C. P. Grams, P. Becker, L. Bohatý, H. Schenck, and J. Hemberger. Critical Slowing Down near the Multiferroic Phase Transition in MnWO$_4$. *Phys. Rev. Lett.*, 114:037204, Jan 2015.

[194] S. Aubry. Unified Approach To Interpretation Of Displacive And Order-Disorder Systems. 1. Thermodynamical Aspect. *J. Chem. Phys.*, 62(8):3217–3227, 1975.

[195] Th. Braun, W. Kleemann, J. Dec, and P. A. Thomas. Creep and Relaxation Dynamics of Domain Walls in Periodically Poled KTiOPO$_4$. *Phys. Rev. Lett.*, 94:117601, Mar 2005.

[196] W. Kleemann, J. Dec, S. Miga, Th. Woike, and R. Pankrath. Non-Debye domain-wall-induced dielectric response in Sr$_{0.61-x}$Ce$_x$Ba$_{0.39}$Nb$_2$O$_6$. *Phys. Rev. B*, 65:220101, May 2002.

[197] W. Kleemann, J. Dec, S. A. Prosandeev, T. Braun, and P. A. Thomas. Universal domain wall dynamics in ferroelectrics and relaxors. *Ferroelectrics*, 334:3–10, 2006.

[198] H. Eugene Stanley. *Introduction to Phase Transitions and Critical Phenomena*. Oxford University Press, 1nd edition, Jul 1971.

[199] G. A. Smolenskii and I. E. Chupis. Ferroelectromagnets. *Sov. Phys. Usp.*, 25(7):475, 1982.

[200] T. Kimura, S. Kawamoto, I. Yamada, M. Azuma, M. Takano, and Y. Tokura. Magnetocapacitance effect in multiferroic $BiMnO_3$. *Phys. Rev. B*, 67:180401, May 2003.

[201] G. Lawes, T. Kimura, C. M. Varma, M. A. Subramanian, N. Rogado, R. J. Cava, and A. P. Ramirez. Magnetodielectric effects at magnetic ordering transitions. *Progr. Sol. State Chem.*, 37(1):40–54, 2009.

[202] M. Kenzelmann, G. Lawes, A. B. Harris, G. Gasparovic, C. Broholm, A. P. Ramirez, G. A. Jorge, M. Jaime, S. Park, Q. Huang, A. Ya. Shapiro, and L. A. Demianets. Direct transition from a disordered to a multiferroic phase on a triangular lattice. *Phys. Rev. Lett.*, 98:267205, Jun 2007.

[203] B. A. Strukov and A. P. Levanyuk. *Ferroelectric Phenomena in Crystals*. Springer, Berlin, 1st edition, Feb 1998.

[204] M. P. Singh, W. Prellier, Ch. Simon, and B. Raveau. Magnetocapacitance effect in perovskite-superlattice based multiferroics. *Applied Physics Letters*, 87(2), 2005.

[205] J. Hemberger, P. Lunkenheimer, R. Fichtl, H. A. K. von Nidda, V. Tsurkan, and A. Loidl. Relaxor ferroelectricity and colossal magnetocapacitive coupling in ferromagnetic $CdCr_2S_4$. *Nature*, 434(7031):364–367, Mar 17 2005.

[206] N. Hur, S. Park, P. A. Sharma, S. Guha, and S-W. Cheong. Colossal Magnetodielectric Effects in $DyMn_2O_5$. *Phys. Rev. Lett.*, 93:107207, Sep 2004.

[207] N. S. Rogado, J. Li, A. W. Sleight, and M. A. Subramanian. Magnetocapacitance and magnetoresistance near room temperature in a ferromagnetic semiconductor: La_2NiMnO_6. *Advanced Materials*, 17(18):2225–2227, Sep 16 2005.

[208] M. Gich, C. Frontera, A. Roig, J. Fontcuberta, E. Molins, N. Bellido, C. Simon, and C. Fleta. Magnetoelectric coupling in epsilon-Fe_2O_3 nanoparticles. *Nanotechnology*, 17(3):687–691, Feb 14 2006.

[209] R. S. Freitas, J. F. Mitchell, and P. Schiffer. Magnetodielectric consequences of phase separation in the colossal magnetoresistance manganite $Pr_{0.7}Ca_{0.3}MNO_3$. *Phys. Rev. B*, 72:144429, Oct 2005.

[210] G. Catalan. Magnetocapacitance without magnetoelectric coupling. *Applied Physics Letters*, 88(10), Mar 6 2006.

[211] P. Lunkenheimer, V. Bobnar, A. V. Pronin, A. I. Ritus, A. A. Volkov, and A. Loidl. Origin of apparent colossal dielectric constants. *Phys. Rev. B*, 66:052105, Aug 2002.

[212] N. Biškup, A. de Andrés, J. L. Martinez, and C. Perca. Origin of the colossal dielectric response of $Pr_{0.6}Ca_{0.4}MnO_3$. *Phys. Rev. B*, 72:024115, Jul 2005.

[213] D. C. Sinclair, T. B. Adams, F. D. Morrison, and A. R. West. $CaCu_3Ti_4O_{12}$: One-step internal barrier layer capacitor. *Applied Physics Letters*, 80(12):2153–2155, Mar 25 2002.

[214] G. Catalan, D. O'Neill, R. M. Bowman, and J. M. Gregg. Relaxor features in ferroelectric superlattices: A Maxwell-Wagner approach. *Applied Physics Letters*, 77(19):3078–3080, Nov 6 2000.

Journal Publications and Proceedings

1. A. M. Kuzmenko, V. Dziom, A. Shuvaev, Anna Pimenov, M. Schiebl, A. A. Mukhin, V. Yu. Ivanov, I. A. Gudim, L. N. Bezmaternykh, and A. Pimenov, „Large directional anisotropy in multiferroic ferroborate", PRB 92, 184409 (2015)

2. M. Schiebl, A. Shuvaev, Anna Pimenov, G. E. Johnstone, V. Dziom, A. A. Mukhin, V. Yu. Ivanov, A. Pimenov, "Order-disorder type critical behavior at the magnetoelectric phase transition in multiferroic DyMnO3", PRB 91,224205

3. H. D. Drew A. B. Sushkov, Ch. Kant, M. Schiebl, A. M. Shuvaev, Anna Pimenov, Andrei Pimenov, Bernd Lorenz, S. Park, S.W. Cheong, Maxim Mostovoy, "Spectral origin of the colossal magnetodielectric effect in multiferroic DyMn2O5",PRB 90,054417,2014

4. A.M. Kuzmenko, A. Shuvaev, V. Dziom, Anna Pimenov, M. Schiebl, AA Mukhin, V. Yu. Ivanov, L.N. Bezmaternykh, A Pimenov, "Giant gigahertz optical activity in multiferroic ferroborate", PRB 89,174407,2014

5. A. Shuvaev, V. Dziom, Anna Pimenov, M. Schiebl, A.A. Mukhin, A.C. Komarek, T. Finger, M. Braden, A. Pimenov, "Electric Field Control of Terahertz Polarization in a Multiferroic Manganite with Electromagnons", PRL 111,22701, 2013

6. Alexander Woschnak, David Krejci, Markus Schiebl, Carsten Scharlemann, "Development of a green bipropellant hydrogen peroxide thruster for attitude control on satellites", Progress in Propulsion Physics, 4, 689-706, 2013

7. David Krejci, Alexander Woschnak, Markus Schiebl, Carsten Scharlemann, Karl Ponweiser, Rachid Brahmi, Yann Batonneau, Charles Kappenstein, "Assessment of catalysts for hydrogen peroxide based thrusters in a flow reactor"JPP 29, 321-330, 2013

8. M. Schiebl, A. Woschnak, D. Krejci, F. Winter, C. Scharlemann, "Modeling of Jet A1-H2O2 Autoignition in a Microrocket Combustion Chamber", JPP 29, 385-395, 2013

9. Schiebl M., "Green Chemical Space Propulsion: Auto Ignition Conditions in a Micro Rocket Combustion Chamber for a Hydrogen Peroxide based Propulsion System", AV Akademikerverlag, 2012

10. Woschnak A., Krejci D., Schiebl M., Scharlemann C., "Development of a Green Bi-Propellant Hydrogen Peroxide Thruster for Attitude Control on Satellites", 4th European Conference for Aerospace Sciences, 2011

11. Schiebl M., Krejci D., Woschnak A., Scharlemann C. et al., "Modeling and Experimental Verification of Auto-Ignition Processes for a Green Bi-Propellant Thruster", IAC-10-C4.3.9, 61st International Astronautical Congress, Prague, 2010

12. Scharlemann C., Schiebl M., Amsüss R., Tajmar M., "Development of Miniaturized Green Propellant Based Mono- and Bipropellant Thrusters", AIAA-2007-5580, 43rd AIAA/ASME/SAE/ASEE Joint Propulsion Conference and Exhibit, Cincinnati, OH, 2007

13. Scharlemann C., Schiebl M., Marhold K., Tajmar M., "Development and Test of a Miniature Hydrogen Peroxide Monopropellant Thruster", AIAA 2006-4550, 42nd AIAA/ASME/SAE/ASEE Joint Propulsion Conference and Exhibit, Sacramento, California, 2006

14. Scharlemann C., Schiebl M., Amsüss R., Tajmar M., et al., "Monopropellant Thrusters Development: Investigation of Decomposition Efficiencies"; 3rd American International Conference on Green Propellant for Space Propulsion, 2006 Poitiers, France

15. Scharlemann C., Schiebl M., Marhold K., Tajmar M., "Test of a Turbo Pump Fed Miniature Rocket Engine", AIAA-2006-4551, 42nd AIAA/ASME/SAE/ASEE Joint Propulsion Conference and Exhibit, Sacramento, California, 2006

16. Scharlemann C., Schiebl M., Marhold K., Tajmar M., "Development and Test of a Miniature Hydrogen Peroxide Monopropellant Thruster", AIAA 2006-4550, 42nd AIAA/ASME/SAE/ASEE Joint Propulsion Conference and Exhibit, Sacramento, California, 2006

Curriculum Vitae

Name: Markus Schiebl
Birth: 26.12.1976
Place of birth: St. Pölten, Austria

Education

since 01/2012	PHD IN PHYSICS	TU WIEN
01/2012	MASTER OF SCIENCE IN PHYSICS	TU WIEN
09/2011	BACHELOR OF SCIENCE IN PHYSICS	TU WIEN
06/2002	MATURA	HTLUVA ST. PÖLTEN
06/1997	TECHNICAL COLLEGE	BFS LANGENLEBARN

Experience

05/2011 – 01/2012	RESEARCH ASSOCIATE	FH WR. NEUSTADT
02/2008 – 05/2011	RESEARCH ASSOCIATE	AUSTRIAN INTITUTE OF TECHNOLOGY
10/2007 – 02/2008	IT SYSTEM MANAGER	COMPUTACENTER SERVICES BARCELONA
08/2005 – 09/2007	RESEARCH ASSOCIATE	AUSTRIAN RESEARCH CENTERS
02/1999 – 09/2002	GIS ENGINEER	LOCAL GOVERNEMENT OF LOWER AUSTRIA